BEHAVIOUR OF SELF CONSOLIDATING STEEL FIBER REINFORCED CONCRETE BEAMS UNDER REVERSED CYCLIC LOADING

by

Nima Aghniaey

Thesis submitted to the
Faculty of Graduate and Postdoctoral Studies
in partial fulfillment of the requirements for the degree of
Master of Applied Science
in Civil Engineering

uOttawa

Department of Civil Engineering
Faculty of Engineering
University of Ottawa

March 2013

Acknowledgement

First and foremost I offer my sincerest gratitude to Dr. Hassan Aoude for his support and restless efforts during all phases of this experimental program, for giving me the opportunity to work with him. It was for his resourcefulness, valuable comments, novel ideas and support during my entire research program that this thesis was prepared and hereby presented. I also would like to thank my co-supervisor, Professor Murat Saatcioglu, for sharing with me his vast knowledge and experience and accommodating me for questions and long discussions despite his limited time and busy schedule.

In addition, I would like to thank the professors of the Department of Civil Engineering at the University of Ottawa and the assistance of the administrative staff who have provided help and support throughout my studies.

I also gratefully acknowledge the support of material supplies from Bekaert Steel Wire Co. (steel fibers) and King Materials (SCC).

Last but not least, I would like to dedicate this thesis to my parents and thank them for their unconditional love and support and giving me the strength to achieve my goals.

Nima Aghniaey

Abstract

Concrete is a very weak and brittle material in tension. It has been shown in previous researches that the addition of steel fibers to a concrete matrix can improve this behavior. The ability of fibers to control and redistribute stresses after cracking results in a number of improvements in the structural behaviour of concrete. A review of existing literature shows that the addition of steel fibers enhances concrete's tensile resistance, crack control properties, ductility and damage tolerance. In beams, fibers can transform brittle shear response into a flexural response and promote ductility, thereby allowing for a full or partial replacement of traditional shear reinforcement. The enhanced shear capacity, ductility and damage tolerance of Steel Fiber Reinforced Concrete (SFRC) can also potentially be used to relax seismic detailing requirements in frames by partially replacing the required transverse reinforcement in the plastic hinge regions of RC beams.

One of the drawbacks associated with SFRC is that the addition of steel fibers to a traditional concrete mix at high fiber contents can result in workability problems. The combined use of Self-Consolidating Concrete (SCC) and fibers can solve this problem and facilitate placement for a wider range of structural applications.

Although several studies have been conducted on the behaviour of SFRC beams subjected to monotonic loading, there is limited research on the behaviour of SFRC beams under cyclic or reverse-cyclic loading. This thesis presents the results of an experimental and analytical study conducted on nine SFRC beam specimens tested under load reversals. The main objective of this research program was to investigate the effect of fibers on structural behaviour and to examine the ability of steel fibers to replace transverse reinforcement. The experimental and analytical results show that use of fibers results in several improvements in behaviour, including enhanced damage tolerance and post-peak ductility. The results also show that steel fibers can potentially be used to allow for a reduction of transverse reinforcement in beams, however further research is required.

Table of Contents

List of Figures

List of Tables

List of Symbols

A_f	Cross-sectional area of fiber
A_s	Cross-sectional area of steel reinforcement
A_v	Transverse reinforcement cross-sectional area
$A_{v,\min}$	Minimum area of shear reinforcement
a/d	Shear span-to-depth ratio
V_f	Factored shear force
w/c	Water-to-cement ratio
d	Effective depth
D_f	Diameter of fiber
d_v	Effective shear depth of the beam
E_s	Modulus of elasticity of longitudinal steel reinforcement
f_c'	Compressive strength of concrete
f_{cf}'	Ultimate compressive strength of fiber reinforced concrete
f_{ct}	Tensile strength of concrete
f_{cu}'	Ultimate compressive strength of plain concrete
f_{fy}	Fiber tensile strength
$f_{\max}$	Peak tensile stress in concrete
θ	Beam rotation
L_1	Top LVDT reading
L_2	Bottom LVDT reading
H	Distance between LVDTs at top and bottom of plastic hinge region
$F_{pullout}$	Pullout strength of a single fiber
f_r	Modulus of rapture of concrete
f_u	Ultimate stress of longitudinal steel reinforcement
f_y	Yield stress of steel reinforcement
f_{yh}	Yield stress of transverse reinforcement

h	Beam height
h_o	Fiber dimension which is a function of hook geometry
K	Fiber participation factor
k	Factor referring to the type of test used to determine the tensile strength of concrete
k_o	Fiber dimension which is a function of hook geometry
k_{f1}, k_{f2}	Parameters used to define the descending branch of SFRC stress-strain curve
L_f	Length of fiber
$L_{f,straight}$	Length of straight portion of fiber neglecting the anchorage
L_f / D_f	Fiber aspect ratio
n	Parameter that describes the shape of SFRC stress-strain diagram
N_{fibers}	Effective number of fibers per unit area
P_1	Load at onset of complete de-bonding during fiber pullout
P_2, P_3	Load plateau at end of first hook contribution during fiber pullout
P_4	Load plateau at end of second hook contribution during fiber pullout
P_{crit}	Load that causes de-bonding to initiate during fiber pullout
$\Delta P'$	Mechanical pullout load contribution of hook due to the formation of two plastic hinges
$\Delta P''$	Mechanical pullout load contribution of hook due to the formation of one plastic hinge
r_f	Fiber radius
s	Center-to-center spacing of transverse steel reinforcement in RC member
s'	Clear spacing of transverse reinforcement in RC member
V	Shear force at a section of RC member
α, α_θ	Fiber orientation factor
Δ_1	Slip of the fiber at full de-bonding
Δ_3	Slip of the fiber at load P_3 during de-bonding
Δ_4	Slip of the fiber at load P_4 during de-bonding

ε_c	Elastic strain in concrete
$\varepsilon_{c,cr}$	Elastic strain in concrete at cracking
ε'_{cf}	Ultimate strain of fiber reinforced concrete
ε'_{cu}	Ultimate strain of plain concrete
ε_{sh}	Strain of longitudinal steel reinforcement at strain-hardening
ε_u	Ultimate strain of longitudinal steel reinforcement
ε_y	Yield strain of longitudinal steel reinforcement
v_f	Volume fraction of fibers
η_1	Length factor that accounts for variability in fiber embedment length
ϕ_u	Curvature of beam at ultimate
ϕ_y	Curvature of beam at yielding of longitudinal reinforcement
ρ	Longitudinal steel reinforcement ratio
M_{cr}	Cracking moment resistance
M_u	Ultimate moment resistance
M_y	Yield moment resistance
σ_c	Elastic stress in concrete
τ_{bond}	Bond shear strength
θ	Angle of inclination of diagonal compressive stresses to the longitudinal axis of the member
F_{m300}	Force at deflection of l/300 in ASTM 4-point bending test
F_{m150}	Force at deflection of l/150 in ASTM 4-point bending test
I'_E	Effective confinement index
f'_{le}	Effective confinement pressure
f'_l	Nominal lateral pressure provided by transverse reinforcement
K_e	Effective confinement factor
A_{shy}	Total cross-sectional area of transverse reinforcement perpendicular to y axis
A_{shx}	Total cross-sectional area of transverse reinforcement perpendicular to y axis
f_{cc}	Transverse reinforcement stress at maximum strength of confined concrete
c_x	Width of concrete core in the x direction

c_y	Width of concrete core in the y direction
Σw^2_i	Sum of squares of clear spacings between adjacent longitudinal bars
ρ_{sey}	Effective ratio of confinement reinforcement in y direction
k	Parameter indicating yielding of transverse reinforcement at maximum strength of confined concrete
f_{cc}	Stress in confined concrete
f'_{cc}	Maximum compressive stress of confined concrete
ε_{cc}	Confined concrete strain
ε'_{cc}	Strain at maximum stress of confined concrete
I_{E50}	Effective confinement index evaluated at the post-peak strain ε_{cc50}
ε_{cc50}	Post-peak strain as defined by equation 6.15
ε'_{cu50}	Post-peak strain measured at 50% of maximum unconfined stress
Δf_{cf}	Stress contribution from steel fibers
A_{ineff}	Ineffectively confined core area
A_{core}	Core area
A_{KE}	Effectively confined core area

Chapter 1 Introduction

1.1 Background

Concrete exhibits weak and brittle behavior under tensile loads. Addition of steel fibers can transform this behaviour due to the ability of fibers to control and redistribute stresses after cracking. Research has shown that the addition of steel fibers to concrete results in several enhancements, including improved tensile resistance, post-cracking strength and toughness (Aoude 2008 & Cohen 2012). Similarly in compression, the addition of steel fibers improves post-peak strength and ductility. In structural members, addition of fibers to concrete leads to enhanced shear resistance due to improvements in diagonal tension capacity of concrete. If added in sufficient quantity, steel fibers can be used to replace traditional shear reinforcement and promote flexural failure and ductility (Cohen, 2012). In columns, the addition of steel fibers enhances confinement and cover spalling (Aoude et al., 2009). Research has also shown that steel fibers can improve energy dissipation capacity at joints and shear walls (Parra-Montesinos, 2005).

Many studies have been conducted on the effect of steel fibers on behavior of beams under monotonic loading and there appears to be fairly good agreement between the obtained results; however, limited research has been done on the behavior of SFRC beams under cyclic and/or reverse-cyclic loading. During earthquakes, flexural members are required to undergo large inelastic deformations while maintaining strength and stiffness under load reversals. To ensure adequate performance, modern codes require the critical regions in such members to be properly detailed with transverse reinforcement that results in congestion of reinforcement. SFRC can be used to relax this detailing requirement and hence ease the construction process.

Several studies have shown that addition of steel fibers to a traditional concrete mix can result in poor workability of concrete (Aoude 2008 & Cohen 2012). Recently, the use of Self Consolidating Concrete (SCC) in combination with steel fibers has been proposed by some researchers (Aoude 2008) in order to obtain workable and uniform fiber reinforced concrete

mixtures. Since the use of SFRC in extreme load applications such as earthquake loads would typically require high fiber contents, the use of SCC is an innovative solution to the workability problems associated with traditional concrete reinforced with steel fibers.

1.2 Research objectives

The primary objective of this research program is to investigate the advantages resulting from the combined use of steel fibers and self consolidating concrete in flexural members subjected to load reversals and to examine the potential of using steel fibers as partial replacement of traditional transverse reinforcement in beams. To improve the placement of concrete, and to allow for high contents of steel fibers without compromising workability, a highly flowable SCC mix was used in this study.

1.3 Experimental Program

The objectives of this experimental program were achieved by testing a number of steel fiber reinforced concrete (SFRC) dual-cantilever specimens constructed using self-consolidating concrete (SCC) under reverse-cyclic loading. Based on a preliminary study and by reviewing previous similar researches (Parra-Montesinos, 2005, Aoude 2008, etc.), nine beams were constructed with varying amounts of transverse reinforcement and fiber contents which included two control beams constructed without fibers. These beams were tested under reverse-cyclic loading and the response of the specimens in terms of hysteretic load-displacement response, flexural strength, post-peak ductility, energy dissipation, crack control and damage tolerance was recorded and is presented in this thesis.

1.4 Analytical Program

As part of the analytical study presented in this thesis, the load-displacement responses of the nine tested specimens were analytically predicted using inelastic static (push-over) analysis. Sectional and member analyses were conducted to establish the moment-curvature and force-displacement relationships for the tested beams. Analytical results were compared to the experimental force-displacement responses and are presented in chapter 6 of this thesis.

1.5 Thesis Organization

This thesis consists of 7 chapters including the introduction chapter:

- Chapter 2 consists of a comprehensive literature review of the topic of this thesis;
- Chapter 3 presents details of the experimental program, including material properties, beam geometry and reinforcement details, loading setup and loading sequence;
- Chapter 4 presents the experimental results for the beams tested in this research program;
- Chapter 5 presents a comparative study of the results in order to investigate the effects of steel fibers and transverse reinforcement on the structural response of the SFRC beams;
- Chapter 6 presents analytical predictions of the response of the beams tested in this study;
- Chapter 7 presents the concluding remarks regarding the experimental and analytical program, and provides recommendations for future research.

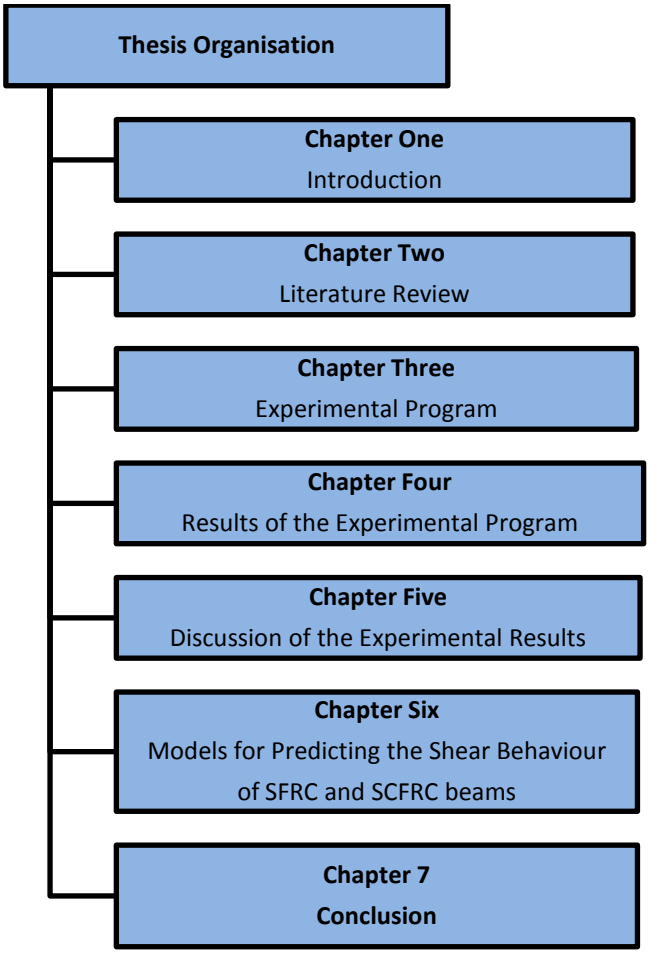

Chapter 2 Literature review

2.1 Chapter overview

Chapter 2 presents an overview of Steel Fiber Reinforced Concrete (SFRC) providing a review of SFRC as a structural material and the concept of using SFRC in structural applications. In this section, different types of steel fibers are introduced and various factors that influence the mechanical properties of SFRC are discussed. In addition, the mechanical behaviour of SFRC under compression and tension is also summarized. The chapter will also discuss the use of self-consolidating concrete (SCC) in combination with steel fibers in self-consolidating fiber reinforced concrete (SCFRC). As this thesis will focus on the behaviour of SFRC beams constructed with SCC under reverse-cyclic loading, existing research on SFRC and SCFRC beams will be discussed, and previous research conducted on the cyclic and reverse-cyclic behaviour of SFRC beams will be summarized. The chapter concludes by reviewing seismic detailing requirements for reinforced concrete (RC) beams in the CSA A23.3 design standard.

2.2 Steel Fiber Reinforced Concrete and its properties

2.2.1 Introduction

Concrete has been used for centuries as a low-cost construction material and has played an important role in shaping our view of modern structures. Nowadays, concrete is used more than any other man-made material in the world. As of 2006, about 7.5 cubic kilometres of concrete has been used each year - more than one cubic meter for every person on earth. The success of concrete as a construction material comes from its unmatched advantages such as its relatively low cost which has persuaded engineers to choose it as their primary choice for design and construction of various types of structures. Despite its benefits, concrete has however always carried certain short-comings and deficiencies. In particular, plain concrete is very weak and brittle in tension. To overcome this shortcoming, reinforced concrete structures combine the high compressive strength of concrete with the tensile strength and ductility of steel reinforcement through the strategic placement of longitudinal and transverse reinforcement in regions subjected to high tensile stresses.

The low tensile capacity and brittle nature of plain concrete as well as the susceptibility of reinforced concrete to cracking under service loads has also tweaked engineers and researchers to search for other alternatives for reinforcing concrete. In recent years, and along with advancements in polymer and steel production technologies, researchers have turned to fibers as a method of improving the tensile behaviour of concrete. In contrast with conventional steel reinforcement, fibers reinforce the matrix is in a multi-directional form acting as miniature crack-arrestors. The result is improvement of many of the properties of concrete including tensile capacity and post-cracking resistance, fracture toughness and ductility. This not only improves the cracking resistance of concrete members under service loads, but can also be used to improve structural behaviour. For example, the use of fiber reinforced concrete (FRC) improves the diagonal tension capacity of concrete and thus can be used to improve the shear resistance of concrete members. In addition, the ductility and energy absorption capacity of FRC can improve the performance of concrete members subjected to extreme load events such as earthquakes and explosions.

This section of the literature review introduces the physical and mechanical properties of Fiber Reinforced Concrete (FRC) in general. Properties of FRC and different types of fibers are discussed and steel fibers are introduced. Various properties of steel fibers which influence the behaviour of steel fiber reinforced concrete (SFRC) are also discussed in this section. Tensile and compressive behaviour of SFRC is summarized and standard test methods for determining tensile properties of SFRC are listed and discussed in brief.

2.2.2 Overview of FRC and various fiber types

Fiber reinforced concrete is a composite material whose components include the traditional constituents of Portland cement concrete (cement, coarse aggregate, sand, water, etc.) and short discrete fibers dispersed randomly in the concrete matrix. Fibers have been used in a variety of applications including slabs on grade, water tanks, tunnels and structural components such as beams. A number of types of fibers commercially used in engineering applications and their properties are listed in **Table 2.1**. These include steel, glass and synthetic fibers. Glass fibers are most commonly used in architectural applications such as building cladding panels. While synthetic fibers can be used to enhance structural performance, they are most commonly used to control plastic shrinkage cracking in concrete slabs (i.e. airport runways). Steel fibers, which come in a variety of forms, can enhance the toughness of concrete. At low fiber contents, steel fiber reinforced concrete can be used to replace secondary reinforcement in slabs and tunnel linings. At higher fiber contents, research has shown that the steel fibers can be used to improve structural response of concrete elements such as beams, columns and walls (Parra-Montesinos, 2005, Aoude 2008, Cohen 2012, Campione et al 2008, Hameed et al 2009). Other types of fibers not listed in **Table 2.1** and are not as commonly used include cellulose fibers and Asbestos fibers.

Table 2.1 Properties of selected fiber types
[Adapted from Kosmatka et al. (2008)]

Fiber Type	*Relative Density*	*Diameter (μm)*	*Tensile Strength, (Mpa)*	*Modulus of Elasticity, (Mpa)*	*Strain at Failure, (%)*
Steel	7.80	100-1000	500-2600	210,000	0.5-3.5
Glass					
AR	2.70	12-20	1500-3700	80,000	2.5-3.6
Synthetic					
Acrylic	1.18	5-17	200-1000	17,000-19,000	28-50
Aramid	1.44	10-12	2000-3100	62,000-120,000	2-3.5
Carbon	1.90	8-10	1800-2600	230,000-380,000	0.5-1.5
Nylon	1.14	23	1000	5,200	20
Polyester	1.38	10-80	280-1200	10,000-18,000	10-50
Polyethylene	0.96	25-1000	80-600	5,000	12-100
Polypropylene	0.90	20-200	450-700	3,500-5,200	6-15

2.2.3 Steel Fiber Reinforced Concrete (SFRC)

Steel fiber reinforced concrete (SFRC) is a composite material whose components include the traditional constituents of Portland cement concrete and short discrete steel fibers that are dispersed randomly in the concrete matrix.

The addition of steel fibers transforms the weak and brittle nature of concrete into a ductile behaviour in tension and enables concrete to have improved post-cracking strength in tension. Other enhancements include improved ductility and toughness in tension and compression, improved impact resistance and increased damage tolerance.

Steel fibers typically are short and discrete elements that can have different lengths to diameter ratios ranging from about 20 to 100, and have tensile strengths ranging from 500 to 2600 MPa. **Figure 2.1** shows typical geometries of steel fibers currently used in structural applications. The bond between the fiber elements and concrete, which has a direct effect on the pullout strength of the fibers, is related to surface roughness and geometry and can be improved by mechanical anchorage properties of fibers. For this reason, fibers typically have deformations either at their ends as in the case of hooked-end fibers, or along their length in the form indentations shown in figure below.

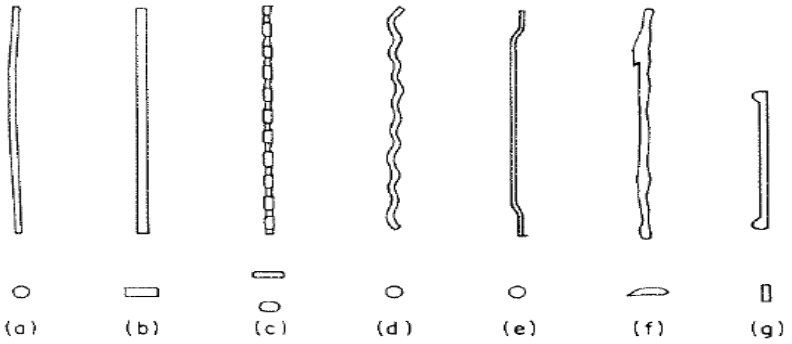

Figure 6.1. Shapes of steel fibres (a) Round, (b) Rectangular, (c) Indented (Duoform, National Standard Patent), (d) Crimped (G. K. N. and Johnson Nephew Ltd.), (e) Hooked ends (Dramix, Z. Bekaerto Ltd. Patent) (f) Melt extract process (Battelle Patent), (g) Enlarged ends (Australian Wire Industries Ltd. Patent)

Figure 2.1 Different Steel Fiber Geometries

[Adapted from Johnston (2001)]

ASTM A 820 categorizes steel fibers into five different types based on the product or process used as a source of steel fiber material; Type I - Cold drawn fibers, Type II - Cut steel fibers, Type III - Melt-extracted fibers, Type IV - Mill-cut fibers and Type V - Modified cold-drawn wire. These categories of steel fibers may be use in straight or deformed shapes such as those shown in **Figure 2.1**.

Steel fiber volumes in typical structural applications range from 0.25% to 2% by volume; and the fiber content has a significant impact on mechanical properties and workability of SFRC. Most current "non-structural" applications such as slabs on grade use fiber contents smaller than 0.5% by volume (or 39 kg/m^3). For most structural applications fiber contents in excess of 1% (or 78 kg/m^3) are typically required. **Table 2.2** lists the range of volume fraction of fibers for SFRC (listed as FRC) and other fiber reinforced concrete composites.

Table 2.2 Range of volume fraction of fibers for typical fiber reinforced cement composites, [Adapted from Naaman, 2003]

Material	Range of V_f	Remark
FRC – Fiber Reinforced Concrete	$V_f \le 2\%$	Fibers are premixed with the concrete matrix. Finer aggregates may be needed.
HPFRCC – High Performance Fiber Reinforced Cement Composites	$V_f \begin{cases} \ge (V_f)_{critical} \\ \ge 1\% \end{cases}$	Strain hardening and multiple cracking characteristics in tension. With proper design, critical V_f can be less than 2%.
Shotcrete (steel fibers)	$V_f \le 3\%$	Applications in tunnel lining and repair.
Spray Technique (glass fibers)	$4\% \le V_f \le 7\%$	Applications is cladding and panels.
SIMCON (steel fibers)	$4\% \le V_f \le 6\%$	Slurry Infiltrated Mat Concrete. A prefabricated fiber mat is needed.
SIMCON (PVA fibers)	$V_f \approx 1\%$	Recently available.
SIFCON (steel fibers)	$4\% \le V_f \le 15\%$	Slurry Infiltrated Fiber Concrete. Fibers are preplaced in a mold and infiltrated by a fine cementitious slurry matrix.

Typical applications of SFRC are in airport pavements and runway/ taxi overlays, slabs on grade bridge decks, industrial floors and structures exposed to high-velocity water flows. Steel fibers are also widely used with shotcrete in thin-layer applications such as rock-slope stabilization and tunnel linings. In addition, some design standards and codes such as the ACI-318 Code have recently permitted the use of steel fibers to replace minimum transverse reinforcement in beams (on the condition that certain SFRC performance criteria are met). **Figure 2.2** summarizes the typical applications of SFRCs.

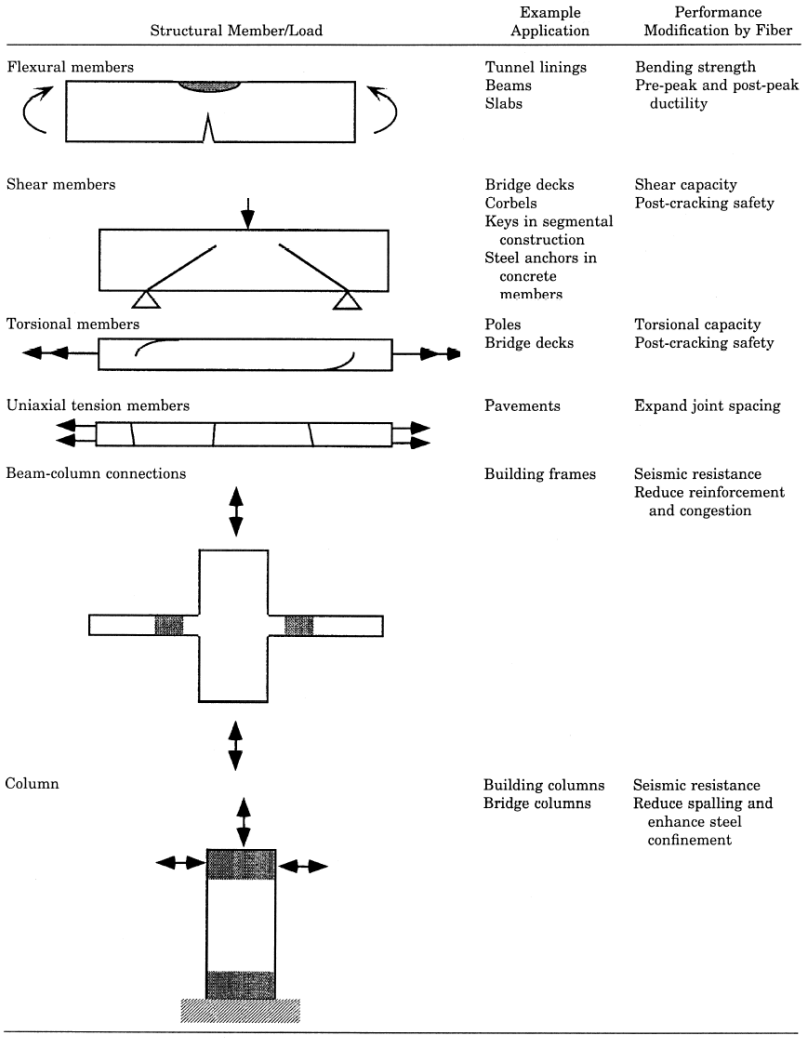

Figure 2.2 Typical applications of SFRCs
[Adapted from Aoude, 2008]

2.2.4 Steel Fiber Typologies

In order to overcome the limitations of straight fibers in bond strength, it is common to induce deformations in the fiber to provide anchoring effects. Several experiments have been conducted to assess the contribution of the anchoring mechanism on pullout strength (Naaman & Reinhardt, 1996; Weiler et al., 1999; Banthia & Trottier, 1994). It can be assumed that the anchoring mechanisms involve processes by which the energy is dissipated as the fiber undergoes plastic deformation while being pulled out.

2.2.4.1 Hooked-end steel fibers

Figure 2.3 shows properties of Dramix hooked-end steel fibers for different types. Hooked end fibers are one of the most commonly used type of steel fibers in the construction industry. These fibers are deformed at the ends in order increase the pullout strength through mechanical clamping. The mechanical clamping of the hook plays a significant role in increasing the pullout load as well as the pullout energy of the fiber. As the fiber is pulled out it undergoes plastic deformations which contributes to dissipation of the pullout energy (energy dissipated during pullout of fibers) and thus impacts the post-cracking behaviour significantly in a positive way. Hooked end fibers are produced in different lengths and diameters to suit various designs and applications. **Table 2.3** shows a list of commonly used *Dramix* brand hooked-end steel fibers (manufactured by *Bekaert*).

Table 2.3 Properties of Dramix hooked end fiber types

[Adopted from Cohen, 2012]

Type	***Tensile Strength (MPa)***	***Diameter (mm)***	***Length (mm)***	***Aspect Ratio***
Dramix RC 65/35 BN	1100	0.55	35	64
Dramix RC 65/60 BN	1000	0.9	60	67
Dramix RC 80/60 BN	1050	0.75	60	80
Dramix RC 80/60 BP	2300	0.71	60	85
Dramix RC 65/60 CN	1000	0.90	60	67
Dramix RC 80/60 CN	1150	0.75	60	80
Dramix RL 45/35 BN	1050	0.75	30	47
Dramix Duo 100	1050	0.75	60	80

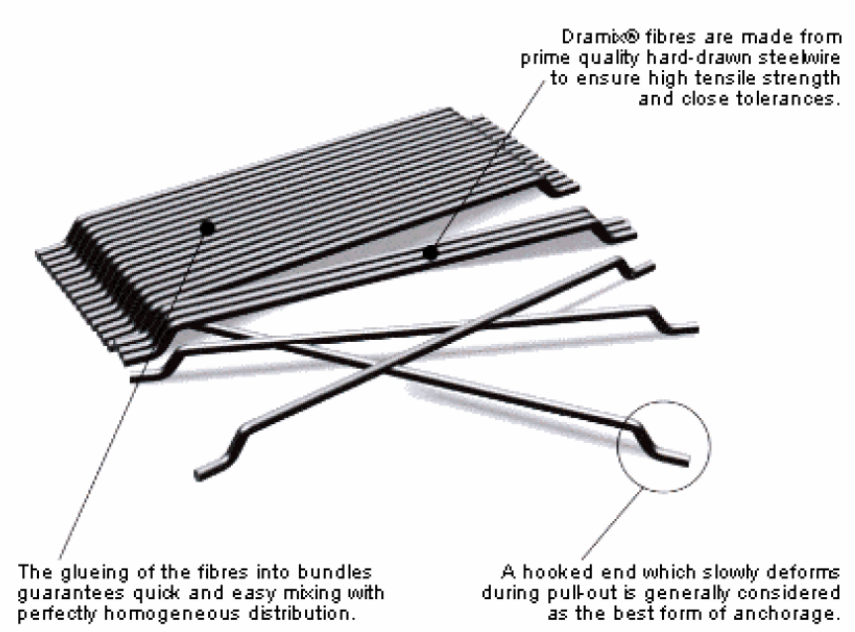

Figure 2.3 Typical *Dramix* hooked end steel fibe

2.2.4.2 Corrugated steel fibers

Corrugated fibers are another type of deformed steel fibers that develop pullout resistance by means of mechanical anchorage and interfacial bonding. A number of researchers have conducted experiments to evaluate the interaction of corrugated steel fibers with cement and concrete (Chanvillard & P. Aitcint, 1996 and others). Two modes of failure are generally observed: in one case the fiber is broken; in the second case, the fiber first de-bonds, then slips in its print until it is finally pulled out. Another important factor is the number of corrugations (or waves) along the length of the fiber. **Table 2.4** presents the energy dissipated during the pullout process for two configurations studied by Chanvillard & Aitcint (1996). As seen in this table, the energy dissipation increases with the number of waves embedded in the matrix. The results also demonstrate that the orientation of the fibers also has a significant effect on the amount of energy dissipated during pullout. In addition, length of fibers directly impact the number of waves embedded in the matrix and thus greater length leads to higher energy dissipation.

Table 2.4 Effect of various parameters on the pullout strength of corrugated fibers [Adapted from Chanvillard & Aitcint (1996)]

	45° angle			90° angle		
w/c	One wave	Two waves	Three waves	One wave	Two waves	Three waves
0.3	372	3056	7428	1094	4760	10382
0.5	269	1855	6478	550	4335	8709
0.7	236	1846	5101	463	3767	7457

2.2.5 Important SFRC properties

SFRC improves the behaviour of concrete in tension. This arises from the ability of fibers to bridge and control cracks, which results in improved post-cracking strength. This crack bridging mechanism is dependent on several parameters including fiber aspect ratio, fiber content, fiber strength, fiber pullout behaviour and fiber orientation.

2.2.5.1 Aspect ratio

One of the key fiber parameters which can influence the properties of SFRC is the fiber aspect-ratio, which is defined as the ratio of the length of the fiber element to its diameter (L_f/d_f). In particular, research has shown that increasing the aspect ratio improves the mechanical properties of SFRC in tension and compression. As shown in **Figure 2.4**, although use of fibers having higher aspect-ratio does not significantly affect peak compressive strength, it does result in important improvements in toughness and slightly increases peak strain of SFRC in compression (Wang et al, 2010).

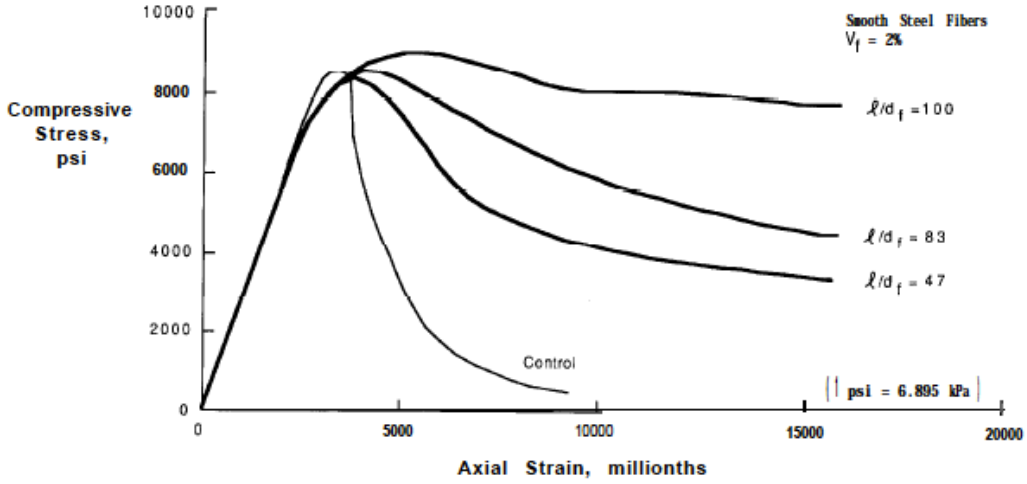

Figure 2.4 Influence of Aspect ratio of fibers on the compressive stress-strain [Adapted from ACI 544 (2008)]

Similarly Bayramov et al. (2004) performed a series of compression tests for SFRC specimens with different fiber aspect-ratios and observed that when fiber aspect-ratio exceeds a certain value, introducing additional steel fibers into concrete may increase the ductility and toughness rather than the strength. The use of higher aspect-ratios can also improve the impact resistance of SFRC. Mohammadi et al. (2009) constructed a drop weight test setup to evaluate the impact resistance of SFRC and observed that specimens which utilized fibers with higher aspect-ratios have higher energy absorption capacities.

It should however be noted that as the aspect-ratio (and generally the length) increases, the workability of the concrete in the fresh-state decreases and thus fibers with larger aspect-ratios (or length) may have lower fiber content limits for a workable mix. Therefore the optimal fiber aspect-ratio must be chosen to satisfy requirements in both the fresh and hardened state (Aoude, 2008).

2.2.5.2 Fiber content

As noted previously, the amount of fibers added to the concrete matrix typically ranges from 0.25% to 1.5% (20 to 120 Kg/m^3) by volume of concrete. Use of higher fiber content improves the post-peak behaviour of concrete in compression as depicted in **Figure 2.5.** Increased fiber content also results in enhanced post-cracking strength in tension. Aoude (2008) suggested that the minimum amount of fibers required for structural applications is 0.5%. Aoude (2008) also suggested that the maximum fiber content that can be used in traditional SFRC without compromising the workability and achieving uniform mix properties is 1.5%. Beyond 1.5% fiber content, SFRC in fresh state becomes very stiff, fibers tend to ball-up and segregation and bleeding of concrete is observed.

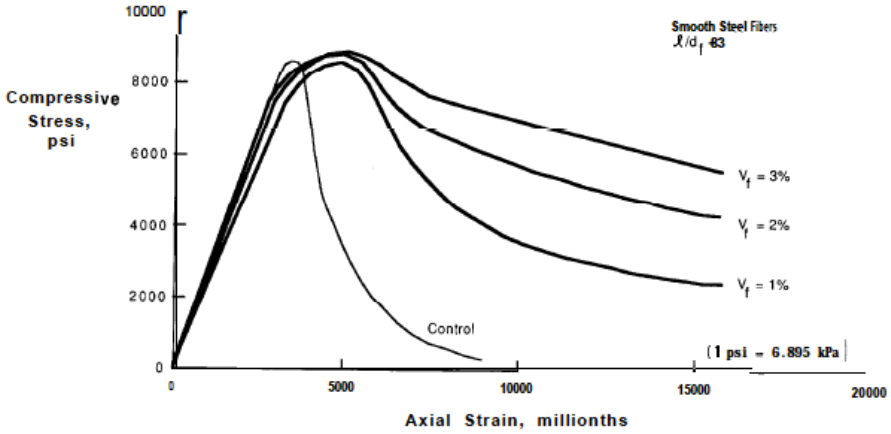

Figure 2.5 Influence of the volume fraction of fibers on the compressive stress-strain [Adapted from ACI 544 (2008)]

2.2.5.3 Steel fiber strength

As with any composite material, the composite behaviour of SFRC is dependent on the characteristics of the various components as well as their interaction with each other. As noted previously, steel fibers aid in controlling cracks by allowing concrete to transfer tensile stress across cracks. Hence, the tensile strength of the steel fibers is a property that can affect the overall performance of SFRC. Although fibers generally do not fracture as they deform, the energy required to deform the fiber (as in the case of hooked-end fibers) is related to the tensile strength of the fibers and hence fiber strength can affect performance.

Van Gysel (2000) conducted pullout tests on steel fibers with high and normal tensile strength fibers. The test results showed that the use of high-strength fibers results in 50-100% improvement in pullout resistance when compared to the results obtained for the normal strength fibers. In applications where higher strength concrete is used, the fibers can indeed fracture and the tensile strength of the fibers becomes even more important. Depending on the manufacturing process and the raw steel material properties, steel fibers can have tensile strengths varying from fu= 1200 MPa (normal tensile strength) to fu=2200-2600 MPa (high tensile strength).

2.2.5.4 Fiber pullout behaviour

Pullout behaviour is another important property that affects the performance of SFRC. This behaviour is a function of fiber typology and differs for straight and hooked-end fibers.

In the case of straight round fibers the pullout strength is directly related to shear bond strength. Shear bond strength refers to the interfacial bond strength between the surface area of an individual fiber element and the cement matrix. For straight round fibers, the pullout strength can be quantified by assuming that a constant bond strength (τ_{bond}) acts along the embedded surface area of the fiber (Hannant, 1978). Equation 2.1 represents the average straight fiber pullout force approximation by considering the shear bond strength as the only contributing factor.

$$F = \tau_{bond} \pi d_f \frac{L_f}{2} \quad (2.1)$$

In equation 2.1, F is the average pullout force, L_f is the length and d_f is the diameter of an individual steel fiber element. **Figure 2.6** shows the various stages in the pullout behaviour of straight round fibers including: fully-bonded, partial de-bonding, full de-bonding and frictional pullout stages. It should be noted that the shear bond strength is directly related to the concrete matrix strength. **Table 2.5** shows suggestions for values for bond strength based on matrix strength range.

Table 2.5 Shear bond stresses of steel fibers
[Adapted from Grunewald (2004) based on work by Kutzing (2000)]

Matrix Compressive strength class	***Compressive strength range*** f'_{co} ***(MPa)***	***Bond shear stress*** τ_{bond} ***(MPa)***
Normal strength	≤ 50	2.0-3.0
Medium strength	≥ 50 & ≤ 70	3.4-4.5
High strength	> 70	5.0-6.0

It should be noted that this representation of the pullout force does not apply to deformed fibers and research has shown that deformed steel fibers results in improved pullout behaviour due to mechanical contribution of the deformations (Alwan et al., 1991).

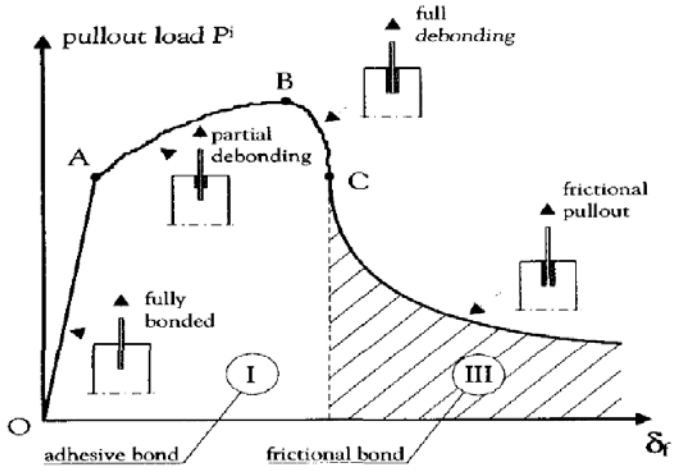

Figure 2.6 Typical pullout load vs. the end-slip relation for a straight steel fiber [Adopated from Naaman et al. (1999)]

Figure 2.7 shows the idealized pullout behaviour of hooked-end fibers. It is noted that the behaviour is similar to the behaviour of straight fibers with the exception being that there are now additional contributions due to the mechanical clamping of the hooks and resulting increases in pullout loads. The model presented by Alwan et. al. (1991) modifies the expected pullout behaviour of smooth-straight fibers to incorporate the contribution of fiber deformation for hooked-end fibers. This contribution consisted of the additional force required to straighten the hooked ends of the fibers before they are pulled out of the concrete matrix (represented by the ΔP values). In his model, Alwan et al. (1991) defined the pullout process to be composed of four stages; stage one is the initial elastic loading phase in which fibers start to become de-bonded at the concrete-fiber interface. In stage two, shear and frictional stresses start to become effective and govern the pullout force until complete de-bonding of the fibers from the concrete matrix. After complete de-bonding in the third stage, the pullout force will be only due to the mechanical clamping of the hooked end of individual steel fibers. At this stage the pullout force will increase due to additional force required to straighten the fibers hence the pullout force will be a function of the hooked end geometry:

$$P_3 = P_1 + \Delta P' \tag{2-2}$$

$$P_4 = P_1 + \Delta P^{''} \tag{2-3}$$

$$\Delta P^{'} = \frac{\left[\frac{f_{fy}\pi r_f^2}{3\cos\theta}\right][1+\frac{\mu\cos\beta}{(1-\mu\cos\beta)}]}{[1-\mu\cos\beta]} \tag{2-4}$$

$$\Delta P^{''} = \frac{\left[\frac{f_{fy}\pi r_f^2}{6\cos\theta}\right]}{[1-\mu\cos\beta]} \tag{2-5}$$

where P_1 is the de-bonding load at the initial stage. P_3 and P_4 are the pullout force plateaus as depicted in **Figure 2.7** respectively. $\Delta P'$ and $\Delta P''$ are the mechanical pullout force contributions. f_{fy} refers to the fiber yield strength, r_f refers to fiber radius and μ is the frictional coefficient at the fiber-matrix interface. The parameters θ and β are related to angle of inclination of the hook with respect to the straight portion of the fiber (Alwan et al., 1999).

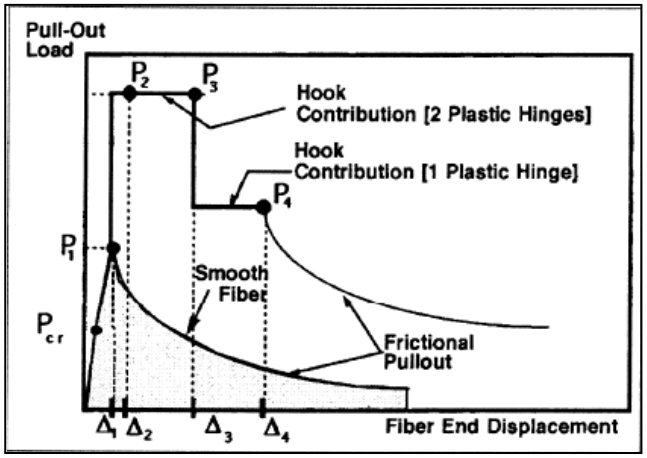

Figure 2.7 Idealized pullout behaviour of hooked-end fibers
[Adpated from Alwan et al., 1999]

The Δ_3 and Δ_4 terms in **Figure 2.7** are calculated as follows:

$$\Delta_3 = \Delta_1 + k_o \tag{2-6}$$

$$\Delta_4 = \Delta_3 + h_o \tag{2-7}$$

where Δ_1 represents the fiber slip length at full de-bonding and k_o and h_o are function of fiber geometry.

2.2.5.5 Orientation & distribution factor

In fiber-reinforced concrete, fibers are assumed to disperse randomly in all directions in order to exhibit isotropic behaviour. However, the real fiber distribution is strongly influenced by various factors such as fiber characteristics (diameter, length, and volume fraction), the fluidity of the matrix, placing method, and shape of the form. Non-uniform fiber distribution decreases the desirable effects of SFRC (Kang et al., 2010).

For fibers randomly dispersed in the three dimensions, the effective number of fibers per unit area can be calculated using equation 2.8 (Lee 1990):

$$N_{fibres} = \frac{v_f}{A_f} \alpha \eta_l \tag{2.8}$$

where A_f is the cross-sectional area of the fiber and v_f is the volume fraction of the fibers in the cement matrix and where the orientation factor α, is used to account for the random orientation of the fibers crossing any arbitrary cracking plane. The orientation of individual fibers implies the position of the fibers with respect to the cracking plane in the cement matrix. This orientation has a significant impact on the pullout behaviour of individual fibers as well as the mechanical properties of the composite. For fibers that are not limited by boundary conditions (fibers in bulk), several authors have suggested using a value of 0.5 for α by integrating fiber pullout length over all possible orientation angles as shown in **Figure 2.8** (Dupont, 2003).

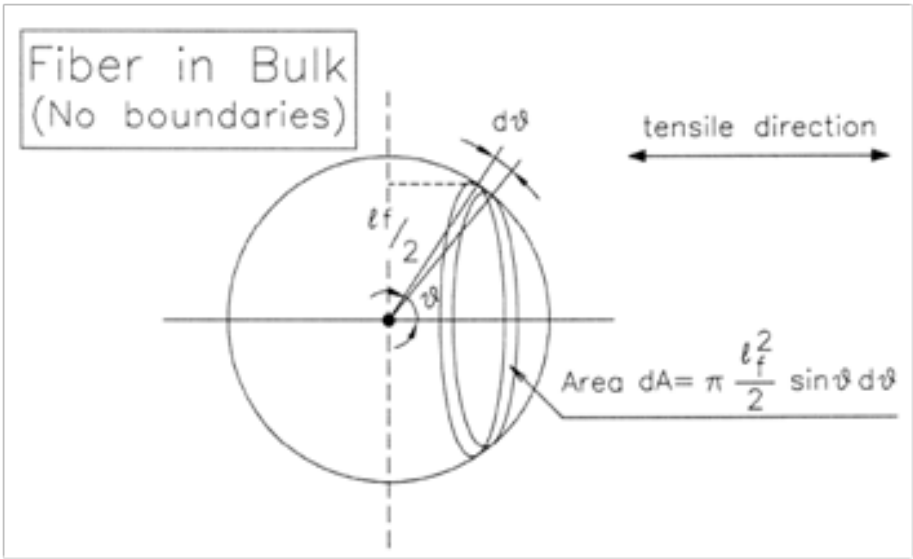

Figure 2.8 Derivation of Orientation factor as suggested by Dupont
[Adapted from Dupont (2003)]

Foster (2003) assumed that fibers orientated in angles of θ=30 ^{o} and less have reduced efficiency and hence suggested that only fibers oriented in θ=30 ^{o} to 90 ^{o} are effective, resulting in an orientation factor of 3/8 (see **Figure 2.9**).

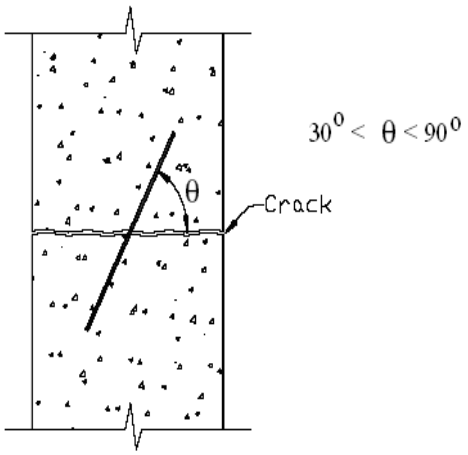

Figure 2.9 Foster's Graphical representation to calculate orientation factor
[Adapted from Foster (2001)]

For fibers with one or two boundary conditions, Dupont (2003) suggests using 0.6 and 0.84 for α, respectively. Suggestions for orientation factors for 2- and 3-dimensional distributions

from other authors are shown in **Table 2.6**. In equation 2.8, η_l accounts for the variability in the fiber embedment length across the cracking plane. Fiber embedment length in concrete can vary from $\frac{L_f}{2}$ to 0 with L_f being the length of the fiber.

Table 2.6 Fiber efficiency factors proposed in several studies [Adapted from Kang et al. , 2010]

Reference	Orientation efficiency factor	
	Random 2-dimension	Random 3-dimension
Aveston et al. [13]	$2/\pi$	1/2
Laws [14]	1/3	1/6
Allen [15]	1/2	–

2.2.6 SFRC in tension

Concrete shows brittle behaviour and can only sustain small loads under tension. Use of steel fibers enhances the tensile resistance of concrete and improves its post-crack behaviour. **Figure 2.10** compares the tensile stress-strain behaviour of traditional concrete and fiber-reinforced concretes. In case of traditional concrete without any fibers (**Figure 2.10 a**), the stress-strain relationship rapidly reaches the peak and follows subsequent softening branch. When fibers are added to the matrix, the new composite material shows higher fracture toughness under uniaxial tension. When a fiber volume fraction of less than 1% is added to the concrete, although the peak tensile strength of SFRC does not differ significantly from that of plain concrete, the post-peak behaviour is enhanced. In this case, SFRC shows higher fracture toughness (area under the stress-strain diagram, see **Figure 2.10 b**). When a higher volume fraction is added to the matrix (V_f >1.5-2%), SFRC show post-crack tension-hardening behaviour, where the ultimate tensile strength is higher than that at first cracking (**Figure 2.10 c**). Such SFRC undergoes multiple cracking in the post-crack stage with $\varepsilon_c > \varepsilon_{c,cr}$ and $f_{ct} < \sigma_c < f_{max}$ (Fantilli et al., 2009). SFRC which exhibits this behaviour is referred to as high performance fiber reinforced concrete in the literature.

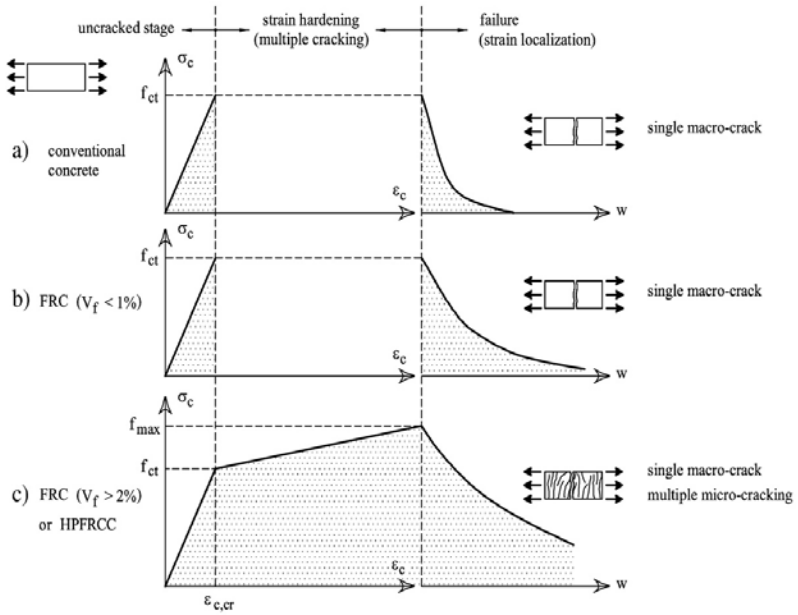

Figure 2.10 Tensile stress-strain behaviour of traditional and fiber reinforced concretes [Adapted from Fantilli et al., 2009]

2.2.6.1 Models for SFRC in tension

Over the years several authors have proposed models for the purpose of predicting the tensile stress-strain behaviour for SFRC. A relatively simple model is detailed in the *Dramix Design Guidelines* proposed by *Bakaert* (the company that provided the steel fibres used in this study). The uniaxial stress-strain curve is derived using forces and deflections determined from standard 4-point bending tests such as the ASTM C1609. The simplified model shown in **Figure** 2.11 is composed of straight ascending branch, followed by a sharp descending branch to 0.1% strain, followed by a third descending branch to 1.0% strain. In the model the maximum tensile stress of SFRC, $f_{fctm,ax}$ is correlated to the maximum compressive stress of SFRC as follows:

$$f_{fctm,ax} = 0.3{f'_{cuf}}^{2/3} \tag{2.9}$$

The stress corresponding to 0.1% and 1% strains respectively are then given by

$$0.37\, f_{fct,eq,300} \tag{2.10}$$

$$0.37 f_{fct,eq,150} \tag{2.11}$$

$$f_{fct,eq,300} = \frac{F_{m300} \times l}{bh^2} \tag{2.12}$$

$$f_{fct,eq,150} = \frac{F_{m150} \times l}{bh^2} \tag{2.13}$$

.

F_{m300} and F_{m150} represent the forces at deflections in mm of l/300 and l/150 where l , b and h refer to the length, width and height of the beam specimens used in the ASTM 4-point bending test, in mm.

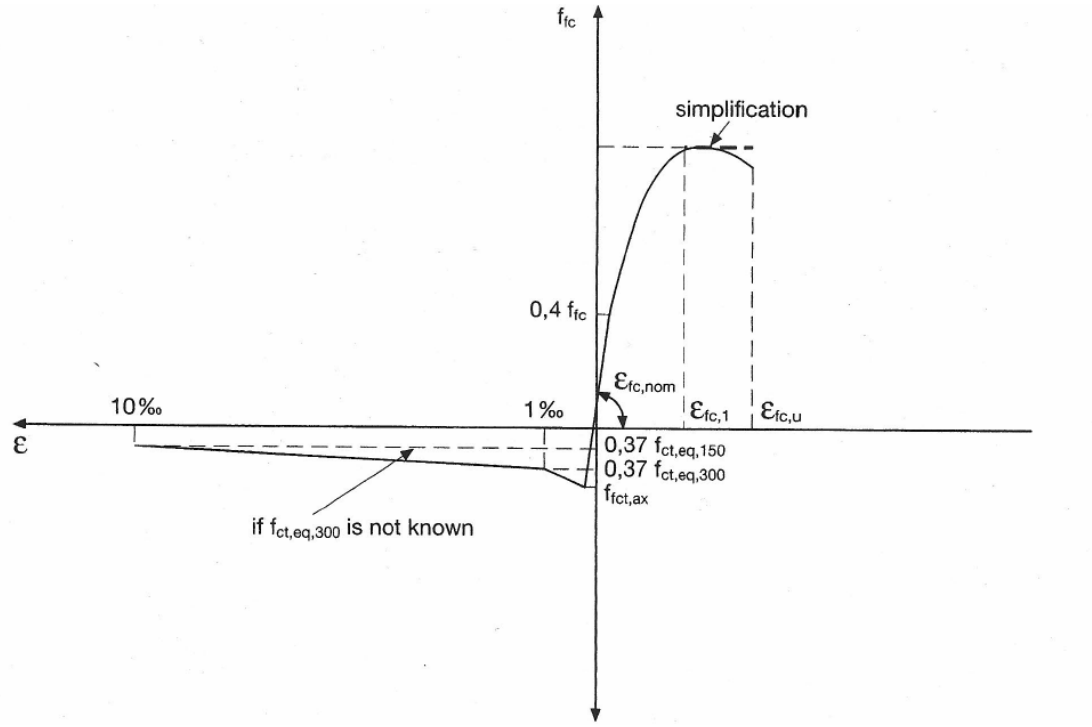

Figure 2.11 Idealized stress-strain curve for concrete reinforced with hooked-end fibres [Adapted from Nemegeer 1998]

Other models such as the one presented by Lok and Pei (1998) recognize that the SFRC in tension can show tension-hardening behaviour at higher fiber contents (see **Figure** 2.12)

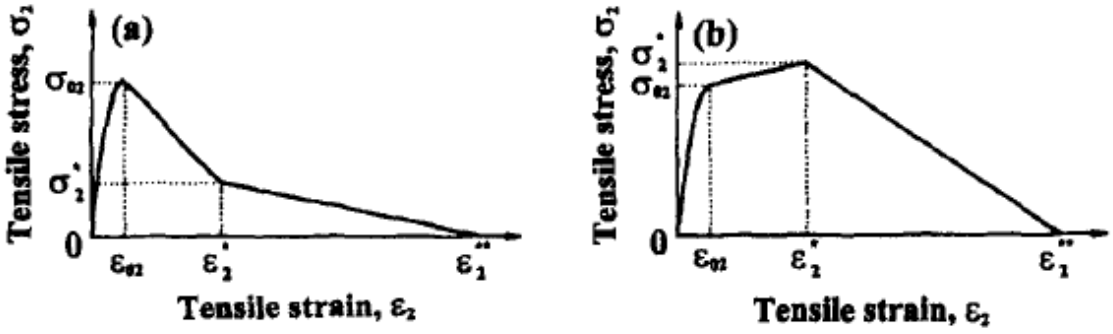

Figure 2.12 Tension softening and tension-hardening behaviour of SFRC in tension [Adapted from Lok and Pei 1998]

2.2.7 SFRC in compression

Several investigations have been conducted to determine the effect of Steel Fibers on the compression behaviour of SFRC (Maidl, 1995; King & Kutzing, 1999; Minelli, 2005; Dupont, 2003; Nataraja et al., 1999); these investigations have lead researchers to believe that addition of steel fibers does not significantly enhance the peak compressive strength of unconfined concrete.

Figure 2.13 shows that the compressive strength of SRFC is almost equal to that of plain concrete however the post-peak ductility increases significantly when steel fibers are used. It is thus assumed that while the presence of steel fibers does not affect the compression strength of concrete, steel fibers can significantly improve post-peak behaviour and this in turn results in improved toughness in compression. During uniaxial compression, lateral swelling of the specimen takes place resulting in combined shear and tensile stresses in the concrete. As the first cracks appear in concrete under compression, the effects of the tensile and shear stresses are better controlled by the improved lateral deformation action due to presence of steel fibers hence resulting in an improved toughness and ductility (Aoude, 2008).

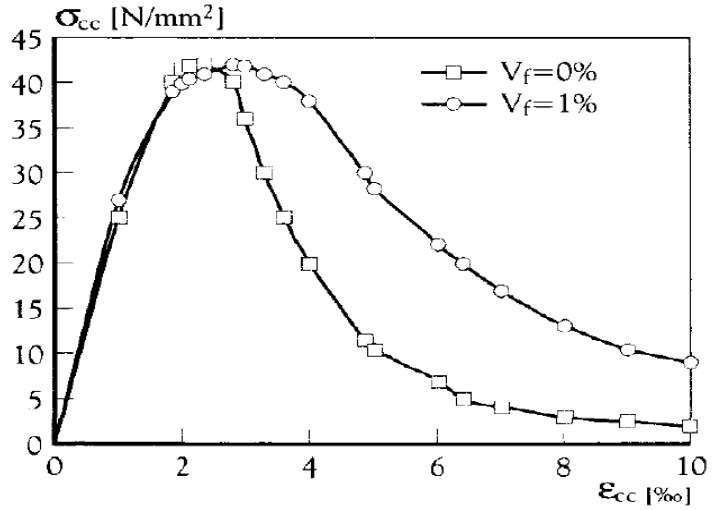

Figure 2.13 Typical behaviour of SFRC in compression
[Adapted from King & Kutzing, 1999]

Examples of stress-strain curves of SFRC in compression are shown in **Figure 2.14** and **Figure 2.15** which illustrate the effect of fiber content and aspect ratio, on performance of SFRC. As shown in the figures, SFRC is characterized by improvements in the descending branch of the stress-strain behaviour in compression. It is shown that increasing fiber content results in a less steep post-peak branch. Similarly, the curves show the enhancement in post-peak ductility in the case of SFRC with fibers having higher aspect ratio.

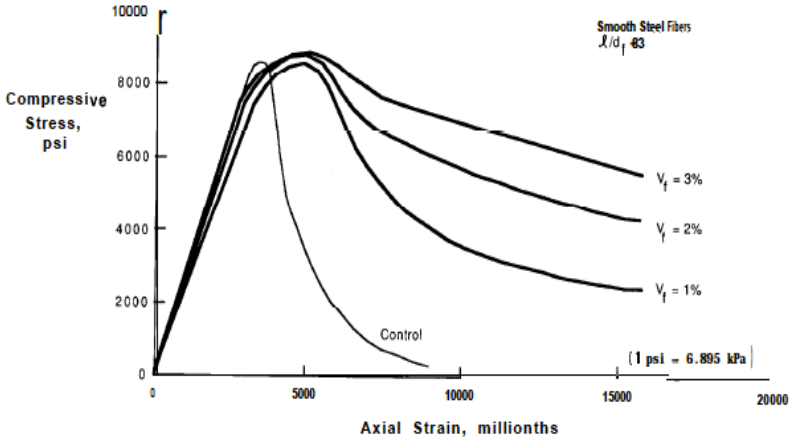

Figure 2.14 Influence of the volume fraction of fibers on the compressive stress-strain [Adapted from ACI 544, 2008]

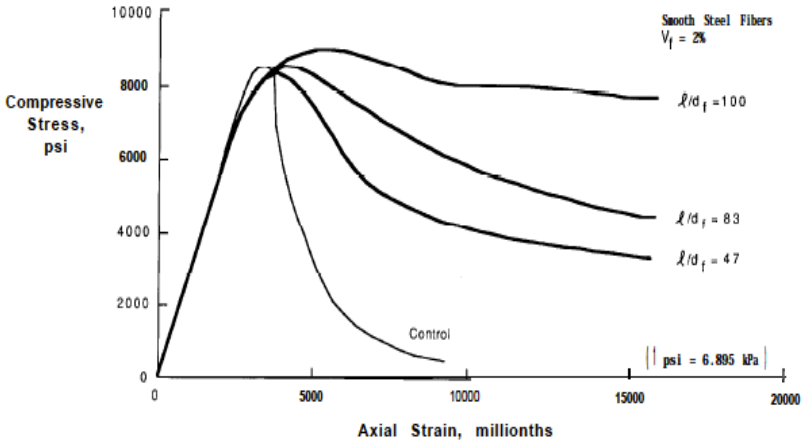

Figure 2.15 Influence of Aspect ratio of fibers on the compressive stress-strain [Adapted from ACI 544 (2008)]

2.2.8 Test methods for characterizing the post-cracking properties of SFRC

2.2.8.1 Direct tensile tests

Theoretically, direct tensile testing is the best method to evaluate the tensile strength, tensile strain capacity and post-cracking behaviour of SFRC as the test result directly reflects material behaviour in tension. However, in practice, it may be difficult to obtain reliable results using this test method. The necessary test setup is somewhat more complex due to the crack initiation behaviour of the specimen under testing. When the tensile strength of the concrete is reached, a crack initiates at one side of the specimen therefore creating bending moment if rotation is restricted (Van Mier, 1997). To avoid this problem, rotating plates can be installed which makes the test setup even more complex (see **Figure 2.16**).

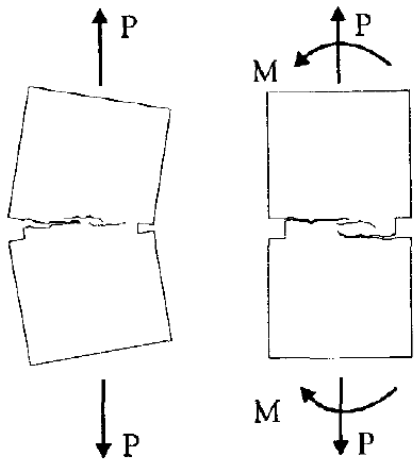

Figure 2.16 Effect of fixed and rotating loading plates in uniaxial tensile tests [Adapted from Van Mier, 1997]

More recently researchers have proposed using the "dog bone" test, in which long concrete specimens with bulked ends (resembling a dog bone) are tested under direct tension, to obtain direct tensile properties. **Figure 2.17** shows a typical dog bone test apparatus. As seen in this figure the ends of the specimen are restrained using steel grips and strain measurement is done by means of LVDTs installed at each side of the specimen. Despite the fact that this test allows for testing of specimens in direct tension, there are no standardized testing procedures for dog bone testing of SFRC and hence there may be inconsistencies in interpreting the obtained results from test to test. For example, Naaman & Reinhardt (2006) showed that different specimen sizes yield different stress-strain responses. **Figure 2.18**

shows the effect of specimen size on stress-strain properties for different fiber types. It can be seen that significant variations are observed when different sizes of specimens are tested under the same direct tensile loading. Hence Naaman & Reinhardt (2006) determined that it is important to specify the size of the specimens prior to testing in order to take into account size effects.

Figure 2.17 Dog-Bone testing apparatus and typical specimens
[Adapted from Liao et al. (2006)]

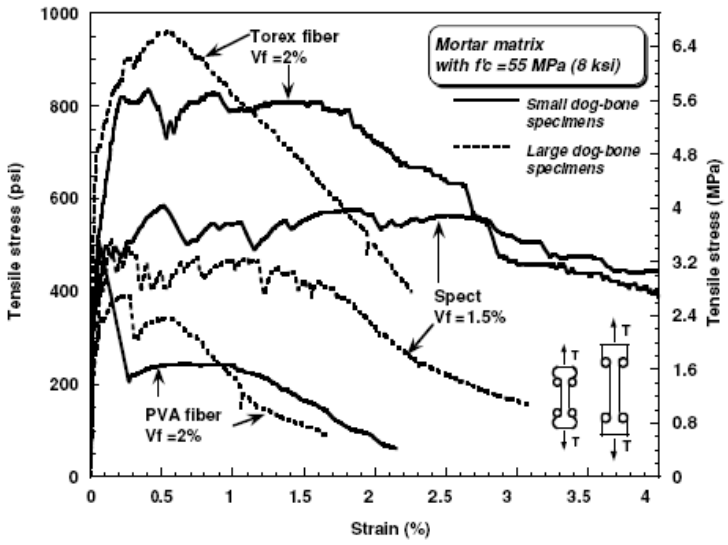

Figure 2.18 Size effect in stress-strain behaviour for different types of fibers
[Adapted from Naaman & Reinhardt (2006)]

2.2.8.2 Indirect tensile tests

Because of the challenges associated with direct tensile testing most standardized tests use more simple indirect tension testing methods to quantify the post-cracking properties of SFRC**.**

2.2.8.2.1 Flexural beam / toughness tests

The two best known and widely used types of tests to indirectly characterize the post-cracking properties of SFRC are the four-point and three-point bending tests (**Figure 2.19**). In a three point bending test (more commonly used in European standards) a notched beam is loaded with a single point load at the mid span, and the Crack Opening Displacement (COD) is measured at the notch giving a relationship between applied moment and crack width.

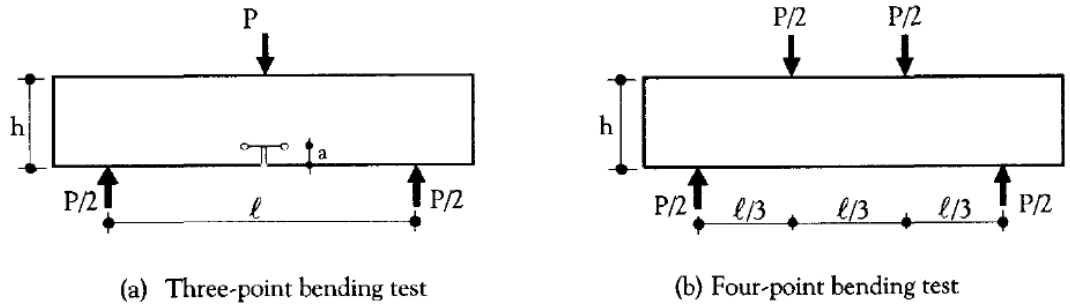

Figure 2.19 Typical behaviour of SFRC in compression
[Adapted from Kooiman, 2000]

In North America, the most commonly used standardized testing method involves testing flexural beams under four-point bending and measuring midspan deflection and applied load. To quantify the toughness of SFRC several toughness "indices" are computed. According to the ACI 318 building code (2008), the ASTM C1609 third-point bending test is considered the standard test to evaluate the flexural performance of SFRC. This test is relatively simple to perform and test results are reproducible in case of constant testing conditions. The predecessor to the ASTM C1609 method was the ASTM C1018 method. Interpretation of results using the ASTM C1018 method was difficult due to the ambiguity involved in interpretation of results based on 'first crack deflection" (Banthia and Trottier, 1995). The ASTM C1609 (much like the JSCE SF-4 method) does not require identification and measurement of the first crack deflection in determining toughness and thus allows for more simple and reliable interpretation of test results. In the case of high-strength SFRC the

ASTM C1399 can be used. In this method the specimen is placed on a steel plate during initial loading; after first crack the plate is removed and the beam is reloaded and the residual strength is recorded. Two load-deflection curves are obtained using this method for a typical specimen, one for the initial loading up to cracking with the steel plate in place and one for the residual strength during reloading as seen. **Figure 2.20** compares the ASTM C1018, C1399 and JSCE SF-4 methods**.**

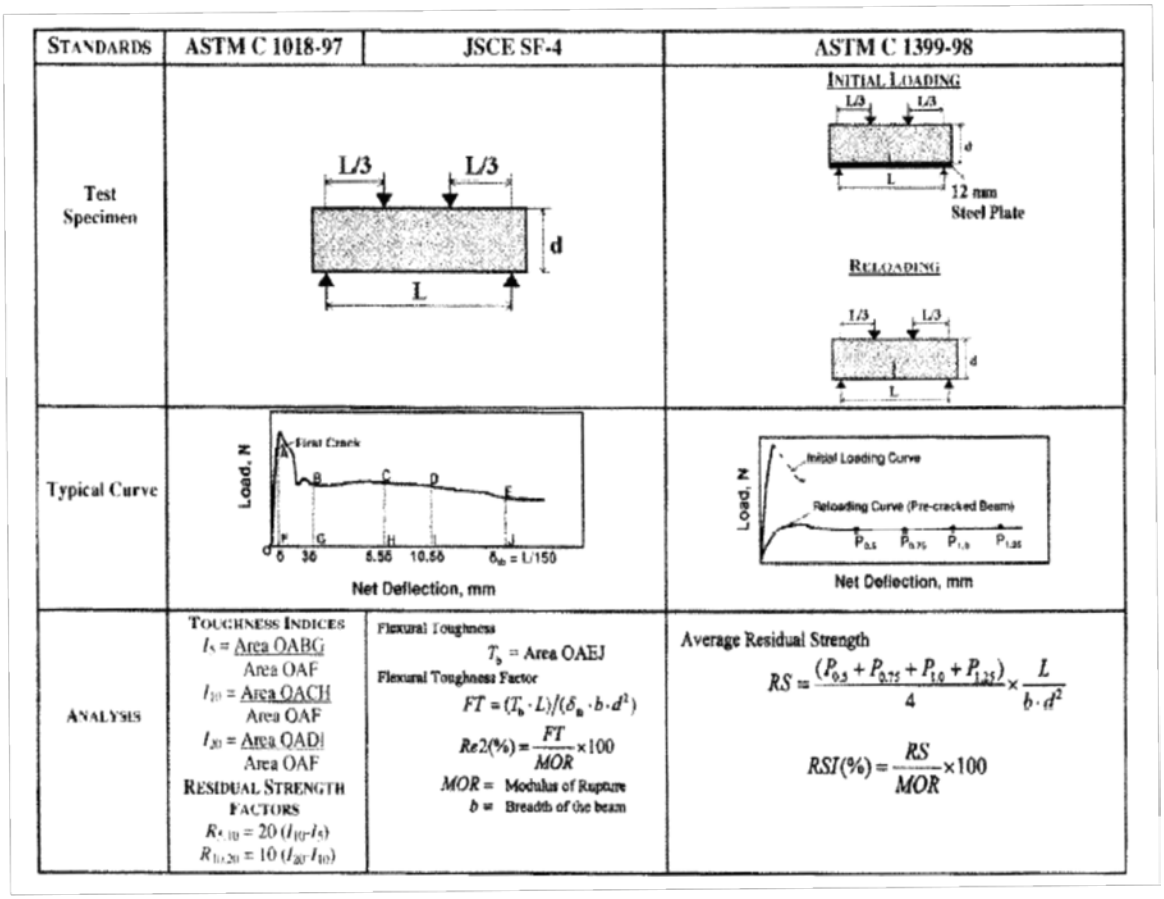

Figure 2.20 A schematic comparison between different toughness test methods [Adapted from Banthia and Mindess, 2004]

2.2.8.2.2 Round panel test

In this test a plate specimen with a diameter of 800mm and thickness of 75mm is placed on three pivots which are equally spaced along the perimeter and is loaded with a concentrated compressive force at the centre of the specimen until failure. Similar to tests discussed previously, a load deflection curve is plotted using the obtained data which is related to the tensile behaviour of the SFRC specimen. This test was standardized by ASTM committee C09 in ASTM C1550 ("Standard Test Method for Flexural Toughness of Fiber-Reinforced Concrete (Using Centrally Loaded Round Panel)"). Advantages of this test method include its relative simplicity, standardized testing equipment and procedure and the reliability of results obtained using the method. However, the large size of the standardized specimens (800mm diameter) and the need to use specialized testing equipment are disadvantages. Typical round panel test equipment can be seen in **Figure 2.21**.

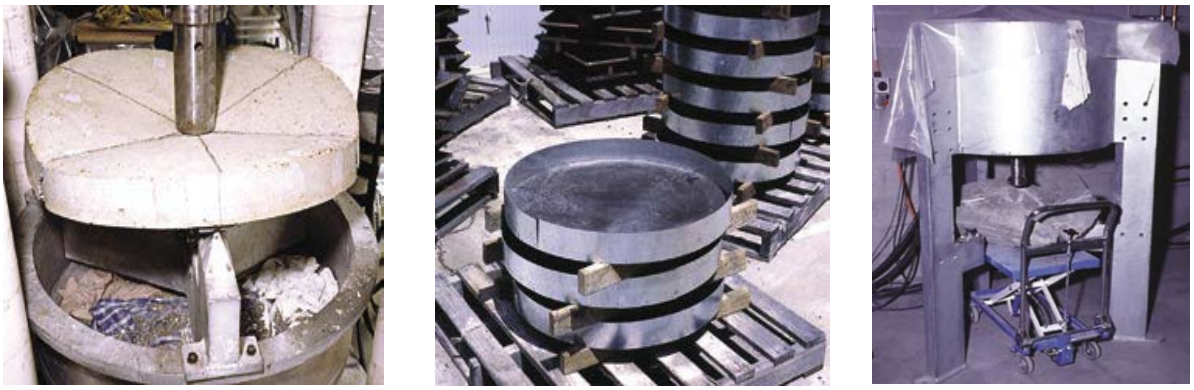

a) Round panel test specimen b) Round panel forms c) Round panel test rig with tested specimen

Figure 2.21 The round panel equipment
[Adapted from Bernard (2003)]

2.3 Self Consolidating Fiber Reinforced Concrete (SCFRC)

2.3.1 Self Consolidating Concrete (SCC)

Self-consolidating concrete, (SCC) is a highly flowable concrete which was developed in Japan in the 1980s to improve the constructability of reinforced concrete structures (Ozyildirim and Lane, 2003). Since no major mechanical vibration is needed when placing this concrete, significant savings in labour costs and construction time can be achieved. Further advantages include noise reduction during construction and a reduction of surface defects leading to a more appealing architectural finish (Gurjar, 2004). The flowable characteristics of SCC are obtained by reducing the coarse aggregate size and volume fraction, increasing the fines content, and by using chemical and mineral admixtures. Chemical admixtures commonly used in SCC include superplasticizers (SP) and viscosity modifying admixtures (VMA), while mineral admixtures include fly ash (FA), silica fume (SF) or micro-silica particles (Khayat et al. 1999; Nowak et al. 2005).

There are three key aspects of workability which should be carefully controlled in order to achieve optimum performance of SCC. Ouchi et al. (2003) classifies these workability aspects into filling ability, resistance to segregation and passing ability. As the name reflects, filling ability refers to a fluid state at which SCC can flow, maintaining homogeneity while undergoing deformations necessary to fill the formwork and voids around the reinforcing steel and achieve consolidation without vibration. Segregation resistance is defined as the ability of particle suspension to maintain a cohesive state throughout the mixing, transportation and casting processes without bleeding or settlement of aggregates. Passing ability refers to the ability of the mix to pass through closely spaced reinforcement or enter narrow sections in formwork and flow around other obstacle without blocking.

To ensure adequate performance, SCC must be tested in the fresh-state for its flowability and its ability to compact under its own weight and pass through reinforcement without blocking. Standard test methods are thus used to measure the filling ability, passing ability and segregation resistance of SCC. These tests include the slump-flow test, J-ring test, and L-box test.

The most commonly used test method is the slump-flow test which provides information on filling ability and passing ability. As depicted in **Figure 2.22,** the testing apparatus consists of a standard Abram's cone, a non-absorbent rigid plate. The procedure involves filling the slump cone with SCC and then allowing the SCC to flow onto the plate and measuring the spread of the SCC in millimetres (sometimes a circle is marked at the centre in order to measure the time for the SCC to reach a 500 mm diameter (referred to as T_{500}(T_{20})).

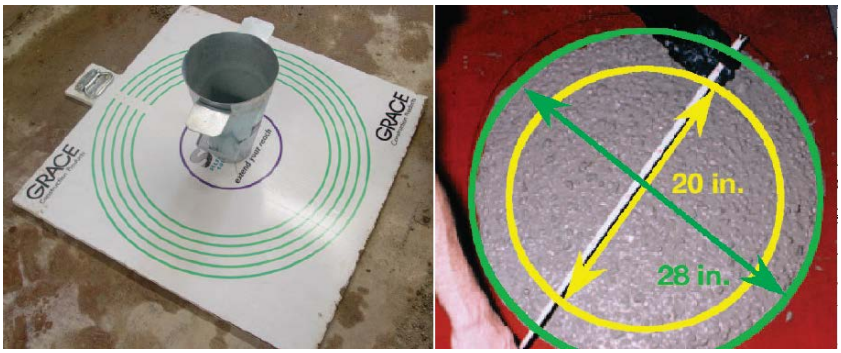

Figure 2.22 Slump flow test apparatus

[Grace Construction, http://www.graceconstruction.com, September, 2012]

The J-Ring test (ASTM C1621) is another fluidity test to measure the passing ability of SCC. The equipment is similar to the slump-flow test with the difference being the 25 mm thick rigid ring supported on sixteen mm diameter rods that are equally spaced along the perimeter of a circle (see **Figure 2.23**).

Figure 2.23 J-Ring test apparatus

[Grace Construction, http://www.graceconstruction.com, September, 2012]

The L-Box test measures the filling and passing abilities of SCC. As seen in **Figure 2.24,** the L-Box test apparatus consists of an L-shaped box which has a component for feeding the SCC that passes through a set of reinforcing bars placed to restrict the flow of concrete into the horizontal portion of the box. The filling ability is described by the ratio of the concrete height at the end of the horizontal section to the height at the beginning of the horizontal section behind the reinforcing bars.

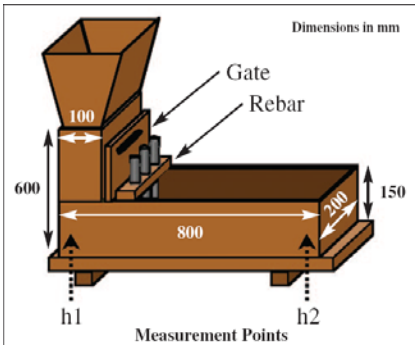

Figure 2.24 L-Box test apparatus

[Grace Construction, http://www.graceconstruction.com, September, 2012]

2.3.2 Self Consolidating Fiber Reinforced Concrete (SCFRC)

Self-Consolidating Fiber Reinforced Concrete (SCFRC) combines the excellent workability of SCC with the mechanical characteristics of fiber reinforced concrete. SCFRC can thus be defined as a highly flowable concrete while benefitting from the cracking resistance properties of fiber reinforced concrete. Liao et al. (2006) also presents a good literature review of SCFRC mix designs proposed by other researchers.

The properties of SCFRC, apart from being influenced by the properties of the SCC mix itself, depend on the type (shape and size) of the fibers added to the mix (for example fibers having longer length or high aspect ratio reduce the workability of SCFRC). Moreover, the volume fraction of fibers in the matrix has a significant impact on the properties of SCFRC in both the fresh-state and hardened-state. As discussed previously fiber contents of 1.5-2% are typically required to achieve tensile strain-hardening behaviour; the enhanced

workability of SCC can thus be utilized to achieve the performance associated with high performance fiber reinforced concretes (HPFRC). It should however also be noted that even in the case of SCFRC, there are limitations on the quantity of fibers that can be added before unfavorably affecting fresh-state properties. According to a study by Grunewald (2004) fiber contents should not exceed 2% to maintain adequate workability in SCFRC.

2.4 Previous research on shear behaviour of SFRC beams

The first research on behaviour of SFRC beams was conducted by Batson et al. in 1972 to investigate the shear capacity of SFRC beams. In his research, several specimens with different steel fiber types and contents were tested in order to demonstrate improvements in shear capacity of beams with use of steel fibers. It was observed that steel fibers could enhance the shear strength of concrete and control cracking through enhanced resistance of concrete in diagonal tension. In addition, if added in sufficient quantity, SFRC was shown to be able to improve flexural strength and ductility of the test specimens. Since Batson's research in 1972, several other research studies have been conducted on the behaviour of steel fiber reinforced concrete beams some of which will be discussed in the following sections.

As an example Colajanni et al. (2008) studied the behaviour of simply supported rectangular beams constructed with high strength concrete and reinforced with hooked end steel fibers. Test specimens consisted of SFRC beams with fibers contents ranging from 0.0% to 1.0%; several series with or without transverse reinforcement were tested. All of the beams that were tested were rectangular in cross-section with width of 150mm and depth of 250mm. The flexural reinforcement (2-20M rebars) were designed to obtain a shear failure for members without transverse reinforcement with 2-10M reinforcement bars used at the top when transverse reinforcement was present. The beams were tested under four-point loading and had a shear-span to depth ratio, a/d, of 1.0 to 3.5. It was observed that beams with 1.0% steel fiber content exhibited enhanced load and deflection capacities as depicted in **Figure 2.25**. It was observed that beams reinforced with steel fibers and without transverse reinforcement failed in shear whereas SFRC specimens with transverse reinforcement were able to reach their full capacity and fail in flexure.

It should however be noted that several other researchers have demonstrated that if added in sufficient quantity, the improved diagonal tension capacity of concrete can be sufficient to transform the brittle failure mode, typical of beams without web reinforcement, into a ductile flexural mode of failure that is typical of beams with adequate shear reinforcement (see **Figure 2.26**).

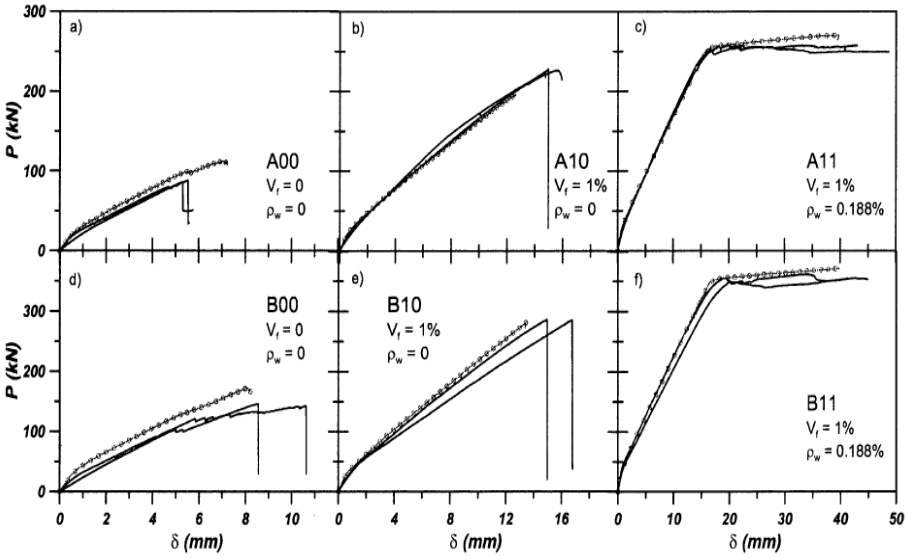

Figure 2.25 Numerical and experimental load-deflection curves for tested specimens [Adapted from Colajanni et al, 2008]

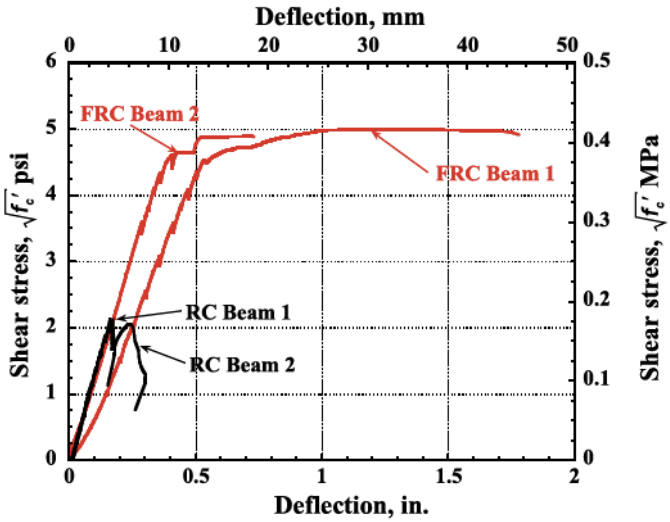

Figure 2.26 Ability of SFRC to transform brittle failure in beams without web reinforcement [Adapted from Parra-Montesinos, 2006]

As noted, there is extensive research available in the literature on the shear behavior of SFRC beams. Parra-Montesinos (2006) investigated a large test database of beams tested by other researchers which included 147 SFRC and 45 companion RC beams. The test data included beams having a wide range of properties in terms of shear span-to-depth ratio, longitudinal reinforcement ratio, steel fiber content, and steel fiber type. Analysis of the database indicated that specimens with fiber contents(v_f) greater or equal to 0.5% failed at applied shear forces corresponding to a shear stress not less than $0.17\sqrt{f_c'}$, which corresponds to the concrete contribution to shear resistance, v_c as defined in the ACI-318 code (2008) (the ACI code requires use of minimum shear reinforcement in beams subjected to shear forces in the range $0.5V_c$ -V_c). Furthermore, the results indicated that specimens with fiber contents greater or equal to 0.75% failed at applied shear forces corresponding to a shear stress not less than $0.3\sqrt{f_c'}$ (see **Figure 2.27**).

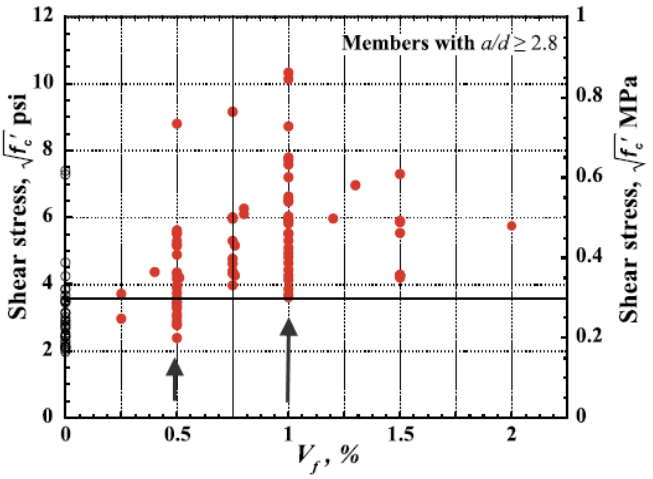

Figure 2.27 Effect of 0.5% and 0.75% fiber content on lower limit of shear stress [Adapted from Parra-Montesinos, 2004]

Based on this research study the 2008 edition of the ACI 318 code permitted for the first time the use of SFRC to replace minimum shear reinforcement in RC beams as long as a minimum requirements related to beam properties, fiber properties and SFRC post-cracking properties were met.

2.5 Previous research on reverse-cyclic behaviour of RC beams

2.5.1 Fenwick and Fong. (1979)

Fenwick et al. (1979) tested five reinforced concrete beams specimens in order to examine the behaviour of concrete beams forming plastic hinges under cyclic load reversals. In particular, the experimental investigated the influence of shear stress level on the performance of the beams. The shear in beams was varied systematically by changing the shear span to depth ratio (a/d) while the flexural reinforcement details were kept the same for all specimens except one which had unequal areas of flexural steel at the top and bottom. Each specimen consisted of two cantilever beams attached to a central rigid concrete block simulating a stiff column. The central block was fixed to a strong floor and the beams were loaded by means of two 300KN capacity hydraulic jacks placed at the top and bottom of the beams at the loading points. Initially the beams were loaded to three quarters of the theoretical flexural yield capacity in each direction for two complete cycles, after which displacements were applied to the beams in both directions for two complete cycles at displacement ductility ratios of 2, 4, 6 and 8 corresponding to 12, 24, 36 and 48mm deflections at a reference point of approximately 1100mm from the face of the centre block (see **Figure 2.28**).

Elastic and inelastic cyclic behaviour of beams including energy dissipation characteristics of the beams were investigated (see **Figure 2.29**). Test results showed that the level of shear stress in plastic hinge zones under reversed loading conditions has a significant effect on beam response. The experimental results demonstrated that as the shear stress level increases the performance of the beam is undermined. Gradual decrease in performance was observed as the shear stress increased from $0.16\sqrt{f_c'}$ to $0.29\sqrt{f_c'}$ but significant decrease was observed from this level of shear stress to $0.41\sqrt{f_c'}$. Based in this observation, the authors suggested a boundary value of $0.29\sqrt{f_c'}$ to ensure adequate performance under load reversals. The beam with unequal areas of flexural steel did not exhibit as good performance as was expected. Also, elongation of the test specimens were observed during testing which could have important implications on performance of frame structures under seismic loadings.

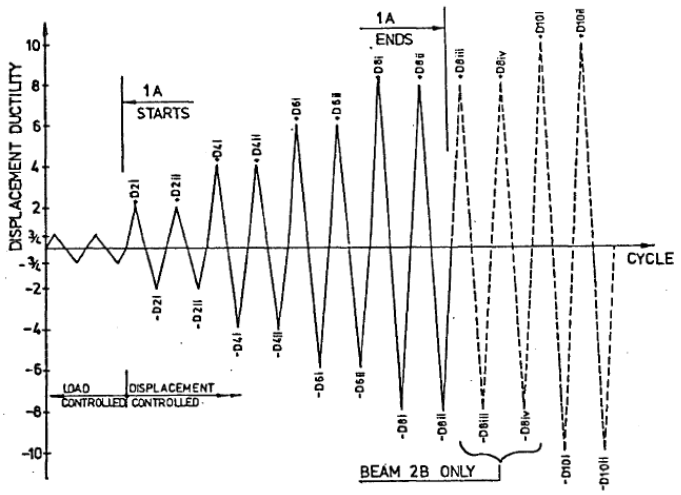

Figure 2.28 Loading Sequence

[Adapted from Fenwick and Fong., 1979]

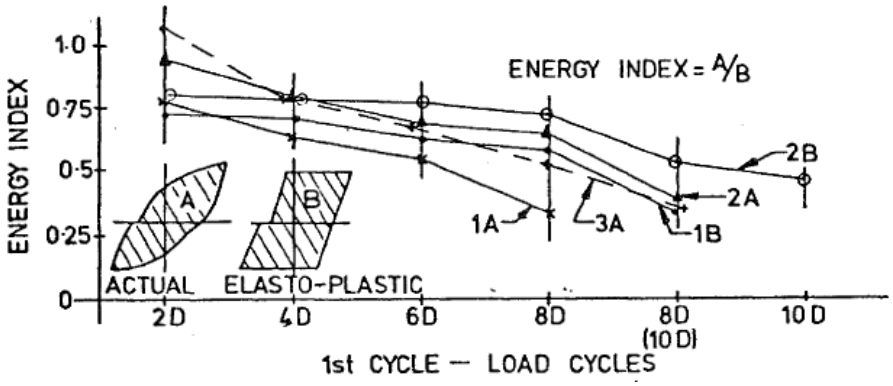

Figure 2.29 Variation of Energy index with load cycle

[Adapted from Fenwick and Fong., 1979]

2.5.2 Marefat et al. (2008)

In this study, the reversed cyclic behaviour of concrete beams reinforced with smooth and deformed steel longitudinal reinforcement was experimentally investigated. The focus of this study was on determining the contributions of varying rebar types on anchorage slip and flexural deformations during loading. Seven beams were tested under reversed cyclic loading, 5 with smooth steel bars and 2 with deformed steel bars. The beams had cross-sectional dimensions and reinforcement details simulating under-reinforced beams in older buildings. The cross-sectional dimensions of the tested beams varied from 200mmx150mm to 300mmx150mm. Beams were placed in an upright position and were attached to the floor by means of a strong concrete foundation and were loaded laterally through hydraulic

actuators installed at the top section of the beams. Beams were loaded at 0.1, 0.5 and 1 ductility ratios up to ductility ratio (Δ/Δy) of 1.0 and then were loaded at ductility ratios with increments of 1.0 as seen in **Figure 2.30**. Loading was repeated (cycled) three times in each ductility ratio stage.

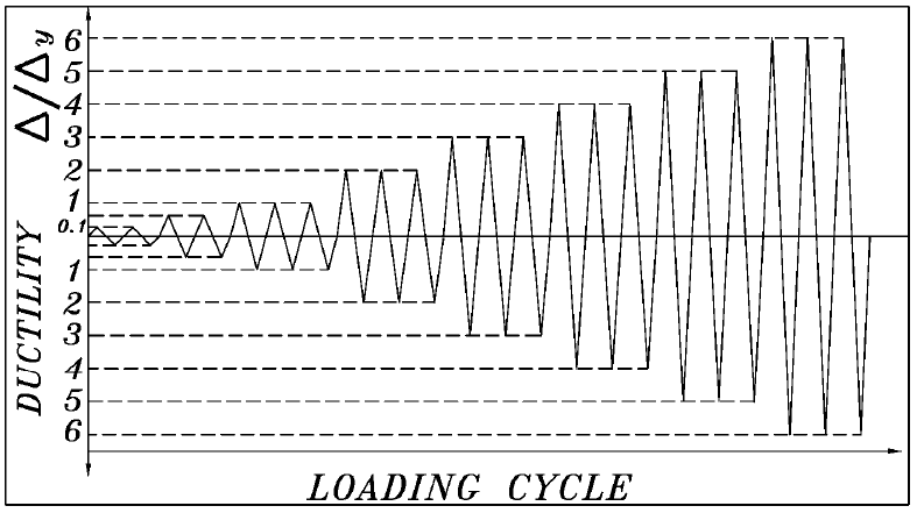

Figure 2.30 Lateral Loading Pattern
[Adapted from Marefat et al., 2008]

Horizontal and vertical displacements were measured by means of LVDT's installed at critical sections to measure the beam deflection due to lateral loads as well as the slip of reinforcing bars at the cracks. Several strain gauges were also installed on reinforcement reinforcing bars in order to measure strains during loading before yielding. Cracking patterns of the beams were examined during and after each test and were compared to other beams tested. Loads were recorded during testing and an experimental hysteresis model of the specimens were generated for each beam. The analysis in this study involved investigating the flexural strengths, drift and ductility capacities and yield strengths of the beams. **Table 2.7** shows ratio of effective stiffness and ductility for the tested specimens. Anchorage slip analyzes were also performed to determine the contributions of the anchorage slip and flexure in lateral deformations of the beams. **Figure 2.31** shows deformation contributions of flexure and anchorage slip for a typical specimen.

The specimens characterized by large cross-sections and small reinforcement ratios could not develop their full flexural strength and failed at about 65% of the nominal sectional strength. Large slip of longitudinal reinforcement was observed. it was concluded from the experimental results that the specimens reinforced by plain bars perform similar to standard specimens with deformed bars, in terms of elastic stiffness and lateral displacement ductility; however, they exhibit larger slip and smaller yield strength.

Table 2.7 Ratio of effective stiffness and ductilty for tested specimens
[Adapted from Marefat et al., 2008]

Type of bar	Specimen	Yield drift ratio (%)		Ultimate drift ratio (%)		Ductility ratio		Effective stiffness ratio
		Δ_y^{PULL}	Δ_y^{PUSH}	Δ_u^{PULL}	Δ_u^{PUSH}	μ^{PULL}	μ^{PUSH}	$EI_{(test)}/EI_{(gross)}$
Plain	PN-CS3	0.23	0.60	2.67	2.67	11.60	4.45	0.07
	PN-CS4	0.18	0.57	1.60	1.87	8.89	3.28	0.12
Plain	PC-M2	1.50	–	12.57	–	8.38	–	–
	PC-C2	1.06	1.27	12.70	12.70	11.98	10.00	0.22
	PN-C1	1.21	2.00	10.50	8.50	8.67	4.25	0.24
Deformed	DC-C2	2.30	1.84	11.50	12.80	5.00	6.96	0.26
	DN-C1	1.60	2.64	9.60	14.70	6.00	5.57	0.28

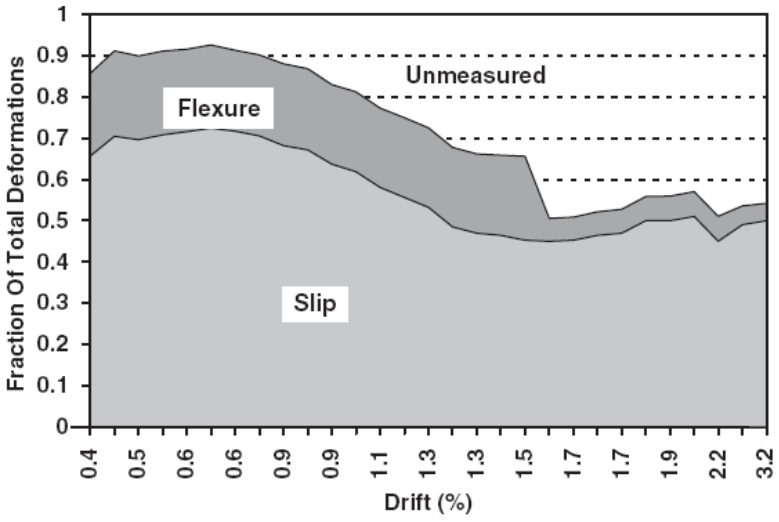

Figure 2.31 Contributionsof slip and flexure in lateral deformations of tested specimens
[Adapted form Marefat et al., 2008]

2.6 Previous research on cyclic behaviour of SFRC beams

2.6.1 Campione et al. (2008)

Campione et al. (2008) conducted an experimental study to evaluate the influence of steel fibers in combination with stirrups in beams tested under cyclic and reverse-cyclic loading. For the beams tested under cyclic loading, the study involved four beams, two of which were made of plain concrete with two spacings for the web reinforcement (198 mm and 98 mm), and two companion specimens with identical properties but reinforced with hooked-end steel fibers. The study demonstrated that the beams reinforced with steel fibers exhibited higher strength and ductility compared to the control specimens due to the bridging action of steel fibers across main and secondary cracks (Campione et al., 2008). **Figure 2.32** shows the behaviour of the control RC specimens, with the results showing a brittle shear failure in the beams with larger pitch (198 mm), while a more ductile flexural failure response was observed in the beams with 98 mm pitch. As seen in **Figure 2.33** the addition of different types of steel fibers in the same two beams results in significant improvement in load-deformation response, energy dissipation capacity and overall ductility in the case of hooked-end fibers in both beam configurations. In addition to the above, Campione et al. (2008) also tested RC beams and SFRC beams under reverse-cyclic loading. Although details on beam properties or testing procedure were not provided in the paper, **Figure 2.34** shows the reverse-cyclic response of a control RC beam with transverse reinforcement and no fibers and the same beam with 1% fiber. It is noted that the addition of steel fibers resulted in enhanced energy-dissipation capacity and post-peak ductility.

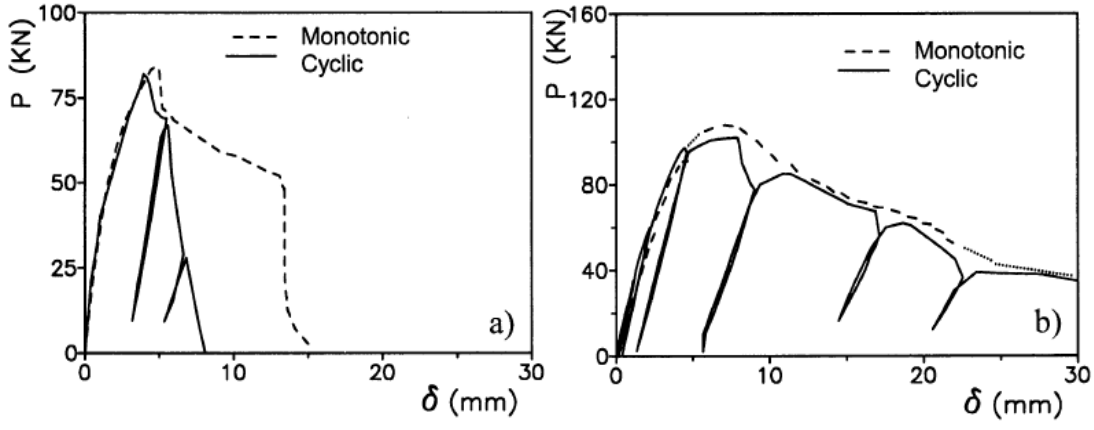

Figure 2.32 RC beams under monotonic/cyclic load: pitch= 198 mm vs. 98 mm [Adapted from Campione et al. (2008)]

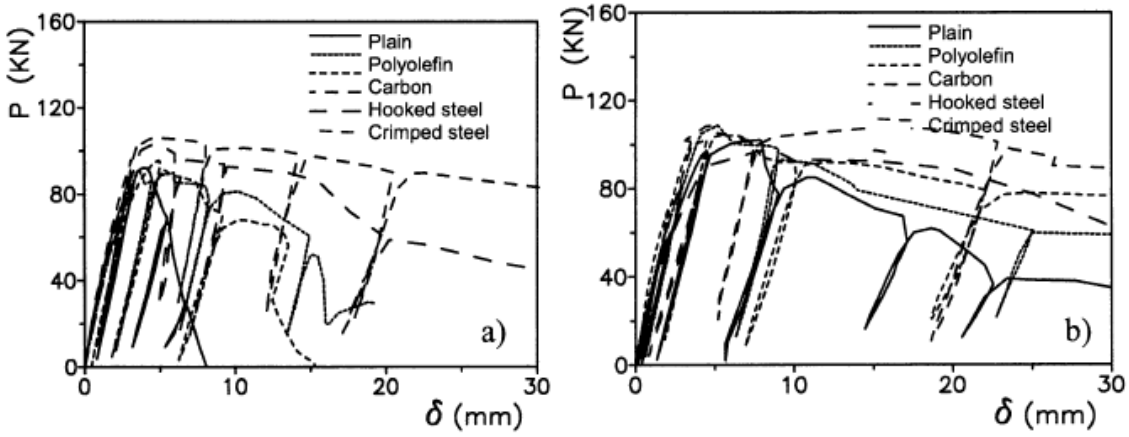

Figure 2.33 The influence of various types of steel fibers on cyclic loading response [Adapted from Campione et al. (2008)]

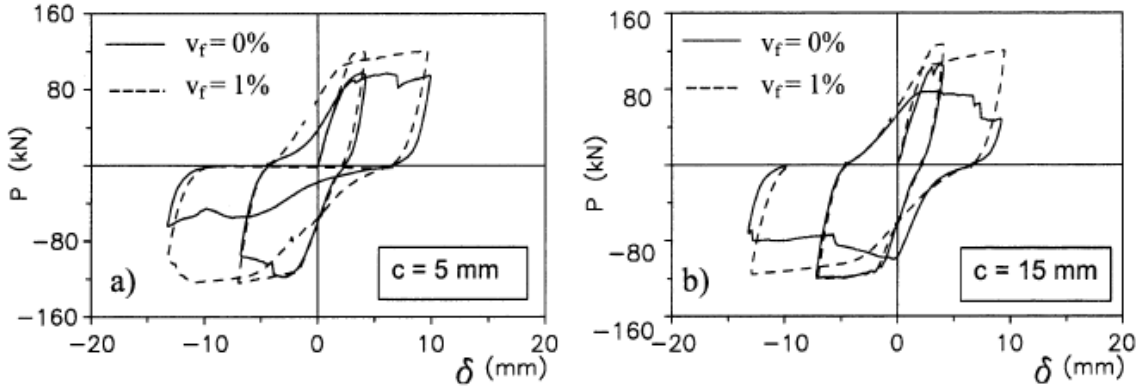

Figure 2.34 Reverse-cyclic response for members with and without fibers [Adapted from Campione et al. (2008)]

2.6.2 Chompreda and Parra-Montesinos (2005)

Chompreda and Parra-Montesinos (2005) investigated the behaviour of fiber reinforced cement composite (FRCC) flexural members under large displacement reversals. The experiments evaluated the displacement capacity and shear strength of members constructed with traditional reinforced concrete and companion specimens constructed with FRCC materials. The FRCC specimens were constructed with either ultrahigh weight polyethylene fibers or hooked-end steel fibers with fiber volume fractions ranging from 1.0% to 2.0%. Eight concrete beam specimens with different fiber contents were tested as part of this research under reversed cyclic loading. Each specimen consisted of two cantilever beams

with a shear span to depth ratio of 3.0 which connected through a stiff and strong middle block used for loading. The specimens were pin-supported at the ends and were loaded vertically at the middle block. **Figure 2.35** shows the schematic the beams tested in this experimental study. One control specimen with no fiber content, two fiber reinforced specimen with web reinforcement and 5 fiber reinforced specimens without web reinforcement were tested in reversed cyclic loading. LVDTs were used to measure the rotations in the plastic hinge area as well as vertical displacement of the middle block. A clinometer was also attached on the middle block to measure the rotation of the middle block which was used to correct the experimental drift values. Results from direct tensile tests conducted by the authors of this study indicated that the FRCC composites reinforced with 2.0% and 1.5% steel fibers exhibited strain hardening and strain softening effects respectively (see **Figure 2.36**).

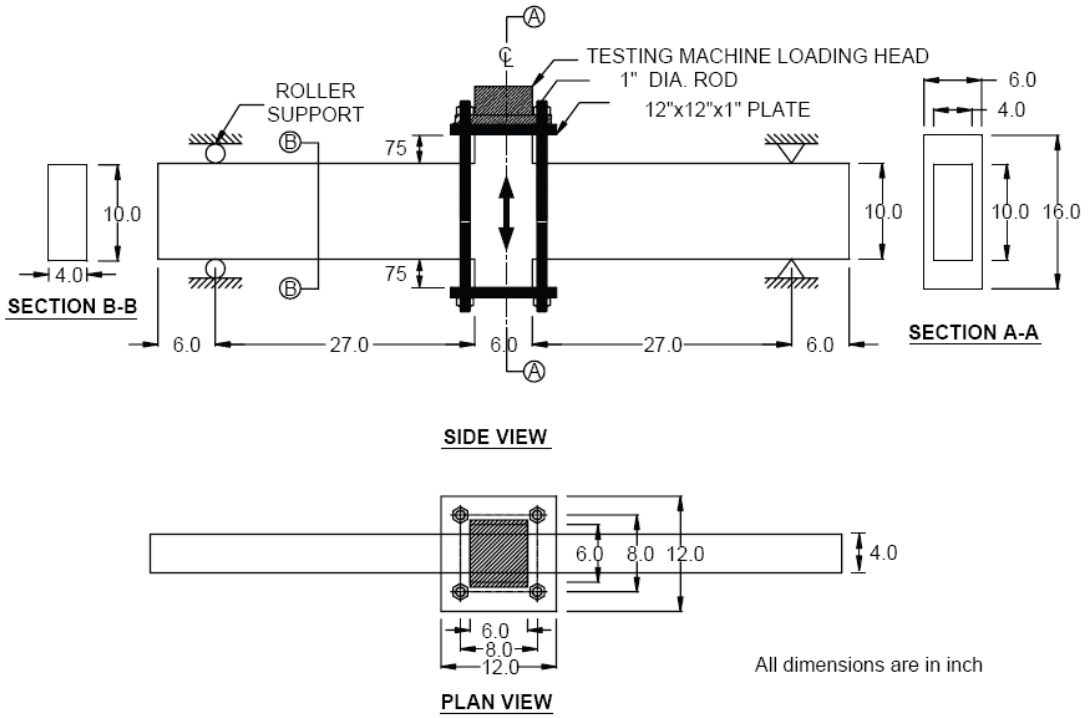

Figure 2.35 Beam specimen setup used in Chompreda & Parra-Montesinos (2005)
[Adapted from Chompreda & Parra-Montesinos, 2005]

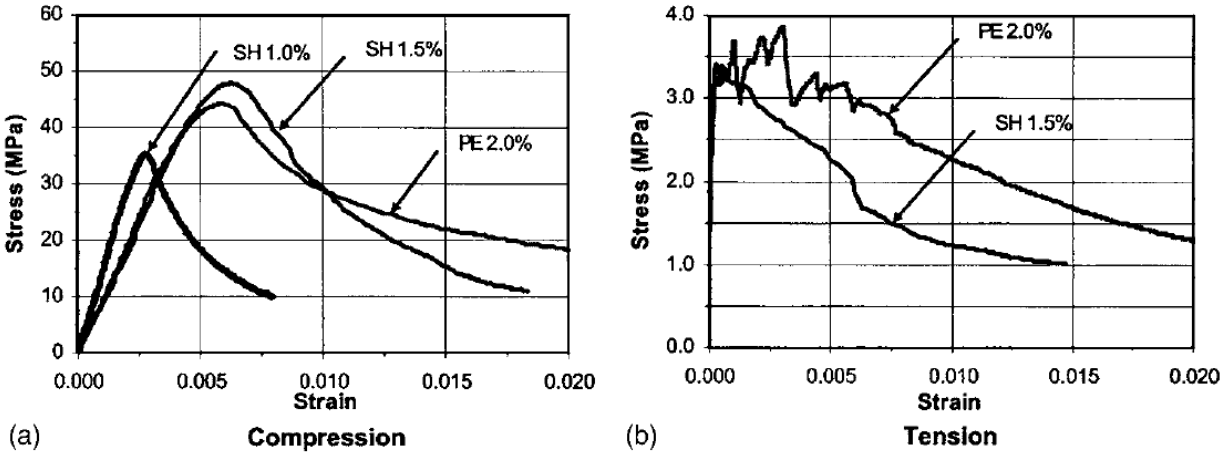

Figure 2.36 Typical Stress-Strain curves for FRCCs
[Adapted from Chompreda and Parra (2005)]

The study reported that peak shear stress demands in the test specimens without web reinforcement ranged from $0.21\sqrt{f_c'}$ to $0.40\sqrt{f_c'}$ [MPa] and was equal to $0.51\sqrt{f_c'}$ [MPa] for the specimen with web reinforcement. The authors of this study observed that all specimens constructed with strain-hardening FRCC, with or without web reinforcement, achieved drift capacities of at least 4.0%. Compared to the control beam, superior damage tolerance with multiple flexural and diagonal cracking was observed in the beam reinforced with steel fibers. In addition, buckling of longitudinal reinforcement in the strain-hardening FRCC members without web reinforcement was not observed up to plastic hinge rotations of 4.0%, whereas the beams with web reinforcement experienced no buckling. The results suggest that shear resistance, confinement, flexural ductility and control of longitudinal steel were improved with addition of fibers. Furthermore, the results indicated that specimens with fiber contents greater or equal to 0.75% failed at applied shear forces corresponding to a shear stress not less than $0.30\sqrt{f_c'}$ (see **Figure 2.37** and **Figure 2.38**). Based on the results the authors suggested that a shear stress level of $0.30\sqrt{f_c'}$ [MPa] can be considered as a lower bound for the shear resistance provided by strain-hardening FRCCs in beams subjected to load reversals.

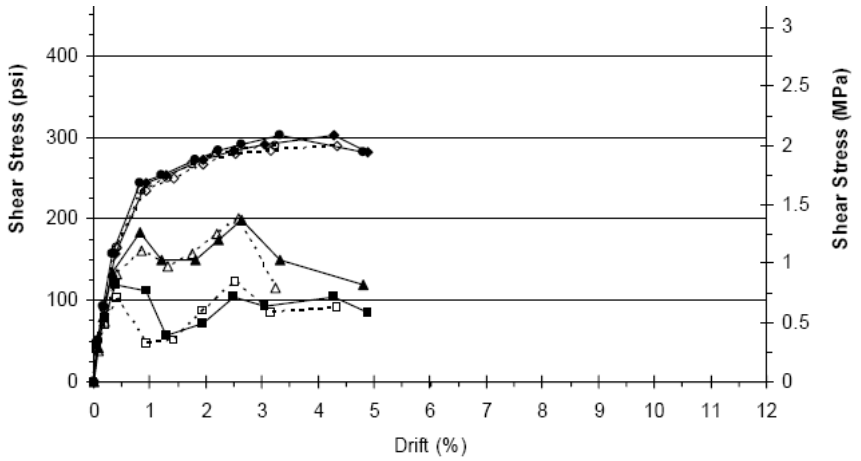

Figure 2.37 Concrete shear stress contribution for beams without web reinforcement

[Adapted from Chompreda & Parra-Montesinos, 2005]

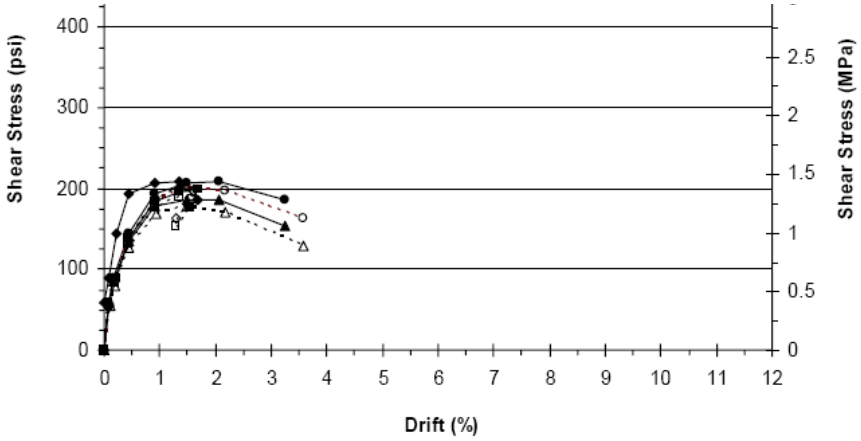

Figure 2.38 Concrete shear stress contribution for beams with web reinforcement and 1.0% steel fiber

[Adapted from Chompreda & Parra-Montesinos, 2005]

2.6.3 Hameed et al. (2009)

In this study six concrete beams, two of which were reinforced with Amorphous Metal Fibers (AMF) and two with hooked-end steel fibers, were tested in reversed cyclic loading in order to investigate the influence of addition of fibers on the behaviour of RC beams subjected to load reversals, and to study the effect of fiber properties on the beam performance. All beams were subjected to a concentrated load at the midspan of the beams while the ends of the beams were simply supported and restrained against vertical displacement. The tests were performed on beams of cross section 150 x 200 mm and a clear span of 1 m. Two steel bars of 6 mm diameter with characteristic yield strength of 500 MPa were used as conventional reinforcement on both faces satisfying the requirement of Eurocode-2 for minimum flexural reinforcement. Flexural failure of the beam was ensured by providing necessary shear reinforcement (bar of 6mm diameter provided at 100mm C/C). **Figure 2.39** shows the reinforcement details and loading setup that was used in this experimental program.

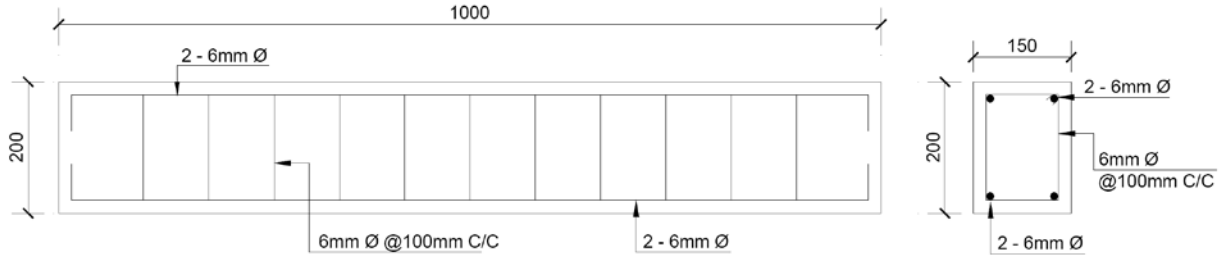

Figure 2.39 Reinforcement details of the beams specimens
[Adapted from Hameed et al., 2009]

It was observed that the addition of steel fibers reduced flexural crack widths at given deflection levels. Also, significant reduction in spalling and deterioration of concrete under load reversals was observed. **Figure 2.40** shows the envelope of the load-deflection curves for beams reinforced with AMF fibers and hooked-end steel fibers which demonstrates improvements in load carrying capacity with the addition of fibers (for both hooked-end steel fibers and AMF fiber typologies). It was shown that the energy dissipation capacity of the beams reinforced with 0.25% steel fibers increased by approximately 28%, and by 38% for the beam reinforced with 0.25% AMF fibers compared to the control beam (see **Figure 2.41**).

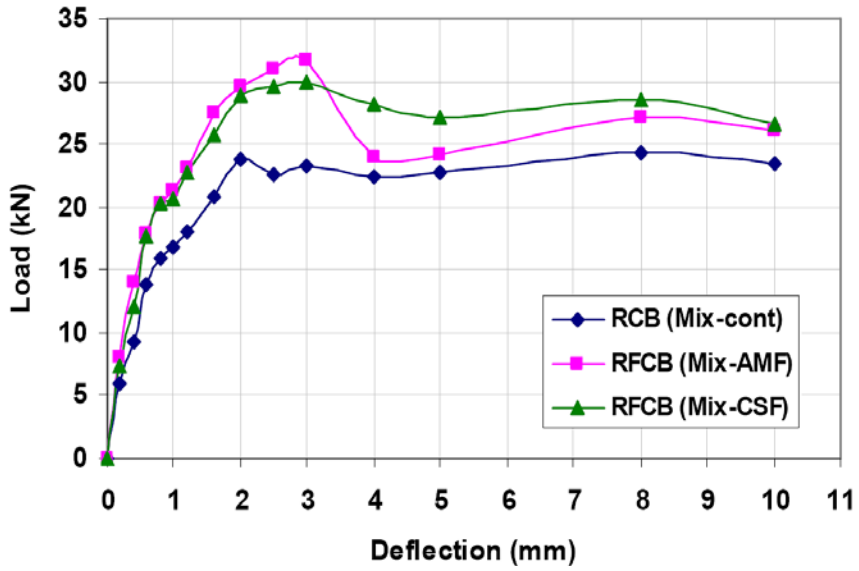

Figure 2.40 Experimental load-deflection envelope curves

[Adapted from Hameed et al., 2009]

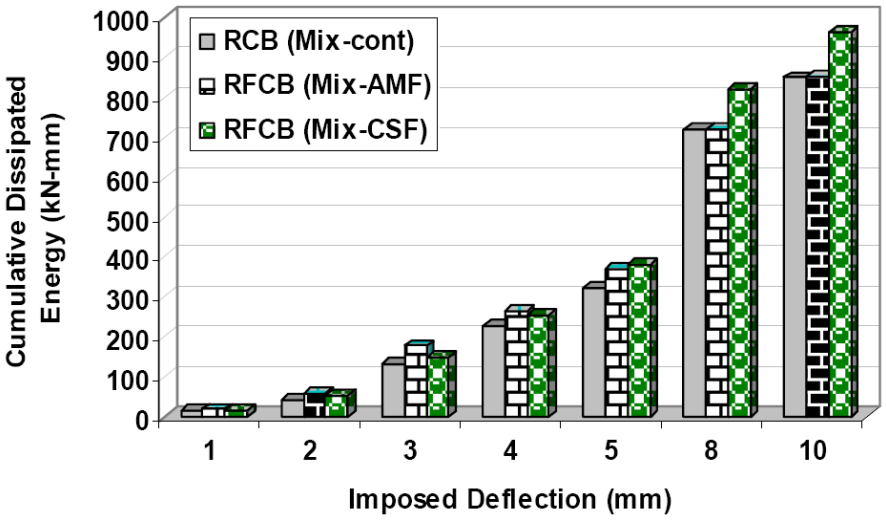

Figure 2.41 Experimental energy dissipation capacities

[Adapted from Hameed et al., 2009]

2.7 Previous research on SCFRC beams

2.7.1 Greenough and Nehdi (2008)

Greenough and Nehdi (2008), tested thirteen SCFRC beams constructed with various steel fiber types (hooked-end, flat-end and wavy), fiber contents (0.5%-1%), and shear span-to-depth ratios (3 and above). By addition of steel fibers, the amount of coarse aggregates used in the mix was reduced and additives were used to achieve the SCC slump flow diameter range of 635mm to 650mm. The results demonstrated that the use of steel fibers enhanced shear strength by up to 128% when compared to companion specimens constructed with plain reinforced concrete. The initial cracking load and ultimate strength of the beams also increased as a result of addition of steel fibers which resulted in higher ductility of the test specimens. It was also reported that the effectiveness of the improvements in shear strength was improved as fiber content increased. **Figure 2.42** shows the relative increase in shear strength of fiber reinforced SCC and regular FRC beams.

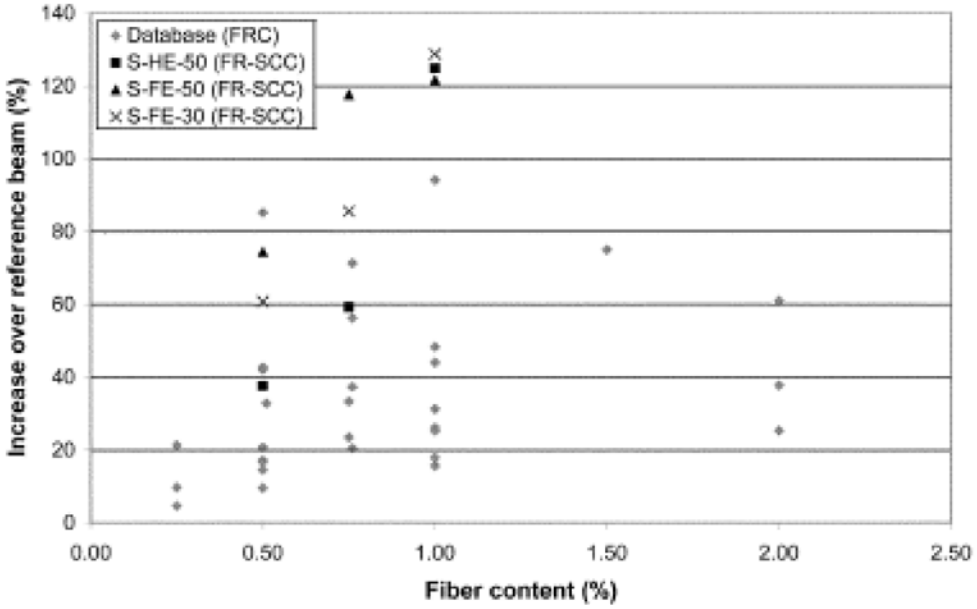

Figure 2.42 Relative increase in shear strength of SCFRC and FRC beams [Adapted from Greenough and Nehdi, 2008]

It was postulated by the authors that this relative increase in the shear strength of SCFRC beams compared to FRC beams is due to the denser microstructure of the matrix and also due to the SCC's ability in achieving better dispersion of fibers within the concrete matrix.

The authors also presented two empirical equations for predicting the shear strength of SCFRC beams and recommended modification to current ACI code provisions for prediction of shear capacity of slender FRC beams by explicitly considering the effect of random orientation of fibers.

2.7.2 Cohen (2012)

12 beams were constructed and tested under monotonic loading as part of this experimental program at the University of Ottawa. Two series of 6 beams each constructed with different longitudinal reinforcement ratios (2-20M and 2-15M bars) were reinforced with varying amounts and types of steel fibers. No transverse reinforcement was used in any of the beams. Normal strength and high strength hooked steel fibers at varying contents (0.75% to 1.5% by volume of concrete) were used in the test specimens. 10 beams out of twelve used normal strength hooked-end fibers whereas 2 beams were constructed with high strength hooked-end fibers. King MS self-consolidating concrete was used in eight of the tested specimens, while the last four beams were constructed using a customized concrete mix developed by the author.

In the first series of the testing program that involved testing beams with 2-15M longitudinal reinforcement steel and no transverse reinforcement, a brittle shear failure was observed in beams with no steel fibers. It was observed the addition of 0.5% steel fibers increased the shear capacity of the beam by 47% however a brittle shear failure was observed. At 1.0% steel fiber content, the brittle shear failure was transformed into a ductile flexural response with 63% increase in shear capacity (see **Figure 2.43**). The ultimate ductility ratio of the beams with 1.0% steel fiber content was approximately 5.5 times higher than that of the control specimen with no steel fibers. Similar behaviour was observed in beams with 1.5% steel fiber content with 28% increase in the ultimate midspan deflection prior to failure compared to that of the beam with 1.0% steel fiber content. Beams constructed with high strength steel fibers resulted in similar but more pronounced improvements in the shear capacity and ductility of the beams. It was also observed that the minimum amount of steel fibers to transform the brittle shear failure behaviour into a ductile manner decreased by 0.25% when high strength hooked-end steel fibers were used.

As seen in **Figure 2.43,** results obtained from the second series of the beams indicated that higher longitudinal reinforcement ratios results in inability of moderate steel fiber contents (1% and below) to transform the brittle shear failure to a ductile behaviour. This was claimed to be due incapability of steel fibers to compensate for the required capacity to alter sudden failure of beams in shear into a ductile response. Beams constructed with the customized concrete mix showed significant increase in shear capacity and exhibited flexural failure pattern when 1.5% steel fibers were used. Beams with 0.0% to 1.0% steel fibers in this group failed in shear.

It was concluded that use of steel fibers in shear dominant beams significantly increases shear capacity of beams, enhances post-peak ductility of the beams and have the potential to replace transverse reinforcement requirements. An analytical model was also proposed for predicting shear capacity of SFRC beams as part of the analytical study conducted in this experimental program.

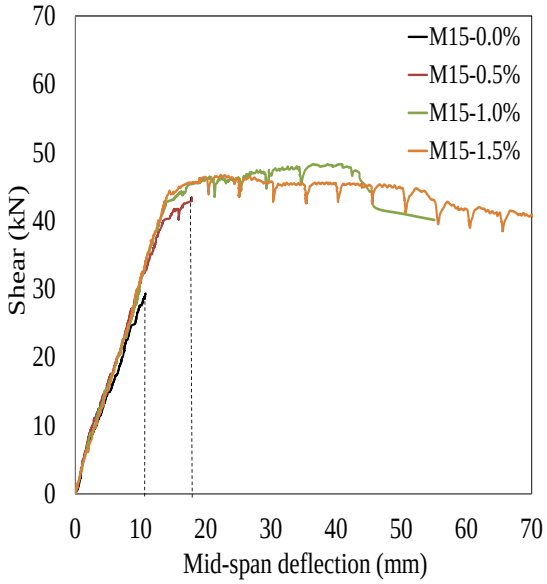

Figure 2.43 Experimental results from the test series of Cohen (2012)
[Adapted from Cohen, 2012]

2.7.3 Alfarra (2012)

This experimental program involved testing of six steel fiber reinforced concrete beams under cyclic loading at the University of Ottawa. Five of the beams were constructed with two 15M longitudinal reinforcing bars as flexural reinforcement and no transverse reinforcement with steel fiber contents varying from 0.0% to 1.5%. The tested beams were 125mm x 250mm in cross-section and had a shear span to depth ratio, a/d of 3.8. The control specimen had no steel fibers and was reinforced with transverse shear reinforcement at 100mm spacing. Two 10M bars were used at the top as support to the steel hoops. All beams were constructed using King MS self-consolidating concrete.

Figure 2.44 depicts the maximum shear force-displacement curves for each tested specimen. The control specimen constructed with the minimum transverse reinforcement required by CSA A23.3 was able to reach its full flexural capacity and showed gradual strength decay until failure at ductility ratio, $\frac{\Delta_u}{\Delta_y} = 4$. It was observed that below 0.75% steel fiber content, despite an increase in the flexural capacity, failure occurs in a brittle shear mode at ductility ratio of approximately 1.5. Beams with steel fiber contents of 0.75% and higher exhibited a flexural failure despite having no transverse reinforcement. Ductility ratios of 4 to 7 were achieved in beams reinforced with 0.75% to 1.5% steel fibers respectively. Addition of steel fibers also increased the peak loads by up to 28% for the beam with 1.5% steel fiber content compared to the control specimen. It was also observed that at steel fiber content, Vf $\geq$ 1%, maximum deflections increase significantly compared to beams with less than 1.0% steel fibers. **Figure 2.45** shows a comparison between the response envelopes for beams reinforced with 0.75% regular strength and high strength hooked-end steel fibers. As it can be seen in this figure, addition of high strength steel fibers increase peak load and higher loads in the post-peak region resulting in a flatter descending branch. Both beams were able to attain their full flexural strengths and failed in a ductile flexural manner.

It is noted that the test programs of Alfarra (2012) and Cohen (2012) used the same concrete and fiber types used in the experimental program presented in this thesis.

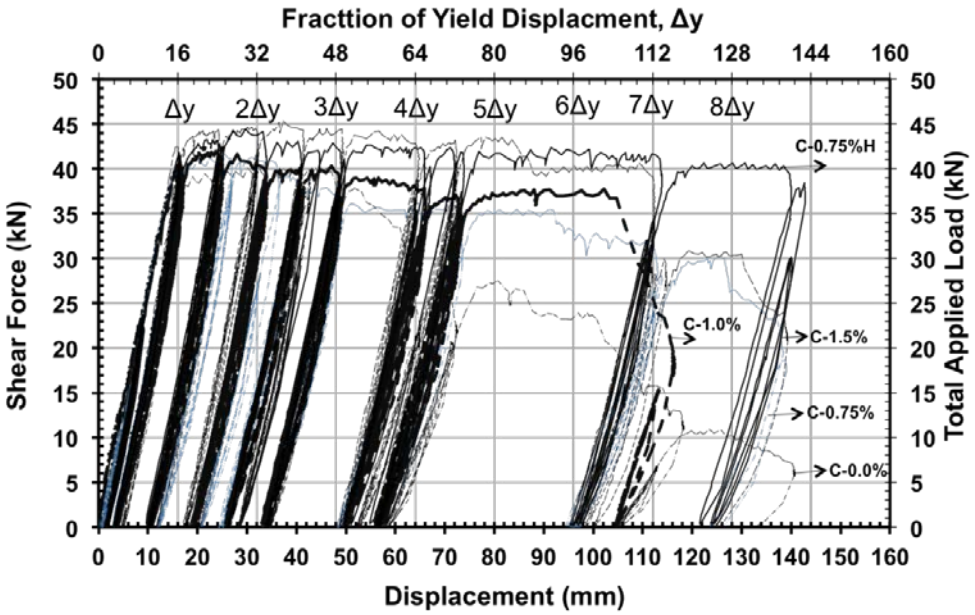

Figure 2.44 Comparison of cyclic response for all tested specimens [Adapted from Alfarra, 2012]

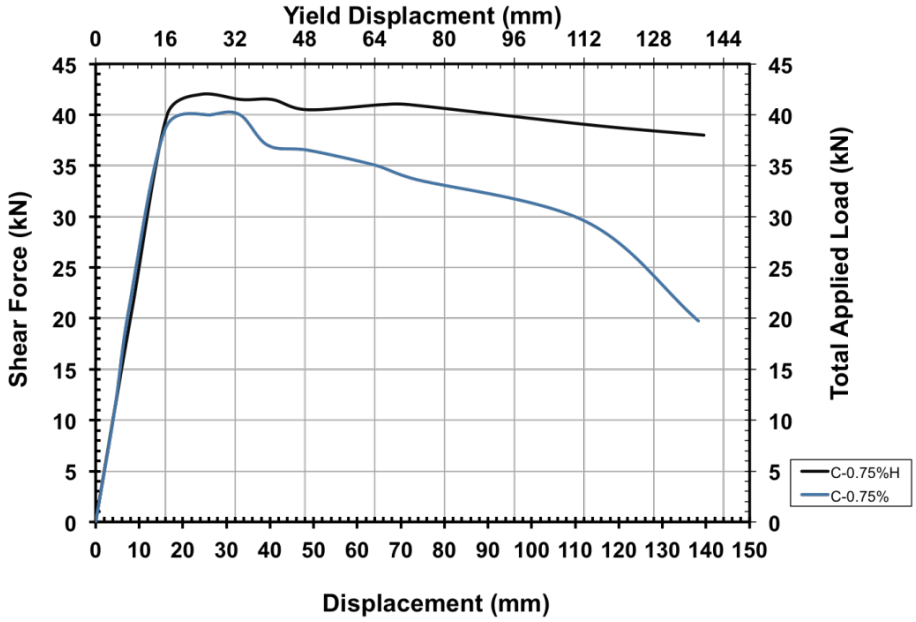

Figure 2.45 Response envelopes for beams with 0.75% regular and high strength steel fibers [Adapted from Alfarra, 2012]

2.8 Code requirements for ductile flexural members

The seismic resistant design of ductile frames requires the provision of adequate detailing of steel reinforcement in the critical regions of columns, joints and flexural members. In the case of flexural members the CSA A23.3-04 design standard (CSA, 2004) requires the provision of transverse reinforcement within the expected plastic hinge regions. Clause 21 of specifies a number of requirements as follows:

- The first hoop needs to be located not more than 50mm from the face of a supporting member (Cl. 21.3.3).
- The maximum spacing of the hoops shall not exceed d/4, eight times the diameter of the smallest longitudinal bars, 24 times the diameter of the hoop bars or 300 mm within a distance 2d from the face of joints, where d refers to the effective depth of the section (Cl. 21.3.3).
- The maximum spacing of transverse reinforcement elsewhere (i.e. outside the hinge regions) should not exceed d/2

Figure 2.46 and **Figure 2.47** list similar seismic provisions for transverse reinforcement in flexural members in other North American design standards (ACI 318, AASHTO).

In addition to the above requirements, cl. 21.3.2.2 of the CSA23.3-04 standard requires the positive bending reinforcement at joints in ductile frames to be at least 50% of the negative moment reinforcement.

Requirement	Flexural Members With $N_u < 0.1A_g f'_c$	Flexural Members With $N_u > 0.1A_g f'_c$
Length over which special transverse reinforcement must be provided; maximum of:	$2h$ from member end or region where inelastic deformations are expected	h $l_n / 6$ 18 inch
Maximum spacing – critical region; minimum of:	$d/4$ 8 $d_{s,\min}$ 24 d_b 12 inch	$b_{min}/4$ 6 $d_{s,\min}$ $4+\left(\frac{14-h_x}{3}\right)$ 3 inch clear spacing (spiral or circular hoops only)
Maximum spacing – elsewhere; minimum of:	$d/2$	6 $d_{s,\min}$ 6 inch
Minimum transverse reinforcement for confinement in plastic hinge regions	Not specified	For spiral or circular hoops: $\rho_s \geq \begin{cases} 0.12\frac{f'_c}{f_{yh}} \\ 0.45\left(\frac{A_g}{A_c}-1\right)\frac{f'_c}{f_y} \end{cases}$ For rectangular hoops: $A_s \geq \begin{cases} 0.3\left(\frac{sh_c f'_c}{f_{yh}}\right)\left(\frac{A_g}{A_{ch}}-1\right) \\ 0.09sh_c\frac{f'_c}{f_{yh}} \end{cases}$
Minimum transverse reinforcement for shear	$A_v = 0.75\sqrt{f'_c}b_w s / f_y \geq 50b_w s / f_y$	
Shear demand used in design	Shear corresponding to expected moment strength at both member ends (calculated assuming a reinforcing steel stress equal to $1.25f_y$) plus shear due to gravity loads	
Maximum shear strength V_s	$8\sqrt{f'_c}b_w d$	
Shear contribution from concrete, V_c	Zero only when the earthquake-induced shear force is greater than one-half the maximum required shear strength, and the factored axial compressive force is less than $A_g f'_c / 20$	

Figure 2.46 ACI 318 requirements for design of transverse reinforcement (seismic provisions)

[Adapted from Chompreda and Parra-Montesions (2005)]

Requirement	For Bridge Columns
Length over which special transverse reinforcement must be provided; maximum of:	h $l_n / 6$ 18 inch
Maximum spacing for confinement in critical region; minimum of:	$b_{min}/4$ 4 inch $6\,d_{bl}$ (for spiral)
Maximum spacing for all regions (shear design); minimum of:	If $v_u < 0.125 f'_c$: $s_{\max} = 0.8 d_v \le 24$ inch If $v_u \ge 0.125 f'_c$: $s_{\max} = 0.4 d_v \le 12$ inch
Minimum transverse reinforcement for confinement in plastic hinge regions	For spiral reinforcement: $\rho \ge \begin{cases} 0.45\left(\frac{A_g}{A_c} - 1\right)\frac{f'_c}{f_y} \\ 0.12\frac{f'_c}{f_y} \end{cases}$ For rectangular hoops: $A_{sh} \ge \begin{cases} 0.30 s h_c \frac{f'_c}{f_y}\left[\frac{A_g}{A_c} - 1\right] \\ 0.12 s h_c \frac{f'_c}{f_y} \end{cases}$
Minimum transverse reinforcement for shear	$A_v \ge \sqrt{f'_c}\frac{b_v s}{f_y}$
Shear demand used in design	Shear corresponding to 1.3 times the moment resistance capacity (calculated using nominal material properties)
Maximum shear strength for $v_c + v_s$	$0.25 f'_c b_v d_v$
Shear contribution from concrete, v_c	Varies linearly from zero when there is no axial load to a value calculated in Section 5.8.3 (Shear Strength Based on Modified Compression Field Theory) when the axial load is equal to $0.1 A_g f'_c$

Note: d_{bl} is the diameter of the longitudinal reinforcement bar, l_n is the member clear span, A_g is

Figure 2.47 AASHTO requirements for design of transverse reinforcement (seismic provisions)

[Adapted from Chompreda and Parra-Montesinos (2005)]

2.9 Conclusions from literature review

The following conclusions are drawn from the literature review presented in this section:

1. The use of fibres results in enhancements in properties of concrete including tensile post-cracking strength, flexural toughness, post-peak strength in compression, ductility and energy absorption capacity.
2. Important properties affecting SFRC performance include fiber properties (typology, aspect-ratio, strength), fiber pullout behaviour, orientation and distribution.
3. SFRC exhibits improved compressive and tensile behaviour and can result in tension-hardening behaviour at higher fiber contents. There are various methods for assessing the tensile post-cracking strength of SFRC, the simplest of which is through indirect testing of flexural beams such as in ASTM C1609;
4. Use of steel fibers reduced workability of traditional concrete, however, combined use SCC and fibers can solve this problem and workable mixes can be achieved ;
5. There has been significant research on SFRC beams under monotonic loading. This research shows that SFRC improves shear resistance and can promote flexural failure and ductility;
6. Research on SCFRC beams is limited, however tests by Cohen (2012) and Alfarra (2012) at the University of Ottawa indicate that SCFRC improves the strength, ductility and cracking resistance of beams;
7. There is limited research on the behaviour of SFRC under cyclic and reversed-cyclic loading, however this research demonstrates that SFRC can potentially improve the performance of flexural members under cyclic loading and load reversals.

The research presented in this thesis examines the potential of using SCFRC to improve the behaviour of beams subjected to reverse-cyclic and therefore contributes to the knowledge on the structural behaviour of SCFRC in general (item 6) and the behaviour of flexure-dominant SFRC beans under load reversals (item 7).

Chapter 3 Experimental Program

3.1 Introduction

The primary objective of this research program is to investigate the behaviour of steel fiber reinforced concrete (SFRC) flexural members constructed with self Consolidating Concrete (SCC) under reversed cyclic displacements. The experimental program involved the construction and testing of nine dual cantilever flexural members under load reversals, including two control reinforced concrete specimens and seven companion specimens in which steel fibers were used. The experimental variables that were investigated included the amount of transverse reinforcement in the plastic hinge region (s = d, d/2, d/3, d/4) and content of steel fibers (0%, 0.75%, 1%, 1.5% by volume of concrete). In addition to studying performance enhancements associated with use of fiber reinforced concrete, the experimental program aimed at examining if use of steel fibers can permit the relaxation of transverse reinforcement requirements in the plastic hinge regions of flexural members. This chapter presents further details regarding the specimens, material properties, construction method and testing procedure.

3.2 Description of Test Specimens

This experimental program involved construction of 9 SFRC dual cantilever flexural members. As shown in **Figure 3.1** to **Figure 3.3**, each specimen consisted of two cantilever beams attached to a middle concrete block which was used for loading. These specimens are referred to as dual cantilever specimens because they are equivalent to two beams with the middle column stub acting as a fixed support.

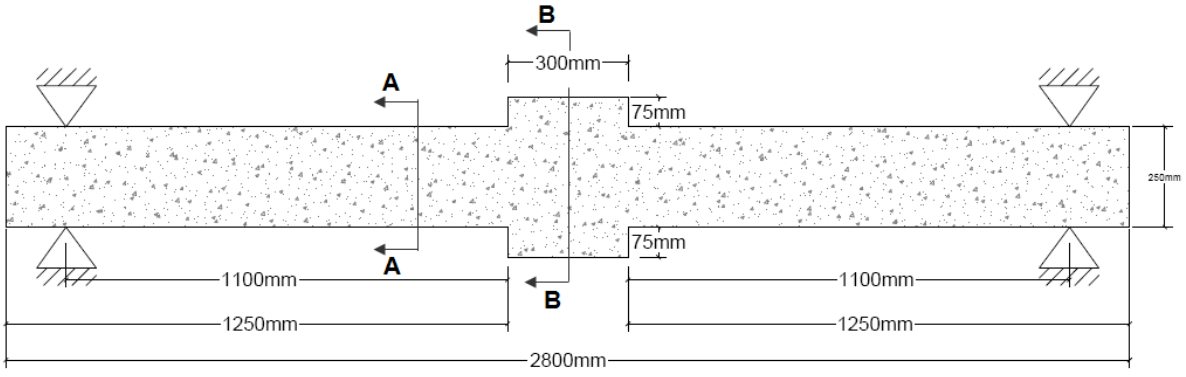

Figure 3.1 Typical beam geometric properties

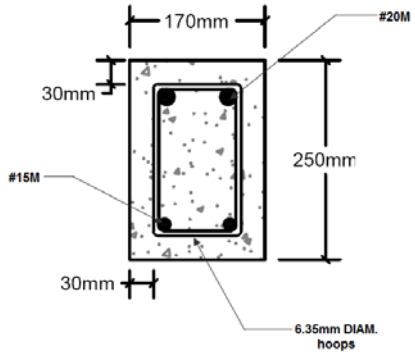

Figure 3.2 Typical beam cross-section (Section A-A)

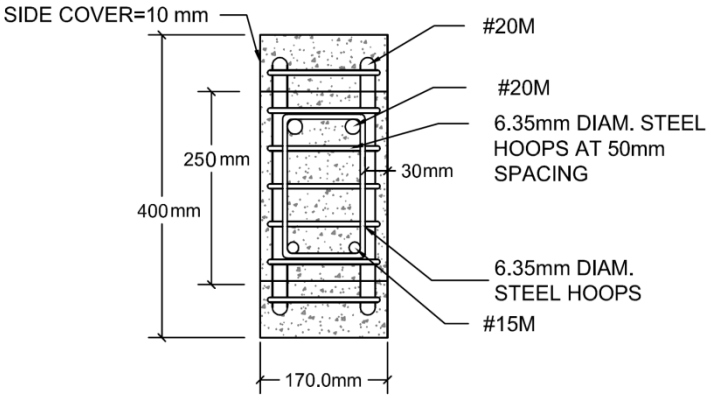

Figure 3.3 Typical cross-section showing details of beam and the middle block (Section B-B)

All specimens had a total length of 2800 mm, simply supported over 2500 mm, with a middle block having length of 300 mm. The block had larger cross-sectional dimensions of 400mm x 170 mm, with 75mm protruding at the top and bottom with respect to the beams. The two cantilever beams had clear spans of 1100 mm and cross-sectional dimensions of 250mm x 170 mm. For each cantilever section the negative moment reinforcement (top) consisted of 2-20M (d_b = 20 mm, A_s = 300 mm^2) reinforcing bars, while the positive moment reinforcement (bottom) consisted of 2-15M (d_b = 16 mm, A_s = 200 mm^2) reinforcing bars. The longitudinal reinforcement details were chosen in accordance with cl. 21.3.2.2 of the CSA23.3-04 (CSA, 2004) in order to better simulate expected performance in real structures; this clause requires the positive bending reinforcement in flexural members to

be at least 50% of the negative moment reinforcement at beam-column joints locations. The beam sections had a top and bottom clear cover of 30 mm to the reinforcing bars, resulting in an average effective depth, d of 204 mm.

As can be seen in **Figure 3.4 (a)** to **(d),** the specimens were grouped into four test series based on spacing of transverse reinforcement in the plastic hinge regions. The D series, D/2 series, D/3 series and D/4 series specimens had transverse reinforcement spacing, s, of 204 mm, 102 mm, 68 mm and 51 mm, respectively, within a distance of 2d from the face of the column-stub. This transverse reinforcement, as the series names imply, thus corresponded to spacings of d, d/2, d/3 and d/4. The transverse reinforcement details for the D/4 series were selected based on the requirements of cl. 21.3.3 of the CSA A23.3-04 design standard for flexural members with ductile detailing. The transverse reinforcement in the D/2, D/3 and D-series specimens was selected to examine if fibers can partially replace transverse reinforcement in the plastic hinge regions of flexural members.

All specimens were constructed using the same self-consolidating concrete mix (KING SCC), but included varying amounts of hooked-end steel fibers ranging from 0% to 1.5% by volume of concrete. The D/2 series consisted of one control specimen without fibers (Beam D/2-0%), and three specimens with 0.75%, 1.0% and 1.5% steel fibers (Beams D/2-0.75%, D/2-1%, D/2-1.5%, respectively). The D/3 series consisted of two specimens constructed with 1.0% and 1.5% steel fibers (Beams D/3-1%, D/3-1.5%, respectively). The D/4 series consisted of one control specimen without fibers (Beam D/4-0%) and one specimen with 1.0% steel fibers (Beam D/4-1%). The D-series specimen (Beam D-1.5%) was constructed with 1.5% steel fibers. Same type of normal strength hooked-end steel fibers was used for all specimens.

It is noted that due to the relatively high shear span to depth ratio, the SCFRC beams tested in this experimental program were subjected to moderate shear stress demands. The research conducted by Chompreda and Parra-Montesinos (2005) reports the results from SFRC beams tested under reversed-cyclic loading and relatively high shear stress demands.

Table 3.1 Design properties for dual cantilever specimens

Series	***Beams***	***Concrete Type***	***Cross-section* (mm x mm)**	***Reinforcement***	***Fiber type***	***Shear span to depth ratio, a/d***	**Transverse reinforcement spacing, s (mm)**	***Fiber content*** (% by volume)
D	D-1.5%	KING SCC	170 x 250	Bottom (M positive): 2 - 15M Top (M negative): 2 - 20M	ZP-305	5.4	s =205 (d)	1.5
D/2	D/2-0.0%						s =103 (d/2)	0
	D/2-0.75%						d/2=103	0.75
	D/2-1.0%						d/2=103	1
	D/2-1.5%						d/2=103	1.5
D/3	D/3-1.0%						d/3=68	1
	D/3-1.5%						d/3=68	1.5
D/4	D/40.0%						d/4=51	0
	D/4-1.0%						d/4=51	1

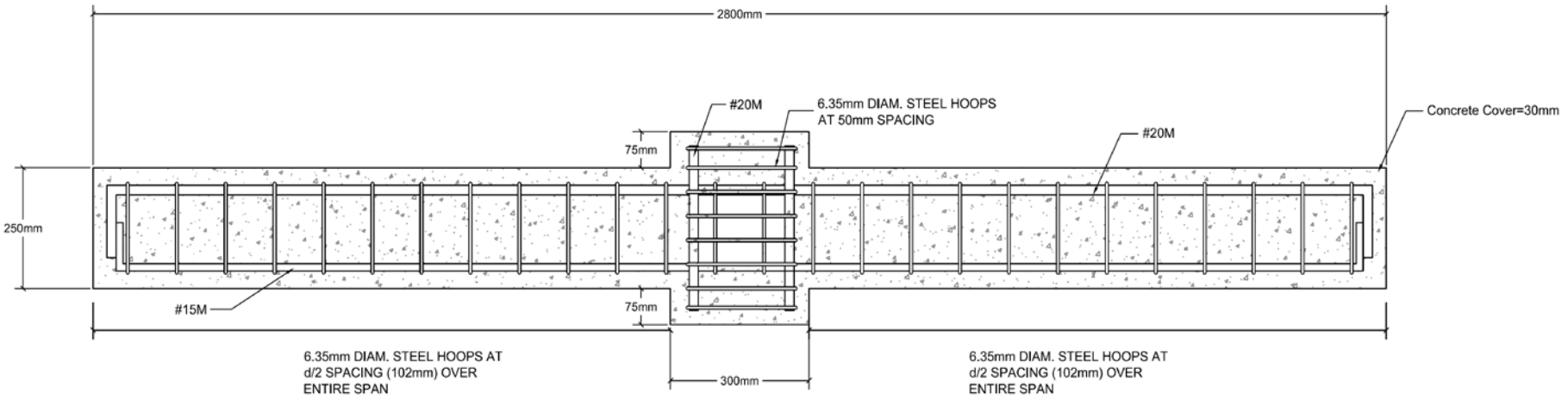

a) D/2 series

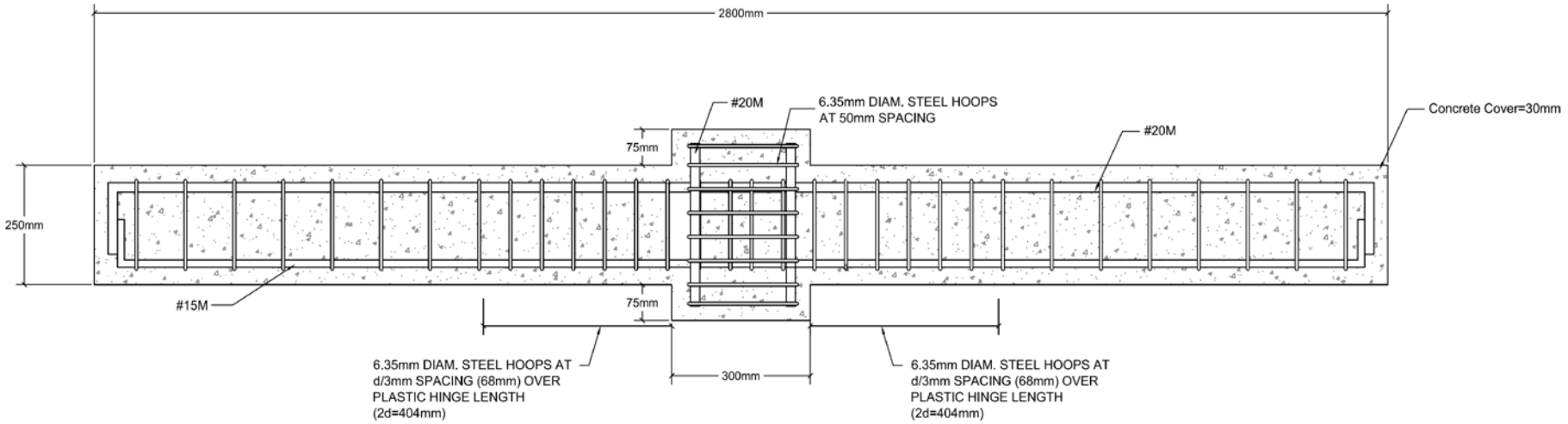

b) D/3 series

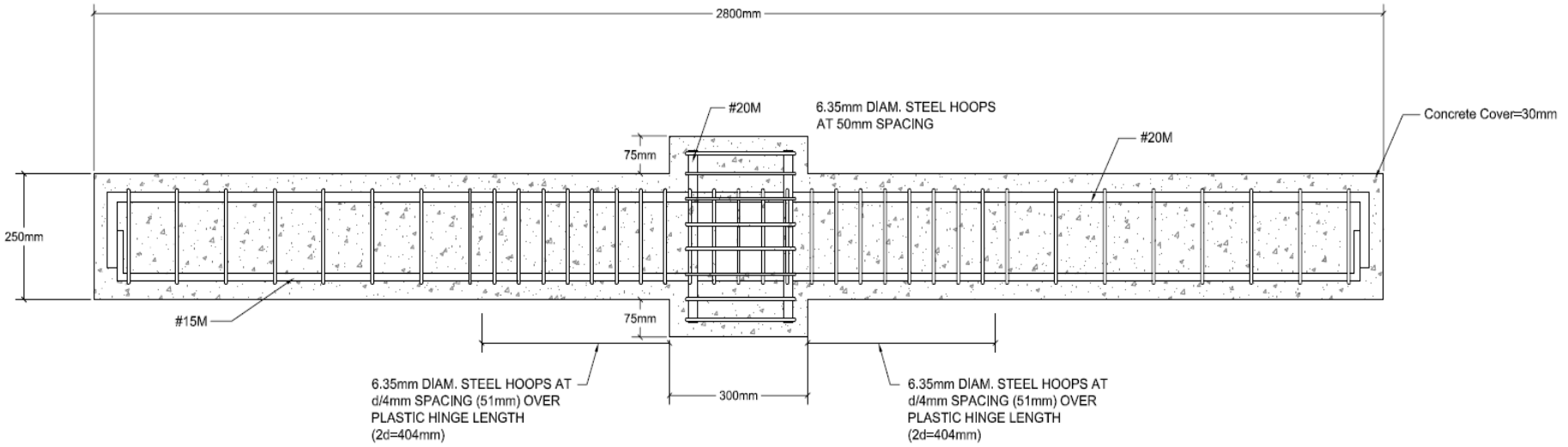

c) D/4 series

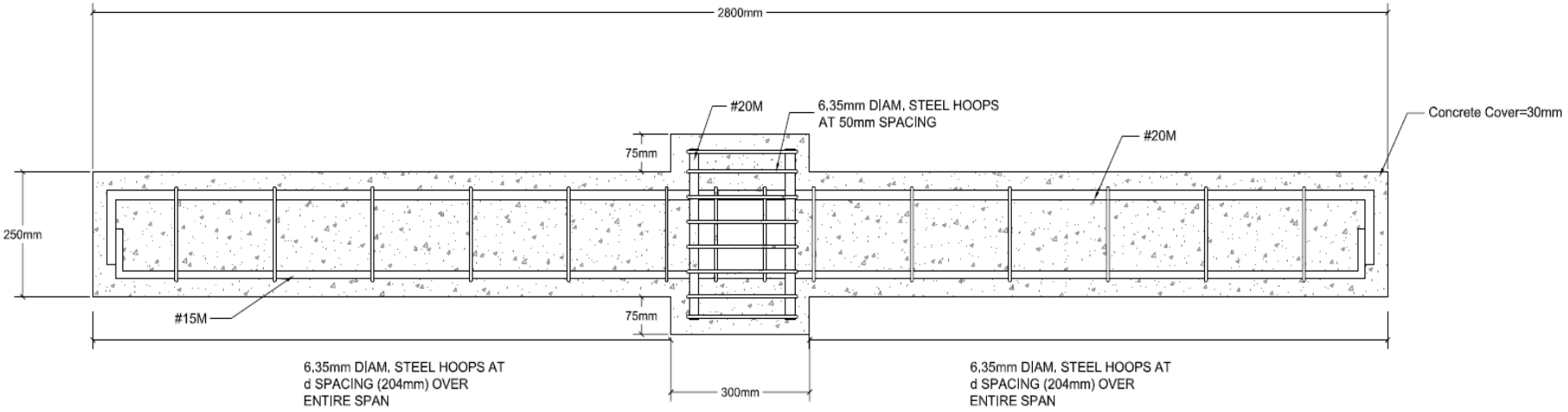

d) D series

Figure 3.4 Details of transverse reinforcement in the D/2, D/3, D/4and D-series specimens

3.3 Material Properties

3.3.1 Reinforcing Steel

The longitudinal reinforcement used in all specimens consisted of 2-15M (d_b =16 mm, A_s = 200 mm^2) for positive moment reinforcement and 2-20M (d_b = 20 mm, A_s = 300 mm^2) reinforcing bars for negative moment reinforcement. 4-20M bars were also used as compression steel in the column stubs. All the reinforcing bars were Grade 400, normal strength steel. The transverse reinforcement was manufactured using 1/4" (6.35mm) diameter steel wire. To determine the properties of the reinforcing bars and wire, standard tensile coupon tests were conducted using a 600KN capacity Galdabini Universal Testing Machine and stress-strain curves for each rebar size were generated.

Figure 3.5 shows these stress-strain curves. Various reinforcing steel properties obtained from the coupon tests are summarized in **Table 3.2** and **Table 3.3**, including yield strength (f_y), ultimate strength (f_u), and strains corresponding to yield, strain-hardening and rupture (ε_y, ε_{sh}, ε_u).

Table 3.2 Properties of 15M and 20M reinforcing bars

Bar description	***Area*** ***(mm^2)***	f_y ***(MPa)*** ***[std. dev.]***	ε_y ***(mm/mm)*** ***[std. dev.]***	ε_{sh} ***(mm/mm)*** ***[std. dev.]***	f_u ***MPa)*** ***[std. dev.]***	ε_u ***(mm/mm)*** ***[std. dev.]***
20M	300	471	0.0032	0.01697	626	142.4
15M	200	436	0.0026	0.0164	588	0.1482

Table 3.3 Properties of 6.35mm steel bars

Yield		**Ultimate**		**Rupture**	
f_y **(MPa)** **[std. dev.]**	ε_y **(mm/mm)** **[std. dev.]**	f_u **(MPa)** **[std. dev.]**	ε_u **(mm/mm)** **[std. dev.]**	f_r **(MPa)** **[std. dev.]**	ε_r **(mm/mm)** **[std. dev.]**
604 **[3.72]**	0.0033 [0.00007]	694 [9.22]	0.0607 [0.01258]	689 [9.97]	0.0706 [0.01695]

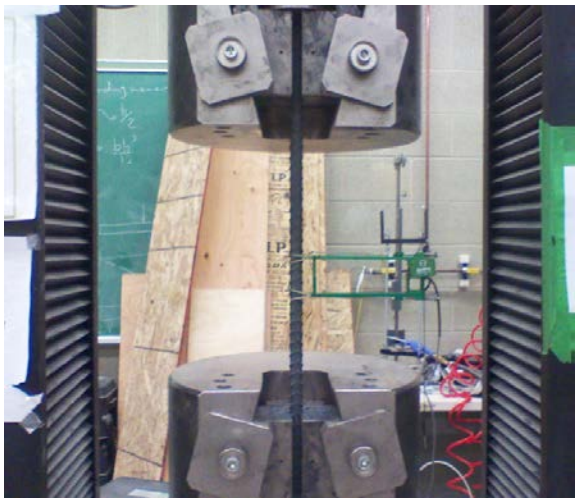

(a) MTS machine used for steel coupon testing

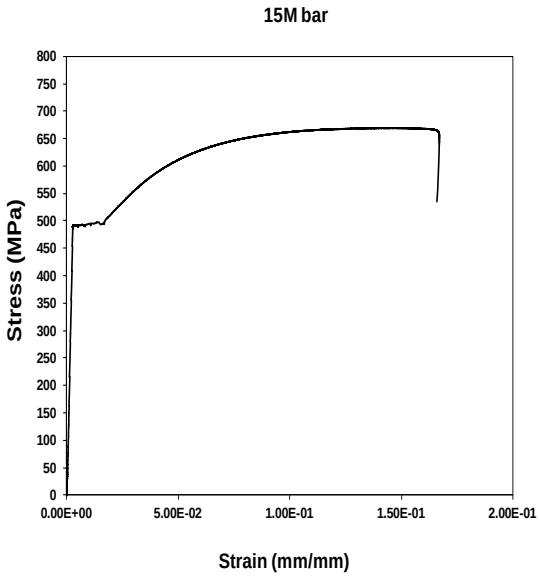

(b) Stress-strain relationship for 15M steel bar

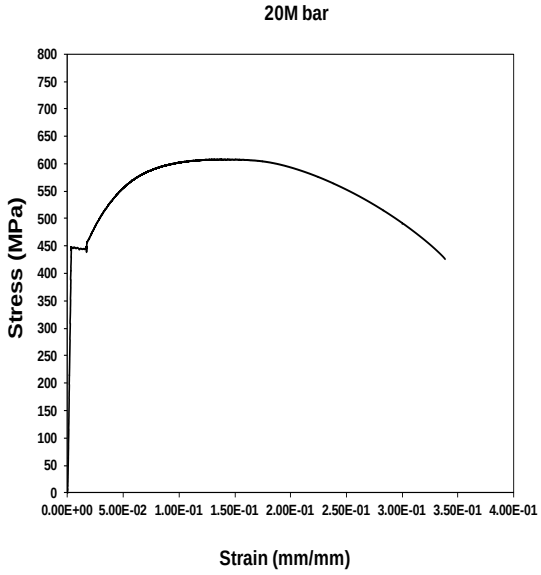

(c) Stress-strain relationship for 20M steel bar

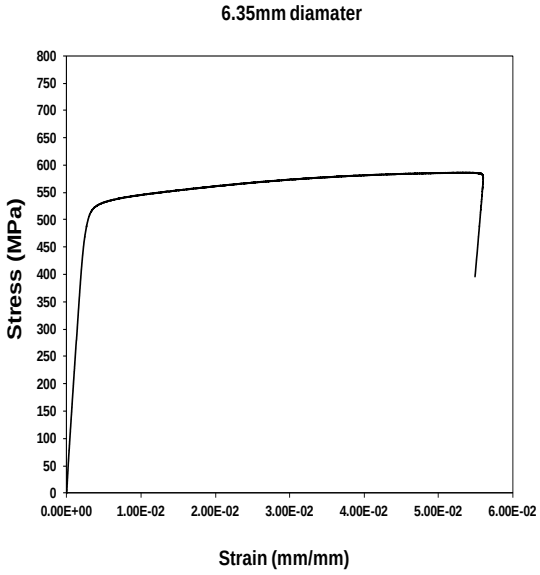

(d) Stress-strain relationship for 6.35mm steel bar

Figure 3.5 Machine used for steel coupon tests and typical stress-strain responses for (a)15M, (b)20M and (c) 6.35mm wire reinforcement

3.3.2 Steel Fibers

All SCFRC specimens were constructed using hooked-end steel fibers. The fibers, which are manufactured by *Bekaert Corporation* as the *Dramix ZP305* brand, have a tensile strength of 1100MPa, length of 30mm, diameter of 0.55mm in and aspect ratio (L_f/D_f) of 55. These fibers come in 20KG packages and are collated into bundles using water-soluble adhesive that dissolves shortly after mixing with concrete letting individual fibers to disintegrate and disperse in concrete during mixing (see **Figure 3.6**). The properties of ZP305 steel fibers as specified by the manufacturer are summarized in **Table 3.4**. As discussed in the previous section, different amounts of fibers were used in the specimens ranging from 0.5% (39 kg/m^3) to 1.5% (117 kg/m^3) by volume of concrete.

Table 3.4 Properties of hooked-end steel fibers used in this study

Fiber type	*Length* L_f *(mm)*	*Diameter* D_f *(mm)*	*Aspect ratio* L_f/D_f *(mm/mm)*	*Tensile strength* f_{fy} *(MPa)*
Dramix ZP-305	30	0.55	55	1345

Figure 3.6 Dramix hooked-end steel fibers

3.3.3 Concrete

The concrete used in construction of the beams was mixed in the University of Ottawa structural laboratory. KING SCC ready-mix concrete was used for all specimens.

3.3.3.1 KING-SCC Mix

The addition of fibers to a traditional concrete mix can cause problems in workability, particularly when high fiber contents (1% and above) are used. In this experimental program self-consolidating concrete was used to improve the workability of the fiber reinforced concrete mixtures. The concrete for all specimens was produced at the University of Ottawa Pomerleau Concrete Laboratory. The concrete consisted of a pre-packaged self-consolidating mix with a specified strength of 50 MPa (*MS Self-Consolidating Concrete, KING Packaged Materials Company*). The mix contained a maximum aggregate size of 10 mm with a sand-to-aggregate ratio of approximately 0.45 and a water-cement ratio of approximately 0.42. An air-entraining admixture, a superplasticizer and a VMA are incorporated into the mix in the form of dry powder. **Table 3.5** lists the composition of KING SCC mix as specified by the manufacturer. This mix was utilized in all nine specimens used in the experimental program. The "control" batches contained no fibers, while the remaining batches contained 0.75%, 1% and 1.5% Dramix ZP305 fibers by volume of concrete.

Table 3.5 Self-Consolidating Concrete composition

Component	***Content***
HSF Cement	500 (kg/m^3)
Water-cement ratio	0.42
Coarse Aggregate	765 (kg/m^3)
Fine aggregate	915 (kg/m^3)
Ratio Fine/Total Aggregate	0.55
Mass Density	2300 (kg/m^3)
Air Content	7 (%)

3.4 Construction of Specimens

3.4.1 Construction of Cages

The first stage of the construction of the test specimens included bending of steel ties, assembly of steel reinforcement cages and application of electrical resistance strain gauges on the steel cages. The reinforcing steel in the test specimens was provided by local steel material suppliers. Bending of the steel ties was done by means of a hand bending jig designed to provide exact dimensions of the steel ties. The *6.3 mm* wire was cut is specified lengths and bend into 90^{o} at the corners and 135^{o} at the hoops. In assembling the steel cages, the first stage was to mark the hoop spacing on a working platform as well as on the longitudinal reinforcement bars. The transverse reinforcement hoops were then placed on the steel bars and tied in place using quick tie wires. **Figure 3.7** and **Figure 3.8** show typical cages with and without seismic detailing after construction.

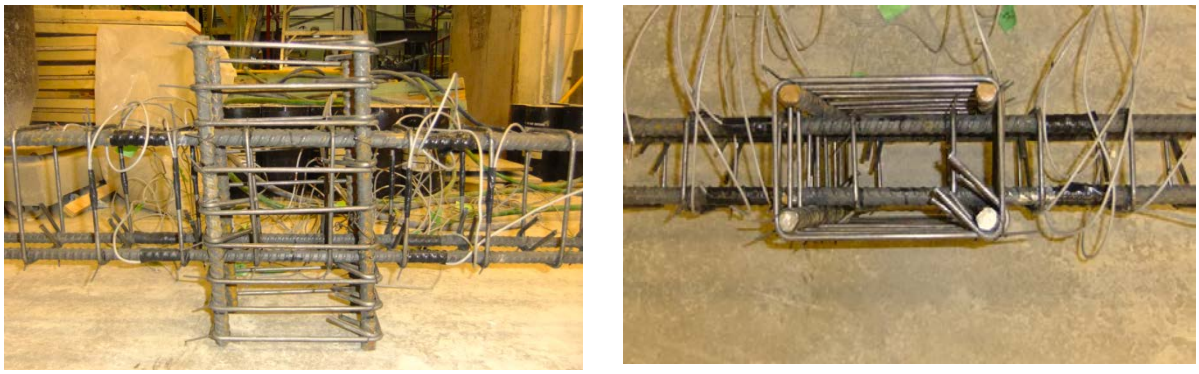

Figure 3.7 Typical cage showing strain gauge instrumentation

Figure 3.8 Typical cage (D/3 series)

3.4.2 Mixing of concrete

A pan mixer was used for mixing the concrete in this experimental program (see **Figure 3.9**). The pan mixer uses 3 fixed paddle blades that are arranged in such a way as to create a forced mixing action as the pan revolves at high velocity. A side scraper blade is also used to scrape the material off of the walls of the pan during mixing. In comparison with other mixer types (such as drum and mortar mixers), this mixer type is well suited for mixing SCFRC due to its ability to force material in to defined flow path at high velocity, and thus ensures good distribution of steel fibers in the concrete, particularly at higher fiber contents. The construction of each beam required 12 bags of KING SCC material (0.17 m^3 of concrete). The capacity of the pan mixer was sufficient for one batch to be used during the construction of each specimen.

Figure 3.9 Pan mixer used in mixing of concrete

3.4.3 Casting and Curing

The mix procedure detailed in the previous section was used to mix the concrete used in all the specimens. After mixing, concrete was poured directly into wheel barrels and moved closer to the formwork for ease of placement. A slump test was performed prior to the start of casting to verify the fresh state properties of the SCC and SCFRC mixtures. **Figure 3.10** to **Figure 3.12** show the wooden formwork details that were used for casting the concrete beams and casting during construction of beam D/2-0.0%. The formwork was designed and constructed for casting 8 specimens. This formwork was later used to cast a ninth specimen. Sheets of rigid insulation foam were used to accommodate for the increased depth of the column section at the middle of the beam. Plaster paste was used to fill the voids and smoothen the rough surface of plywood inside the formwork. The interior surfaces of the formwork were covered with hydraulic oil prior to casting to ease their removal after curing. Plastic chairs with specified heights (30mm) were placed at the bottom of the formwork to maintain the required concrete cover during placement of concrete.

Concrete was poured into the forms in layers requiring occasional vibration in cases of higher fiber contents (1% and above) to prevent voids and to ensure proper consolidation of around the reinforcement. This was especially necessary in the case of the D/4 series fiber reinforced specimen since the spacing of the hoops and spaces between the reinforcement at the beam-column joint location were close to the length of the fibers; additional vibration was required to ensure sure that fibers completely filled the areas between the steel reinforcement. Once casting of concrete was finished, the surface was levelled and smoothened. Two steel hooks were embedded at the ends of the beam to facilitate lifting and moving of the beam after curing. Concrete beams were then covered with plastic sheets and a layer of moist burlap. Concrete beams were watered regularly during the curing period. Curing of concrete beams continued for seven days after casting then the formwork was removed and the beams were let to cure in room conditions until the day of testing.

Figure 3.10 Formwork used to cast concrete beam specimens

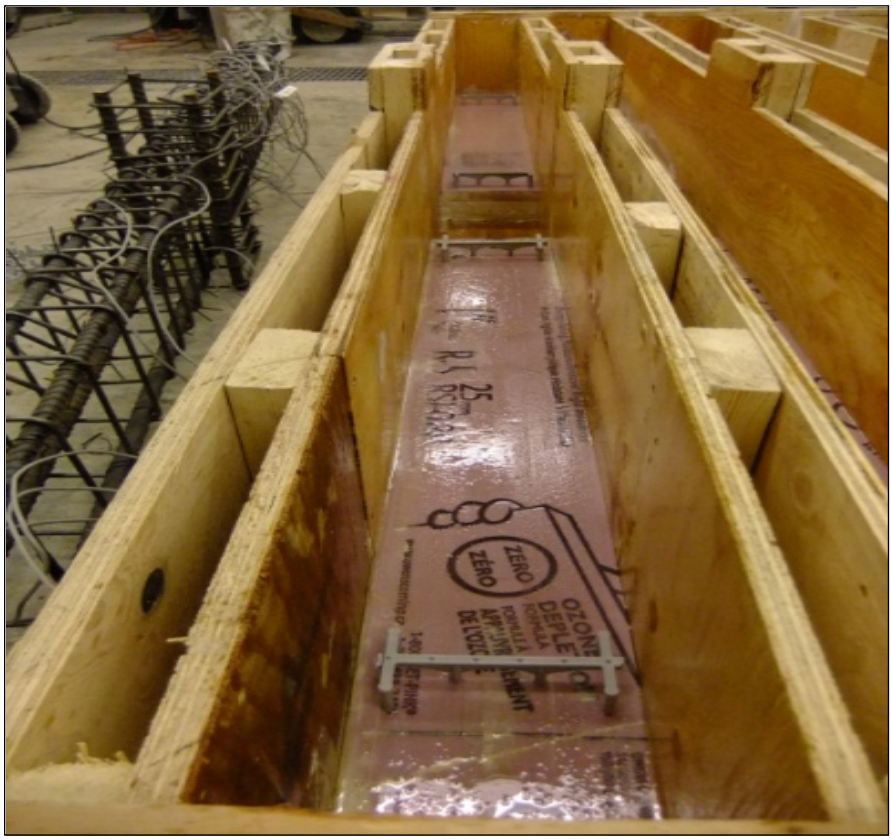

Figure 3.11 Reinforcement chairs and insulation foam used in formwork prior to casting

Figure 3.12 Casting beam D/2-0.0%

It is to note that the first D/4-1.0% specimen that was built turned out to have excessive voids and honey combing within the hinge region. This was due to poor consolidation of concrete within the heavily congested plastic hinge region and the middle concrete block. **Figure 3.13** shows the first D/4-1.0% after opening the formwork. Hence a new specimen was built and used as part of the testing program.

Figure 3.13 Poor consolidation of concrete in the plastic hinge region for first D/4-1.0% beam

3.5 Concrete Properties

3.5.1 Fresh-State Concrete Properties

Workability and resistance to segregation are two important characteristics of fresh state SCC which should be checked prior to placement of concrete. In this experiment the slump flow test was used to check for workability of the SCC and SCFRC for each batch of concrete mix before casting. The diameter of the spread of concrete was measured in two directions in mm and the average was recorded as slump flow for the batch before casting. In addition, the SCC and SCFRC mixtures were visually inspected for segregation and bleeding prior to casting.

Figure 3.6 shows photos of the slump flow spread for each batch of concrete with associated average slump flow values in mm. For the case of the control SCC mix, the average slump flow for both control specimens was approximately 600 mm and due to the high workability of the SCC mix, placement of concrete in the formwork was possible without vibration in specimen D/2-0%, while only slight vibration was required when casting SCC in the congested hinge areas of specimen D/4-0%. Many factors can affect the workability of SCFRC including fiber content, including fiber properties (geometry, length, aspect-ratio, anchorage properties) and SCC mix properties (aggregate size, admixture type and content). For the case of the SCFRC batches used in this experimental program the same base SCC mix and fiber type were used, as such the main variable was fiber content. As expected, addition of fibers progressively reduces workability as the fiber content increases, and this reflected in the slump flow results (reduces slump readings as fiber content increases). In this test series, although self-consolidation was no longer possible at a fiber content of 1% ZP305 fibers, the mix was sufficiently workable. During casting of the specimens, good workability and uniformity of concrete mix was observed in batches with fiber contents less that 1.0% with only slight vibration required during casting. More important vibration was required for the mixtures with 1.5% fibers, particularly in the highly congested D/4 series specimen. Aoude et al. (2009) suggest that 1.5% fiber content is an upper limit for a semi-workable SCC mix; the results from this experimental program confirm this finding.

Table 3.6 Slump properties

Slump Flow Photos			
Batch	D/2-0.0%	D/4-0.0%	D/2-0.75%
Slump flow (mm)	600	600	520
Slump Flow Photos			
Batch	D/2-0.1.0%	D/3-1.0%	D/4-1.0%
Slump flow (mm)	480	490	440
Slump Flow Photos			
Batch	D/2-1.5%	D/3-1.5%	D-1.5%
Slump flow (mm)	405	380	385

3.5.2 Hardened- State Concrete Properties

To measure the concrete material properties for each batch, a series of lab cured cylinders and flexural beams were prepared during the mixing of the concrete. The concrete compressive strengths were obtained by testing standard cylinders having a diameter of 100 mm and a height of 200 mm at the day of testing (see **Table 3.7**). The majority of the cylinders were tested using a hydraulic compression testing machine located at the University of Ottawa Structures Laboratory (see **Figure 3.14 (a)**). To illustrate the effect of fibers on complete response, **Figure 3.15 (a)** shows the complete stress-strain behaviour of cylinders constructed using the same SCFRC mixtures used in this study for fiber contents of 0%, 1% and 1.5% (tested by Alfarra (2012)). It is seen that the fibers do not have an important effect on peak strength, however post-peak ductility improves with addition of fibers. To examine the effect of fibers on flexural toughness, the ASTM C1609 test method was used for a sample of the SCFRC mixtures. The tests were conducted on flexural beams having cross-section dimensions of 100 mm by 100 mm and a length of 400 mm. The beams were subjected to third point loading over a span of 300 mm using a 600KN capacity Galdabini Universal Testing Machine (see **Figure 3.14 (b)**). **Figure 3.15 (b)** plots typical load-deflection responses for SCFRC mixtures having 0%, 1% and 1.5%; it is noted that fibers improve toughness of concrete. It is also noted that although an indirect tension test, the beam with 1.5% demonstrates some deflection-hardening behaviour with an enhanced post-cracking strength.

(a) Concrete cylinder test setup

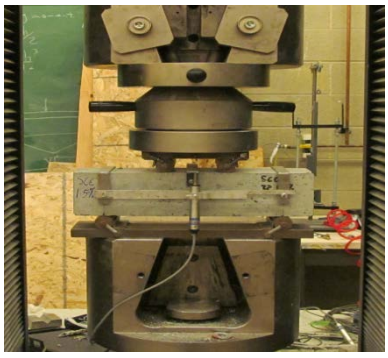

(b) Flexural beam test setup

Figure 3.14 Machines and test setup for concrete cylinder and flexural beam tests

Table 3.7 Concrete Properties

Concrete Type	Label	Fiber type	Fiber Content v_f (%)	Average Compressive strength at day of testing, f'_{co} (MPa)
SCC	D/2-0.0%	ZP305	0	58.5
	D/2-0.75%		0.75	53.8
	D/2-1.0%		1	59.7
	D/2-1.5%		1.5	60.8
	D/3-1.0%		1	49.5
	D/3-1.5%		1.5	60.9
	D/4-0.0%		0	53.0
	D/4-1.0%		1	49.3
	D-1.5%		1.5	54.5

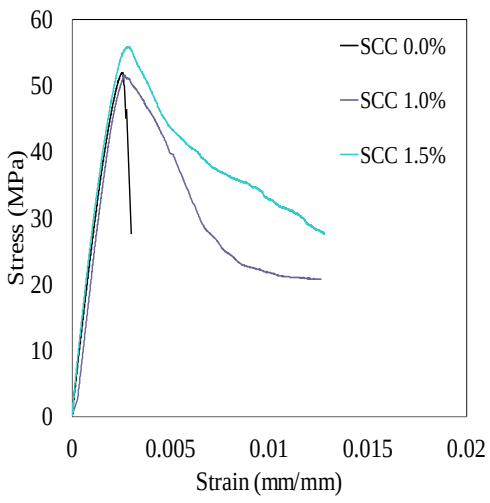

(a) Stress-strain response in compression

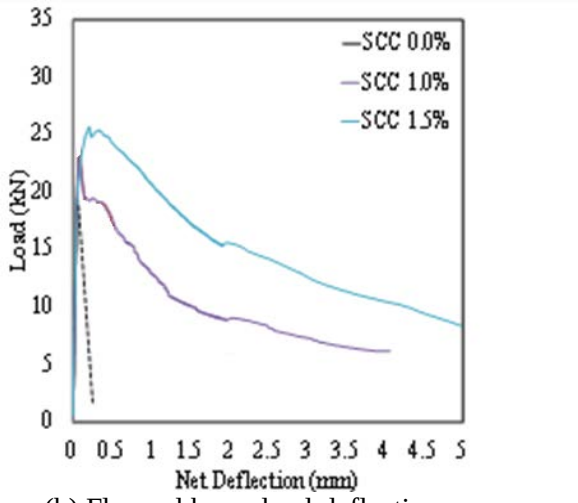

(b) Flexural beam load-deflection curves

Figure 3.15 Typical behavior in compression and flexure (toughness) for SCC and SCFRC

3.6 Test Setup

3.6.1 Load setup

Figure 3.16 and **Figure 3.17** shows the test setup that was used for testing all specimens in the experimental program. As discussed previously the specimens consisted of two beams joined by a strong stiff block at the midspan. All specimens were simply supported over a span of 2500mm and were subjected to a point load using the stiff middle block. The point load was transferred to the column-stub through an assembly of steel plates and rods which allowed the load to be transferred uniformly within the plate area. The same type of assembly was used at the supports with the addition of a roller bearing at the bottom of the left support to allow for small horizontal movements under flexure. The shear span of the dual cantilever beams from the supports to the face of the column-stub was 1100mm, resulting in a shear-span to depth ratio, *a/d*, of 5.4.

The loading setup was designed to allow for load reversals to allow for testing under reverse-cyclic loading. Two 1/5” steel plates were placed at the top and bottom of the enlarged block and were connected by means of four high strength threaded steel rods drilled through the corners of the steel plates as shown in **Figure 3.16** and **Figure 3.17.** A double valve hydraulic jack having a travel length of 6” (152 mm), equivalent to a travel length of 3” (76 mm) in each direction, was connected to a load-cell and the top plate loading assembly. This hydraulic jack was suitable for drift stages up to 7% in each direction, after which the loading assembly was manually adjusted to allow for further travel in each direction. The hydraulic jack was fixed to a square HSS section at midspan. The HSS section was positioned on top of the beam and was vertically fixed via *Dywidag* bars which were attached to the strong floor of the structures laboratory.

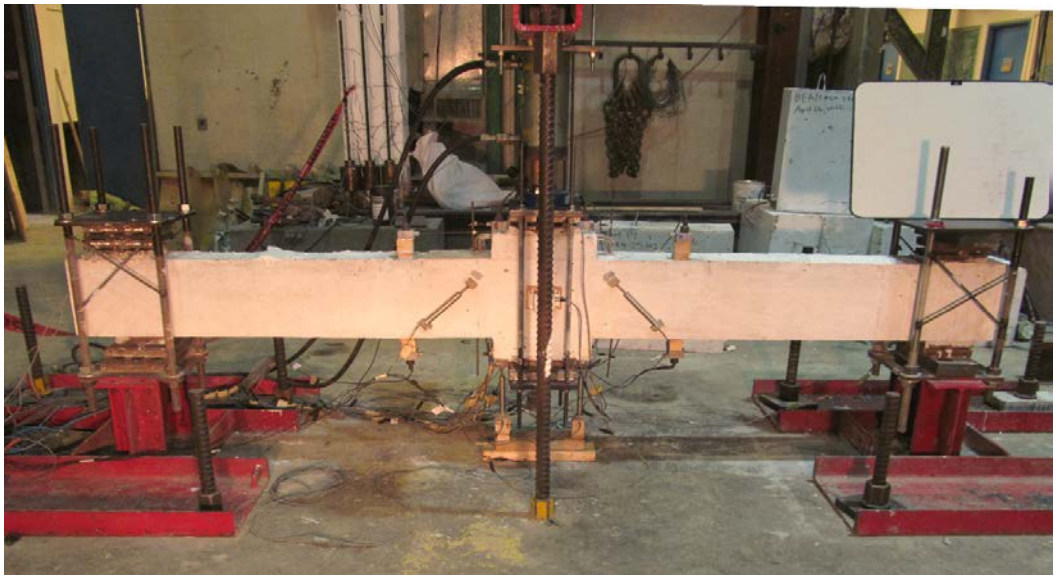

Figure 3.16 Beam specimen prior to testing

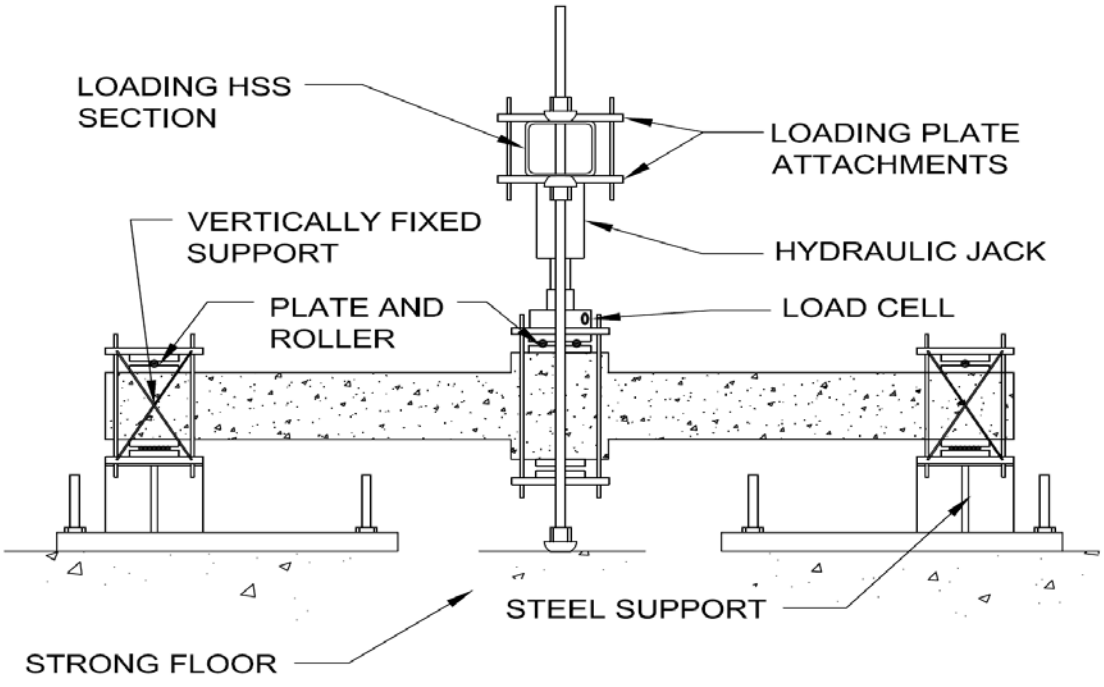

Figure 3.17 Schematics of the loading setup

3.6.2 Instrumentation

In order to study the response of the dual-cantilever specimens, several parameters were monitored and recorded during testing. These included load-displacement measurements, general rotation of the rigid block, anchorage slip deformations, rotation of the beams within the hinging region, shear deformation in the beams within the hinging region, strains in the longitudinal reinforcement at the faces of the column and strains in the transverse reinforcement at various hoop locations within the hinge region.

Figure 3.18 shows details of the loading device setup and support system. The loading was recorded using a load cell attached to the loading assembly while vertical displacement measurements were recorded using two cable transducers installed at midspan. General rotation of the middle loading block was measured using a digital inclinometer that was glued to the front face of the column and zeroed before start of each test. Anchorage slip rotation of the beam on both sides of the column was measured by means of Displacement Cable Transducers (DCT's) installed as close as possible to the face of the column as seen in **Figure 3.19** and **Figure 3.20.** DCT's were installed at four corners of the column to measure anchorage slip rotations at these locations. Flexural rotation of the beam within the hinging region was measured in a similar fashion by installing DCT's at a specified distance of 9" (228mm) from the faces of the column. This distance was chosen to match the dimensional characteristics of the DCT's, and to ensure that the flexural rotation deformation is captured over a net distance of at least d≈205mm. The linear deformations obtained from the DCT readings were converted to rotation then the rotation resulting from the anchorage slip was deducted to yield the rotation due to flexure only. Shear deformations within the hinging region were measured using LVDT's installed diagonally (45^o angle) on the faces of the beam within a distance d≈205mm from the faces of the column on both the front and back sides of the beam. LVDT's installed for this purpose were positioned in opposite diagonal directions in the front and back sides of the column to capture shear deformation in positive and negative bending. Tensile strains in longitudinal and transverse reinforcement were measured using electrical resistance strain gauges glued to the surface of the reinforcement steel at control locations. Strain gauges were installed on all four longitudinal reinforcement within the hinge region at the face of the rigid block.

Figure 3.18 View of loading and support setup

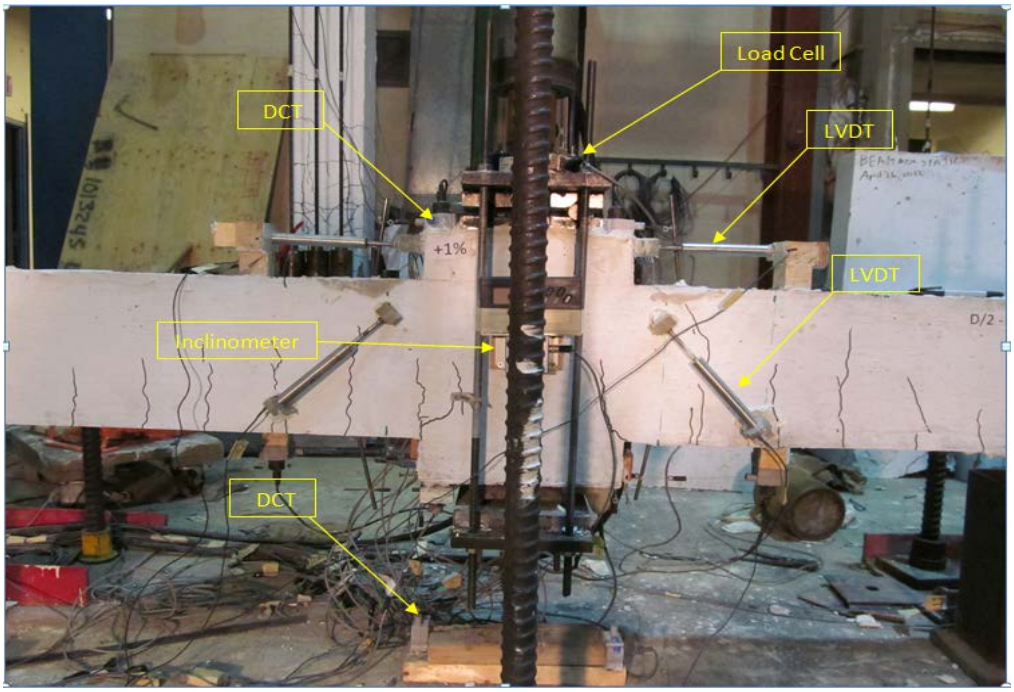

Figure 3.19 Instrumentation used in beam tests

Figure 3.21 show the instrumentation and DCT/LVDT labels for the various specimens, while **Figure 3.22 (a) to (d)** shows the locations and labels for strain gauges for the beams in the D/2-series, D/3 -series, D/4-series and D-series specimens.

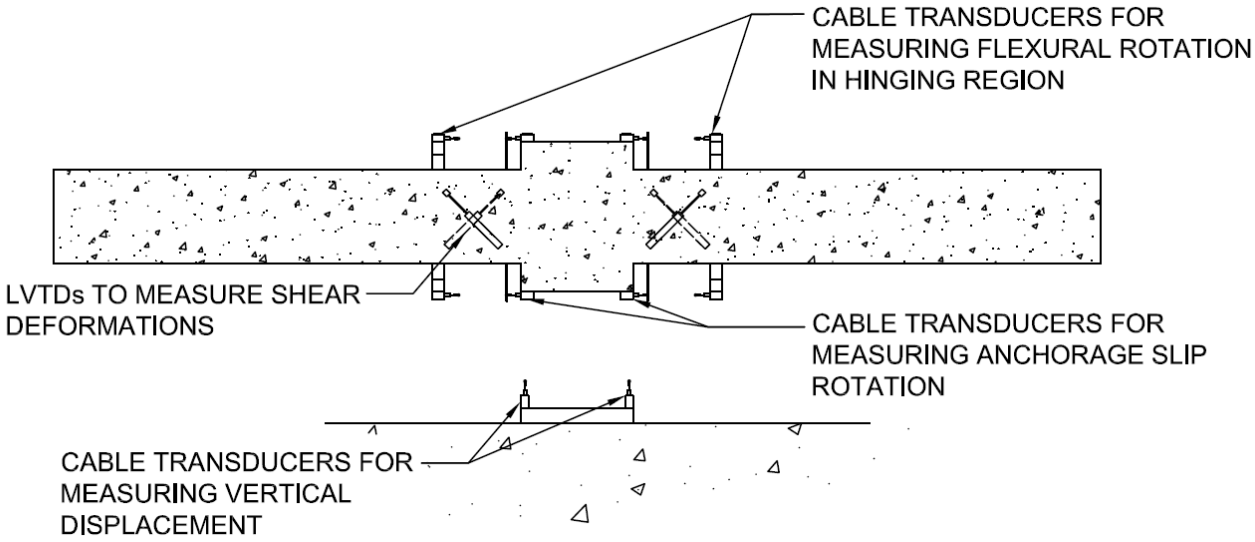

Figure 3.20 Displacement and rotation measurement instrumentation

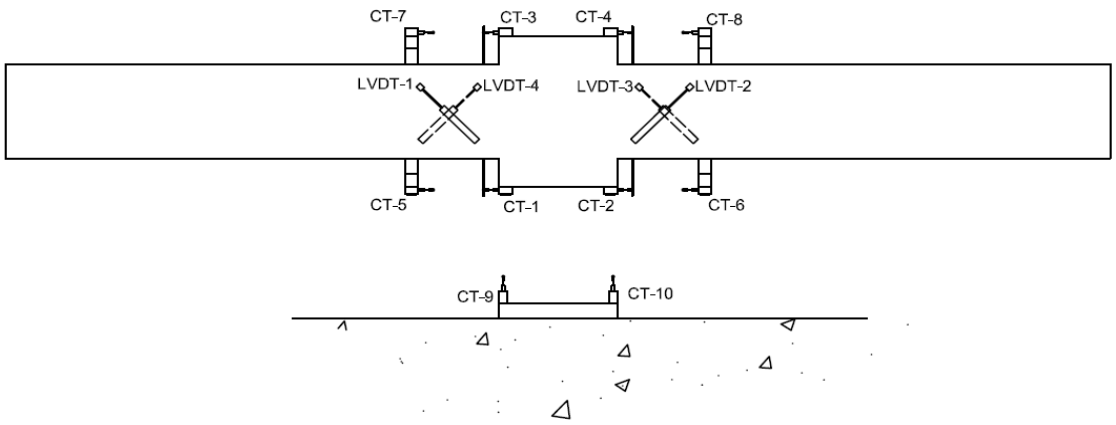

Figure 3.21 DCT and LVDT instrumentation labels

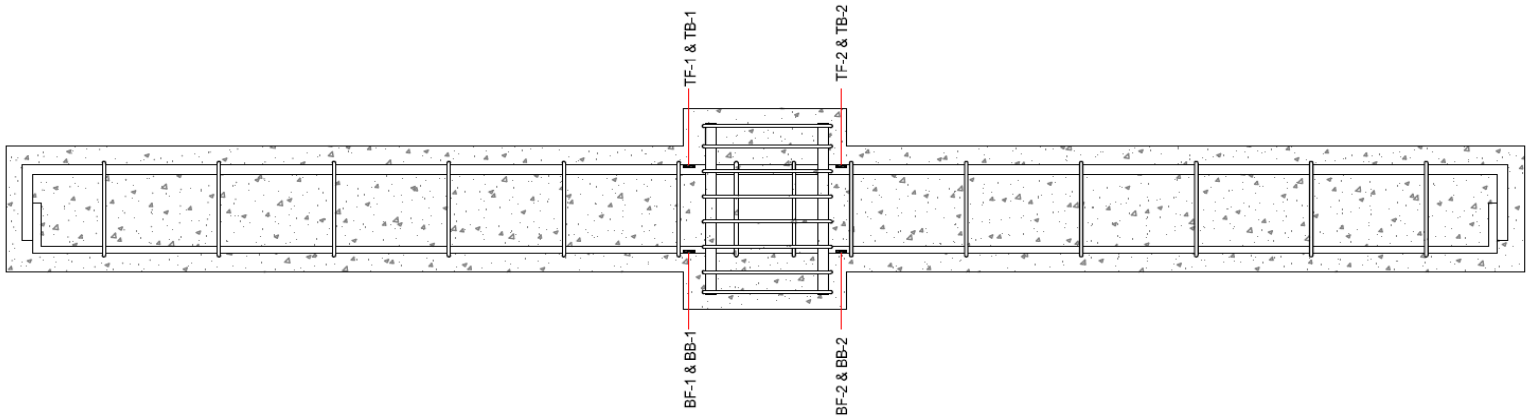

b) Strain gauge labels for D series

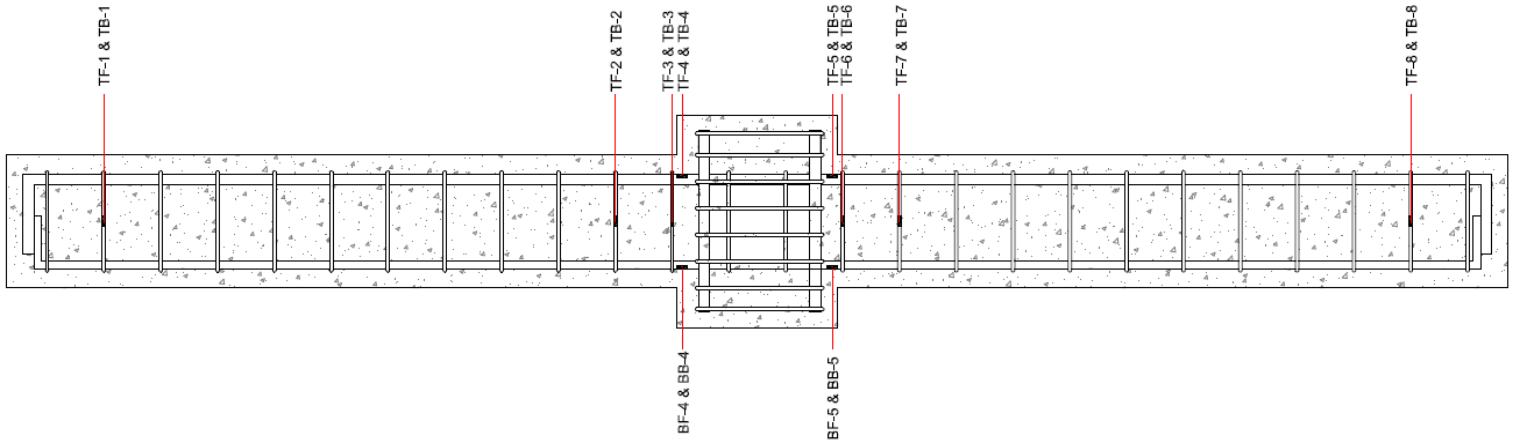

c)Strain Gauge labels for D/2 series

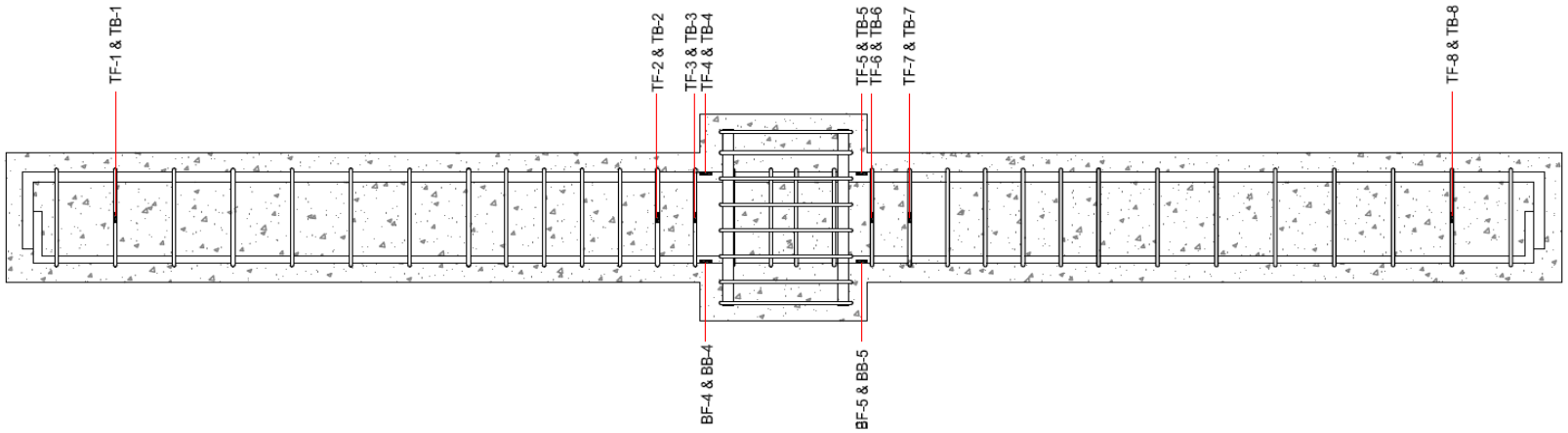

d) Strain gauge labels for D/s series

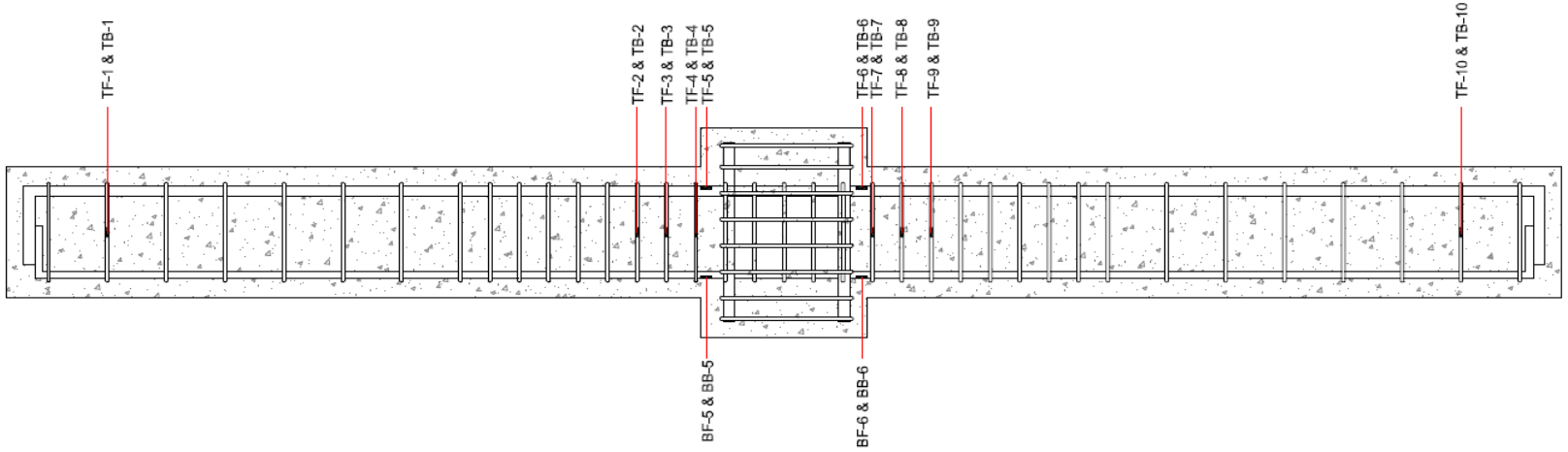

e) Strain gauge labels for D/4 series

Figure 3.22 Location and Labels for strain gauges in various test series.

3.6.3 Testing Sequence

All specimens were subjected to the same loading sequence. The load sequence in this experimental program was based on the conventional load sequence used in reverse-cyclic loading similar to one adopted by Parra-Montesinos (2005). Initially drift increments of 0.25% drift were used up to 1.5% drift, followed by 0. 5% drift increments up to 3% drift. The drift increments increased to 1.0% thereafter up to failure. Generally 3 cycles (designated as cycles A, B, C) were used at each drift stage (see **Figure 3.23**). In case of failure of the beam the positive bending direction, loading continued under cyclic loading depending in the negative bending direction. At this stage increments of 1% to 2.0% drift were used keeping in mind the residual strength of the beams and limitations of the testing apparatus. It is noted that under cyclic loading the beams were cycled only two times for each drift stage.

Throughout testing, cracks were marked and their widths were measured using a transparent crack-width reader. Measurement were taken, labelled and recorded up to a crack width of 2mm. Visual inspection was conducted at each drift stage and the general conditions of the beam including spalling, disintegration and crushing of concrete were recorded. A photographic record of the specimens at each load stage was also taken.

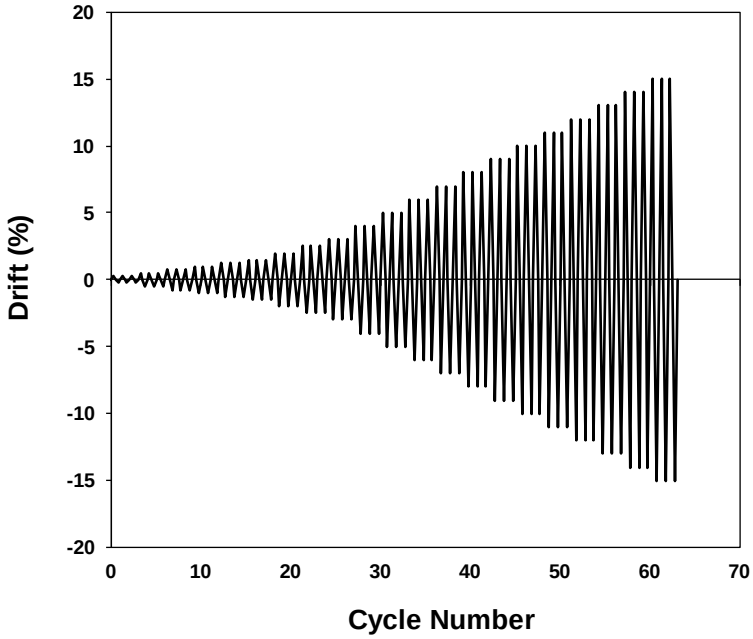

Figure 3.23 Loading Sequence

Chapter 4 Results of the Experimental Program

4.1 Background

In this section, the results obtained from the experimental program are described. A total of nine beams were tested, including two control reinforced beams and seven companion SCFRC beams. The beams had varying amounts of transverse reinforcement (s = d, d/2, d//3 and d/4) and fiber contents to illustrate the effects of transverse reinforcement and steel fibers on member response. The behavior of the beams is presented in terms of load-displacement response, load-drift response, crack development and strains in reinforcement steel. In addition a photographic record of the tests at major drift stages is presented and key events (such as development of cracks, spalling and crushing of concrete, rupture of steel reinforcing bars, etc.) are summarized

Each beam was loaded with a similar loading protocol. Initially drift increments of 0.25% and 0.5% drift were used up to 3% drift. The drift increments increased to 1.0% thereafter. Generally 3 cycles which were designated as cycles A, B and C were used at each drift stage. At later load stages, drift increments of 2% to 4% were used in some beams. The same loading pattern was applied to all beams until the rupture of the steel reinforcing bars or when a major drop in load was observed. It is noted that testing continued in the negative moment direction after rupture of the positive moment reinforcing bars if sufficient residual capacity remained. In this case, cyclic loading continued considering the residual capacities of the beams and limitations of the test setup.

4.1.1 Beam D/2 -0.0%

All beams in the D/2 test series were reinforced with transverse reinforcement at a hoop spacing of 100 mm, corresponding to half the effective depth of the beams. The same self-consolidating concrete mix was used in all beams with the difference being the quantity of fibers in the mix. Beam D/2-0.0% was the control specimen for this series and was constructed without fibers.

Figure 4.1 and **Figure 4.2** shows the reverse-cyclic response of the specimen in terms of applied load (and Mid-span moment) as a function of displacement (mm), drift (%) and ductility ratio (Δ/Δ_y). The figure also highlights the major events during testing. **Figure 4.3 (a)** and **(b)** show the backbone response in terms of drift and ductility ratio (Δ/Δ_y), respectively. and **Figure 4.3 (c)** and **Figure 4.3 (d)** show the strains in the longitudinal and transverse reinforcement. Major events during the testing of the specimen are graphically presented in **Table 4.1** and **Table 4.2** for the positive and negative bending cycles, respectively.

For this specimen the first vertical flexural cracks started appearing at 0.5% drift in both negative and positive bending cycles with crack widths of less than 0.2mm. Major cracks started concentrating at the faces of the column at subsequent cycles at ±0.5% drift. The first diagonal shear crack appeared at +1.0% drift; the load at this stage was recorded to be 47 KN (moment=26KN.m) for positive bending. Yielding of the longitudinal reinforcement was observed at displacements of 12.9mm (1.2% drift) and 18.1mm (1.7% drift) for the positive and negative bending moment cycles, respectively. The loads at these stages were recorded to be 54.2KN (moment=29.8KN.m) and 78.6 KN (moment=43.2KN.m), respectively. At the 1.5% drift stage (16mm displacement), the major vertical cracks widened considerably compared to the previous stages to reach crack widths of 1.5mm and 0.75mm in positive and negative bending, respectively. At the drift stages of ±2.0% (±22mm displacement) drift the diagonal shear cracks also widened slightly further.

At the -3.0% drift stage (-33mm displacement), the direction of the cracks near the face of the column was aligned with the 15M reinforcing bars such that the cover concrete beyond the level of 15M reinforcing bars began to spall and disintegrate. The first spalling of concrete occurred near the edges of the major vertical cracks near the faces of the column-stub and this was followed by general disintegration of concrete within the plastic hinge area (d from the faces of the middle block) at ±4.0% drift (±44mm displacement). Severe spalling and disintegration of the concrete including crushing of concrete within the core concrete area near the right face of the column was observed at ±4.5% (±49.5mm displacement) drift.

Clockwise rotation of the column-stub was also observed at this stage and recorded by the inclinometer.

Failure of the beam occurred at the ±4.5% drift stage. Recorded loads at failure for the positive and negative bending were 54.5KN (moment=30KN.m) and 59.7 KN (moment=32.8KN.m) respectively. At the cycle corresponding to -4.5%B, the 20M reinforcing bars were completely exposed and the 15M reinforcing bars had buckled; in addition one of the exposed hoops had partially opened up. Significant drop in load was observed at this stage. The concrete cover at the bottom of the beam near the column had also completely spalled off (in the compression zone for negative bending with 20M reinforcing bars in tension); failure of the beam in negative bending was deemed to be due to crushing of concrete and excessive loss of concrete in the compression zone. The residual loads at failure were recorded to be 18.3 KN (moment=10.1KN.m) and 28 KN (moment=15.4KN.m) for the negative and positive bending moment cycles, respectively.

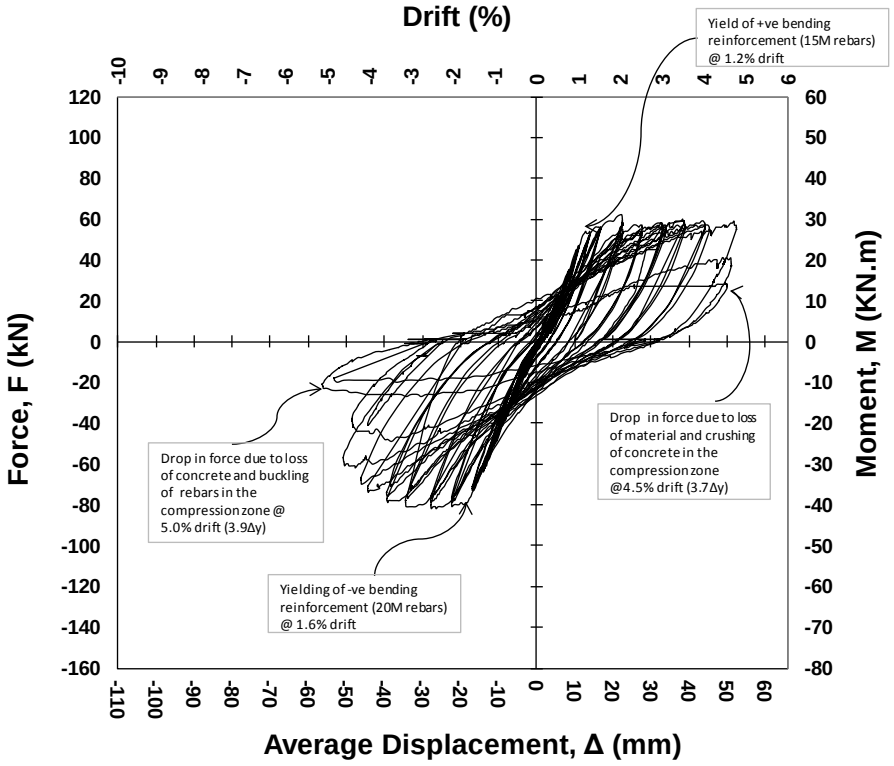

Figure 4.1 Force-displacement diagram for beam D/2-0.0%

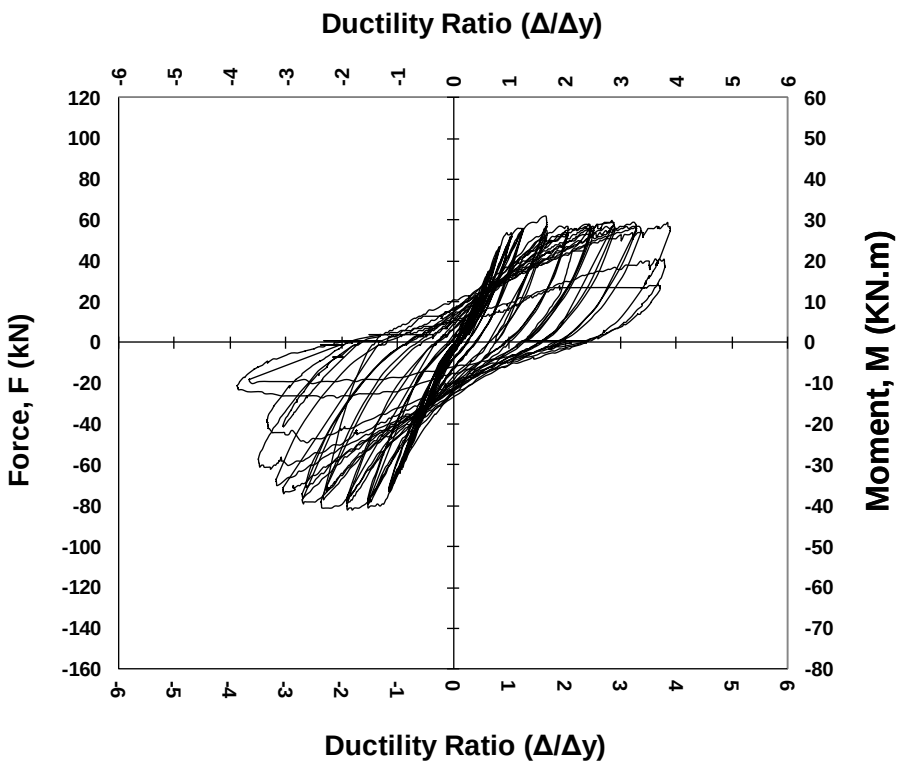

Figure 4.2 Force vs. ductility ratio for beam D/2-0.0%

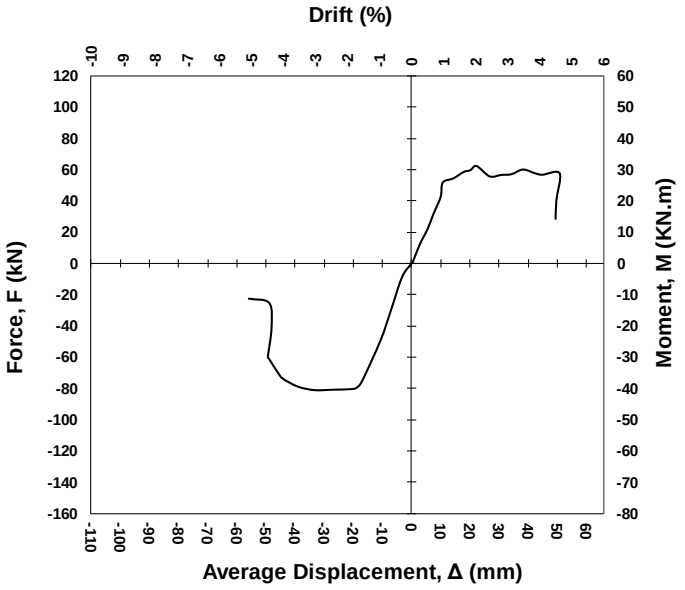

(a) Force-displacement response envelope

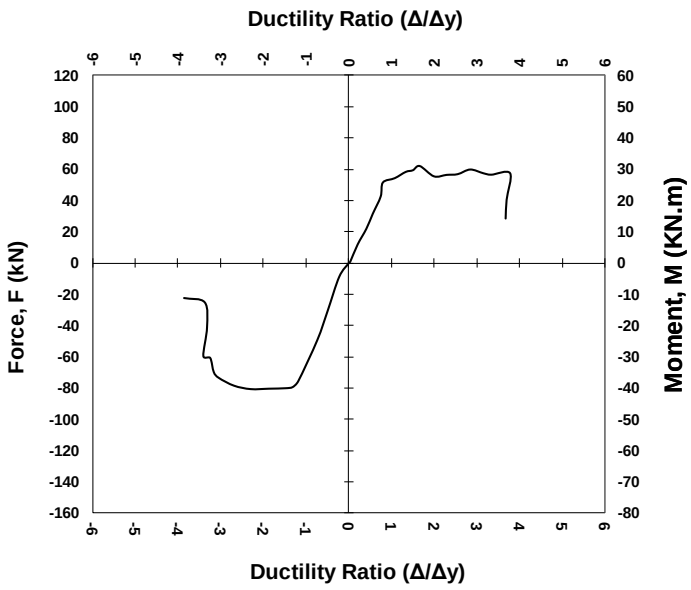

(b) Force-ductility ratio response envelope

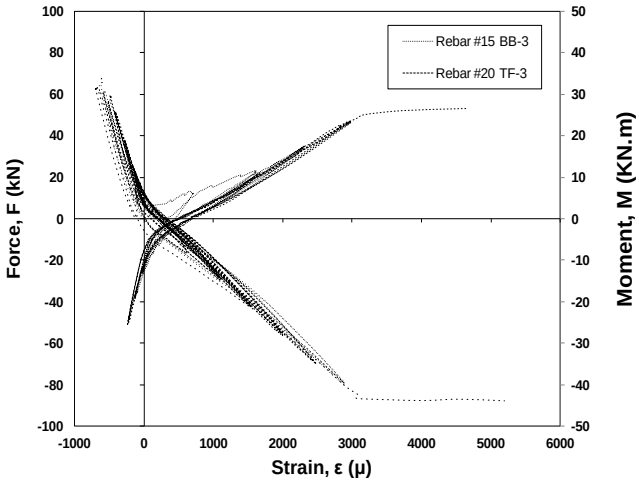

(c) Strain in longitudinal reinforcement at the face of t he middle block

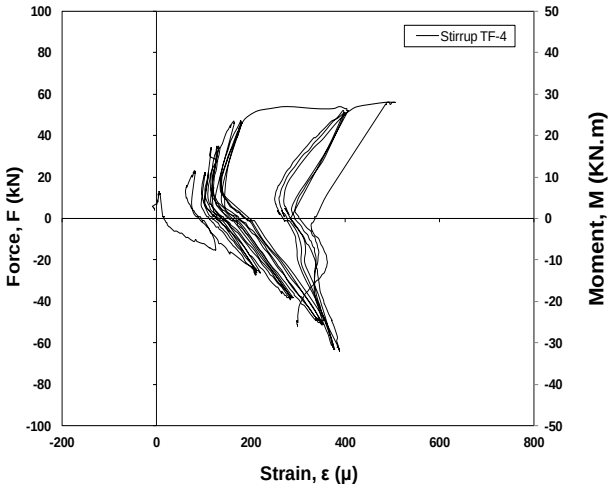

(d) Strain in a typical steel stirrup near the face of the middle block

Figure 4.3 Experimental results for beam D/2-0.0%

Table 4.1 Major events during positive bending for specimen D/2-0.0%

D/2-0.0%	Positive bending - #15 rebars in tension		
Δ(mm)	Drift (%)	Δ/Δy	Comments
5.5	0.5	0.4	Vertical cracks appeared at approximately D/2 spacing.
			
Δ(mm)	Drift (%)	Δ/Δy	Comments
11	1	0.9	First diagonal cracks appeared in the right side cantilever beam. A vertical crack appeared near the center of the middle block
			
Δ(mm)	Drift (%)	Δ/Δy	Comments
22	2	1.7	Vertical cracks at the faces of the middle block opened up almost equally on both sides. Other cracks stopped widening. Diagonal cracks extended.
			
Δ(mm)	Drift (%)	Δ/Δy	Comments
38.5	3.5	3.0	Minor spalling around the vertical cracks at the faces of the middle block at the bottom was observed.
			

Table 4.1 Major events during positive bending for specimen D/2-0.0% - continued

Δ(mm)	Drift (%)	Δ/Δy	Comments
44	4	3.0	General disintegration of concrete within the plastic hinge area Increased spalling at the bottom was seen.. Small spalling between the disintegrated chunks of concrete within the hinging area mostly at the right side of the middle block. In-plane rotation of middle block slightly increased.

Δ(mm)	Drift (%)	Δ/Δy	Comments
49.5	4.5	3.8	4.5% cycle B - Severe spalling of the core concrete was observed. Dowel action at the face of the middle block was more pronounced. Bottom rebar completely exposed within the spall zone. Significant drop in load (approximately to half of initial).

Δ(mm)	Drift (%)	Δ/Δy	Comments
49.5	4.5	3.8	4.5% cycle C - Significant spalling and loss of material was observed. Bottom cover was completely lost; core concrete was significantly disintegrated/ spalled. Failure occurred due to loss of material and severe spalling of the cover and disintegration of the core region, slight buckling of the bottom rebars and dowel action of the rebars was observed.

Table 4.2 Major events during negative bending for specimen D/2-0.0%

D/2-0.0%	Negative bending - #20 rebars in tension		
Δ(mm)	Drift (%)	Δ/Δy	Comments
-5.5	-0.5	-0.3	Vertical hairline cracks appeared at approximately D/2 spacing.
			
Δ(mm)	Drift (%)	Δ/Δy	Comments
-11	-1.0	-0.5	More vertical cracks appeared; cracks mostly concentrated at the face of the middle block and extended into the middle block.
			
Δ(mm)	Drift (%)	Δ/Δy	Comments
-22	-2	-1.2	A few more vertical and diagonal cracks appeared; existing diagonal cracks extended slightly. Cracks at the faces of the support opened up unequally (more on the right hand side face of the middle block 2.00 mm vs.1.25 mm)
			
Δ(mm)	Drift (%)	Δ/Δy	Comments
-38.5	-3.5	-2.1	Cracks started aligning with top longitudinal rebars. Dowel action may have occurred. Slight drop in load was observed (possibly due to the slight spalling in the bottom).
			

Table 4.2 Major events during negative bending for specimen D/2-0.0%- continued

D/2-0.0%			
Δ(mm)	Drift (%)	Δ/Δy	Comments
-44	-4	-2.4	First small spalling at the top of the middle block appeared immediately to the right of the middle block. The horizontal cracks along the longitudinal rebars widened and were more pronounced at the right side of the middle block. It seemed that the cover above the top rebars was about to spall.
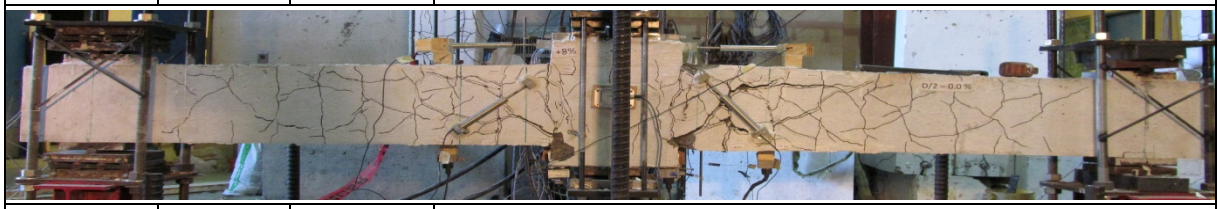			
Δ(mm)	Drift (%)	Δ/Δy	Comments
-49.5	-4.5	-2.7	4.5% Cycle A - Horizontal crack aligned with the top rebar was well defined and shifted the cover outward. Top concrete cover was separated from the core by this crack. Increased spalling and disintegration of concrete was seen mostly at the right side. Longitudinal reinforcement and hoops were exposed at the right side as the cover concrete was spalled. Core concrete was also disintegrated to a moderate extent.
			
Δ(mm)	Drift (%)	Δ/Δy	Comments
-49.5	-4.5	-2.73	4.5% Cycle C - Top rebars were completely exposed. Slight buckling of the bottom rebars (#15) and significant drop in load was observed. One of the hoops within the hinge region started to open up.
			

4.1.2 Beam D/2 0.75%

This beam was the second beam in the D/2-series and had identical properties to the control specimen D/2-0% with the exception being the provision of steel fibers. The beam was the first of three fiber-reinforced specimens in this series and was reinforced with 0.75% fibers by volume of concrete.

Figure 4.4 and **Figure 4.5** show the reverse-cyclic response of the specimen in terms of applied load (and Mid-span moment) as a function of displacement (mm), drift (%) and ductility ratio (Δ/Δ_y). **Figure 4.4** also highlights the major events during testing. **Figure 4.6 (a)** and **(b)** show the backbone response in terms of drift (%) and ductility ratio (Δ/Δ_y). **Figure 4.6 (c)** and **Figure 4.6 (d)** show the strains in the longitudinal and transverse reinforcement. Major events during the testing of the specimen are graphically presented in **Table 4.3** and **Table 4.4** for the positive and negative bending cycles, respectively.

Flexural cracks started appearing for this specimen at about 0.5% drift (11mm displacement) with maximum crack width of less than 0.2mm. More cracks developed at approximately d/2 spacing with two major cracks at the left and right sides of the column. At about 1.5% drift (16.5mm displacement) the major cracks were widening further while all other cracks appeared to retain the same width. Yielding of the 15M reinforcing bars was observed at approximately +1.1% drift (12.5mm displacement) under a load of 58.8KN (moment=32.3KN.m). Small diagonal cracks appeared at +1.3% drift (13.8mm displacement). The 20M reinforcing bars yielded at approximately -2.0% drift (21mm displacement) at a load of 89.9KN (moment=49.4KN.m).

The first signs of cover spalling were observed at +3.0% drift (33mm) at the top right side of the column-stub. A small wedge of concrete was also disintegrated at the bottom right side. At this point the major cracks had significantly widened while mo major changes were occurring at the other cracks. In addition, a horizontal crack appeared at the top right side aligned with the top longitudinal reinforcement.

Slight drop in load was observed in the first cycle of +4.0% drift stage (44mm displacement) followed by further sudden drop of 15% in the second +4.0% cycle. Some shifting of the middle block with respect to the beam was observed in the first cycle of +4.5% drift stage (49.5mm displacement). This was followed by rupture of one of the 15M reinforcing bars in the second +4.5% cycle at a load of 50.6KN (moment=27.83KN.m). A 21.0% drop in load was observed at the third +4.5% cycle. Both top and bottom reinforcing bars were exposed at the 5.0% drift stage (55mm displacement). The second 15M reinforcing bar ruptured at the second +5.0% drift stage which was followed by significant drop (61.0%) in load. The specimen was deemed to have completely failed at the second cycle of the -5.0% drift stage.

The ultimate capacities of this beam were 89.9KN (moment=49.4KN.m) for negative bending and 58.8KN (moment=32.3KN.m) which were approximately 14.5% and 8.0% higher than what was observed in the control specimen for negative and positive bending, respectively. The strength at yield also increased in negative bending by about 16.0%; yield strength in positive bending was almost the same as the control beam.

When compared to the control beam, specimen D/2-0.75% exhibited slight improvements in response. Cracking and spalling behaviour was significantly improved and not as much disintegration of concrete (in both the cover and core region) was observed compared to the control specimen. In terms of hysteretic response, behaviour was similar to what was observed in the control specimen however pinching was reduced. The improvements in response can be linked to the improved crack control, damage tolerance and confinement in the fiber reinforced specimen. It is also noted that due to the addition of the fibers this specimen showed a different cracking pattern in the plastic hinge region; only two major cracks developed at the right and left sides of the column-stub while all other cracks remained well controlled (this was also observed in the remaining SCFRC specimens). It is also noted that the positive moment reinforcement (2-15M) which corresponded to 50% of the reinforcement in the negative moment region ruptured during testing and limited the overall performance of this specimen

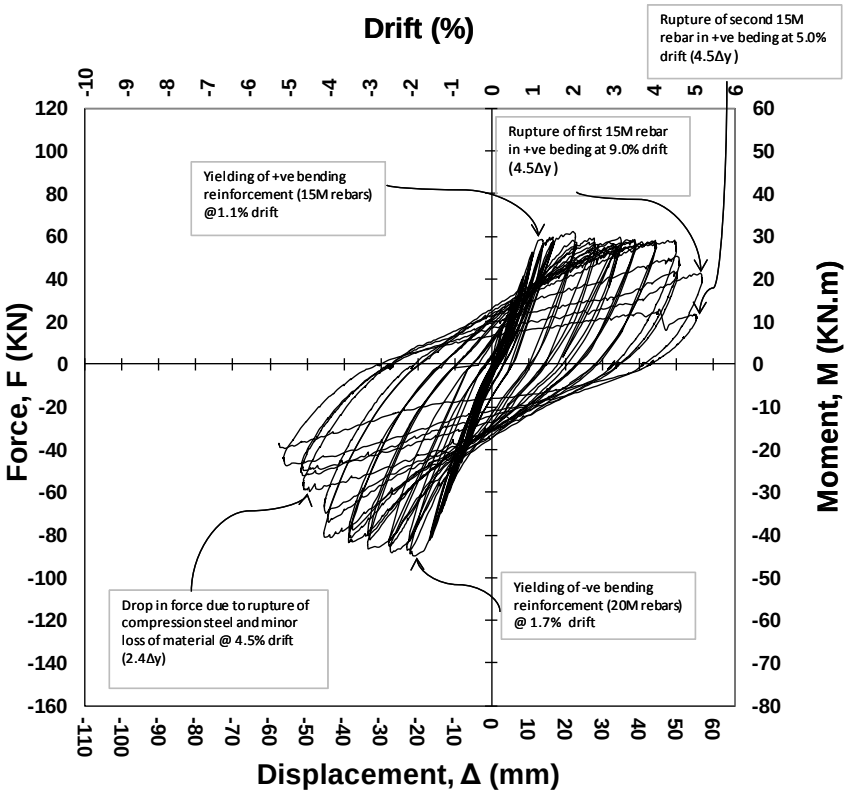

Figure 4.4 Force-displacement diagram for beam D/2-0.75%

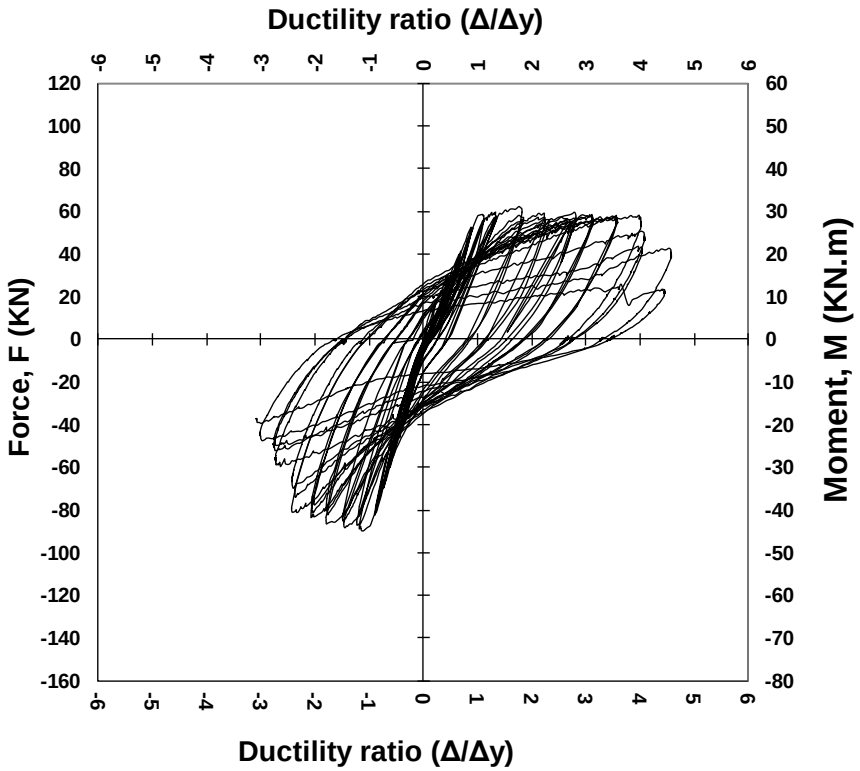

Figure 4.5 Force vs. ductility ratio for beam D/2-0.75%

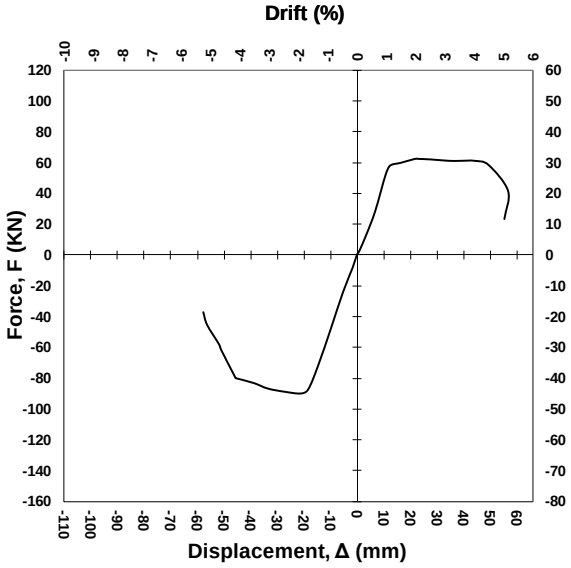

(a) Force-displacement envlope

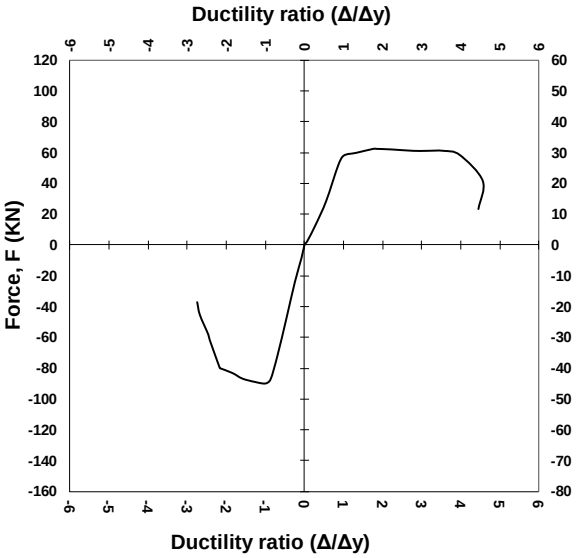

(b) Force-ductility ratio response envelope

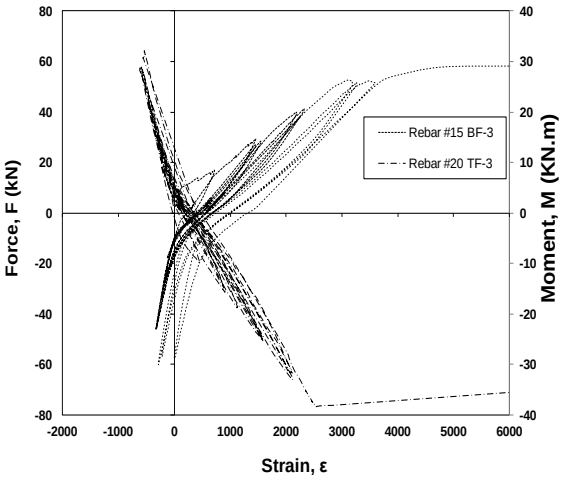

(c) Strain in longitudinal reinforcement at the face of t he middle block

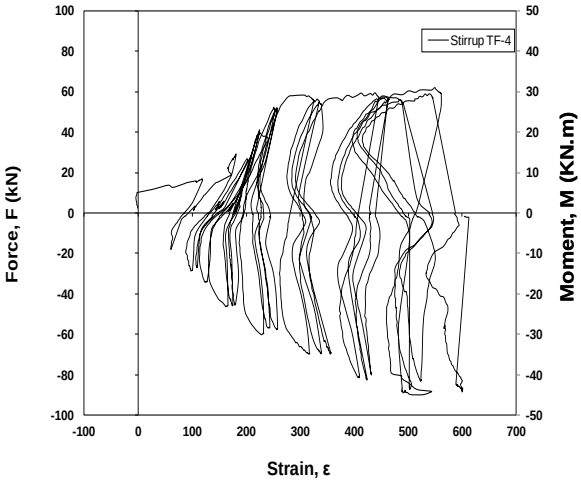

(d) Strain in a typical steel stirrup near the face of the middle block

Figure 4.6 Experimental results for beam D/2-0.75%

Table 4.3 Major events during positive bending for specimen D/2-0.75%

D/2-0.75%	Positive bending - #15 rebars in tension		
Δ(mm)	Drift (%)	Δ/Δy	Comments
5.5	0.5	0.4	Vertical cracks appearing at the bottom at approximately D/2 spacings.
			
Δ(mm)	Drift (%)	Δ/Δy	Comments
16.5	1.5	1.3	Vertical crack at the bottom at the face of the support opened up considerably. Diagonal cracks extended further.
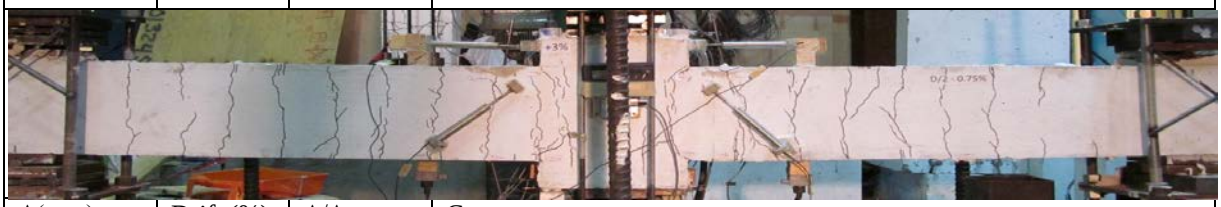			
Δ(mm)	Drift (%)	Δ/Δy	Comments
22	2	1.8	widening of cracks was seen at only two cracks on each side of the middle block. Other cracks remained at almost the same width. Yielding of #20 rebars was observed at approximately 1.9% drift (21mm displacement).
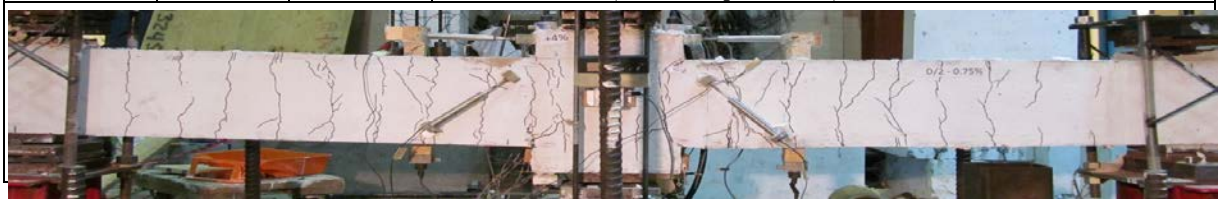			

Table 4.3 Major events during positive bending for specimen D/2-0.75%- continued

D/2-0.75%			
Δ(mm)	Drift (%)	Δ/Δy	Comments
33	3	2.7	Major cracks widened further. First signs of cover spalling was seen at around the cracks specially at the right side. A small wedge at the bottom in the right side seemed to be disintegrated but was still in place. Load slightly decreased.
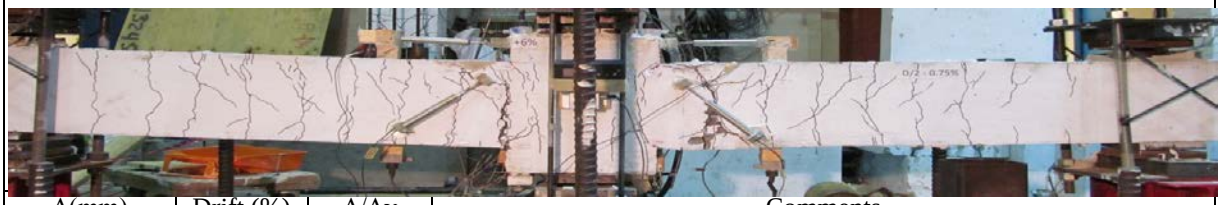			
Δ(mm)	Drift (%)	Δ/Δy	Comments
38.5	3.5	3.1	Slight loss of material was observed in the right hand side crack. In-plane rotation of middle block was visible. Middle block was slightly shifting down against the right hand side crack.
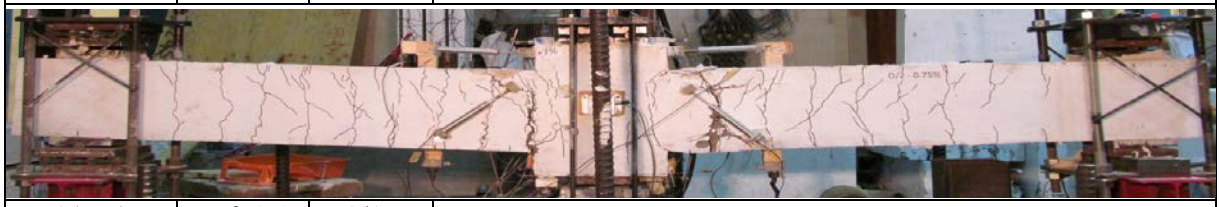			
Δ(mm)	Drift (%)	Δ/Δy	Comments
44	4	3.5	4% Cycle A - Slight drop in load was seen compared to previous negative stage. Further minor spalling at the cracks specially the bottom right hand side major cracks was observed. Concrete wedge at the bottom right hand side seemed to be completely disintegrated but was still in place. Middle block shifted downward against the right hand side crack.
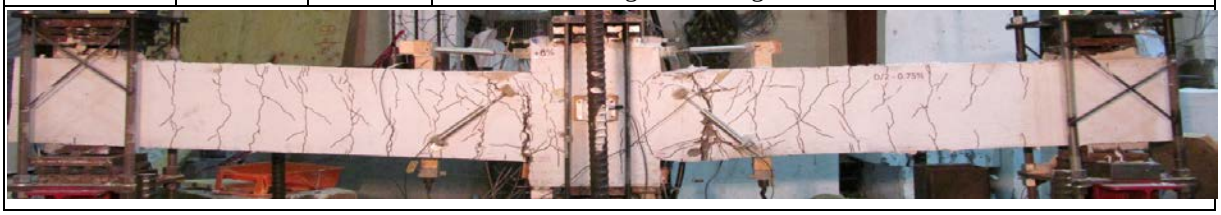			

Table 4.3 Major events during positive bending for specimen D/2-0.75%-continued

D/2-0.75%			
Δ(mm)	Drift (%)	Δ/Δy	Comments
49.5	4.5	3.9	+4.5% Cycle A - Major shift in the middle block at the right hand side crack was observed with no reduction in load. The disintegrated wedge at the bottom of the right hand side crack started to spall out of place.

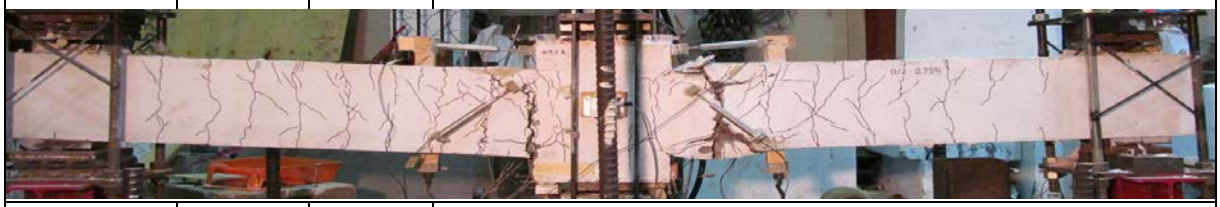

Δ(mm)	Drift (%)	Δ/Δy	Comments
49.5	4.5	3.9	4.5% Cycle B - Rupture of one of bottom (#15) rebars. Drop in load of 12% was recorded in the positive bending compared to +4.5% A.

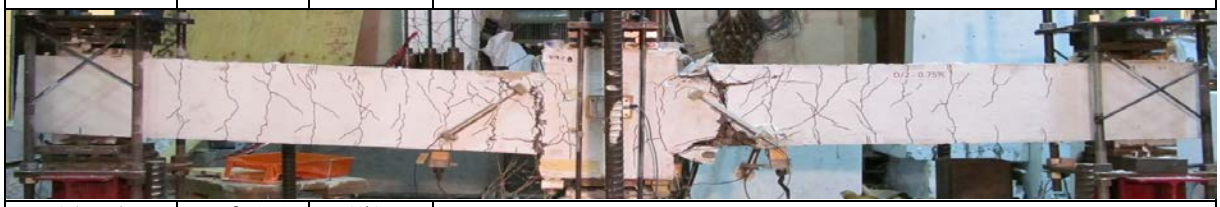

Δ(mm)	Drift (%)	Δ/Δy	Comments
55	5	4.4	5% Cycle B - Both of the bottom rebars (#15) ruptured. Significant drop (61%) in load down to 23KN was observed. Significant shift in middle block against the crack (~50mm) was observed. Beam was considered failed at this stage of the positive bending.

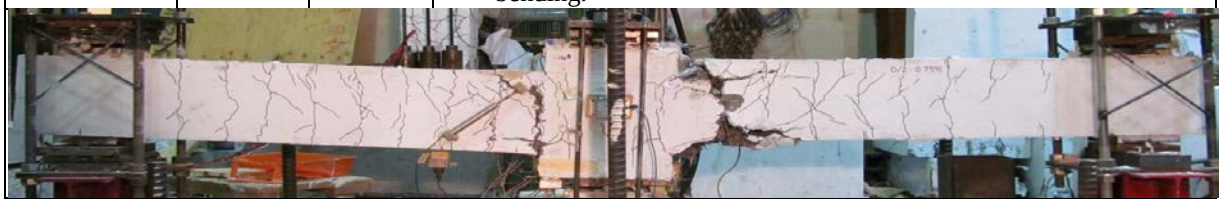

Table 4.4 Major events during negative bending for specimen D/2-0.75%

D/2-0.75%	Negative bending - #20 rebars in tension		
Δ(mm)	Drift (%)	Δ/Δy	Comments
-11	-1.0	-0.4	Several vertical hairline cracks appeared; cracks concentrated at the face of the middle block and extended into the middle block.
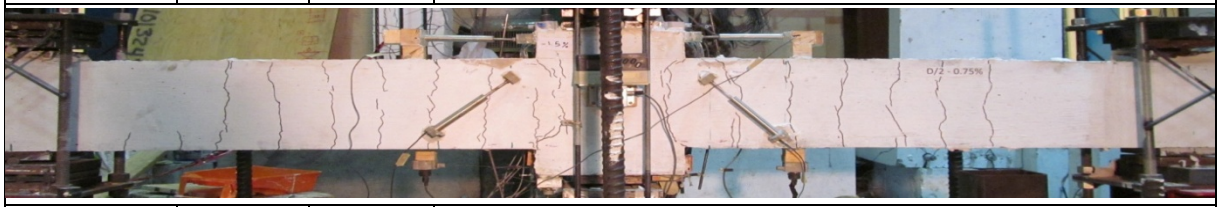			
Δ(mm)	Drift (%)	Δ/Δy	Comments
-16.5	-1.5	-0.7	Almost same number of vertical and diagonal cracks as the previous drift stage was recorded. Forking of cracks was seen around existing cracks. Yielding of #15 rebars was recorded at approximately 1.2% drift (22.5mm displacement).
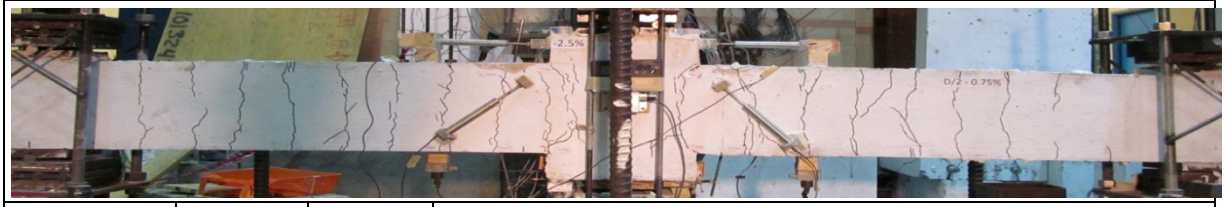			
Δ(mm)	Drift (%)	Δ/Δy	Comments
-27.5	-2.5	-1.3	Crack widths were well beyond 2 mm at this stage. First horizontal crack at the rebar level appeared at the top of the middle block. Crack on the left changed to a diagonal path to reach the top of the middle block.
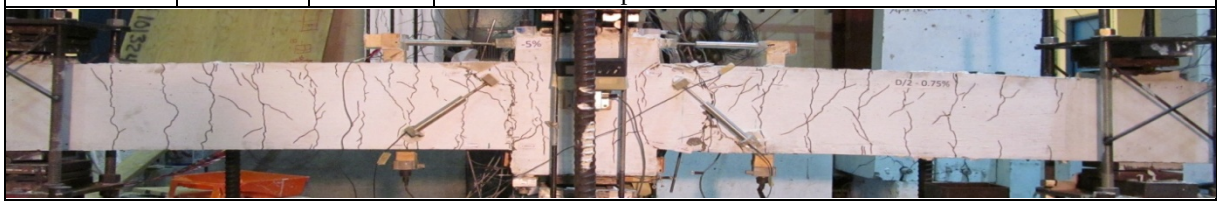			

Table 4.4 Major events during negative bending for specimen D/2-0.75%-continued

Δ(mm)	Drift (%)	Δ/Δy	Comments
-44	-4	-2.1	4% Cycle A - Further minor drop in load was observed. Middle block shifted up against the right hand side crack. Left hand side major crack was not widening as much. The middle block seemed to be hinging at the right hand side crack. Further minor cover spalling was seen at the left hand side crack.
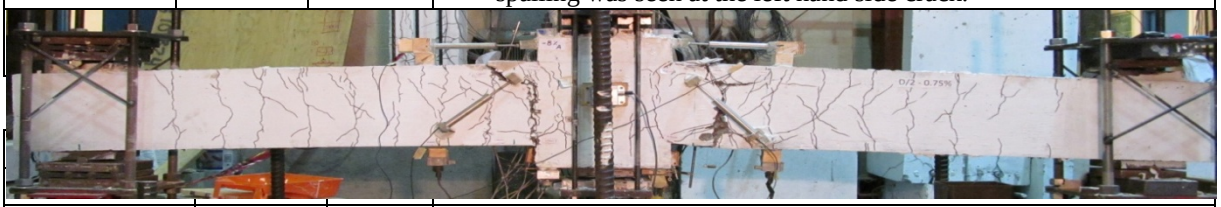			
-44	-4	-2.1	4% Cycle B - Sudden ~15% drop in load was recorded compared to -4%A.
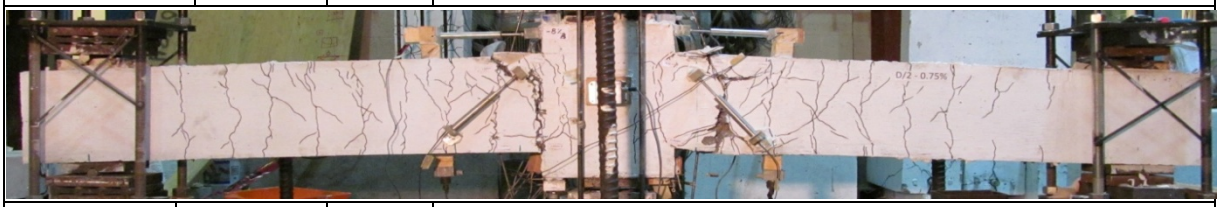			
Δ(mm)	Drift (%)	Δ/Δy	Comments
-55	-5	-2.6	5% Cycle A - Bottom rebars and hoops were exposed within the plastic hinge zone at the right side. Significant drop in load to 58 KN (28% compared to -4.5%A) was recorded. Shifting of the middle block in the upward direction was not as pronounced as the in the downward direction. Bottom rebars had buckled.
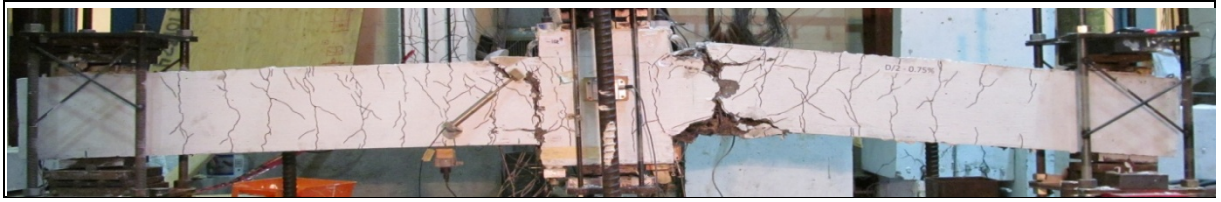			

4.1.3 Beam D/2 1.0%

This beam is the third specimen in the D/2-series. The steel fiber content in this beam was 1.0% by volume of concrete. This specimen allows for an investigation into the effect of increasing fiber content on member response.

Figure 4.7 and **Figure 4.8** show the reverse-cyclic response of the specimen in terms of applied load (and Mid-span moment) as a function of displacement (mm), drift (%) and ductility ratio (Δ/Δ_y). The figure also highlights the major events during testing. **Figure 4.9 (a)** and **(b)** show the backbone response in terms of drift (%) and ductility ratio (Δ/Δ_y). **Figure 4.9 (c)** and **(d)** show the strains in the longitudinal and transverse reinforcement. Major events during the testing of the specimen are graphically presented in **Table 4.5** and **Table 4.6** for the positive and negative bending cycles, respectively..

For this beam, hairline cracks (<0.2mm) started appearing at the load stage corresponding to 0.5% drift (5.5mm displacement) and slightly wider flexural cracks, at approximately D/2 spacing, appeared at about 1.0% drift (11mm displacement). Similar to previous beams, cracks started concentrating near the faces of the column-stub with two major cracks developing at each side. At about 1.0% drift (11mm displacement) only the major cracks began widening further. The 15M reinforcing bars in the positive moment region began yielding at +1.5% drift (16.5mm displacement) at a load of 68.1KN (moment=37.5KN.m). Slight surface spalling was observed at 2.0% drift (22mm displacement) which was followed by a 8.0% drop in load in the second cycle. The 20M reinforcing bars began yielding at -2.0% drift (-44mm displacement) in negative bending at a load of 79.6KN (moment=43.67KN.m). The largest crack widths were over 2mm at the end of the +2.0% drift stage (+22 displacement). The first signs of spalling were also observed at this drift stage. For the negative bending side, the crack width limit of 2mm was reached at the -2.5% drift stage (27.2mm displacement). Further surface spalling was observed at the ±3.0% drift stages (±33nn displacement) which were accompanied by drops in load of 6.0% and 14.0% in the positive and negative bending cycles, respectively.

Significant opening of the major crack at the left side of the column-stub was noted at the +3.5% drift (+38.5mm displacement) stage with disintegration of the cover concrete at the top and bottom faces of the beam. This was accompanied by 9.0% and 18.0% drops in load carrying capacity in positive and negative bending at the same drift stages respectively. One of the 15M reinforcing bars ruptured in positive bending during the first +4.0% drift stage (44mm displacement) resulting in a 42.0% drop in load compared to the previous drift stage. The second 15M reinforcing bar ruptured at the second +4.0% drift cycle at which point the top concrete cover showed signs of spalling but the cover concrete was still hanging in place. This was followed by a 92.0% drop in load compared to the previous drift stage. Significant in-plane rotation of the column was also observed at this stage. Although the beam had essentially failed, it was decided to continue loading the beam under cyclic loading in the negative moment direction under cyclic loading. Loading continued until a load stage corresponding to -6% drift (66mm displacement) after which testing was stopped. It can also be observed that the load drops at about -3.5% drift (38.5mm displacement) in negative bending which can be related to the rupture of compression steel.

When comparing to the control specimen, it is to note that no major crushing or spalling was observed during the test; while some disintegration was observed mainly near major cracks, the core concrete showed little signs of crushing and the cover remained in place to the end of testing. However similar to was observed in the previous fiber-reinforced specimen crack opening within the plastic hinge region concentrated at major cracks near the face of the column stub while all other cracks remained well controlled. In terms of hysteretic response, the behavior of the beam in positive bending remained similar to the control specimen and the beam with 0.75% fibers with no major improvements in peak strength or ductility. As was observed in the other fiber-reinforced specimen rupture of the positive moment reinforcement occurred during testing. Nonetheless, in negative bending the beam did show ability to carry residual load in negative bending under cyclic loading. Unlike the specimen with 0.75% fibers, as the beam was cycled to drifts corresponding to -6% (66mm displacement) the beam still had significant residual capacity. However the overall performance of the specimen was limited due to the rupture of the positive moment reinforcing bars.

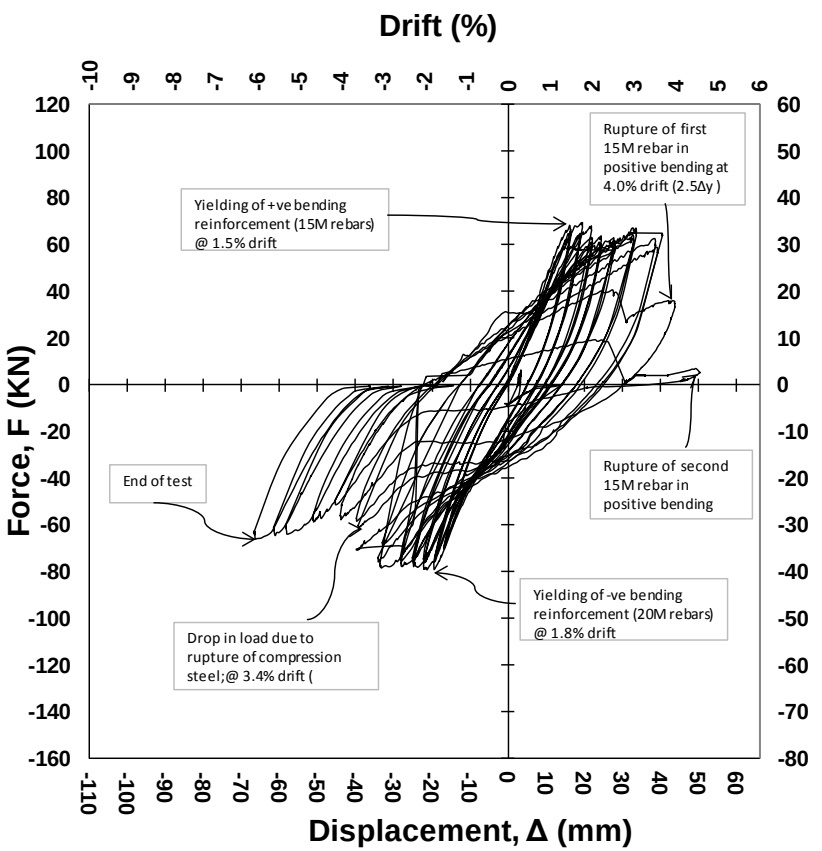

Figure 4.7 Force-displacement diagram for beam D/2-1.0%

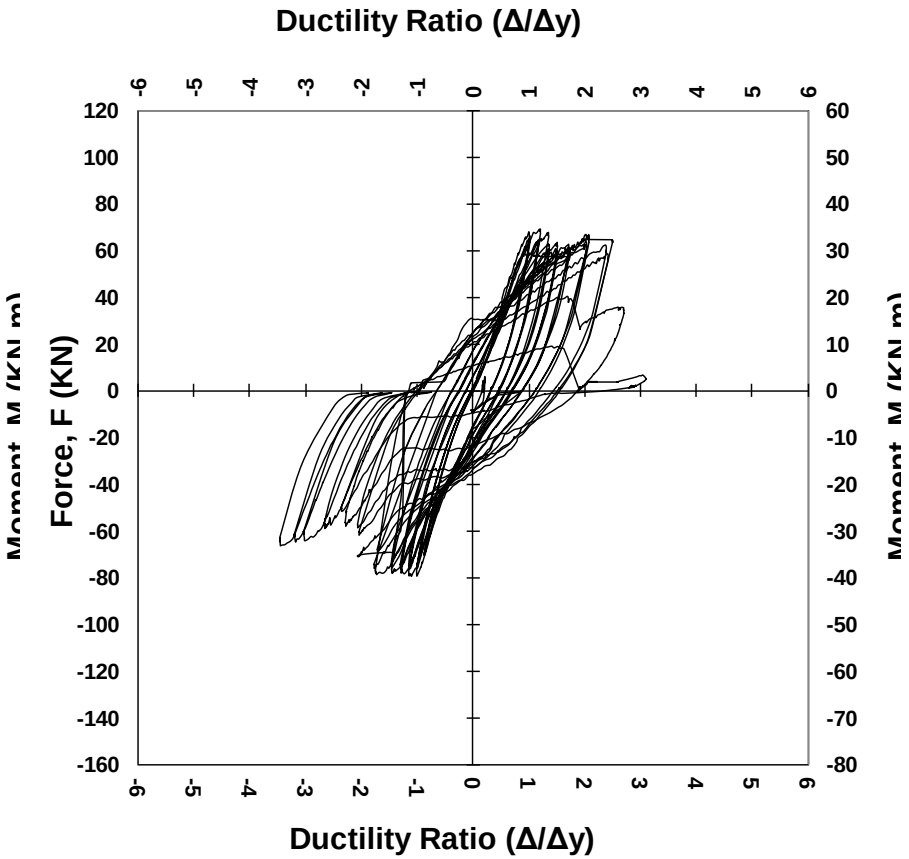

Figure 4.8 Force vs. ductility ratio for beam D/2-1.0%

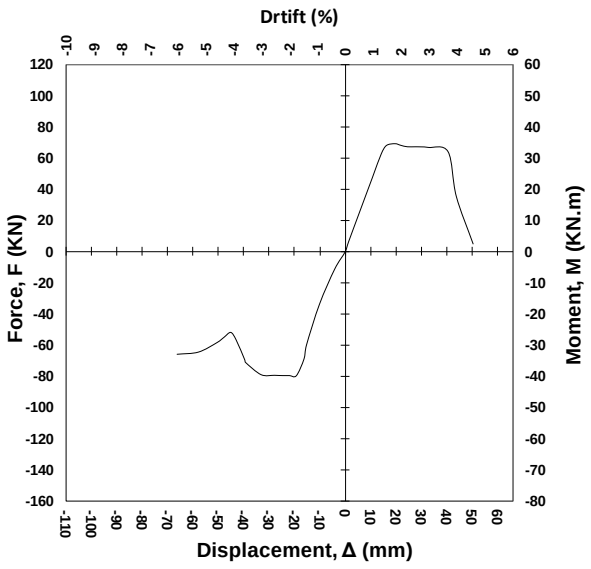

(a) Force-displacement response envelope for beam D/2-1.0%

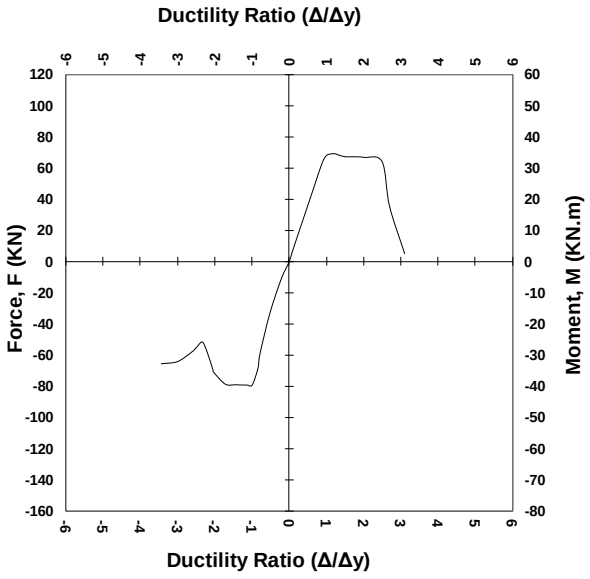

(b) Force-ductility ratio response envelope for beam, D/2-1.0%

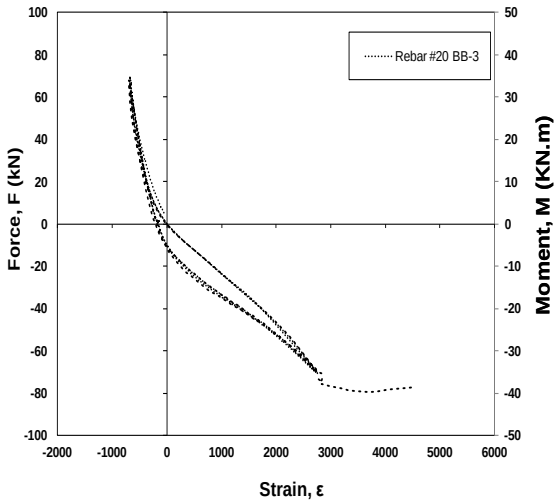

(c) Strain in longitudinal reinforcement at the face of t he middle block

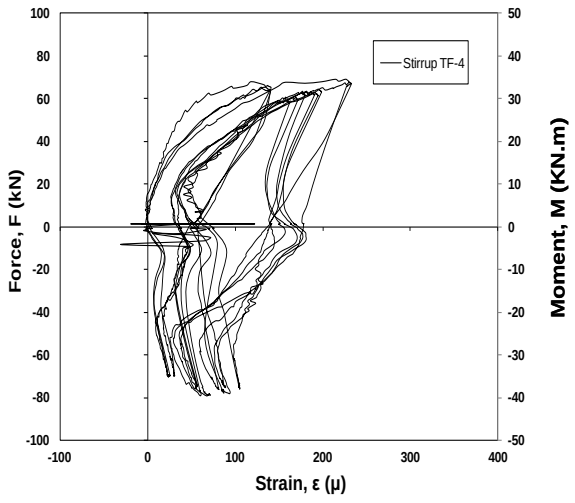

(d) Strain in a typical steel stirrup near the face of the middle block

Figure 4.9 Experimental results for beam D/2-1.0%

Table 4.5 Major events during positive bending for specimen D/2-1.0%

D/2-1.0%	Positive bending - #15 rebars in tension		
Δ(mm)	Drift (%)	Δ/Δy	Comments
5.5	0.5	0.3	Vertical cracks appearing at the bottom at approximately D/2 spacings. A diagonal crack appeared at about D from the right face of the middle block.
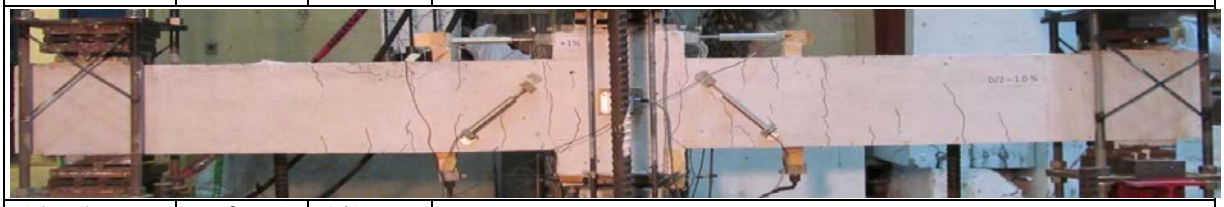			
Δ(mm)	Drift (%)	Δ/Δy	Comments
16.5	1.5	1.0	Major cracks at the faces of the middle block widening. Cracks at other location not changing much. Bottom rebars (#15) are yielding.
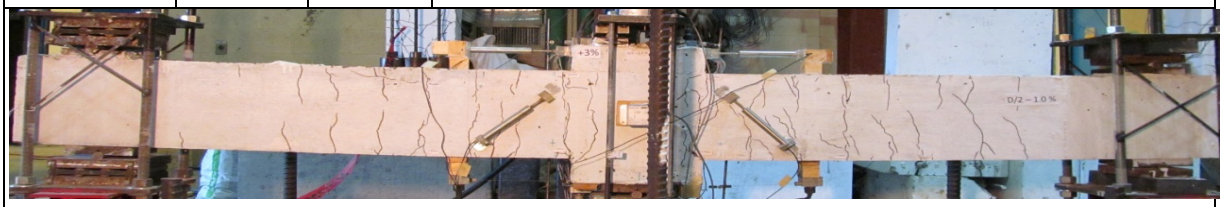			
Δ(mm)	Drift (%)	Δ/Δy	Comments
22	2	1.3	widening of cracks seen at almost only two cracks at each side of the middle block. Other cracks remaining at almost the same width. Slight spalling of the surface at the bottom left face of the middle block. Slight drop (8%=~6KN) in load in the second 2% cycle to ~62KN.
			

Table 4.5 Major events during positive bending for specimen D/2-1.0% - continued

D/2-1.0%	Negative bending - #20 rebars in tension		
Δ(mm)	Drift (%)	Δ/Δy	Comments
33	3	2.0	Load increased slightly (6%=4 KN) compared to 2.5% drift stage. Slight progression of the surface spall was observed at the crack at the top left face of the middle block. Major crack at the left face of the middle block widened. Width of the major crack at the right face of the middle block remained almost the same as the previous stage. Disintegration of a small chunk of concrete at the crack at the bottom left face of the middle block was observed.
			
Δ(mm)	Drift (%)	Δ/Δy	Comments
38.5	3.5	2.4	Significant widening of the left side crack at the bottom. Diagonal/horizontal cracks at the rebar levels opened up at the top and the bottom at the left side of the middle block. 9% drop in load compared to the +3% stage (+33mm displacement) was recorded. Disintegration of concrete at the left side crack was observed.
			
Δ(mm)	Drift (%)	Δ/Δy	Comments
44	4	2.7	4% Cycle A - One of the bottom rebars (#15) ruptured. 42%=26 KN drop in load was recorded. Significant opening of the major crack at left side of the middle block was seen. Complete disintegration of the bottom cover concrete at the left side was observed while concrete wedges remained in place.
			
Δ(mm)	Drift (%)	Δ/Δy	Comments
44	4	2.7	4% Cycle B - 'Second bottom rebar (#15) ruptured. Significant drop in load (92%=33KN) was recorded compared to +4% B stage. Load decreased to 4 KN. Beam was considered failed in positive bending.
			

Table 4.6 Major events during negative bending for specimen D/2-1.0%

D/2-1.0%	Negative bending - #20 rebars in tension		
Δ(mm)	Drift (%)	Δ/Δy	Comments
-5.5	-0.5	-0.3	Vertical cracks appeared at the top at approximately D/2 spacings. A horizontal crack appeared at about 2D from the left face of the middle block.
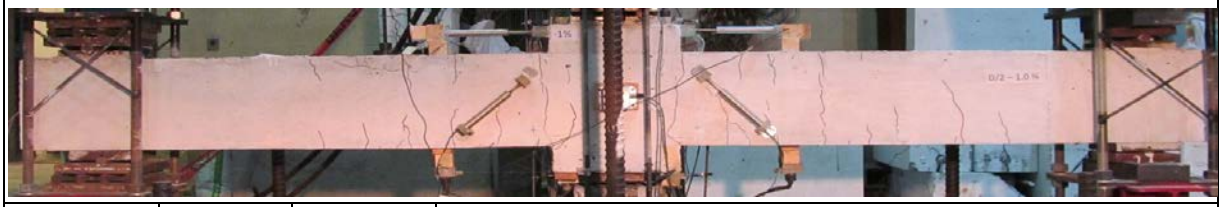			
Δ(mm)	Drift (%)	Δ/Δy	Comments
-16.5	-1.5	-0.7	Almost same number of cracks with existing cracks that extended slightly further. A minor spalled surface at the crack at the bottom right face of the middle block appeared.
			
Δ(mm)	Drift (%)	Δ/Δy	Comments
-22	-2	-1.1	Major cracks' widths remained the same. Top (#20) rebars yielded and minor spalling of the surface at the top left face of middle block was observed.
			
Δ(mm)	Drift (%)	Δ/Δy	Comments
-33	-3	-1.7	14% drop in load at the third 3% cycle (33mm displacement) compared to the first 3% cycle. Major crack at the left face of the middle block widened further. Width of the major crack at the right face of the middle block remained almost the same as the previous stage. Cracks at the right side of the middle block remained almost unchanged.
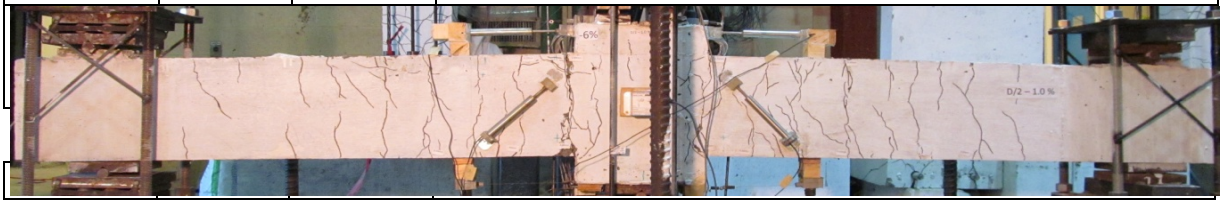			

Table 4.6 Major events during negative bending for specimen D/2-1.0%-continued

D/2-1.0%	Negative bending - #20 rebars in tension		
Δ(mm)	Drift (%)	Δ/Δy	Comments
-38.5	-3.5	-2.0	18% drop in load was recorded in the third 3.5% cycle (38.5mm displacement) compared to the first 3% cycle (33mm displacement).
			
Δ(mm)	Drift (%)	Δ/Δy	Comments
-44	-4	-2.3	-4% Cycle B - 10% drop in load was recorded compared to -4% A stage. Significant in-plane rotation of the middle block was observed.
			
Δ(mm)	Drift (%)	Δ/Δy	Comments
-49.5	-4.5	-2.6	4.5% Cycle A - 14%=7KN increase in load compared to -4% B stage. No major progression of spalling or disintegration of concrete was seen at this stage..
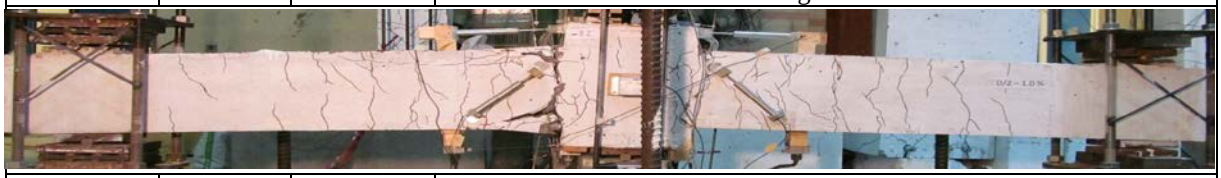			
Δ(mm)	Drift (%)	Δ/Δy	Comments
-55	-5	-2.8	12%=7KN increase in load was recorded compared to -4.5% stage. In-plane rotation of the middle block increased. No major progression of spalling/ disintegration was obsered.
			
Δ(mm)	Drift (%)	Δ/Δy	Comments
-66	-6	-3.4	Load slightly increased. Only minor spalling was observed; beam remains almost in the same condition as the last few stages. End of Test.
			

4.1.4 Beam D/2-1.5%

This beam was the last specimen in the D/2 series. This beam was constructed with a high content of steel fibers (1.5% by volume of concrete). This specimen was meant to investigate the influence of increasing the fiber content beyond 1% on behavior in terms of flexural ductility and crack control.

Figure 4. and **Figure 4.11** show the reverse-cyclic response of the specimen in terms of applied load (and Mid-span moment) as a function of displacement (mm), drift (%) and ductility ratio (Δ/Δ_y). The figure also highlights the major events during testing. **Figure 4.12 (a)** and **(b)** show the backbone response in terms of drift (%) and ductility ratio (Δ/Δ_y). **Figure 4.12 (c)** and **(d)** show the strains in the longitudinal and transverse reinforcement. Major events during the testing of the specimen are graphically presented in **Table 4.7** and **Table 4.8** for the positive and negative bending cycles, respectively.

Hairline cracks started appearing at the first cycle of ±0.5% drift (5.5mm displacement). Further cracks with widths less than 0.2mm appeared up to second and third cycles of ±0.5% drift (5.5mm). More cracks appeared at ±1.0% drift (11mm displacement) with major crack concentrating in the beams at the faces of the column-stub. The maximum width of the cracks at -1.0% drift (-11mm displacement) was recorded 0.2mm which is noticeably less compared to previous specimens which had cracks widths exceeding 0.75mm at this load stage.

At approximately ±1.5% drift (16.5mm displacement), new secondary cracks appeared to be forking off of existing cracks. This forking action also occurred in previous specimens which were reinforced with steel fiber and can be related to redistribution of forces at the crack interface due to presence of fibers. During cycling at this stage the major crack at the right side of the column suddenly widened significantly to width of greater than 2.0mm and the crack on the left side of the column widened to 1.25mm whilst other existing cracks remained well controlled. Examination of strain data indicated that the 15M reinforcing bars yielded at approximately +1.2% drift (12.8mm displacement) at a load of 65.7KN (moment=36.1KN.m); while yielding of the 20M reinforcing bars occurred at -1.5% drift

(16.5mm displacement) at a load of 110.3KN (moment=60.7KN) after which slight drops in load (~5.0% compared to previous drift stages) were observed in the positive and negative bending cycles.

Minor loss of material and surface spalling was first observed at -2.0% drift (-22mm displacement). A small concrete wedge at the top right corner of the column became disintegrated at +2.5% drift (27.5mm displacement) but was hanging in place. Small spalling and disintegration was observed around the major cracks at 2.5% drift and 11.0% drop in load was observed during this stage. Crushing and further disintegration of concrete at the top was observed at -3.5% drift (38.5mm displacement) followed by a 23.0% drop in load. A further drop in load was observed at 4.0% drift (44mm displacement) accompanied by further spalling and disintegration of concrete around major cracks. During the next stage of +4.5% drift stage (49.5mm displacement) the two 15M reinforcing bars in the positive moment region ruptured suddenly during the second cycle resulting in total loss of load carrying capacity in positive bending and hence the specimen failed.

As in the previous specimen it was nonetheless decided to continue cycling the beam in negative bending as significant load carrying capacity remained despite the rupture of the compression reinforcing bars. After the initial drop in load due to loss of compression steel, the load carrying capacity stabilized at -5.5% drift (60.5mm displacement) and from -6.0% (66mm displacement) to -15.0% (155.5mm displacement) drift, load increased slightly without major changes in the condition of the beam under cyclic loading in negative bending. At this stage, the two 20M reinforcing bars ruptured and testing was stopped. It is to note that small disintegrated concrete wedges were still in place and minimal loss of material was recorded even at this large drift.

As expected the cracking behavior and damage tolerance was significantly improved when comparing to the other specimens in this series. As discussed and is visible in the photographic record the cover concrete remained in place until the end of testing. As was observed in the previous fiber reinforced specimens major cracking was concentrated at the column faces with all other cracks remaining well controlled. Unlike other SCFRC

specimens in this series showed an increased peak capacity in both positive and negative bending. As was the case in the previous specimens with fibers, rupture of the 15M reinforcing bars occurred in this specimen and thus no major improvements in terms of hysteretic response were observed in the positive bending cycles. Nonetheless important improvements in negative bending were observed after rupture of the 15M bars, with the beam showing some residual capacity in negative bending up to -15% drift (165mm displacement).

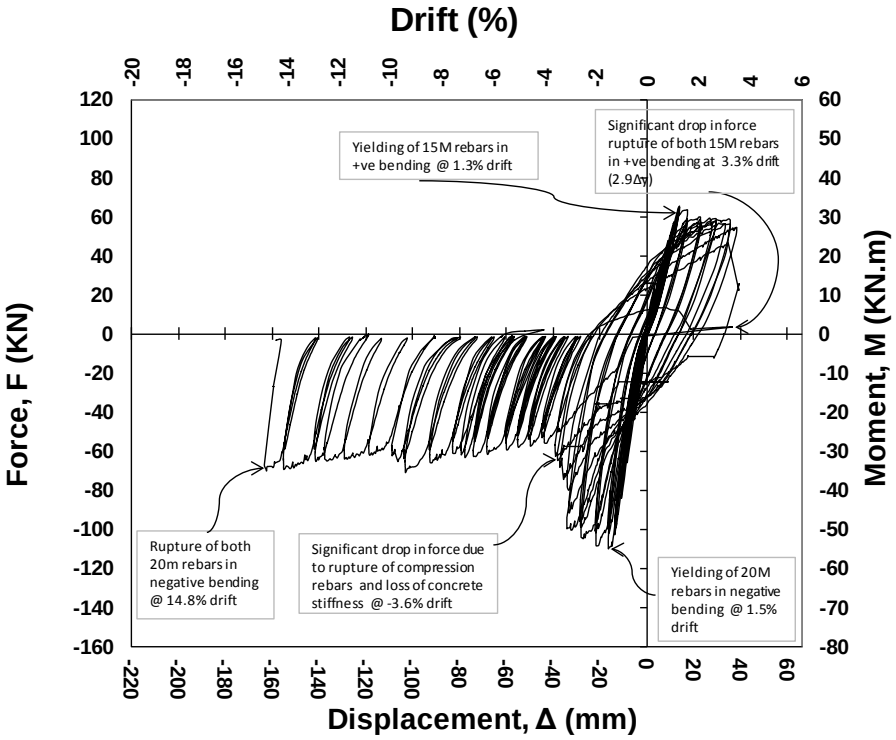

Figure 4.10 Force-displacement diagram for beam D/2-1.5%

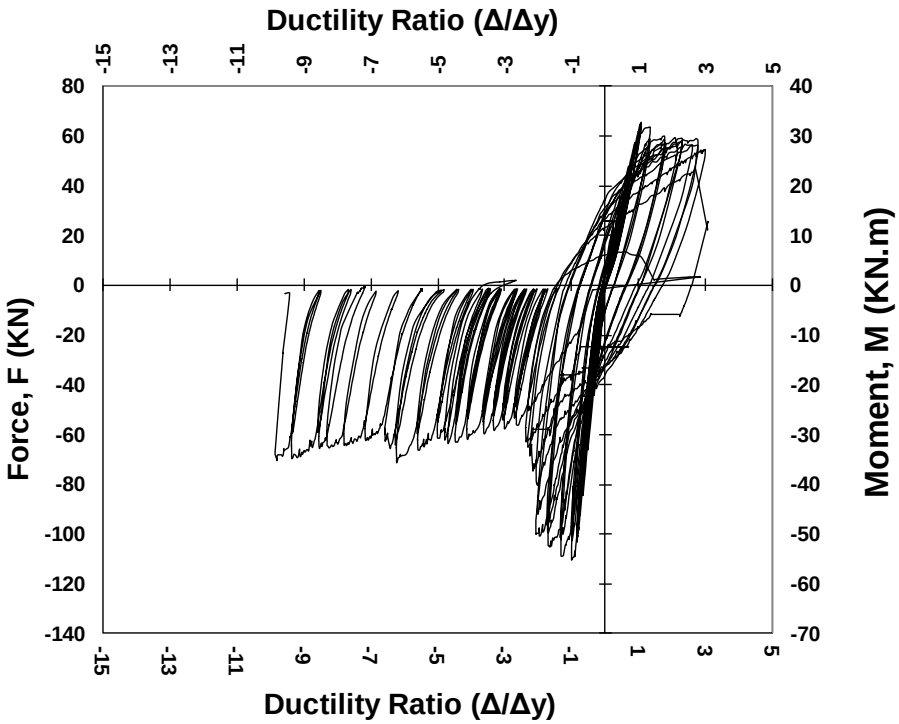

Figure 4.11 Force vs. ductility ratio for beam D/2-1.5%

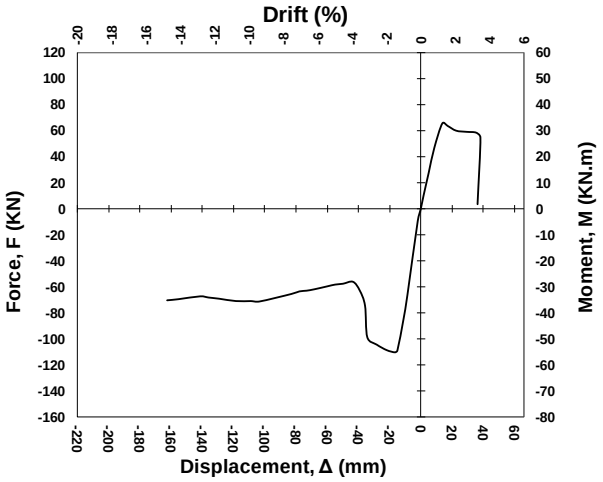

(a) Force-displacement response envelope

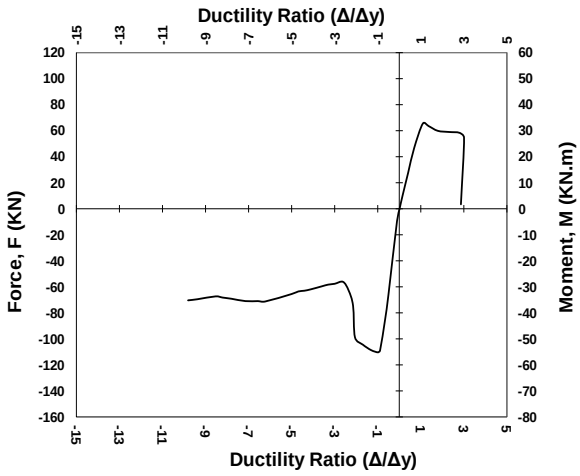

(b) Force-ductility ratio response envelope

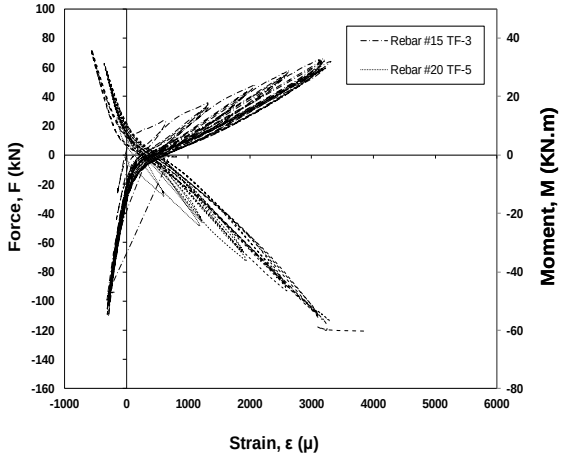

(c) Strain in longitudinal reinforcement at the face of t he middle block

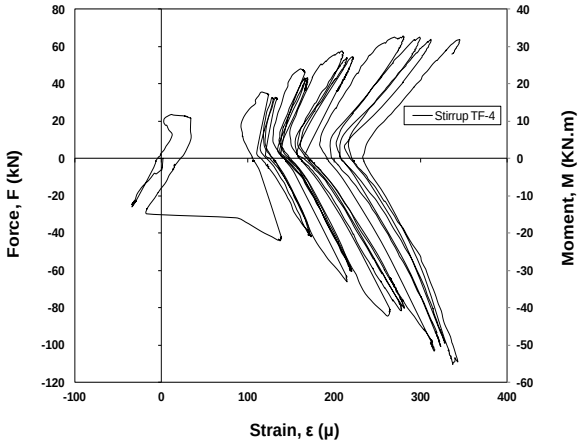

(d) Strain in a typical steel stirrup near the face of the middle block

Figure 4.12 Experimental results for beam D/2-1.5%

Table 4.7 Major events during positive bending for specimen D/2-1.5%

D/2-0.0%	Positive bending - #15 rebars in tension		
Δ(mm)	Drift (%)	Δ/Δy	Comments
5.5	0.5	0.05	A few cracks appeared close to the faces of the middle block with some of the cracks extending into the middle block.
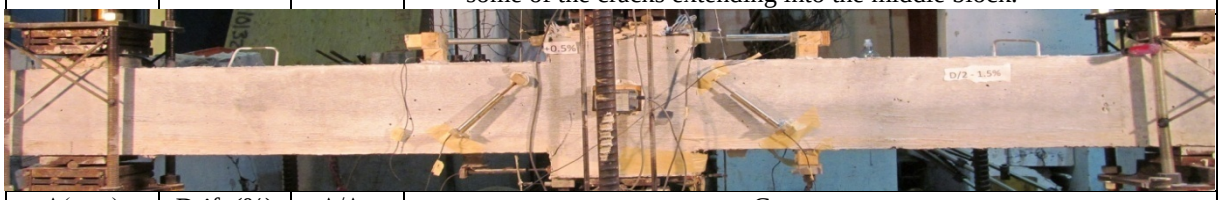			
Δ(mm)	Drift (%)	Δ/Δy	Comments
11	1	0.2	A few more new cracks appeared. Cracks concentrated at the right face of the middle block.
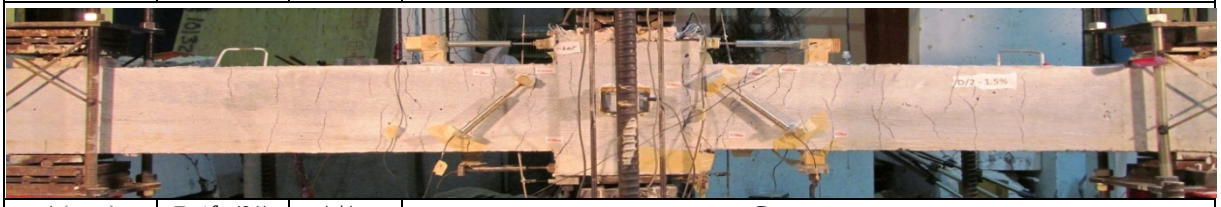			
Δ(mm)	Drift (%)	Δ/Δy	Comments
16.5	1.5	0.3	The Major crack at the top right face of the middle block opened up to be 2mm wide. This major crack was located inside the middle block at approximately 20mm in from the right face of the middle block. Other cracks appeared to be unchanged since the previous drift stage. 5.5% (3.5KN) drop in load compared to previous drift stage.
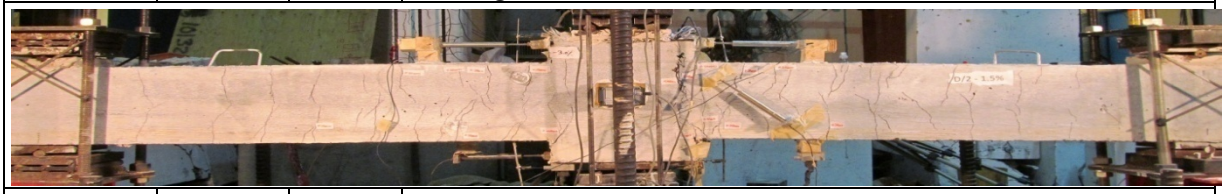			
Δ(mm)	Drift (%)	Δ/Δy	Comments
27.5	2.5	0.5	Loss of material at the top right major crack was observed. The concrete wedge at the top right face of the middle block was almost completely disintegrated but was still in place.
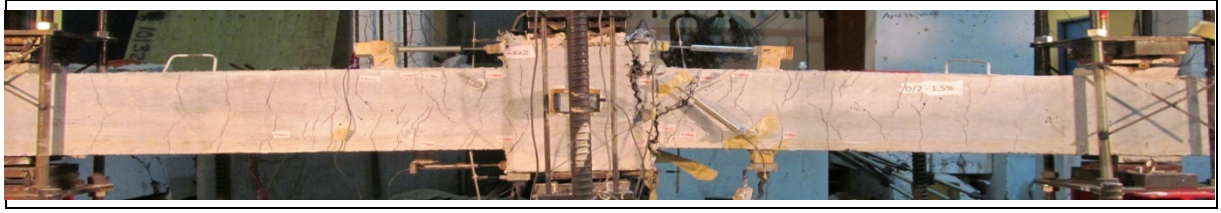			

Table 4.7 Major events during positive bending for specimen D/2-1.5% - continued

D/2-0.0%			
Δ(mm)	Drift (%)	Δ/Δy	Comments
38.5	3.5	0.7	Significant opening of the major crack inside the middle block and at the top right face of the middle block was seen. Further surface spalling and loss of material occurred around the major cracks. Slight drop in load (~6.8%=4KN) in the first stage followed by further drop due to rupture of #15 rebars in the second cycle down to 3.5 KN final load was recorded.
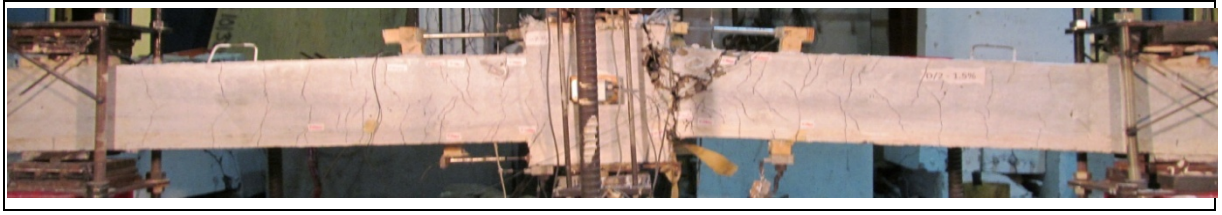			

Table 4.8 Major events during negative bending for specimen D/2-1.5%

D/2-0.0%	Negative bending - #20 rebars in tension		
Δ(mm)	Drift (%)	Δ/Δy	Comments
-5.5	-0.5	-0.1	Only one crack appeared at the left face of the middle block that was extending into the middle block.

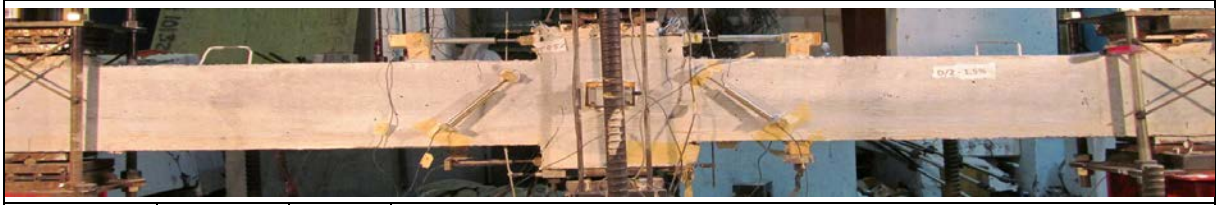

Δ(mm)	Drift (%)	Δ/Δy	Comments
-11	-1	-0.3	Few more new cracks appeared. Cracks appeared to be concentrated along the right side of the middle block specially at the right face of the middle block. More forking of cracks was observed at the right face of the middle block. Considerable crack width control was noted compared to specimens with lower fiber contents (D/2-1.0% had cracks width of 0.5mm at this drift stage).

Δ(mm)	Drift (%)	Δ/Δy	Comments
-22	-2	-0.7	The major crack at the bottom right face of middle block opened up severely. A small chunk of concrete spalled but was still place at the bottom right face corner of the middle block.

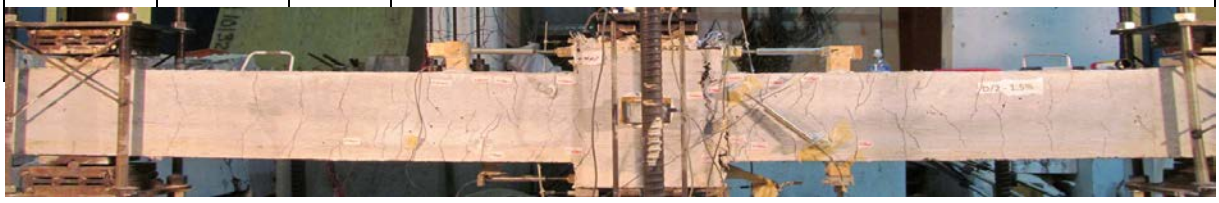

Table 4.8 Major events during negative bending for specimen D/2-1.5% - continued

Δ(mm)	Drift (%)	Δ/Δy	Comments
-27.5	-2.5	-0.8	The two major cracks at the right face and inside of the middle block are now connected at mid-height. The top right corner of the middle block (middle block cover beyond the vertical reinforcement) was disintegrated but was still in place. Slight drop in load (~3.5%=4KN) in the first stage was recorded followed by further drops in the second and third cycle of -2.5% totalling 11%=12KN compared to previous drift stage).
			
-38.5	-3.5	-1.2	Bottom right crack retained almost the same width. Crushing and further disintegration of the top concrete wedge was observed. 7.5% =6KN drop in load in -3.5%A and further drop in the second and third cycles totalling ~23%=18KN compared to previous drift stage.
			
Δ(mm)	Drift (%)	Δ/Δy	Comments
-44	-4	-1.3	Significant disintegration and moderate spalling of concrete at the top right cracks. Concrete was still in place. 14.5%=9KN drop in load was recorded compared to -3.5%C drift cycle.
			
Δ(mm)	Drift (%)	Δ/Δy	Comments
-55	-5	-1.7	12%=7KN increase in load was recorded compared to -4.5% stage. In-plane rotation of the middle block increased. No major progression of spalling/ disintegration was observed.
			
Δ(mm)	Drift (%)	Δ/Δy	Comments
-60.5	-5.5	-1.8	10%=6KN drop in load compared to -4% A stage was recorded. Significant in-plane rotation of the middle block was observed.
			

Table 4.8 Major events during negative bending for specimen D/2-1.5% - continued

Δ(mm)	Drift (%)	Δ/Δy	Comments
-66	-6	-2.0	~3%=2KN increase in load was recorded. Top right concrete wedge was almost completely crushed.
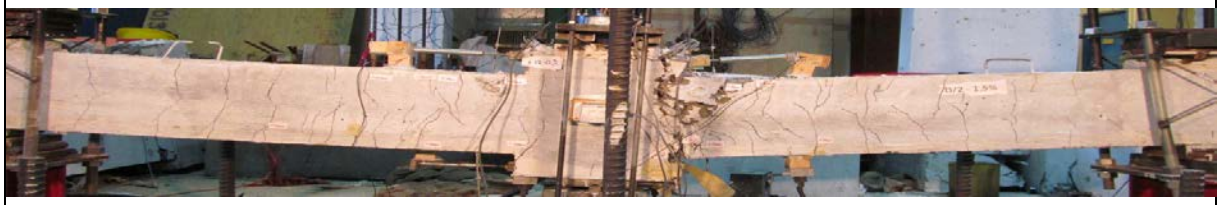			
Δ(mm)	Drift (%)	Δ/Δy	Comments
-71.5	-6.5	-2.2	~5%=3KN increase in load was recorded compared to the previous drift stage. No major change in the condition of the cracks/ beam was noted.
			
D/2-0.0%			
Δ(mm)	Drift (%)	Δ/Δy	Comments
-165	-15	-5.0	Both #20 rebars ruptured. Load increased by ~8%=5KN compared to previous drift stage before rupture of the rebars. Slightly further spalling at the top right corner. No other major changes in the condition of the concrete. Concrete chunks were still holding together despite severe disintegration and vertical displacement at the midspan. End of test.
			

4.1.5 Beam D/3-1.0%

The D/3 series beams had identical cross-sectional details to all beams in the experimental program. The longitudinal reinforcement in the D/3 series were identical to the D/2 series with 2-15M reinforcing bars in the bottom (Negative bending) and 2-20M reinforcing bars in the top (Positive bending). However, in this series the transverse reinforced was reduced to d/3. It is noted that both beams in this series were constructed with fibers, thus this series allows an investigation into the effect of combined use of fibers and transverse reinforcement on response. The first beam in this series was reinforced with 1.0% of steel fibers by volume of concrete and thus the response of Beam D/3-1.0% can be compared to Beam D/2-1.0%.

Figure 4.and **Figure 4.15** show the reverse-cyclic response of the specimen in terms of applied load (and Mid-span moment) as a function of displacement (mm), drift (%) and ductility ratio (Δ/Δ_y). The figure also highlights the major events during testing. **Figure 4.15 (a)** and **(b)** show the backbone response in terms of drift (%) and ductility ratio (Δ/Δ_y). **Figure 4.15 (c)** and **(d)** show the strains in the longitudinal and transverse reinforcement. Major events during the testing of the specimen are graphically presented in **Figure 4.9** and **Table 4.10** for the positive and negative.

As in the previous tested specimens, hairline cracks for the beam started appearing at ±0.5% drift (5.5mm displacement). Further flexural cracks appeared with maximum width of approximately 0.5mm at ±1.0% drift (11mm displacement) at which point some diagonal cracks also appeared. As with previous SCFRC specimens major cracking began concentrating near the faces of the column during cycling at this drift stage with other cracks remaining well controlled. In addition smaller secondary cracks started to fork off of existing major cracks. Analysis of strain data shows that the 15M reinforcing bars started to yield in positive bending at 1.5% drift (16.5mm displacement) at a load of 59.4KN (moment=32.7KN.m), while the 20M reinforcing bars yielded at approximately 1.3% drift (14.3mm displacement) at a load of 87.5 KN (moment=48.1 KN.m). Major cracks near the faces of the column widened to widths of 2mm and 0.75mm in positive and negative

bending respectively at the end of the cycling at this stage with all other cracks remaining well controlled. Minor surface spalling was observed at -2.0% drift (22mm displacement) near the bottom left corner of the column-stub. At ±2.5.0% drift (27.5mm displacement) cracks widths exceeded 2mm and a slight drop in load was recorded.

The load started to increase slightly at +3.0% drift (33mm displacement). Minor loss of concrete cover was seen at +4.0% drift (44mm displacement) and the load slightly increased at this stage. Further increase in load was observed at +4.5% drift (49.5mm displacement) cycle which was followed by the sudden rupture of both 15M reinforcing bars in the second cycle at this stage. The major crack in the right-side cantilever beam (which corresponds to the location of rupture of the 15M reinforcing bars) widened significantly at this point. The major crack at the left side of the column remained almost unchanged and was not as wide as the right side major crack. Some rotation of column-stub was observed at this point. Despite failure of the beam in positive bending, testing continued under cyclic loading in negative bending. Due to the loss of the 15M bars, 20.0% and 39.0% drops in load were recorded in the second and third -4.5% cycles (49.5mm displacement). A horizontal crack appeared at the level of 20M reinforcing bars at this point and slight loss of material was observed at the major cracks. After this initial loss in capacity, the load stabilized and eventually began to increase with further load cycling. A 16.0% increase in load was recorded at the drift stage corresponding to -5% which was followed by a further 24.0% increase in load in -5.5% drift (60.5mm displacement). No major changes in the condition of concrete was recorded at -6.5% drift (71.5mm displacement) when one of the 20M reinforcing bars rupture in negative bending. The Load increased by 4.0% before the rupture of the 20M reinforcing bar. The beam was considered to have failed at this stage and the test was discontinued. Comparing to the Beam D/2-1.0%, similar behaviour was observed for D/3-1.0%; slight improvement in cracking behaviour and increased ductility in negative bending was seen compared to the specimen without fibers (Beam D/2-0%). As was observed in the previous SCFRC specimens rupture of the 15M reinforcing bars in positive bending limited the performance of this specimen.

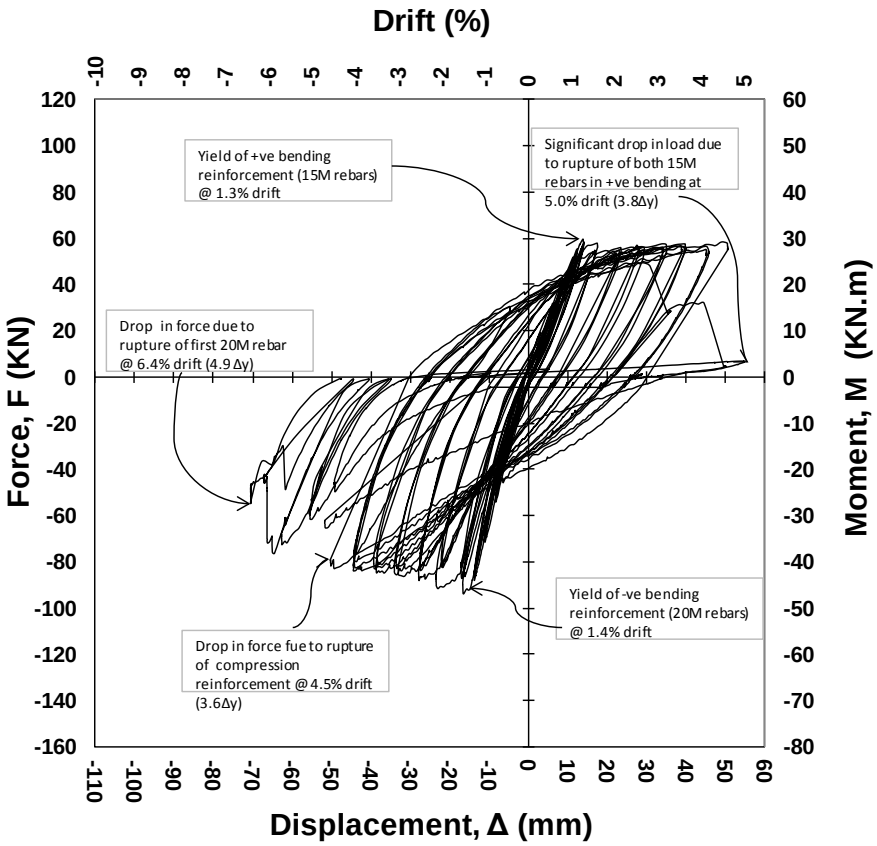

Figure 4.13 Force-displacement diagram for beam D/3-1.0%

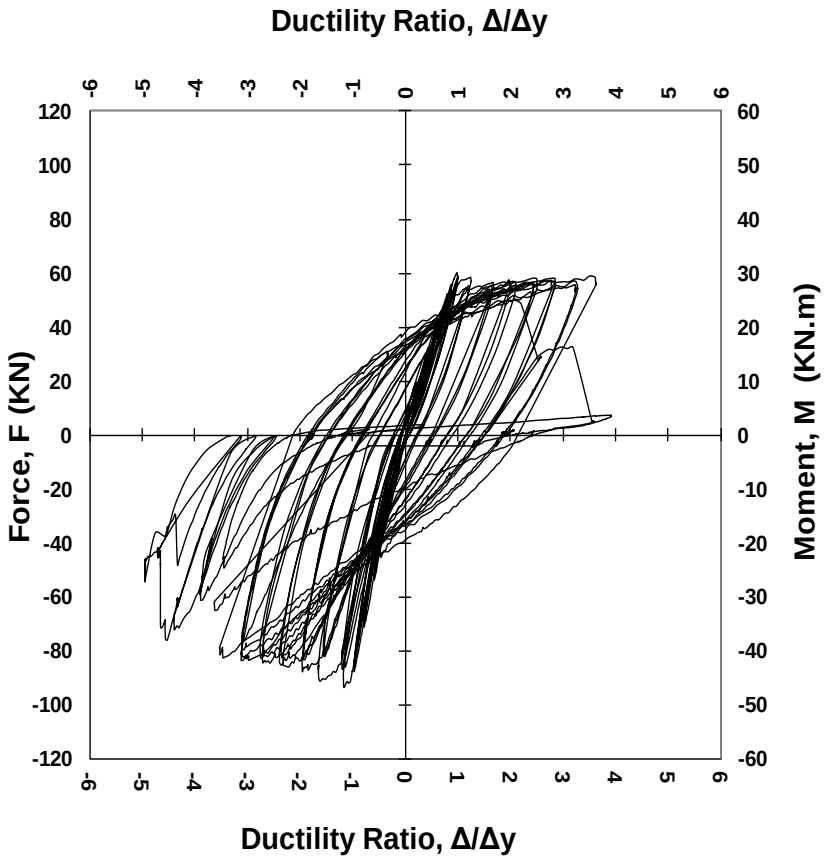

Figure 4.14 Force vs. ductility ratio for beam D/3-1.0%

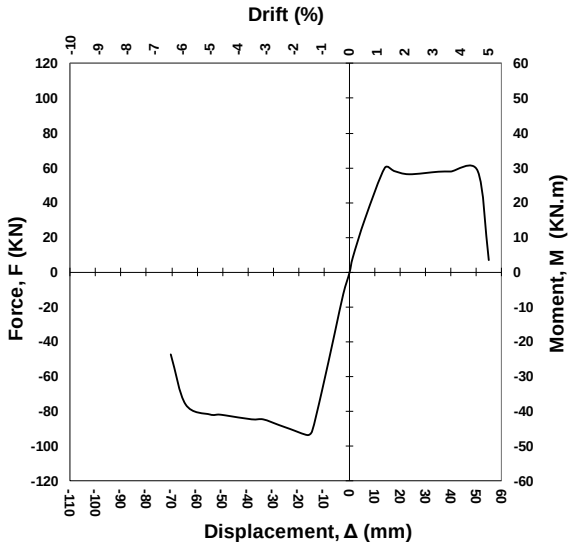

(a) Force-displacement response envelope

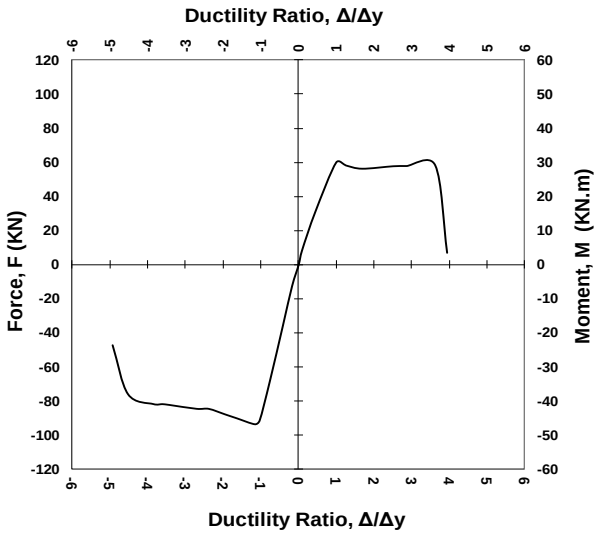

(b) Force-ductility ratio response envelope

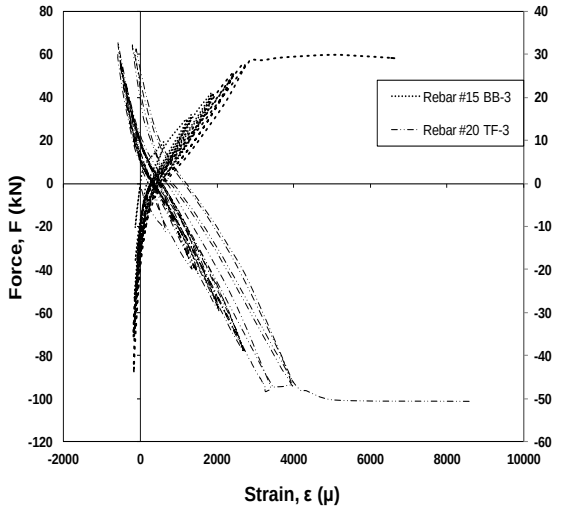

(c) Strain in longitudinal reinforcement at the face of t he middle block

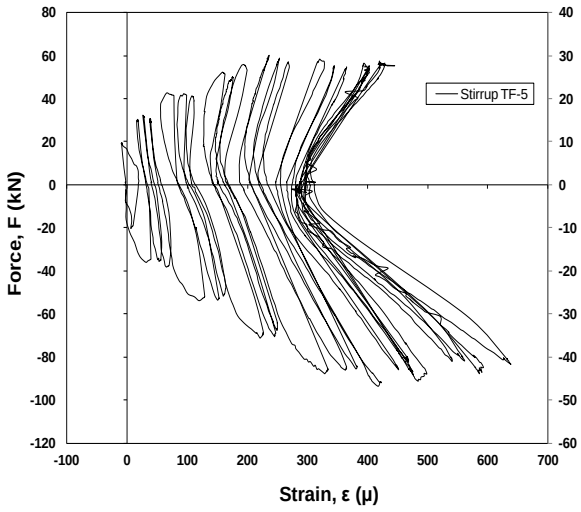

(d) Strain in a typical steel stirrup near the face of the middle block

Figure 4.15 Experimental results for beam D/3-1.0%

Table 4.9 Major events during positive bending for specimen D/3-1.0%

D/3 - 1.0%	Positive bending - #15 rebars in tension		
Δ(mm)	Drift (%)	Δ/Δy	Comments
5.5	0.5	0.4	Vertical cracks appeared. No diagonal cracks. Cracks starting at the face of the middle block have extended into the middle block.

Δ(mm)	Drift (%)	Δ/Δy	Comments
11	1	0.8	More vertical cracks appeared at approximately D/2 spacings. Cracks at the faces of the middle block on each side became wider. Other cracks remained at almost the same width or widened at a slower rate.

Δ(mm)	Drift (%)	Δ/Δy	Comments
16.5	1.5	1.2	Major cracks at the top faces of the middle block widened considerably. Other cracks seem to be widening at a slower rate or remained unchanged.

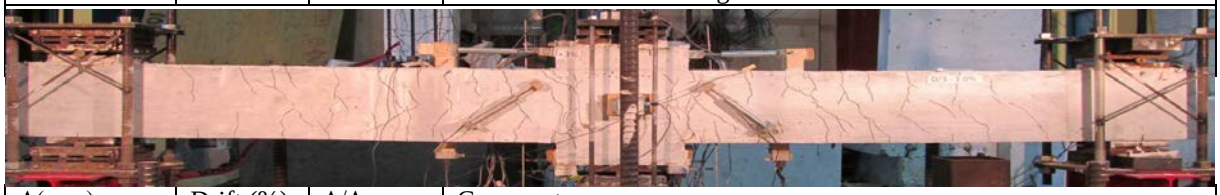

Δ(mm)	Drift (%)	Δ/Δy	Comments
22	2	1.6	~3.4%=2KN drop in load compared to previous drift stage. Cracks considerably opened up compared to previous drift stage. Minor shifting of the middle block against the major crack at the left side of the middle block was observed. Other cracks appeared to be unchanged k.

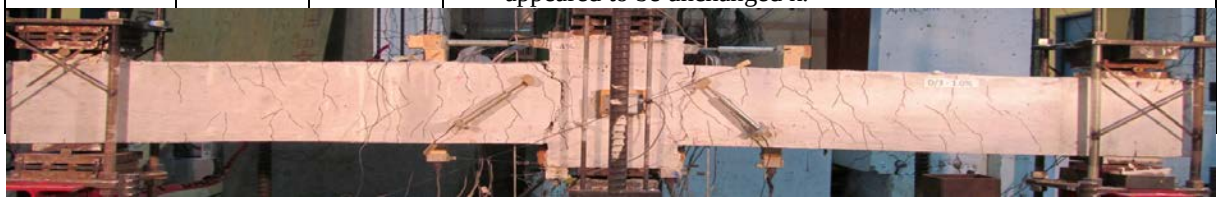

Table 4.9 Major events during positive bending for specimen D/3-1.0% - continued

Δ(mm)	Drift (%)	Δ/Δy	Comments
33	3	2.4	Major opening of the two major cracks. Other cracks remained unchanged and the crack openings were concentrating at the two major cracks. Disintegration of a small concrete wedge at the top right side of the middle block. Load slightly increased.

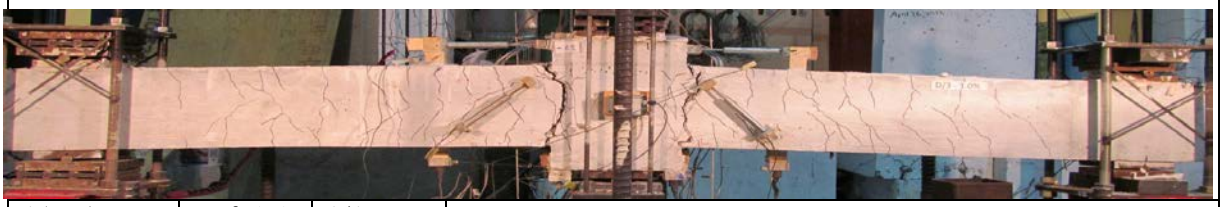

Δ(mm)	Drift (%)	Δ/Δy	Comments
38.5	3.5	2.8	Permanent opening of cracks was more pronounced at this drift stage. Slight shifting of the middle block against the left side cracks is at about 5mm at this stage. Slight increase in load was recorded.

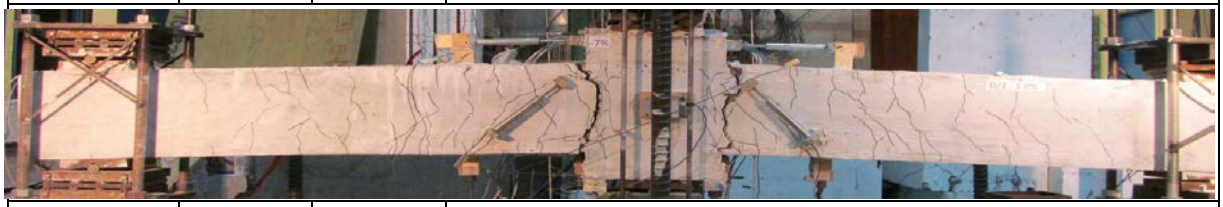

Δ(mm)	Drift (%)	Δ/Δy	Comments
49.5	4.5	3.5	One of the #15 rebars ruptured in the first +4.5% cycle and the second #15 rebar ruptured at the second +4.5% cycle before reaching the 4.5% drift. Load slightly increased to be 58.3KN before rupture of rebars. Left crack significantly opened up at this stage. Right crack was completely closed and middle block had significantly rotated clockwise. Beam was considered failed in positive bending.

Table 4.10 Major events during negative bending for specimen D/3-1.0%

D/2-0.0%	Negative bending - #20 rebars in tension		
Δ(mm)	Drift (%)	Δ/Δy	Comments
-5.5	-0.5	-0.4	Vertical and diagonal cracks appeared. Cracks starting at the face of the middle block have extended into the middle block.
			
Δ(mm)	Drift (%)	Δ/Δy	Comments
-11	-1	-0.8	More cracks appeared. Diagonal cracks appeared in the same orientation (direction) on both sides of the beam. The number of diagonal cracks is more in the right side of the middle block.
			
Δ(mm)	Drift (%)	Δ/Δy	Comments
-16.5	-1.5	-1.2	More cracks appeared at the faces of the middle block mostly forking off of existing cracks. Major cracks on each side of the middle block appeared to be widening at almost the same rate. #20 rebars started to yield.
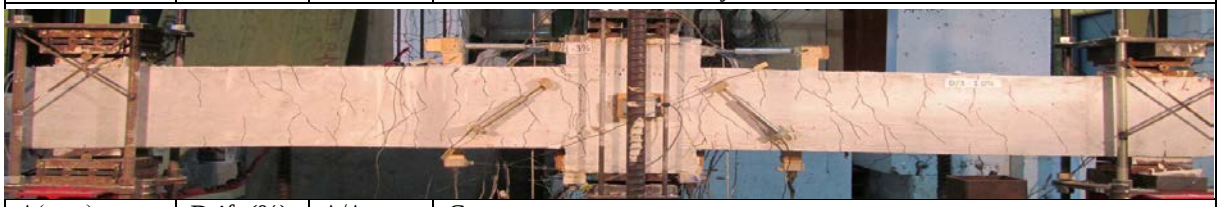			
Δ(mm)	Drift (%)	Δ/Δy	Comments
-22	-2	-1.5	Minor surface spalling at the major crack at the bottom left side of the middle block. Bottom left crack opened up to be more than 2mm wide. Other cracks remained almost unchanged.
			
Δ(mm)	Drift (%)	Δ/Δy	Comments
-27.5	-2.5	-1.9	~3.3%=3KN drop on load compared to previous drift stage. Further widening of the major cracks at each side of the middle block. Hinging appeared to be in the major cracks only, specially in the major crack to the left of the middle block

Table 4.10 Major events during negative bending for specimen D/3-1.0%- continued

Δ(mm)	Drift (%)	Δy	Comments
-44	-4	-3.1	Minor crushing of concrete at the edges of the major cracks was observed.
			
D/2-0.0%			
Δ(mm)	Drift (%)	Δy	Comments
-49.5	-4.5	-3.5	~20%=147 KN and 39%=32Kn drop in load in the second and third -4.5% cycle compared to the first -4.5% cycle. A chunk of concrete started to disintegrate at the left face of the middle block. A horizontal crack appeared at the level of the #20 reabrs. Slight loss of material and spalling at the cracks was observed.
			
Δ(mm)	Drift (%)	Δy	Comments
-55	-5.0	-3.8	Crack width almost the same at the level of the #20 rebars. The chunk of concrete at the left face of the middle block appeared to be completely disintegrated; it popped out slightly. 16%=8 KN increase in load was recorded compared to -4.5%C cycle.
			
Δ(mm)	Drift (%)	Δy	Comments
-71.5	-6.5	-5	No major changes in the condition of the cracks/beam compared to the previous stage was observed. No further spalling/ disintegration was observed. ~4%=3KN increase in load compared to the previous drift stage. One of the #20 rebars ruptured in the -6.5%B cycle. Beam was considered failed at this stage. considerable spalling/ disintegration control at failure. End of test.
			

4.1.7 Beam D/3-1.5%

This is the second beam in the D/3 series and had identical properties to the previous beams but was reinforced with 1.5% fibers by volume of concrete. Comparison with the previous specimen allows an investigation into the effect of increasing fiber content from 1% to 1.5%. Furthermore comparison with Beam D/2-1.5% allows further investigation into the effect of combined use of fibers and transverse reinforcement on response.

Figure 4.16 and **Figure 4.17** show the reverse-cyclic response of the specimen in terms of applied load (and Mid-span moment) as a function of displacement (mm), drift (%) and ductility ratio (Δ/Δ_y). The figure also highlights the major events during testing. **Figure 4.18 (a)** and **(b)** show the backbone response in terms of drift (%) and ductility ratio (Δ/Δ_y). **Figure 4.18 (c)** and **(d)** show the strains in the longitudinal and transverse reinforcement. Major events during the testing of the specimen are graphically presented in **Table 4.11** and **Table 4.12** for the positive and negative bending cycles, respectively**.**

As with other beams, hairline cracks appeared at ±0.5% drift (5.5mm). Further cracks appeared at ±1.0% drift (11mm displacement) which was accompanied by formation of secondary cracks which branched off of existing cracks. At this stage, two major cracks running all the way to the top and bottom formed on either side of the column. Examination of strain data indicates that yielding of the 15M reinforcing began in positive bending at 1.0% drift (11mm displacement) at a load of 59.5KN (moment=32.7KN.m). The first diagonal crack appeared at -1.0% drift (-11mm displacement) at the left side of the column-stub. During the next load stage of -1.5% drift (16.5mm displacement) the 20M reinforcing bars yielded with a recorded load of 95.5KN (moment=52.5KN.m).

At +2.0% drift (22mm displacement), only the major cracks at the column faces were widening and other cracks appeared to remain unchanged. Maximum crack width exceeded 2.0mm at ±2.0% drift (22mm displacement). A diagonal crack at the right side of the column widened considerably at +3.0% drift (33mm displacement). Crushing of concrete at the top

left side of the column was observed at this stage which was followed by minor loss of material at ±3.5% drift (38.5mm displacement).

During the next load stage of +4.0% drift (44mm displacement), one of 15M reinforcing bars ruptured under positive bending at a load of 56.3KN (moment=30.9 KN.m) after which the load dropped by 50%. Despite this, only a slight decrease in load was observed during -4.0% cycle (-44mm displacement) which was followed by further minor decreases in load up to -6.5% drift (71.5mm displacement). This was accompanied by minor spalling and disintegration of concrete at and near major cracks.

Cyclic loading continued under negative bending and after stabilizing the load began to increase at -9.0% drift (99mm displacement). Crushing of compression concrete along with significant widening of major cracks was observed at -10.5% drift (115.5mm displacement), and the load dropped by 4.5% at this stage prior to rupture of one of the 20M reinforcing bars at -11.5% drift (126.5mm displacement). The beam was deemed to have failed at this stage and hence the test was discontinued. In general, other than at the major crack locations minimal disintegration of concrete and loss of material was recorded at the end of testing.

When compared to the previous specimen with 1% fibers this specimen showed some improvements in response in the negative bending (this was also observed in the D/2 series when going from 1% to 1.5% fibers). In addition in the post-peak region significant improvement was observed in post-peak strength; the load increases to a maximum of 117 KN (moment=64.3KN.m) (due to strain hardening in the tension steel) while the initial peak load was 103KN (moment=56.6KN.m). However as was observed in all other SCFRC specimens, performance was limited due to the early rupture of the 15M bars.

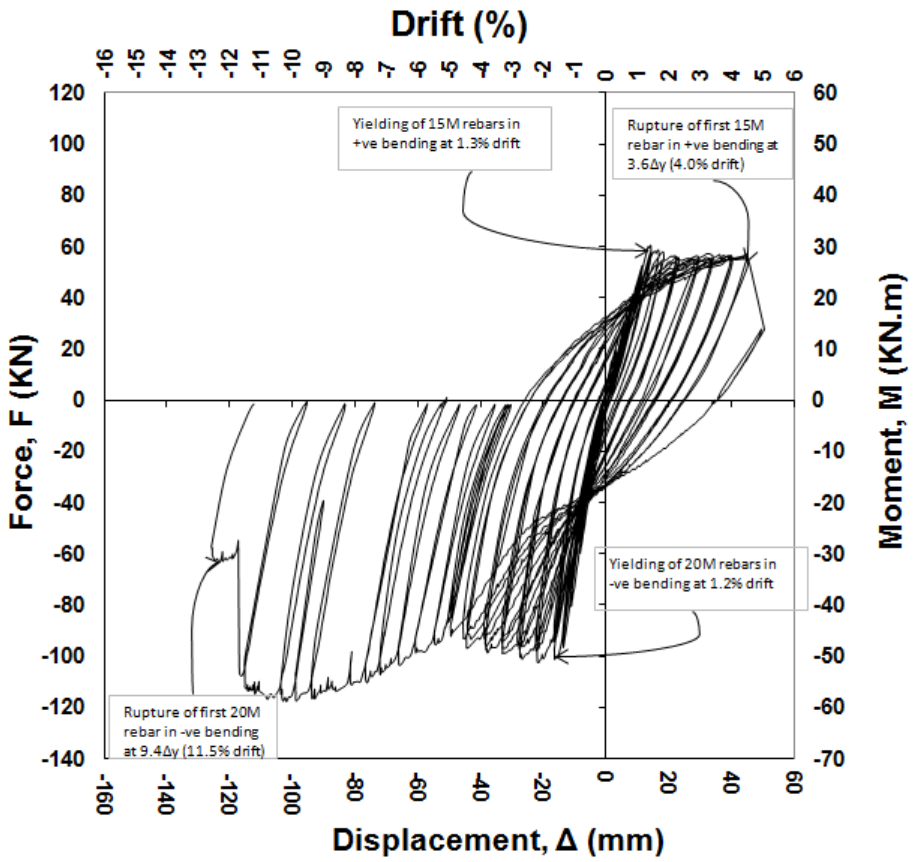

Figure 4.16 Force-displacement diagram for beam D/3-1.5%

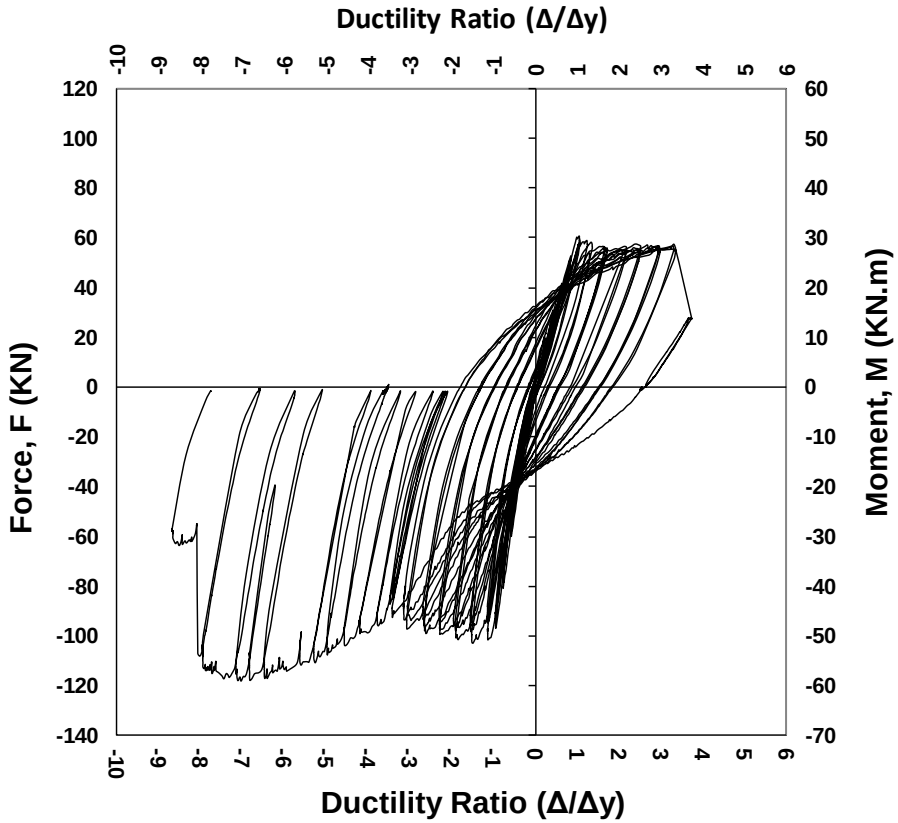

Figure 4.17 Force vs. Ductility ratio for beam D/3-1.5%

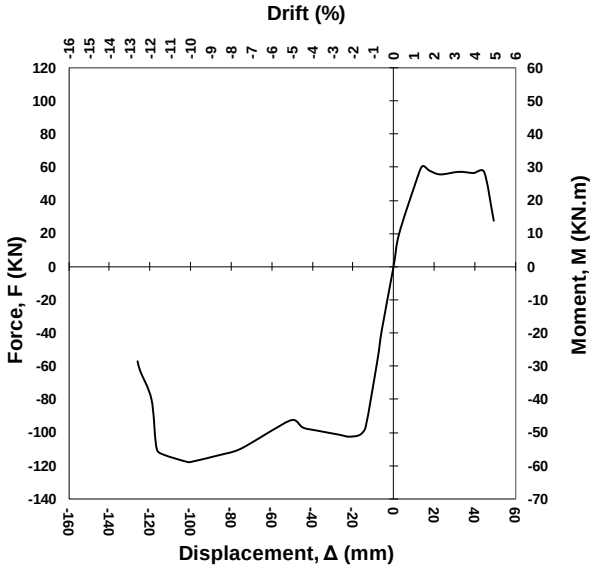

(a) Force-Displacement Diagram

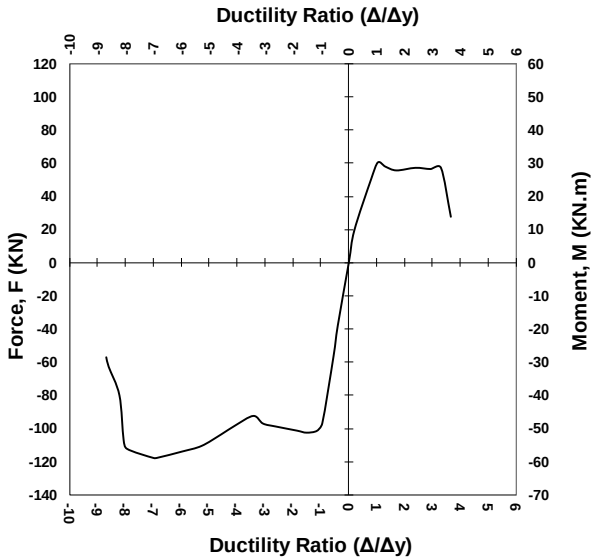

(b) Force-ductility ratio response envelope

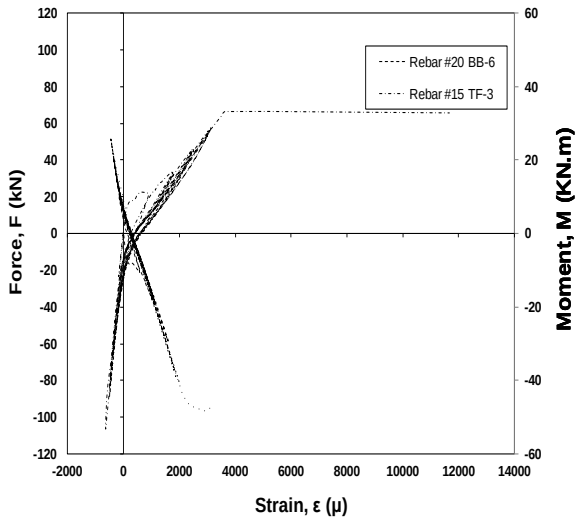

(b) Strain in longitudinal reinforcement at the face of t he middle block

Figure 4.18 Experimental results for beam D/3-1.5%

Table 4.11 Major event during positive bending of beam D/3-1.5%

D/3-1.5%	Positive bending - #15 rebars in tension		
Δ(mm)	Drift (%)	Δ/Δy	Comments
5.5	0.5	0.4	A few small cracks appeared at approximately D/2 spacing.
			
Δ(mm)	Drift (%)	Δ/Δy	Comments
11	1	0.8	#15 rebars started to yield. Further forking of existing cracks specially at the faces of the middle block.
			
Δ(mm)	Drift (%)	Δ/Δy	Comments
16.5	1.5	1.2	A small chunk of concrete at the top left face of the middle block started to disintegrate.
			
Δ(mm)	Drift (%)	Δ/Δy	Comments
22	2	1.6	Widening of cracks was seen at almost only two cracks at each side of the middle block. Other cracks remained at almost the same width. Slight spalling of the surface at the bottom left face of the middle block. Slight drop (8%=~6KN) in load in the second 2% cycle to ~62KN.
			
Δ(mm)	Drift (%)	Δ/Δy	Comments
44	4	3.3	One of the #15 rebars ruptured. ~50%=30Kn drop in load. Significant widening of the major crack at the left face of the middle block.
			

Table 4.12 Major event during negative bending of beam D/3-1.5%

D/2-0.0%	Negative bending - #20 rebars in tension		
Δ(mm)	Drift (%)	Δ/Δy	Comments
-5.5	-0.5	-0.4	Some small vertical cracks appeared at approximately D/2 spacing.

Δ(mm)	Drift (%)	Δ/Δy	Comments
-11	-1	-0.8	A diagonal crack appeared at the right face of the middle block. A few more cracks forked off of existing cracks. Not many new individual cracks.

Δ(mm)	Drift (%)	Δ/Δy	Comments
-16.5	-1.5	-1.1	The diagonal crack at the right face of the middle block widened. #20 rebars started to yield. Signs of surface spalling (very minor) at the major crack at the left side of the middle block.

Δ(mm)	Drift (%)	Δ/Δy	Comments
-22	-2	-1.5	A small concrete wedge started to disintegrate at the bottom right face of the middle block. Signs of crushing at the top left corner of the middle block. The major crack at the left side of the middle block opened up.

Δ(mm)	Drift (%)	Δ/Δy	Comments
-27.5	-2.5	-1.9	Minor surface spalling at the cracks. Left crack opened up. Slight decrease in load was recorded .

Table 4.12 Major event during negative bending of beam D/3-1.5% - continued

Δ(mm)	Drift (%)	Δ/Δy	Comments
-38.5	-3.5	-2.7	Minor loss of material at the top left face of the middle block. Disintegration of small pieces of concrete at the bottom left face of the middle block. Permanent crack openings were observed at the compression side. Slight decrease in load was recorded.
			
Δ(mm)	Drift (%)	Δ/Δy	Comments
-44	-4	-3.0	~4%=4KN drop in load in the third -4% cycle compared to -3.5% drift stage. Widths of the major vertical cracks were almost the same as the previous stage. A horizontal crack at the #20 rebar level at the bottom left face of the middle block opened up.
			
Δ(mm)	Drift (%)	Δ/Δy	Comments
-66	-6	-4.6	Small chunks of concrete started to disintegrate and spall at the top of the major crack in both sides. ~6%=6KN increase in load was recorded.
			
Δ(mm)	Drift (%)	Δ/Δy	Comments
-99	-9	-6.8	%4.5%=5KN increase in load was recorded. Further crushing and slight spalling of the concrete was observed at the top left crack.
			

Table 4.12 Major event during negative bending of beam D/3-1.5% - continued

Δ(mm)	Drift (%)	Δ/Δy	Comments
-115.5	-10.5	-8.0	Further crushing of the top left face of the middle block. Further widening of the major cracks especially at the left face of the middle block. A concrete wedge at this location was crushed and appeared to be disintegrating. 4.5% =5KN drop in load was recorded compared -9% drift stage.
			
Δ(mm)	Drift (%)	Δ/Δy	Comments
-126.5	-11.5	-8.7	One of the #20 rebars ruptured. ~42%=45 KN drop in load. Top left wedge of concrete was significantly crushed but was still in place. More surface spalling at this location. The bottom left concrete wedge was further disintegrated. End of test.
			

4.1.8 Beam D/4-0.0%

The D/4 series is the third series of beams in this test program. All beam properties were kept identical however in this series the transverse reinforcement in the plastic hinge region was reduced to d/4, corresponding to requirements for ductile design in the CSA A23.3 design standard. This series includes two beams. The first specimen, Beam D/4-0.0%, is constructed without fibers and when compared to Beam D/2-0% allows for an investigation into the effect of transverse reinforcement on response. Comparison with the other beams in this research program allows for an investigation into the ability of fibers to replace transverse reinforcement.

Figure 4.19 and **Figure 4.20** show the reverse-cyclic response of the specimen in terms of applied load (and Mid-span moment) as a function of displacement (mm), drift (%) and ductility ratio (Δ/Δ_y). The figure also highlights the major events during testing. **Figure 4.21 (a)** and **(b)** show the backbone response in terms of drift (%) and ductility ratio (Δ/Δ_y). **Figure 4.21 (c)** and **(d)** show the strains in the longitudinal and transverse reinforcement. Major events during the testing of the specimen are graphically presented in **Table 4.13** and **Table 4.14** for the positive and negative bending cycles, respectively.

During testing of this specimen (and has been observed in all other specimens), several hairline cracks appeared at ±0.5% drift (5.5mm displacement). At the next load stage of ±1.0% drift (11mm displacement), two major cracks also appeared at each side of the column-stub and started to extend into the column area. With further cycling additional cracks appeared including two diagonal cracks in the right side of the beam. At ±1.5% drift (16.5mm displacement), it was noted that contrary to beams reinforced with steel fibers, widening of cracks was observed in most cracks in the plastic hinge region and was not limited to the cracks near the column. Strain data shows that 15M reinforcing bars yielding at +1.2% drift (+12.8mm displacement) at a load of 52.1 KN (moment=28.7 KN.m). The major cracks near the faces of the column widened considerably at this stage. Yielding of the 20M reinforcing bars occurred at -1.5% drift (16.5mm displacement) and was accompanied by 7.0% increase in load to 85 KN (moment=46.8 KN.m).

Minor crushing and disintegration of concrete near major cracks was observed at +2.0% drift (22mm displacement). At -2.0% drift (-22mm displacement), further diagonal cracks appeared while the load increased by 5.3% in the first cycle and decreased by 12% in the second cycle of -2.0% drift. Major cracks near the faces of the column kept widening and further disintegration of concrete within the plastic hinging area was observed. At +4.0% drift (44mm) significant spalling of concrete cover was observed. A 4.5% drop in load was observed during the +4.5% drift (49.5mm displacement) stage; this was accompanied by significant crushing of core concrete and loss of remaining concrete cover. At this stage the 15M reinforcing bars and some hoops were exposed. The Load increased by 7% in -4.5% cycle, however this was followed by further spalling and loss of material was observed at this stage.

During the next drift stage of +5.0% drift (55mm displacement), one of 15M reinforcing bars ruptured followed by 41% drop in load and severe spalling at the bottom face of the beam. A 60% drop in load was recorded in the -5.0% drift (-55mm displacement) cycle; this was deemed to be due to the loss of the compression steel as well as severe loss of concrete material in the compression zone. Following this, the load dropped significantly and testing was stopped.

Overall this specimen showed a response which was slightly improved when compared to the other control specimen (Beam D/2-0%). When examining the hysteretic response significantly less pinching is observed, however energy dissipation remained similar. This is to be expected due to the relatively low shear stress demand imposed on the beams in this test program. When comparing to the fiber reinforced specimens, severe spalling, crushing and loss of material were observed in beam D/4-0.0%; this was better controlled in the previous fiber-reinforced specimens.

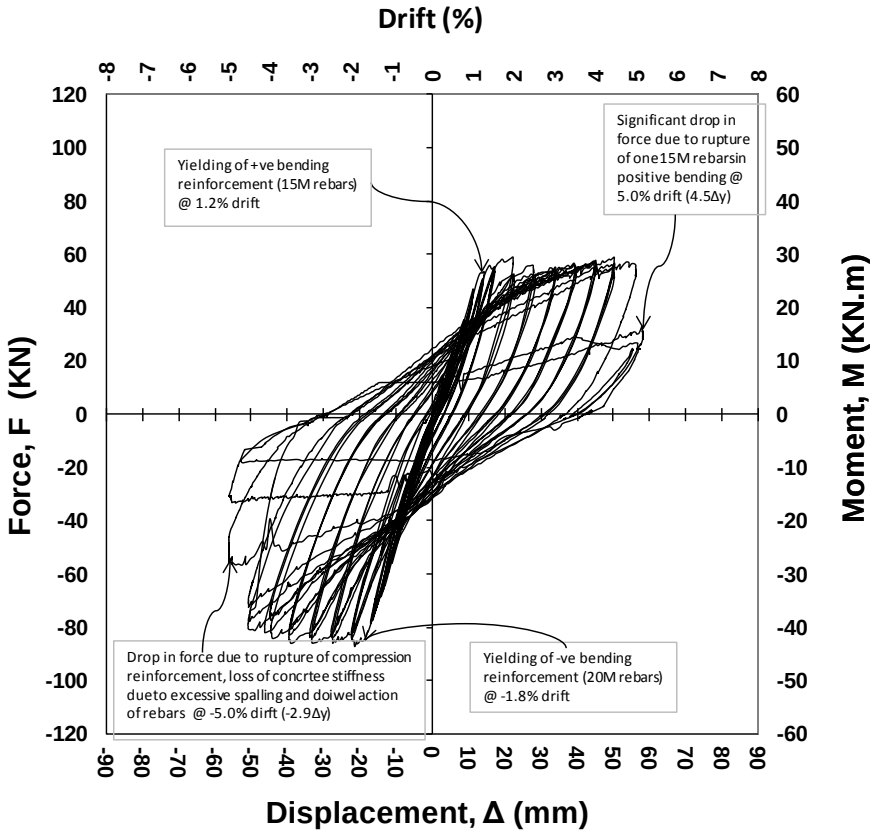

Figure 4.19 Force-displacement diagram for beam D/4-0.0%

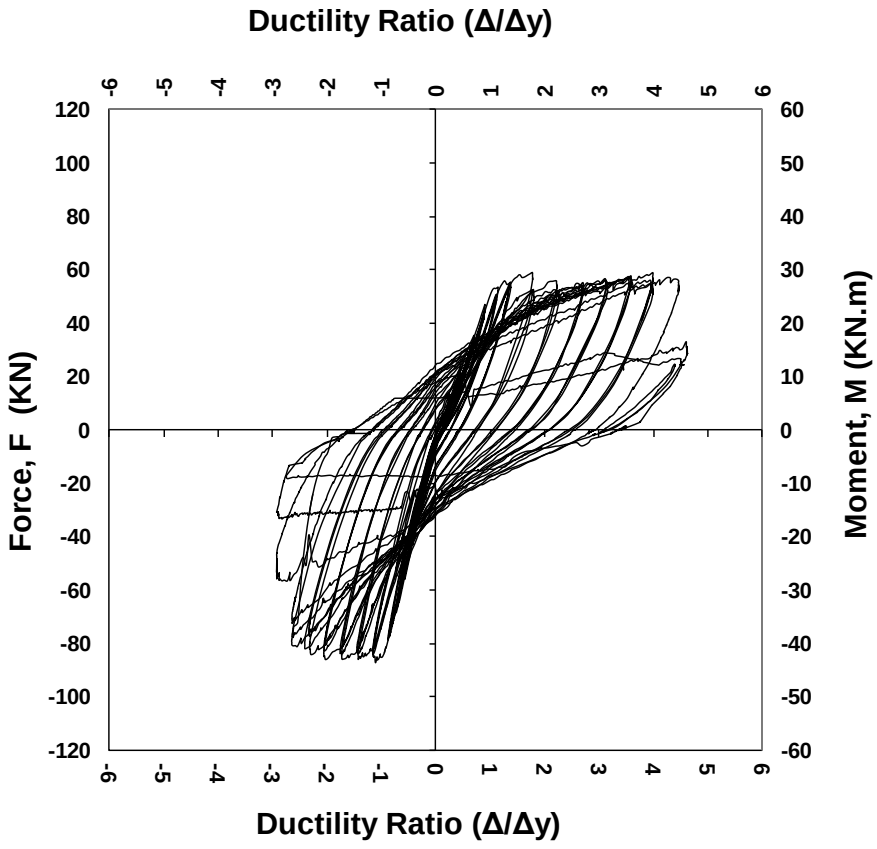

Figure 4.20 Force vs. ductility ratio for beam D/4-0.0%

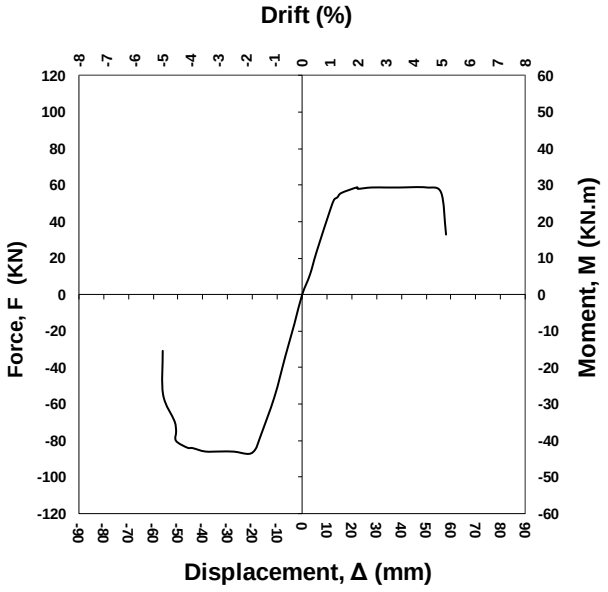

(a) Force-displacement response envelope

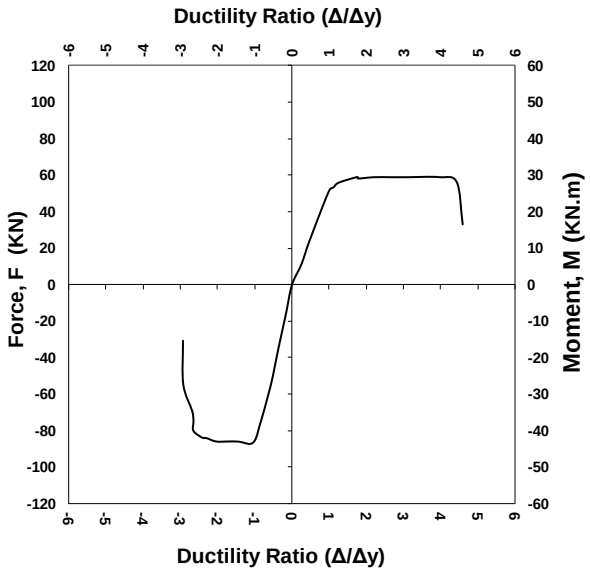

(b) Force-ductility ratio response envelope

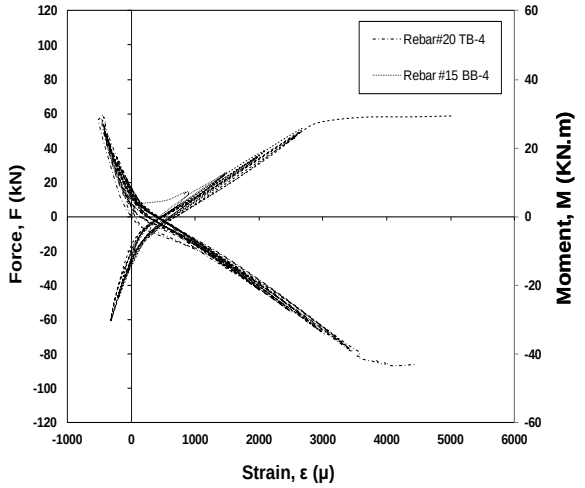

(c) Strain in longitudinal reinforcement at the face of the middle block

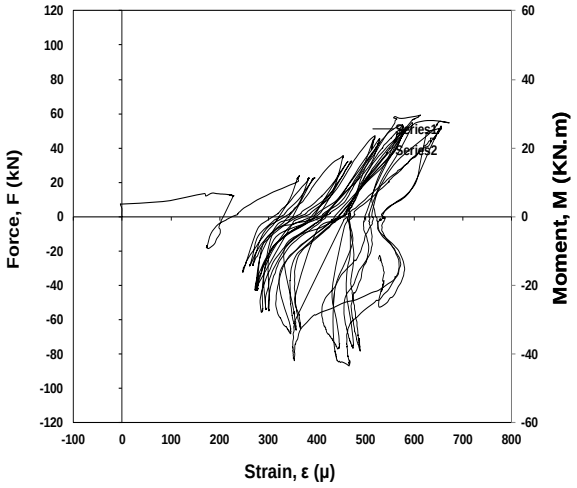

(d) Strain in a typical steel stirrup near the face of the middle block

Figure 4.21 Experimental results for beam D/4-0.0%

Table 4.13 Major event during positive bending of beam D/4-0.0%

D/4-0.0%	Positive bending - #15 rebars in tension		
Δ(mm)	Drift (%)	Δ/Δy	Comments
5.5	0.5	0.2	Several vertical hairline cracks appeared. Major cracks at each face of the middle block extended into the middle block.
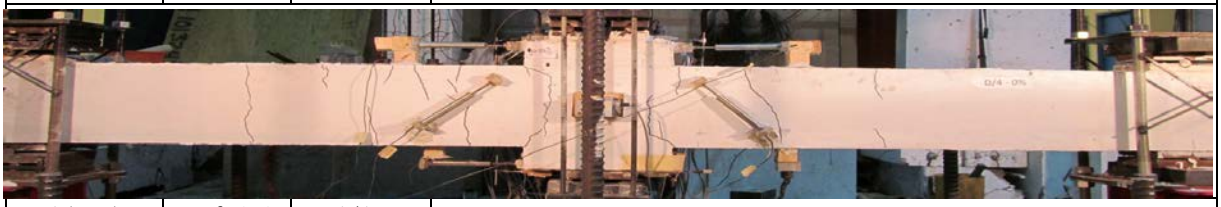			
Δ(mm)	Drift (%)	Δ/Δy	Comments
16.5	1.5	0.6	#15 rebars started to yield. Some new appeared. Major cracks opened up further. Other cracks widened at a slower rate.
			
Δ(mm)	Drift (%)	Δ/Δy	Comments
22	2	1.7	Major cracks widened further. Minor surface spalling and disintegration of a chunk of concrete is observed at the left face of the middle block. Slight crushing/disintegration of a small area at the top left face of the middle block.
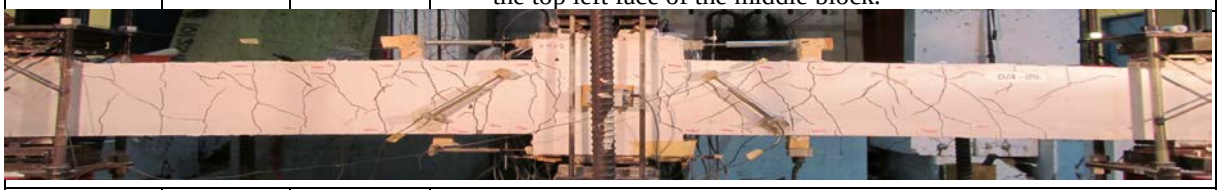			
Δ(mm)	Drift (%)	Δ/Δy	Comments
27.5	2.5	2.1	Cracks opened up further. Minor spalling at a crack location a distance d (=204mm) to the left of the face of the middle block.
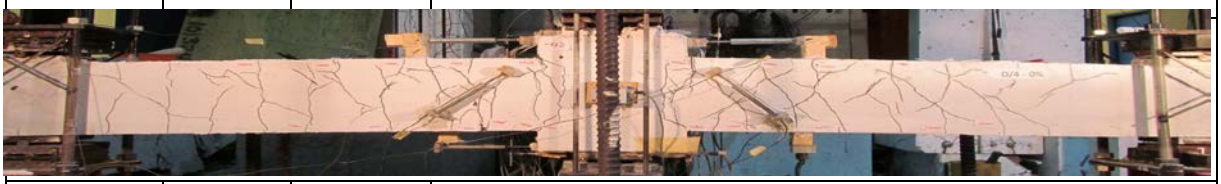			
Δ(mm)	Drift (%)	Δ/Δy	Comments
44	4	3.4	Disintegration and spalling of a large area of the concrete wedge at the bottom left side of the middle block. The major cracks at the right side of the middle block widened further.
			

Table 4.13 Major event during positive bending of beam D/4-0.0% - continued

Δ(mm)	Drift (%)	Δ/Δy	Comments
55	5.0	4.3	#15 rebars are completely exposed at the spalled locations. One of the #15 rebars ruptured at the second cycle; 41%=23KN drop in load. Significant loss of material and spalling at both sides of the middle block. Chunks of concrete spalled off at the bottom of the beam at both sides of the middle block.
			

Table 4.14 Major event during negative bending of beam D/4-0.0%

D/4-0.0%	Negative bending - #20 rebars in tension		
Δ(mm)	Drift (%)	Δ/Δy	Comments
-5.5	-0.5	-0.1	Several vertical cracks appeared. Major cracks at each face of the middle block are extending into the middle block.
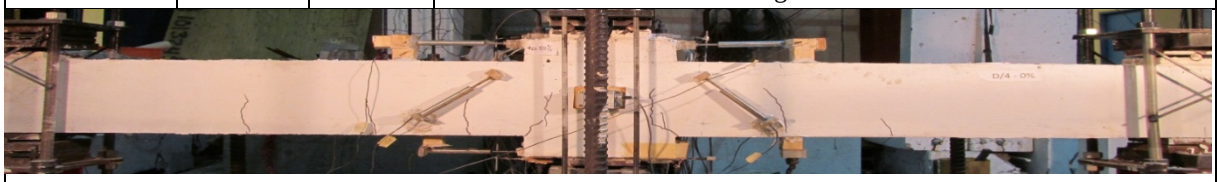			
Δ(mm)	Drift (%)	Δ/Δy	Comments
-11	-1	-0.6	A diagonal cracks appeared at the right face of the middle block. A few more cracks forked off of existing cracks. Not many new individual cracks.
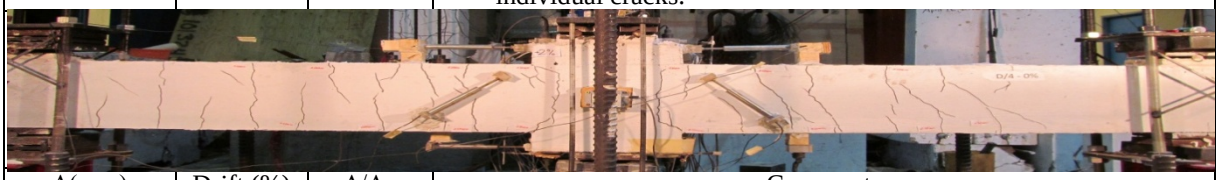			
Δ(mm)	Drift (%)	Δ/Δy	Comments
-16.5	-1.5	-0.9	~7%=4KN increase in load was recorded. Major cracks at the faces of the middle block widened further. Cracks at other locations did not change much. Bottom rebars (20) yielded.
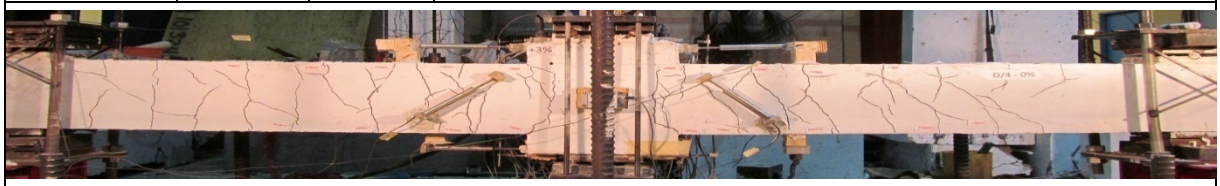			
Δ(mm)	Drift (%)	Δ/Δy	Comments
-22	-2	-1.2	~5.3%=3KN increase in load was recorded in the first cycle. ~12%=6.5KN drop in load after the second and the third cycle. Cracks opened up further. More diagonal cracks appeared.
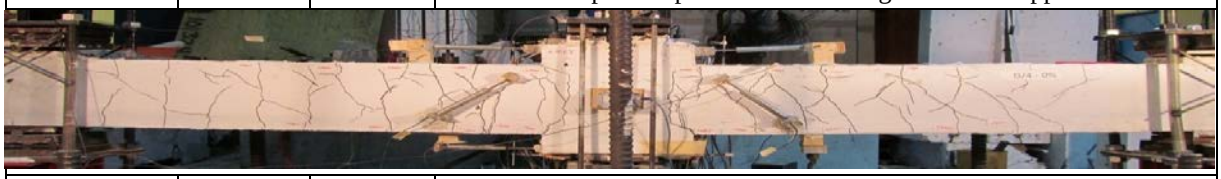			
Δ(mm)	Drift (%)	Δ/Δy	Comments
-44	-4	-2.3	Slight increase in load. Spalling of a large area of the concrete wedge at the bottom left side of the middle block.
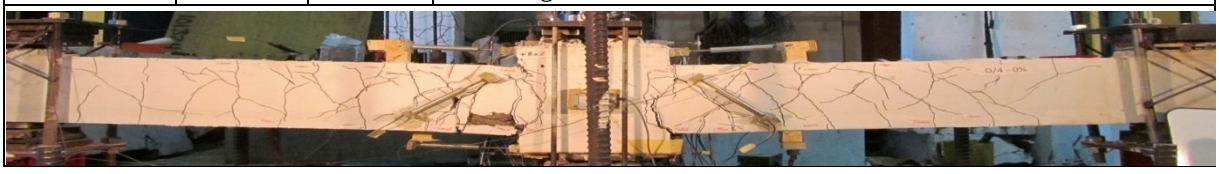			

Table 4.14 Major event during negative bending of beam D/4-0.0%- continued

Δ(mm)	Drift (%)	Δ/Δy	Comments
-49.5	-4.5	-2.6	- Slight increase in load and subsequent drops a total of 7%=4KN in the second and third cycles. Further spalling/ loss of material at the left side of the middle block. The concrete wedges at both sides disintegrated further.

Δ(mm)	Drift (%)	Δ/Δy	Comments
-55	-5	-2.9	- ~31%=25KN drop in load.. Drop in load was suspected to be due to loss of compression zones at the bottom of the beam. Significant spall/ disintegration of the concrete wedges at both sides of the middle block. End of test.

4.1.9 Beam D/4-1.0%

Beam D/4-1.0% was constructed with the details as beam D/4-0.0% but contained 1.0% steel fibers by volume of concrete. This beam allows an investigation into the benefits that arise from the combined use of closely spaced transverse reinforcement and fibers.

Figure 4.22 and **Figure 4.23** show the reverse-cyclic response of the specimen in terms of applied load (and Mid-span moment) as a function of displacement (mm), drift (%) and ductility ratio (Δ/Δ_y). The figure also highlights the major events during testing. **Figure 4.24 (a)** and **(b)** show the backbone response in terms of drift (%) and ductility ratio (Δ/Δ_y). **Figure 4.24 (c)** and **(d)** show the strains in the longitudinal and transverse reinforcement. Major events during the testing of the specimen are graphically presented in **Table 4.15** and **Table 4.16** for the positive and negative bending cycles, respectively.

The first hairline cracks for this specimen appeared at ±0.5% drift (5.5mm displacement) at approximately d/2 spacing. At +1.0% drift (11mm displacement), the spacing between the cracks reduced to match the spacing of the hoops, d/4, within the expected plastic hinge region. As was observed in previous SCFRC specimens, cracks started to concentrate near the faces of the column-stub. Smaller secondary cracks forked off of existing major cracks at this stage. Two small diagonal cracks also appeared during subsequent cycling at -1.0% drift (-16.5mm displacement). Maximum widths of cracks at +1.0% and -1.0% drift were 0.4mm and 0.5mm. This is slightly less than crack widths observed in beams D/2-1.5% and D/3-1.5% which had widths near 0.75mm at this stage. Strain data indicates that the 15M reinforcing bars started yielding under positive bending at +1.4% drift (15.5mm displacement) at a load of 63.4 KN (34.9KN.m). The 20M reinforcing bars yielded at -1.5% drift (-33mm displacement) at a load of 91.8KN (moment=50.5KN.m).

An 8% drop in load was observed at +2.0% drift (22mm displacement); this was followed by some surface spalling of concrete around the major cracks at -2.0% drift (-22mm displacement). Widening of cracks was observed mostly at the major cracks near the faces of the column-stub. Further drops in load were observed at -2.5% drift (5% drop) and -3.0%

drift (5% drop). A 7.1% drop in load was observed at +4.0% drift (44mm displacement). During the next load stage of +4.5% drift (49.5mm displacement), one of the 15M reinforcing bars ruptured in positive bending at a load of 56KN (30.8KN.m). Some minor spalling of concrete was observed at this stage.

The beams was then cycled in negative bending and the load dropped by 5.5% and 9.3% in the second and third -4.5% drift cycles (-49.5mm displacement). Major cracks kept widening after this stage. After stabilizing the load started increasing with a 6% increase at -5.5% drift, 8.3% increase at 8.0% drift and 6.5% increase at -9.0% drift. Additional cover spalling was observed at -8.0% drift (176mm displacement). At -11.0% drift (220mm displacement), the major cracks at the bottom face of the beam widened considerably; this was followed by rupture of one of 20M reinforcing bars in negative bending at -11% drift (132mm displacement) at a load of 83.1 KN (45.7KN.m).

Comparing to the previous specimen, the addition of fibers resulted in some improvements in terms of crack control and damage tolerance. The response in positive bending was similar, however some improvements in performance were observed in negative bending. The overall response was similar to that of beam D/3-1.5% and showed some improvements compared to beams D/2-1.0%, D/3-1.0% and the control beams D/2-0.0% and D/4-0.0%.

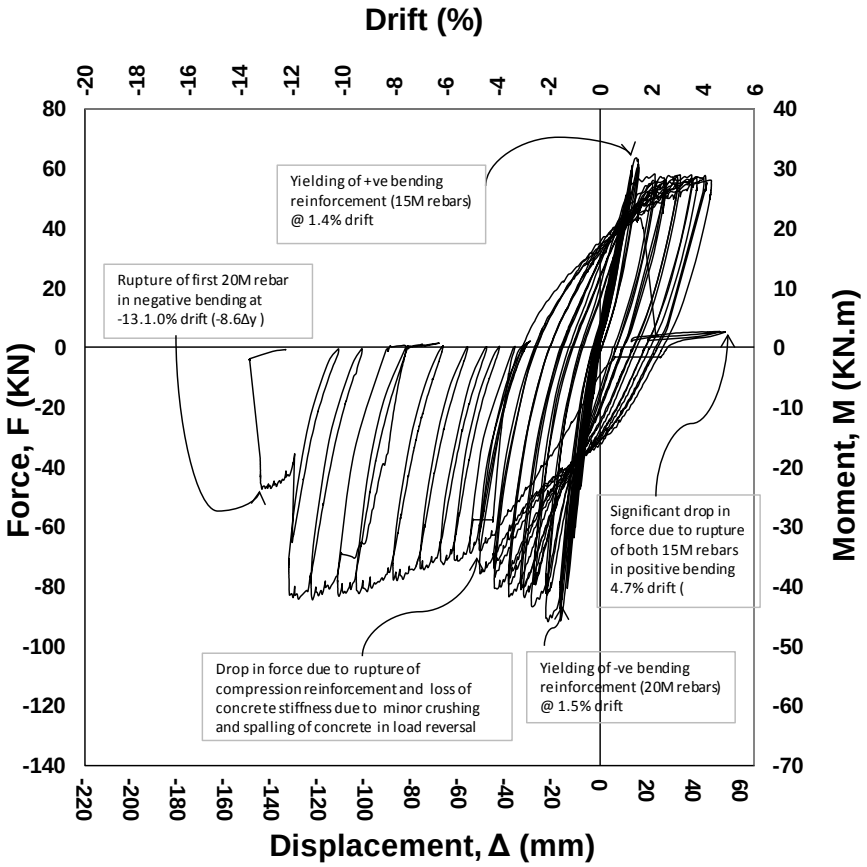

Figure 4.22 Force-Displacement Diagram for Beam D/4-1.0%

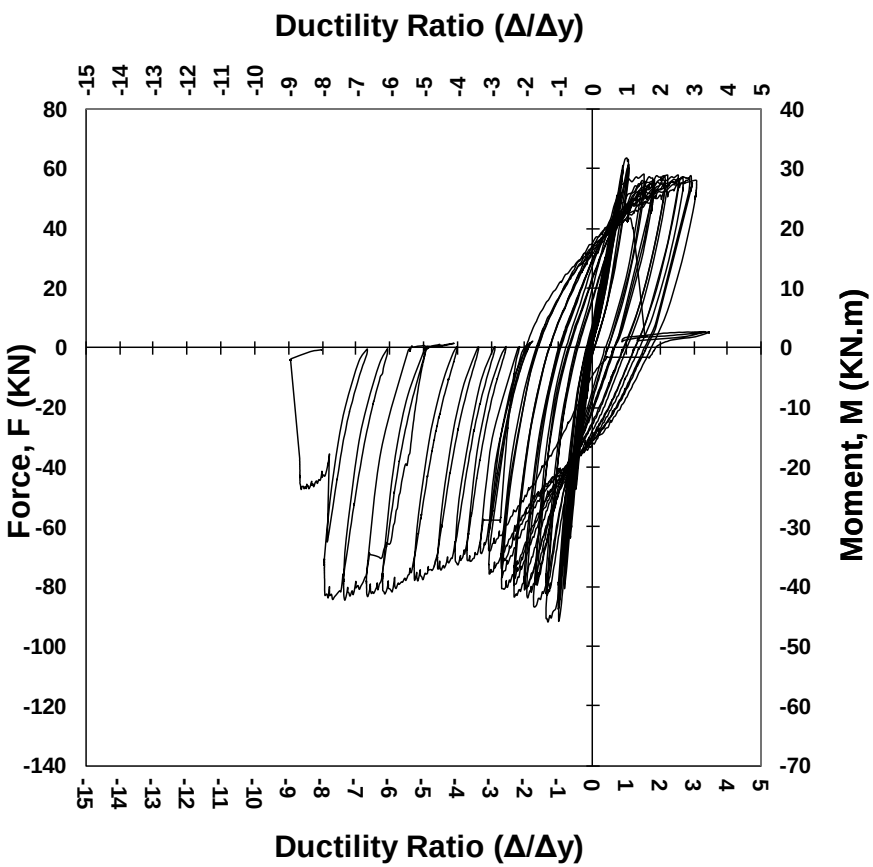

Figure 4.23 Force vs. Ductility Ratio for Beam D/4-1.0%

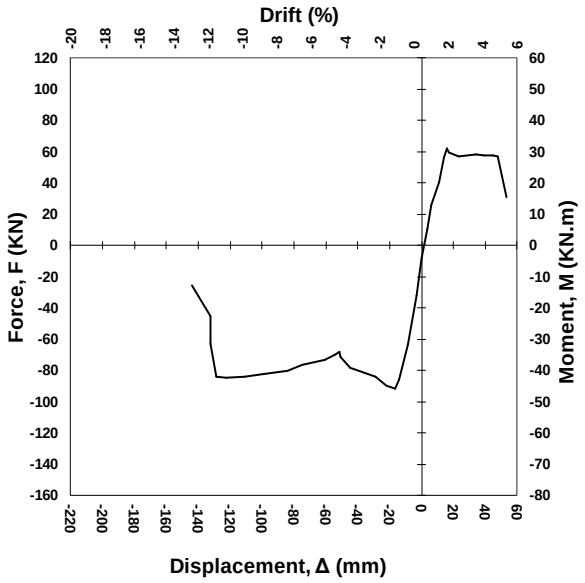

(a) Force-displacement response envelope

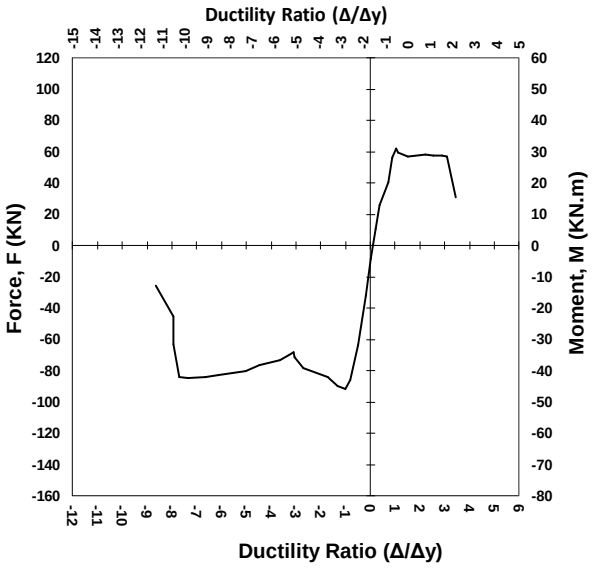

(b) Force-ductility ratio response envelope

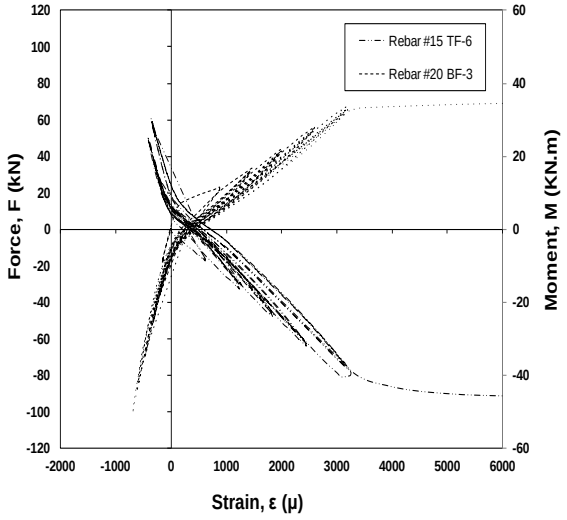

(c) Strain in longitudinal reinforcement at the face of t he middle block

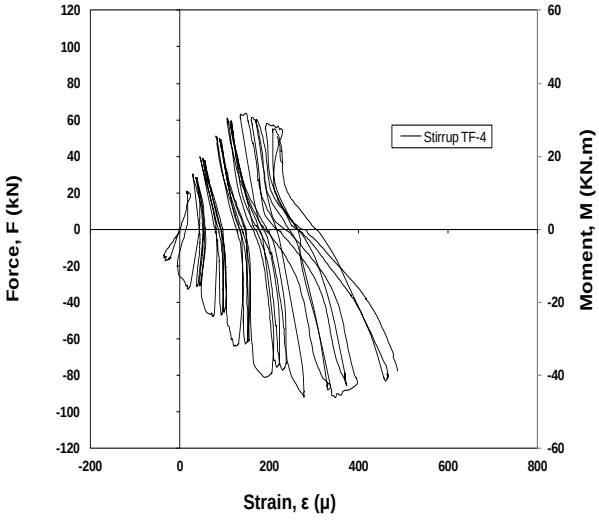

(d) Strain in a typical steel stirrup near the face of the middle block

Figure 4.24 Experimental results for beam D/4-1.0%

Table 4.15 Major event during positive bending of beam D/4-1.0%

	Positive bending - #15 rebars in tension		
Δ(mm)	Drift (%)	Δ/Δy	Comments
5.5	0.5	0.2	7 cracks appeared along the top of the beam.
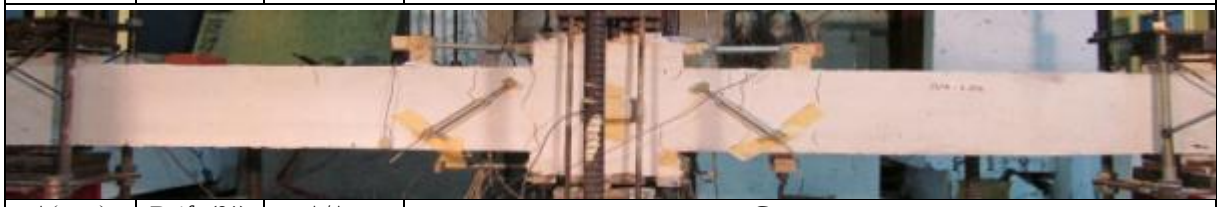			
Δ(mm)	Drift (%)	Δ/Δy	Comments
11	1	0.8	More cracks appeared along the top of the beam at approximately D/4 spacings Mostly in the right side of the middle block.
			
Δ(mm)	Drift (%)	Δ/Δy	Comments
16.5	1.5	1.2	Cracks started to concentrate at the faces of the middle block. The major crack with smaller cracks forking off of it was located approximately d from the right face of the middle block. The major crack on the left side was located right at the left face of the middle block. #15 rebars started to yield (they yield at 1.4% drift).
			

Table 4.15 Major event during positive bending of beam D/4-1.0%- continued

Δ(mm)	Drift (%)	Δ/Δy	Comments
22	2	1.6	~8%=5KN drop in load compared to +1.5% drift stage. Widening of the major cracks at both sides of the middle block. Further minor surface spalling at the major cracks is observed.

Δ(mm)	Drift (%)	Δ/Δy	Comments
27.5	2.5	2.0	Further widening of both major cracks plus slight loss of material at the left side crack. The horizontal crack at the #20 rebars level at the bottom right side of the middle block extended.

Δ(mm)	Drift (%)	Δ/Δy	Comments
38.5	3.5	2.9	A medium size chunk of concrete at the right major crack was disintegrated. A horizontal crack at the #15 rebar level appeared at the top right face of the middle block. The horizontal crack at the #20 rebar level at the bottom right face of the middle block widened further.

Δ(mm)	Drift (%)	Δ/Δy	Comments
49.5	4.5	3.7	One of the #15 rebars ruptured in the first cycle. The second #15 rebar ruptured at the second cycle. A small chunk of concrete spalled off at the top left face of the middle block. Other than above the condition of the cracks/ beam is almost the same as the previous stage. Concrete is considerably preserved compared to other specimens with lower fiber contents/ larger hoop spacing. Beam is considered failed in positive bending at this stage.

Table 4.16 Major event during negative bending of beam D/4-1.0%

D/4-1.0%	Negative bending - #20 rebars in tension		
Δ(mm)	Drift (%)	Δ/Δy	Comments
-5.5	-0.5	-0.2	4 cracks appeared along the bottom of the beam.
			
Δ(mm)	Drift (%)	Δ/Δy	Comments
-11	-1.0	-0.7	Existing cracks extended slightly further. More vertical cracks appeared further away from the plastic hinging region specially in the left side.
			
Δ(mm)	Drift (%)	Δ/Δy	Comments
-16.5	-1.5	-1.1	#20 rebars started to yield. Further Diagonal cracking was observed specially in the left side of the beam. More forking of existing cracks.
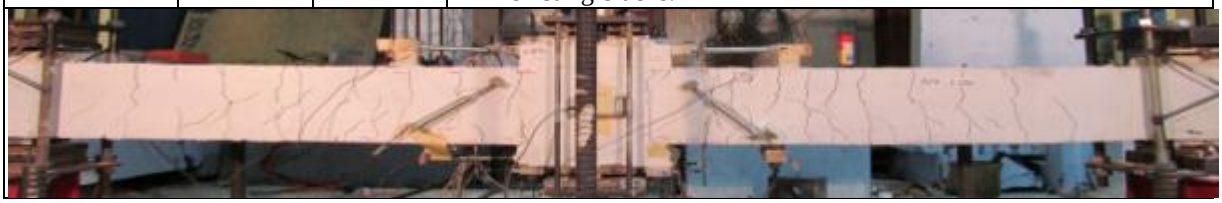			

Table 4.16 Major event during negative bending of beam D/4-1.0% - continued

Δ(mm)	Drift (%)	Δ/Δy	Comments
-22	-2	-1.5	Major surface spalling at the major cracks at the right and left faces of the middle block. As mentioned in +1.5 stage, the major crack at the right side of the middle block was located a distance of approximately d from the right face of the middle block.

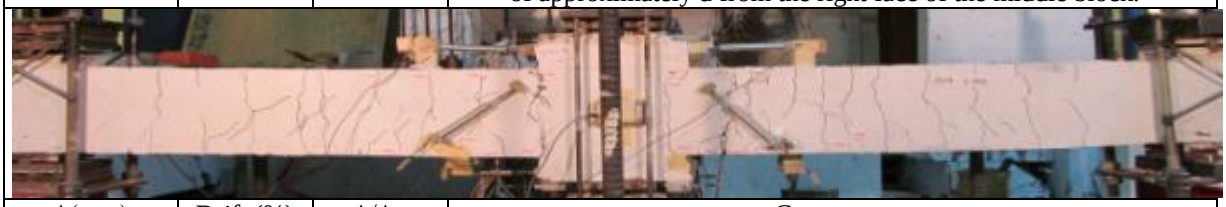

Δ(mm)	Drift (%)	Δ/Δy	Comments
-27.5	-2.5	-1.9	~5.4%=5KN drop in load compared to previous drift stage. Further widening of the major cracks. Other cracks seemed to remain unchanged. Further minor disintegration/crushing at the crack at the top left crack.

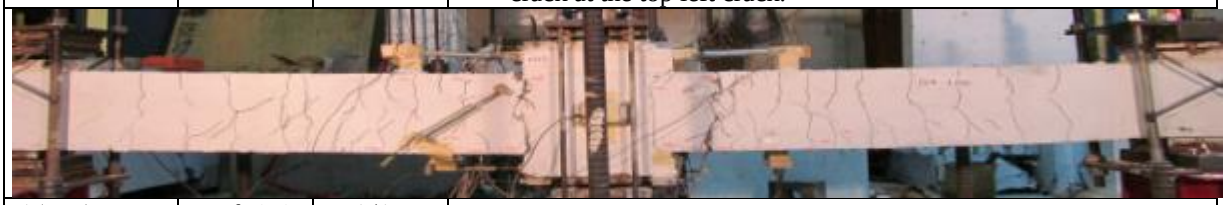

Δ(mm)	Drift (%)	Δ/Δy	Comments
-33	-3	-2.3	~5%=4KN drop in load compared to previous drift stage. Further minor disintegration and surface spalling at the major cracks (only). Other cracks seemed to remain unchanged.

Δ(mm)	Drift (%)	Δ/Δy	Comments
-44	-4	-3.0	~5%=4KN drop in load in the first cycle and further drops totalling 7.1%=6KN at the second and third cycles.

Table 4.16 Major event during negative bending of beam D/4-1.0% - continued

Δ(mm)	Drift (%)	Δ/Δy	Comments
-55	-5	-3.8	Slightly further opening of the major cracks at the bottom. Other than this the condition of the cracks remained unchanged.

Δ(mm)	Drift (%)	Δ/Δy	Comments
-60.5	-5.5	-4.2	~6%=4KN increase in load compared to the previous cycle. No major changes observed in the condition of the cracks/ beam.

Δ(mm)	Drift (%)	Δ/Δy	Comments
-88	-8	-6.1	~8.3%-6Kn increase in load compared to -5.5% drift stage. A large concrete wedge at the top left side of the middle block was disintegrated and seemed to be popping out of place.

Δ(mm)	Drift (%)	Δ/Δy	Comments
-99	-9	-6.8	~6.5%=5KN increase load compared to -8% drift stage. The major crack at the right side of the middle block remained almost unchanged. The concrete wedge at the left face of the middle block popped out slightly further but was still in place. The cracks around this wedge widened further. The counter-clockwise in-plane rotation of the middle block was easily seen at this stage.

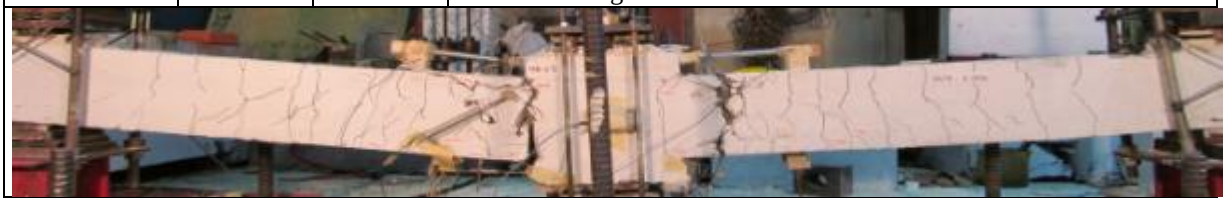

Table 4.16 Major event during negative bending of beam D/4-1.0% - continued

Δ(mm)	Drift (%)	Δ/Δy	Comments
-132	-12	-9.1	One of the #20 rebars ruptured at halfway to -13% (at almost the same displacement as -12% drift, this point is labeled as -12B in the graph); the load at this point was 65KN approximately 22% less than the first -12% cycle. .Slightly further in-plane rotation of the middle block and penning of the major crack at the bottom left side of the middle block is observed. No major changes in the condition of the cracks is observed.
			
Δ(mm)	Drift (%)	Δ/Δy	Comments
-143	-13	-9.9	Second #20 ruptured. No major changes in the condition of the cracks compared to the previous stage other than widening of the left side major crack. No major spalling was observed despite disintegration of large chunks of concrete at the left face of the middle block. End of test.
			

4.1.10 Beam D-1.5%

Beam D-1.5% was constructed with the same details of longitudinal reinforcement as all other specimens in the experimental program, however in this specimen the transverse reinforcement consisted of 6.35mm diameter steel hoops spaced at 204mm, corresponding to the effective depth of the beams. The beam was reinforced with 1.5% hooked end steel fibers. The objective of this test was to examine if provision of fibers could be used to fully replace required transverse reinforcement in the plastic hinge regions of flexural members.

Figure 4.25 and **Figure 4.26** show the reverse-cyclic response of the specimen in terms of applied load (and Mid-span moment) as a function of displacement (mm), drift (%) and ductility ratio (Δ/Δ_y). The figure also highlights the major events during testing. **Figure 4.27 (a)** and **(b)** show the backbone response in terms of drift (%) and ductility ratio (Δ/Δ_y). **Figure 4.27 (c)** and **(d)** show the strains in the longitudinal and transverse reinforcement. Major events during the testing of the specimen are graphically presented in **Table 4.17** and **Table 4.18** for the positive and negative bending cycles, respectively.

Hairline cracking appeared in this specimen at 0.5% drift (5.5mm displacement) in negative and positive bending. Diagonal cracks appeared at 1.0% drift (11 mm displacement) at the right side of middle block. Strain data indicates that the 15M and 20M reinforcing bars began to yield at approximately +1.6% drift (+17.6mm displacement) and -1.4% drift (-15.4mm displacement) with corresponding loads of 56.8KN (moment=32KN.m) and -93KN (moment=-51.2KN.m), respectively. Decrease in load of 6.5% and 3.0% were recorded during the cycles of ±2.0% drift. This was accompanied by the development of diagonal shear cracks in the hinge regions. Diagonal cracking was prevented in all other beams as they were reinforced with closely space transverse reinforcement.

It is noted that the condition of concrete (both in the cover and within the core) did not change significantly until rupture of first 15M rebar in positive bending at +4.0% drift (44mm displacement) at an applied load of 50KN (moment=27.5KN.m). At this point, the major vertical crack at the right face of the middle block widened considerably and load

dropped by 52%. With further cycles of loading at this stage horizontal cracks aligned with the longitudinal reinforcing bars widened and extended indicating that the longitudinal reinforcing bars in the compression were beginning to show signs of buckling due to the large spacing between the transverse hoops. At this stage the major vertical crack had widened to such an extent that slight dowel action of longitudinal reinforcing bars could be observed. When loading was switched to negative bending, the load initially increased by approximately 25% in the first -4.0% drift (44mm displacement) cycle. However this was followed by drops in load of 10% and 41% in the second and third cycles of -4.0% drift. Slight buckling of the remaining 15M reinforcing bar which in turned caused the fiber reinforced concrete cover to effectively spall as the bars pushed against the large pieces of cover. The second 15M rebar ruptured during the first +5.0% drift (55mm displacement) cycle. Top cover concrete was completely detached at this point. The load began to increase by approximately 30% at the first -5.0% drift (-55mm displacement) and was followed by 38% drop in the second cycle due to failure of the 15M rebar in the previous positive drift stage. Despite failure of the specimen, the beam was cycled under negative bending for the remainder of the test. The was observed to increase slightly between drift cycles of -6.0% (66mm displacement) to -13.0% (143mm displacement). Further crushing and spalling of concrete was observed at the -13.0% drift and -15.0% drift (176mm displacement) stages. Testing could not continue beyond this point as the maximum displacement of the testing apparatus was reached. The test ended at a -15.0% drift with the specimen having a residual load of 67KN (moment=37KN.m).

Compared to the control specimens (D/2-0% and D/4=0%) this beam showed some improvement in terms of crack control and damage tolerance. As in the previous SCFRC specimens, behaviour in positive bending was limited due to rupture of the 15M reinforcement. Following rupture of the 15M bars the beam showed improved response during subsequent negative bending cycles. The test results also demonstrated that SCFRC beams with large hoop spacing can be susceptible to reinforcing bar buckling.

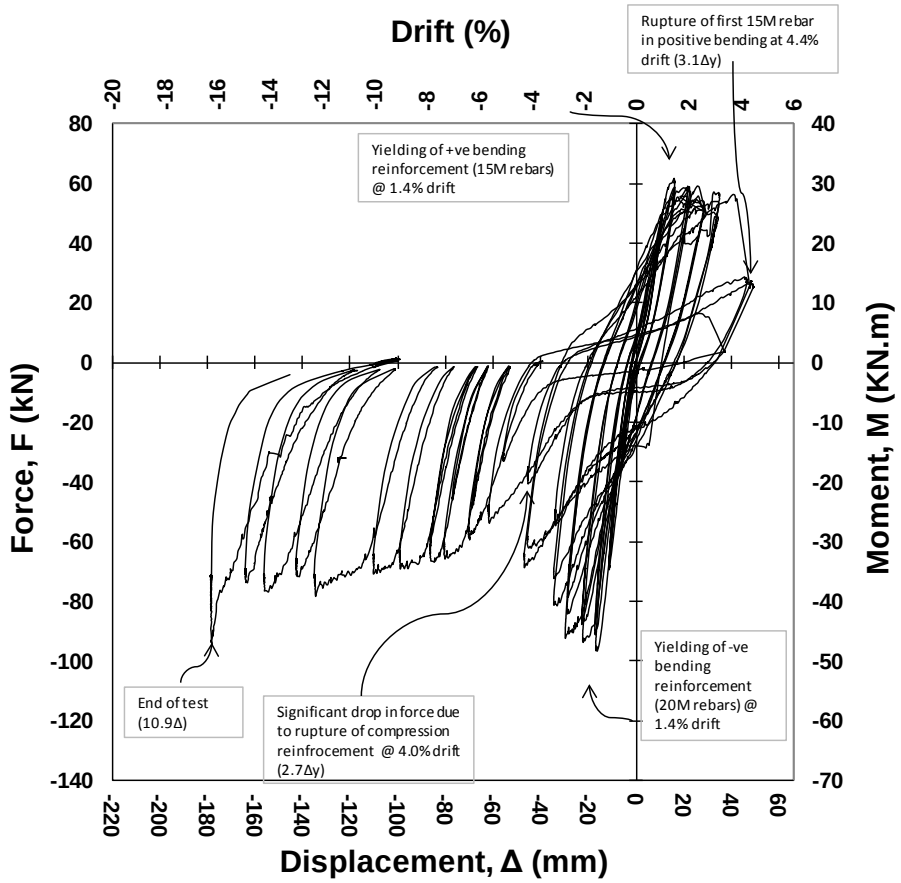

Figure 4.25 Force-displacement diagram for beam D-1.5%

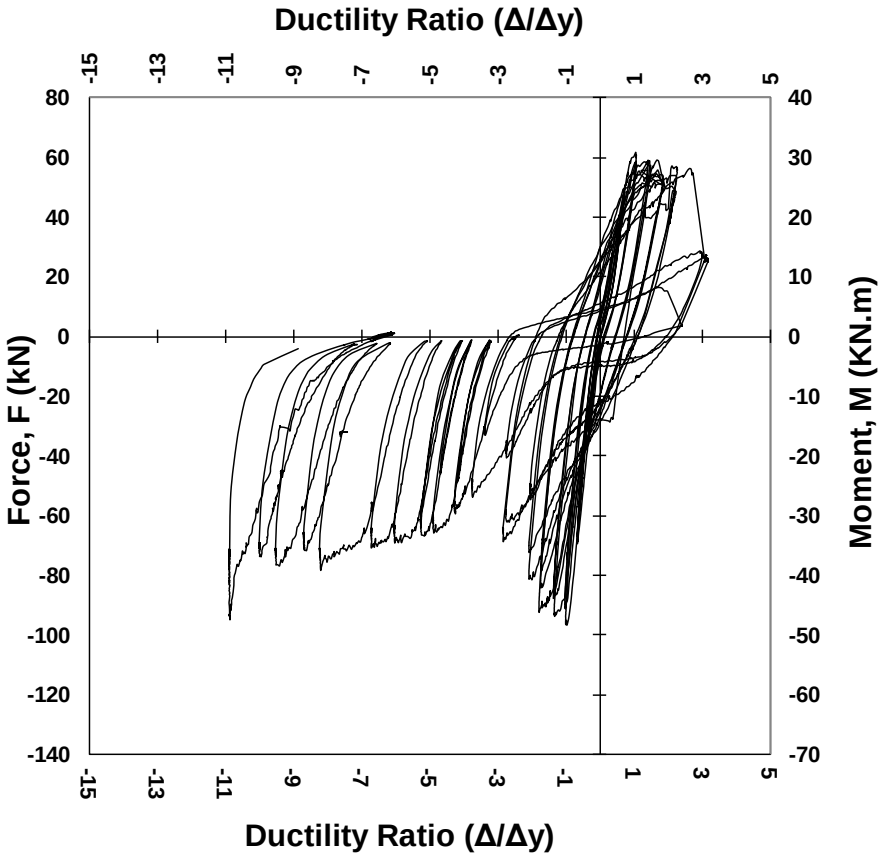

Figure 4.26 Force vs. ductility ratio for beam D-1.5%

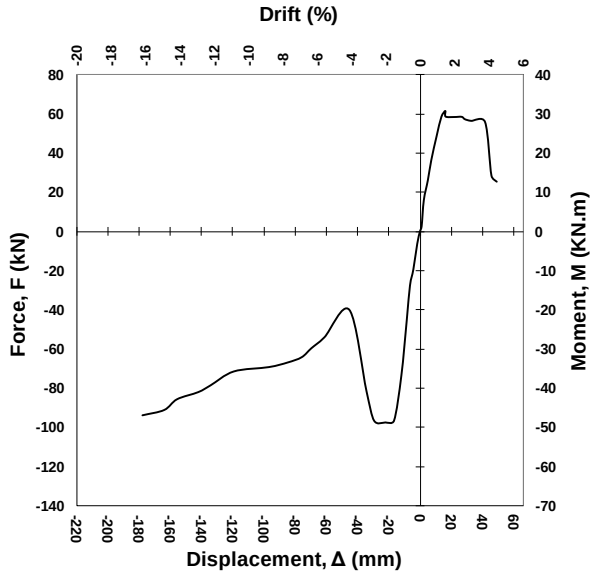

(a) Force-displacement response envelope

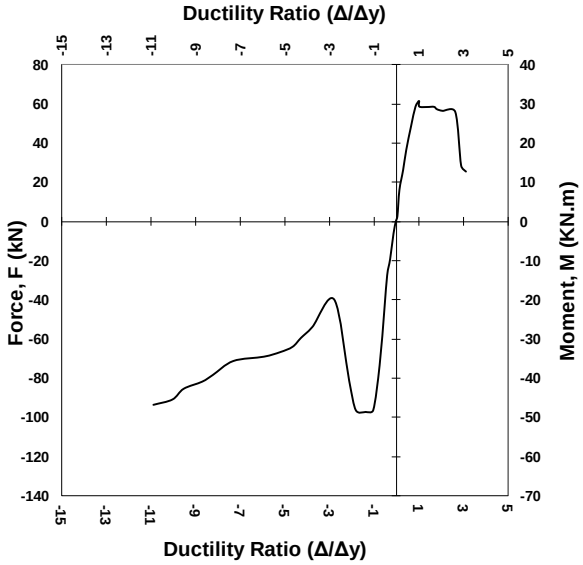

(b) Force-ductility ratio response envelope

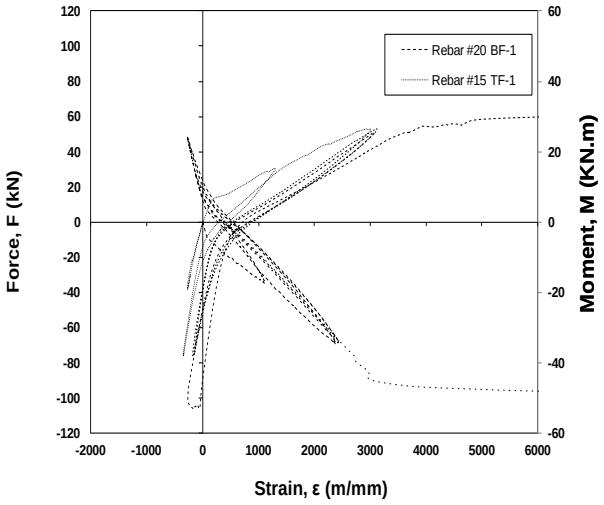

(c) Strain in longitudinal reinforcement at the face of t he middle block

Figure 4.27 Experimental results for beam D-1.5%

Table 4.17 Major event during positive bending of beam D-1.5%

Δ(mm)	Drift (%)	Δ/Δy	Comments
11	1	0.4	Several cracks appeared including diagonal cracks at the right side of the beam; forking of the existing cracks is observed.

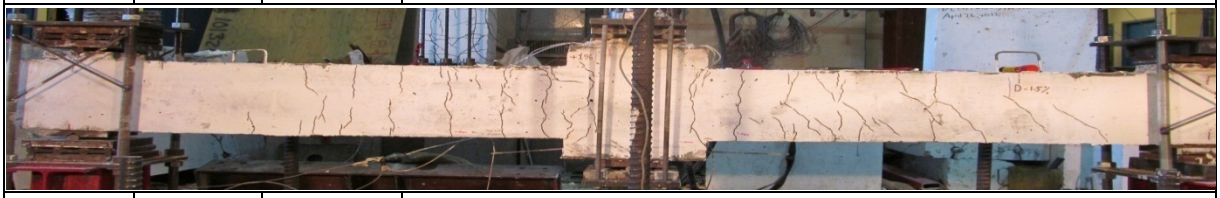

Δ(mm)	Drift (%)	Δ/Δy	Comments
16.5	1.5	0.6	More diagonal cracks and a few more vertical cracks appeared. More forking of the existing cracks was observed. #15 rebars started to yield.

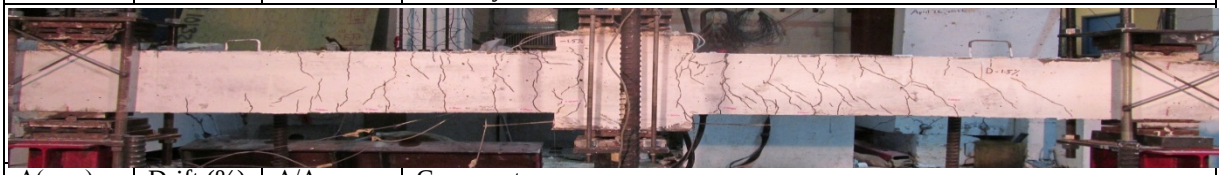

Δ(mm)	Drift (%)	Δ/Δy	Comments
22	2	0.814815	6.5%=3KN drop in load. A major straight crack formed of other existing cracks at the right side of the beam. The crack was almost perfectly vertical which may be related to higher stiffness of concrete due to high fiber content. This major crack opened up considerably at the top right side of the middle block. A small horizontal crack appeared at the #15 rebar level at the top right side of the middle block.

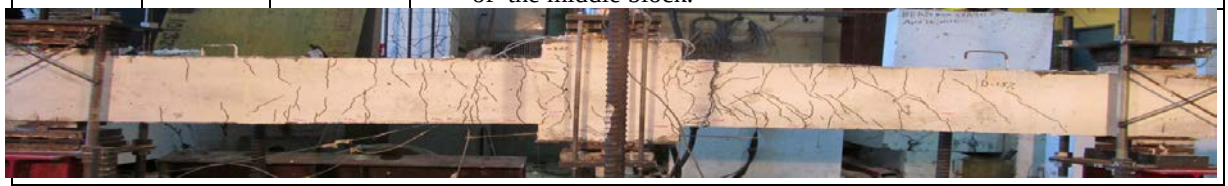

Δ(mm)	Drift (%)	Δ/Δy	Comments
44	4	1.6	One of the #15 rebars ruptured. 52%=29KN drop in load. The crack at the right and the horizontal cracks at the top and bottom at the rebar levels opened up significantly. Further disintegration of concrete was observed at the major crack in the right side of the middle block.

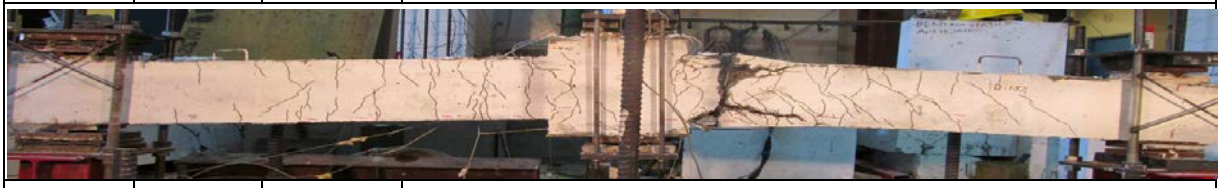

55	5	2.0	Second #15 rebar ruptured. Load dropped to almost zero. Beam considered failed in positive bending.

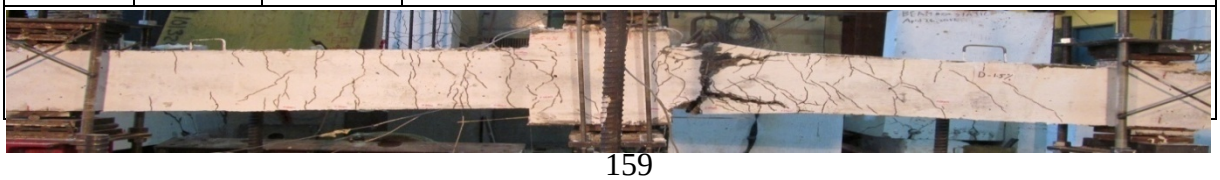

Table 4.18 Major event during negative bending of beam D-1.5%

Δ(mm)	Drift (%)	Δ/Δy	Comments
-5.5	-0.5	-0.2	8 vertical hairline cracks appeared at the bottom of the beam.

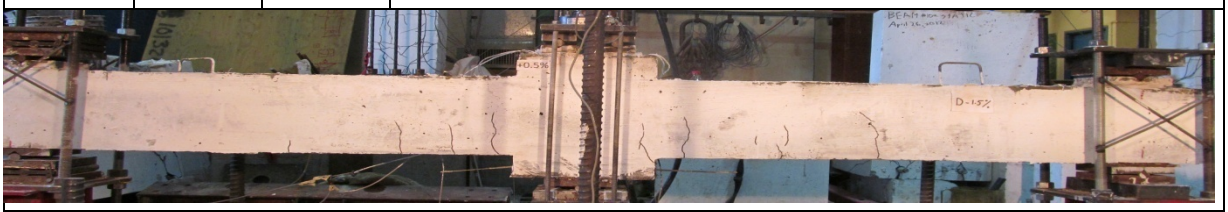

Δ(mm)	Drift (%)	Δ/Δy	Comments
-11	-1	-0.4	More cracks appeared at the bottom of the beam. More diagonal cracking appeared at the right side of the beam. More forking of the cracks is observed.

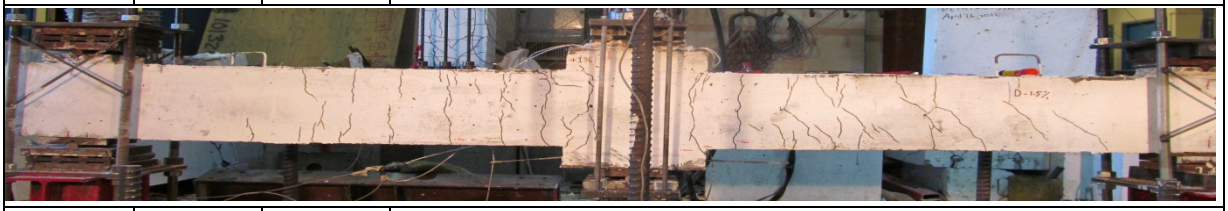

Δ(mm)	Drift (%)	Δ/Δy	Comments
-16.5	-1.5	-0.6	Several more diagonal cracks appeared specially at the right side of the beam. #20 rebars start to yield.

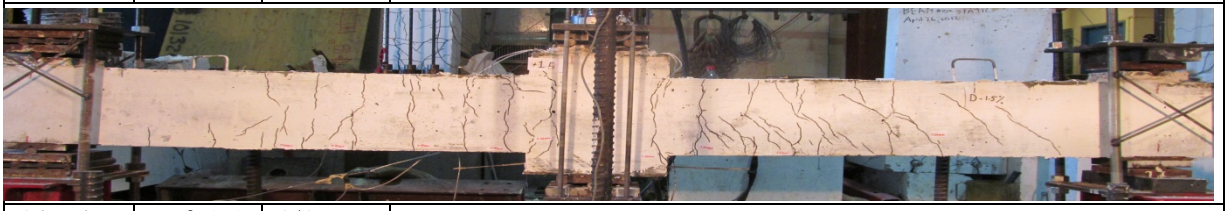

Δ(mm)	Drift (%)	Δ/Δy	Comments
-22	-2	-0.8	3% drop in load. Condition of the crack/ beam was almost unchanged compared to the previous cycle.

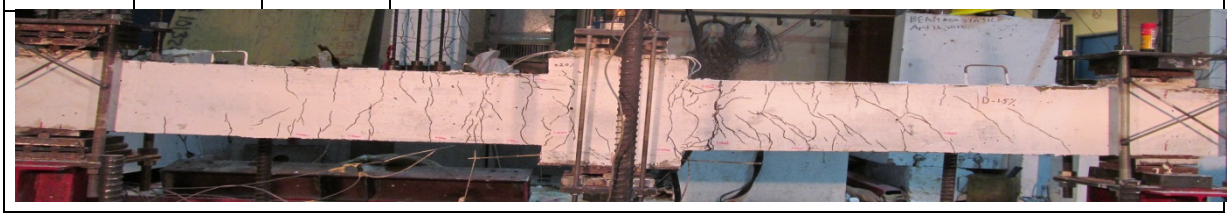

Table 4.18 Major event during negative bending of beam D-1.5% - continued

Δ(mm)	Drift (%)	Δ/Δy	Comments
-44	-4	-1.6	~28%=15KN increase in load in the first cycle. Load dropped by 10%=7KN and 41%=28KN in the second and third cycles respectively. The width of the cracks at the right side of the middle block was almost the same as the previous drift stage. Top concrete cover completely disintegrated and spalled. Bottom cover disintegrated but was still in place. Further loss of material at the crack. Major shift of the middle block against right crack was observed. Dowel action was evident at this stage.
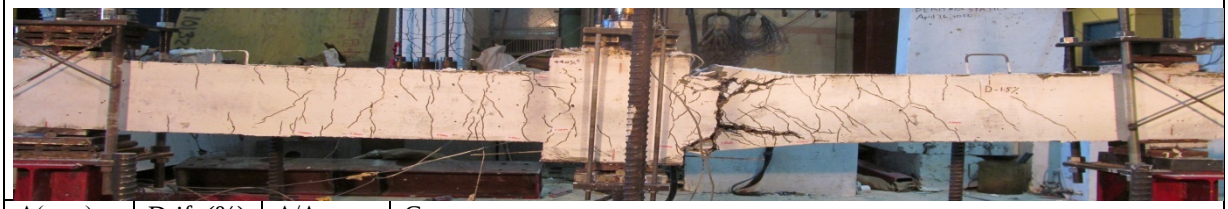			
Δ(mm)	Drift (%)	Δ/Δy	Comments
-55	-5	-2.0	30%=12KN increase in load in the first cycle compared to the previous drift stage and 38%=20KN drop in load in the second cycle (compared to first stage). Top cover had completely spalled off. Bottom cover was still remaining but had spalled out of place. Significant rotation of the middle block was observed.
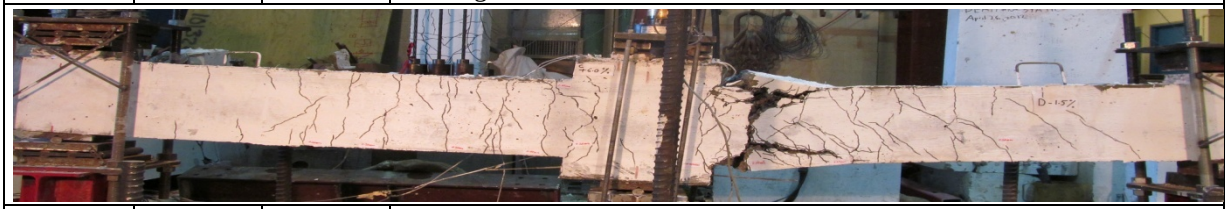			
Δ(mm)	Drift (%)	Δ/Δy	Comments
-66	-6	-2.4	9.5% increase in load compared to the previous drift stage. Condition of cracks/ beam was almost unchanged compared to previous drift stage.
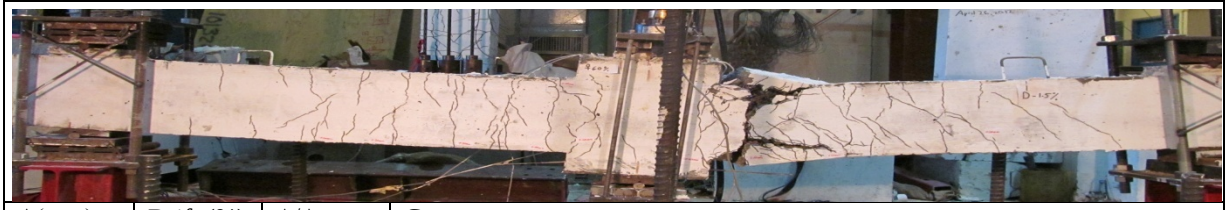			
Δ(mm)	Drift (%)	Δ/Δy	Comments
-77	-7	-2.9	10%=6KN increase in load compared to the previous stage. Further rotation of the middle block was observed. Crack / beam condition was almost unchanged from previous stage.
			

Table 4.18 Major event during negative bending of beam D-1.5% - continued

Δ(mm)	Drift (%)	Δ/Δy	Comments
-99	-9	-3.7	Slight increase in load. Crushing/ surface spalling was seen at a horizontal crack at mid-height of the beam next to the right side major crack. Further rotation of the middle block was observed.

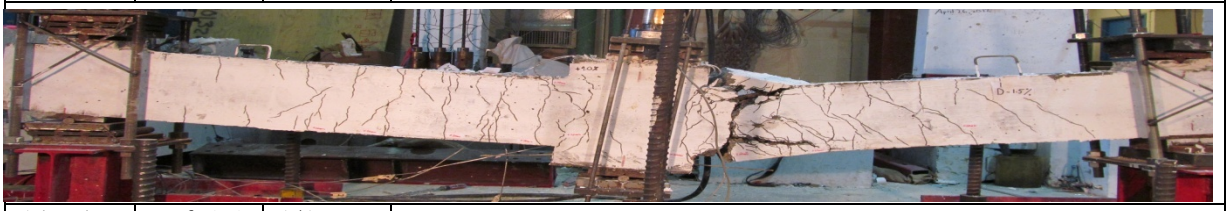

Δ(mm)	Drift (%)	Δ/Δy	Comments
-132	-12	-4.9	~9%=7KN increase in load compared to the previous stage. Further rotation of the middle block was observed. No other major change was observed in the condition of the cracks/ beam.

Δ(mm)	Drift (%)	Δ/Δy	Comments
-143	-13	-5.3	~7%=5KN increase in load compared to the previous drift stage. Significant clockwise rotation was observed in the middle block. The condition of the cracks was almost unchanged except further crushing/ surface spalling at the mid-height horizontal crack.

Δ(mm)	Drift (%)	Δ/Δy	Comments
-176	-16	-6.5	Further small disintegration at the right side crack including the mid-height horizontal crack which extended slightly further. Significant clockwise rotation of the middle block was observed. The bottom right edge of the middle block was touching the instrumentation board at the bottom. Test could not continue further.

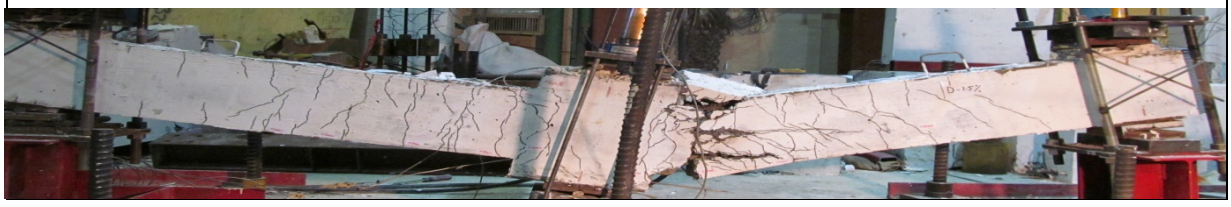

Chapter 5 Analysis of Experimental Results

5.1 Introduction

Detailed behavior of the various specimens in terms of force versus displacement response, strains in steel reinforcement, and major changes during testing was presented in chapter 4. In this chapter, the results are compared in order to investigate the effect of steel fibers and transverse reinforcement on the structural behavior of the SFRC flexural members tested in this experimental program.

5.2 Test Parameters

Four different series of specimens with different levels of transverse reinforcement, constructed with varying amounts of steel fibers were tested in this research program. As such the test parameters in this experimental program consist of steel fiber content and transverse reinforcement ratio. In order to evaluate the effects of these parameters on structural response the following factors were analyzed and compared:

- Flexural capacity
- Initial stiffness of beams
- Energy dissipation and post-peak ductility
- Buckling and rupture of Longitudinal reinforcement
- Crack control and damage tolerance

5.2.1 General comparison of member hysteretic response

Figure 5.1 to **Figure 5.4** present the force-displacement curves for the tested specimens (also expressed in terms of Moment and drift). The effects of the test parameters on the structural response can be examined by comparison of the force-displacement curves for the beams in different series with varying steel fiber contents and transverse reinforcement ratios.

The beams in each series (D/2, D/3, D/4) had constant transverse reinforcement ratios and varying steel fiber contents. Thus comparison of the beams within each series allows for an investigation of the improvements in structural response due to addition of steel fibers. Comparison of the beams shows that while modest changes in flexural capacity are observed for beams with up to 1% fiber

content, addition of 1.5% fibers results in more pronounced improvements. All beams with steel fibers experienced rupture of the 15M reinforcing bars during positive bending, nonetheless beams with steel fibers in each series show higher ductility in the post-peak region in negative bending; this enhancement in performance becomes more significant as the fiber content increases as is demonstrated in the responses of the beams with 1.5% fiber content. Comparison of the hysteretic response of the beams in each series also demonstrates that the beams reinforced with steel fibers exhibit significant reductions in 'pinching' which is an indication of higher energy dissipation capacity. The improvements in response can be linked to the enhancements in tensile resistance and post-cracking capacity of concrete, and contributes to damage tolerance of SFRC beam members.

Furthermore, increasing transverse reinforcement ratios while keeping all other parameters constant generally resulted in improvements in structural behaviour of the beams. While this improvement was small in case of the control beams without steel fibers (D/2-0.0 % vs. D/4-0.0%**)**, significant improvements were observed in the beams having same fiber content of 1% but varying amounts of transverse reinforcement (compare D/2-1%, D/3-1% and D/4 1.0%). It can be seen that increasing the amount of transverse reinforcement improves energy dissipation when considering the negative bending cycles. In addition, higher transverse reinforcement ratio (in both the control series and the 1% series) resulted in reduced slightly pinching and hence higher energy dissipation capacity.

The results also show that combination of high fiber contents with closely spaced hoops in beams D/3-1.5% and D/4-1.0% results in more significant improvements in overall response and contributes to development of strain hardening in the longitudinal reinforcement and hence improves ductility.

Beam D-1.5%, which was reinforced with a the minimum amount of transverse reinforcement (with spacing corresponding to d=204mm) and 1.5% steel fibers, showed significant improvements in post-peak ductility and flexural strength in negative bending, however the very large spacing of the transverse reinforcement resulted in increased pinching when compared to other beams with

same amount of steel fibers and higher transverse reinforcement ratios (D/2-1.5%, D/3-1.5% and D/4-1.5%). In addition, this beams showed severe buckling of reinforcement and thus results indicate the importance combining steel fibers with at least a minimum level of transverse reinforcement.

Unequal flexural reinforcement in positive and negative bending generally resulted in poor performance of the SCFRC beams as the beams failed in positive bending at earlier stages of loading due to rupture of positive bending reinforcement (2-15M bars). Beams reinforced with 1.0% or higher steel fibers were able to undergo larger displacements in negative bending at drift stages of up to 16.0% while they failed in positive bending at drifts of approximately 5.0%. This finding (i.e. effect of unequal longitudinal reinforcement) has previously been reported for traditional RC beams by Fenwick and Fong (1979). Better performance may have been possible had equal amounts of reinforcement (2-20M at both top and bottom) been used in the SFRC specimens.

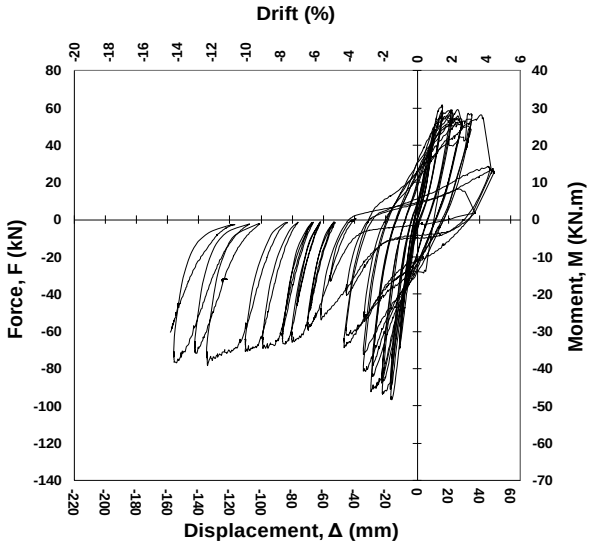

Figure 5.1 Force-displacement diagram for beam D-1.5%

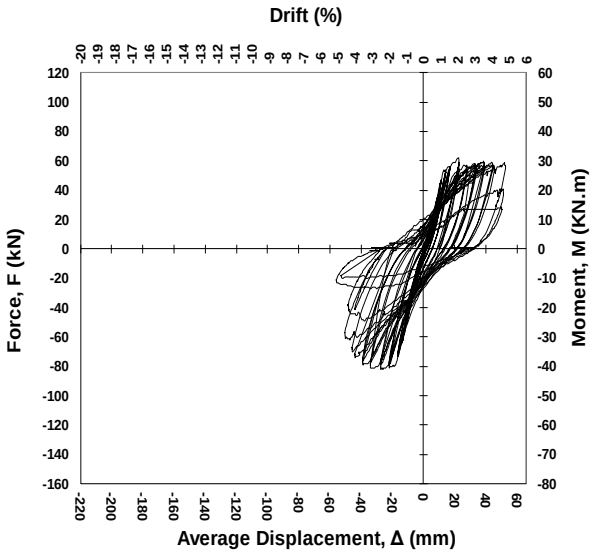

(a) D/2-0.0%

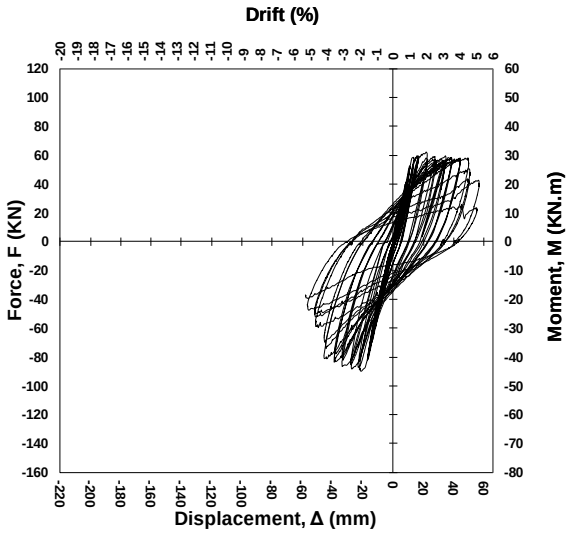

(b) D/2-0.75%

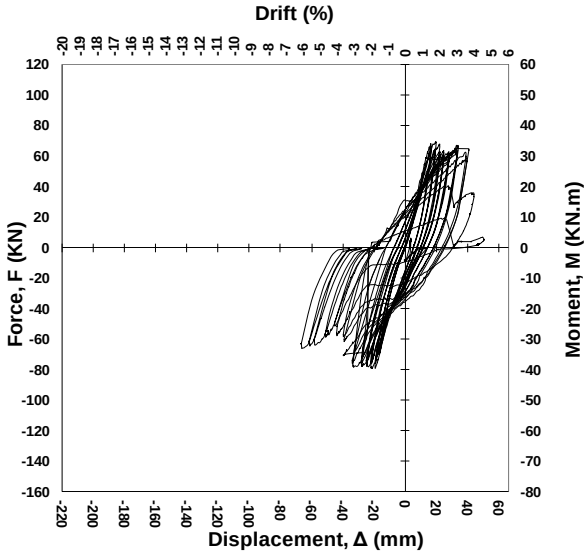

(a) D/2-1.0%

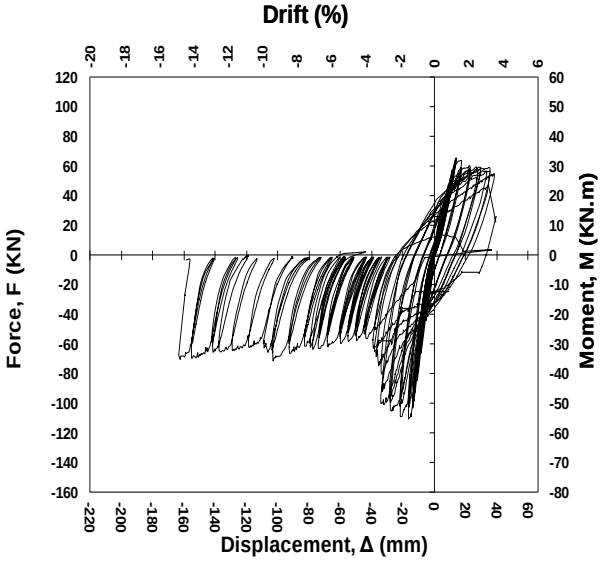

(b) D/2-1.5%

Figure 5.2 Force-displacement diagrams for the D/2-series specimens

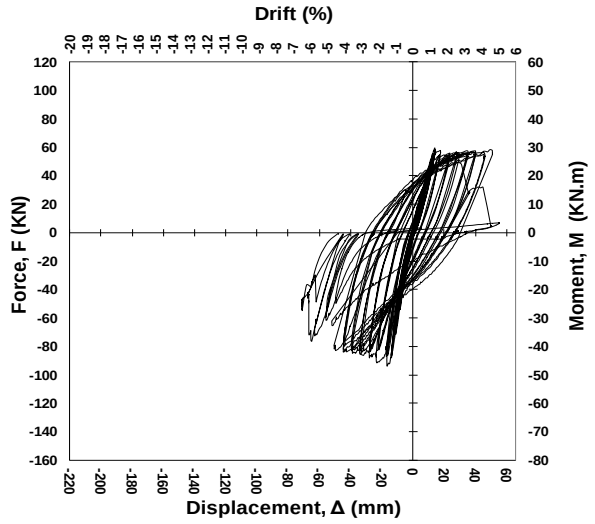

(b) D/3-1.0%

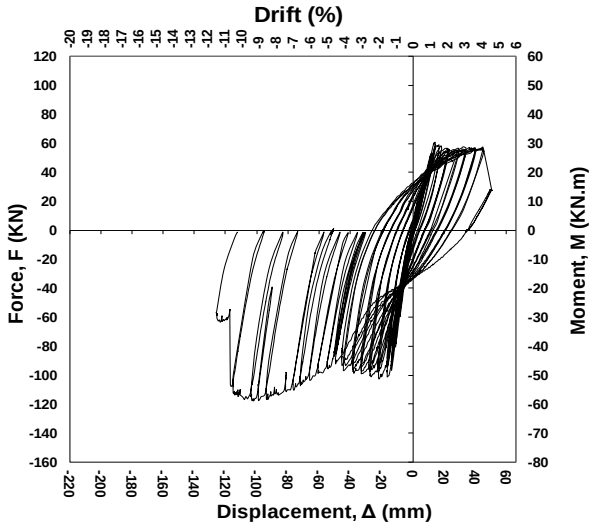

(b) D/3-1.5%

Figure 5.3 Force-displacement diagrams for the D/3 series specimens

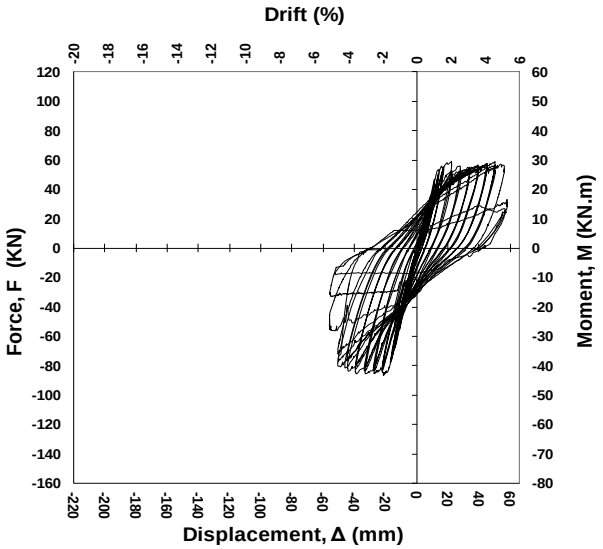

(a) D/4-0.0%

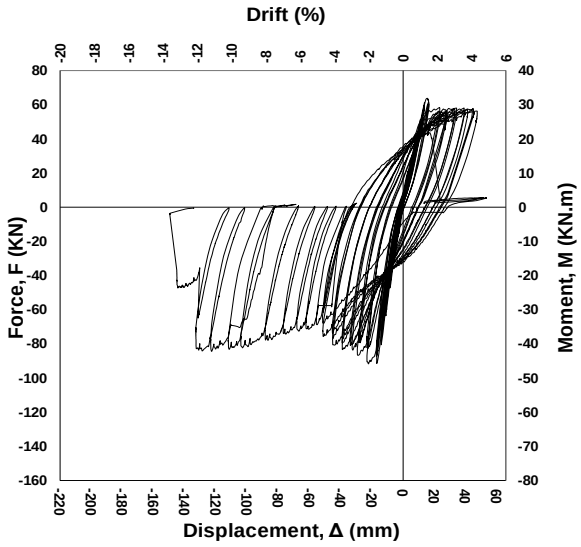

(b) D/4-1.0%

Figure 5.4 Force-displacement diagrams for the D/4 series specimens

5.3 Effect of test parameters on Flexural capacity

Table 5.1 shows the flexural capacities of the various beams tested in the experimental program. **Table 5.2** also shows the improvements in flexural strengths due to addition of steel fibers by comparing the results of the beams in each respective series (D/2, D/3 and D/4). Generally, the test data demonstrates that addition of steel fibers results in increase in the flexural strengths in both positive and negative flexure for the tested specimens. Comparison of the results from all three series also shows that as the fiber content increases the relative improvement in flexural strength also increases. This increase was more significant in specimens with 1.5% steel fibers. For example in the D/2 series, while addition of 0.75% fibers resulted in modest increases of 0.3% and 9.6% in positive and negative bending strength, respectively, doubling the fiber content to 1.5% resulted in 6% and 34.5% increase in positive and negative bending strength when compared to the control specimen without fibers. It is noted that Beam D/2-1.0% in this series, does not follow this trend, showing a 3.96% drop in negative bending strength when compared to the control specimen. This could be related to experimental errors during casting which may include improper mixing of steel fibers, and testing of this specimen.

Comparing the beams in D/3 series, specimen D/3-1.5% showed 1.17% and 25.75% increase in the positive and negative flexural strengths, respectively, when compared to specimen D/3-1.0%. It is to note that the maximum flexural strength in negative bending for beam D/3-1.5% occurred at -9.4% drift ($\Delta/\Delta y = -7.11$) due to strain hardening in the 20M reinforcing bars. The additional flexural strength in negative bending due to the strain hardening effect was 18% compared to the peak strength recorded at the onset of yielding for this beam.

Comparing the results for the D/4 series, beam D/4-1.5% showed 7.5% and 5.8% increase in negative and positive bending, respectively, when compared to the specimen without fibers.

The results also generally show that the effect of fibers in increasing flexural strength is more important in negative bending when compared to the case of positive bending. Research has shown that in addition to improving tensile behavior, the addition of steel fibers significantly

improves behavior of concrete in compression. Tests on columns by Aoude et al. (2009) has shown that addition of steel fibers to concrete results in significant improvements in the behavior of confined and unconfined concrete columns. Unequal amounts of flexural reinforcement in positive and negative bending resulted in unequal compression zone depths due to the variation in the location of the neutral axis, with the larger compression zone in negative bending due to higher negative flexural reinforcement ratio. Thus, the effects of steel fibers were more evident in the case of negative bending.

Table 5.1 Experimental flexural strengths of tested specimens

Specimen	*Positive Moment (KN)*	*Δ/Δy*	*Drift (%)*	*Negative Moment (KN)*	*-Δ/Δy*	*Drift (%)*
D/2-0/0%	34.1	1.7	2.0	-45.1	1.5	-2.5
D/2-0.75%	34.2	1.8	2.0	-49.5	-1.0	-1.9
D/2-1.0%	37.7	1.2	1.8	-43.3	-1.0	-1.7
D/2-1.5%	36.1	1.1	1.3	-60.7	-1.0	-1.5
D/3-1.0%	33.0	1.0	1.3	-51.5	-1.2	-1.6
D/3-1.5%	33.4	1.0	1.3	-64.8	-7.1	-9.4
D/4-0.0%	32.5	1.7	2.0	-47.9	-1.1	-2.0
D/4-1.0%	34.9	1.0	1.5	-50.6	-1.3	-2.0
D-1.5%	33.8	1.0	1.5	-52.3	-0.9	-0.7

Table 5.2 Effect of steel fibers on flexural strength

Specimen	*% change in positive moment strength*	*% change in negative moment strength*
D/2-0/0%	Control	Control
D/2-0.75%	0.3	9.6
D/2-1.0%	10.5	-4.0
D/2-1.5%	6.0	34.5
D/3-1.0%	Control	Control
D/3-1.5%	1.2	25.8
D/4-0.0%	Control	Control
D/4-1.0%	7.5	5.8
D-1.5%	-	-

Table 5.3 shows the effect of hoop spacing on flexural strengths for beams relative to the control specimens for beams with the same steel fiber content. The results demonstrate that varying hoop spacing generally does not show a consistent trend in enhancing the flexural

strengths of the beams in positive bending. While there is no trend for the case of strength in positive bending (which has reduced flexural reinforcement ratio), increasing the amount of transverse reinforcement generally resulted in increased negative bending strength when comparing beams having same fiber content. The exception to this trend is beam D/4-1.0% which showed reduced strength when compared to beam D-1.5%. This can partly be explained by the fact that this beam was constructed with a different batch of 20M reinforcing bars which had reduced yield strength. As noted in Chapter 3, initial casting of beam d/4-1.0% resulted in excessive voids due to poor consolidation of the concrete in the heavily congested hinge regions. Subsequently a second beam was cast using this new set of reinforcing bars.

Table 5.3 Effect of transverse reinforcement on flexural strength

Specimen	***% change in positive bending***	***% change in negative bending***
D/2-0/0%	Control	Control
D/4-0.0%	-4.8	6.2
D/2-1.0%	Control	Control
D/3-1.0%	-12.5	18.9
D-1.5%	Control	Control
D/2-1.5%	6.8	16.1
D/3-1.5%	-1.4	23.9
D/4-1.5%	3.1	-3.3

5.4 Effect of test parameters on initial stiffness

Experimental results show that steel fibers slightly increase the initial stiffness of the beams. This effect is only observed in negative bending while no major improvement is seen in initial stiffness of the beams in positive bending.

Figure 5.5 (a) to **(c)** show Force-displacement response envelopes for beams with the same amount of transverse reinforcement and varying steel fiber contents. It can be seen than the initial stiffness of the beams, defined here as the slope of the elastic portion of the Force-displacement response envelope, increases as the fiber contents increases. This increase is not significant for beams with fiber contents of 1.0% or lower, however, beams with 1.5% steel fiber content show a more pronounced increase in initial stiffness. As discussed previously the SFRC mixtures containing 1.5% were expected to show enhanced behavior in tension with tension-hardening response and improved crack control due to the high amount of fibers; this may partly explain this trend.

Figure 5.6 (a) to (c) compare the Force-displacement response envelopes for beams with equal amount of steel fibers and varying transverse reinforcement spacing. As seen in these figures, the initial stiffness of the beams does not change significantly with increasing amount of transverse reinforcement in the hinge regions.

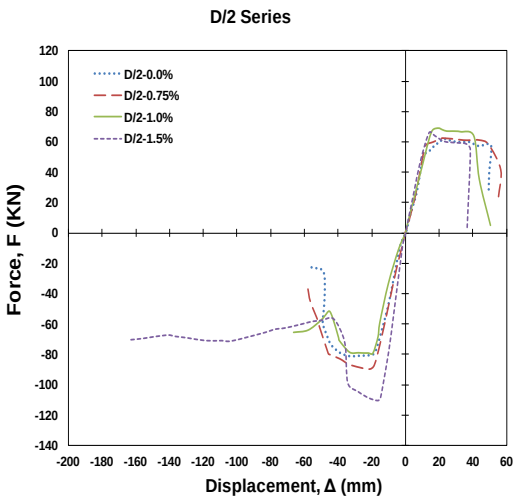

a) Comparison of experimental force-displacement curves for D/2 series

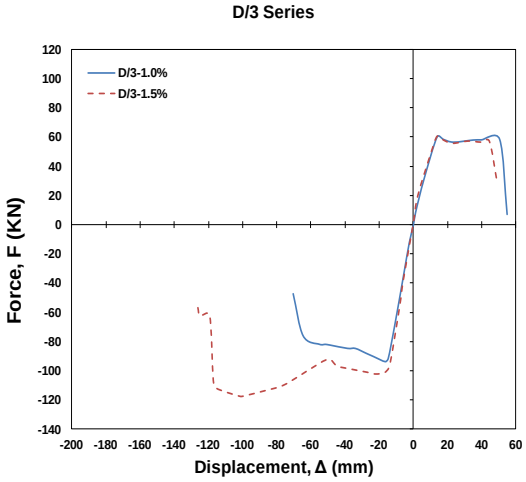

b) Comparison of experimental force-displacement curves for D/3 series

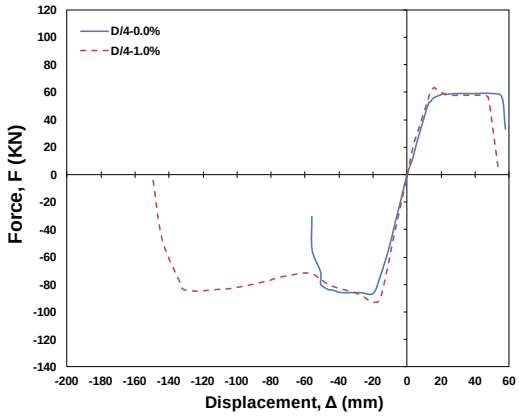

c) Comparison of experimental force-displacement curves for D/4 series

Figure 5.5 Comparison ofexperimental Force-displacement response envelopes for beams with equal transverse reinforcement spacing

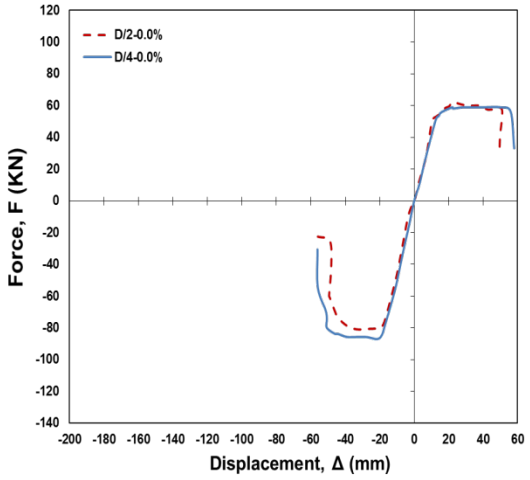

a) Comparison of experimental force-displacement curves for 0.0% series

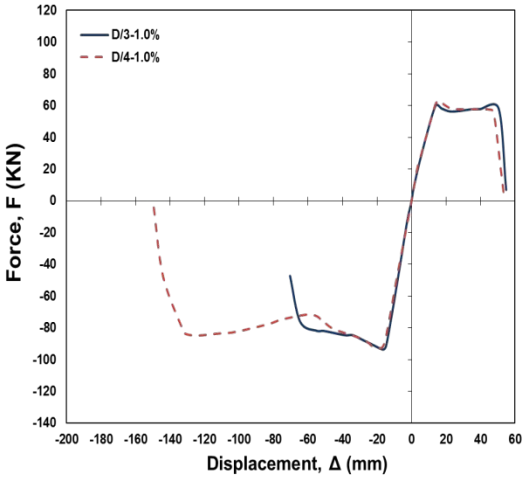

b) Comparison of experimental force-displacement curves for 1.0% series

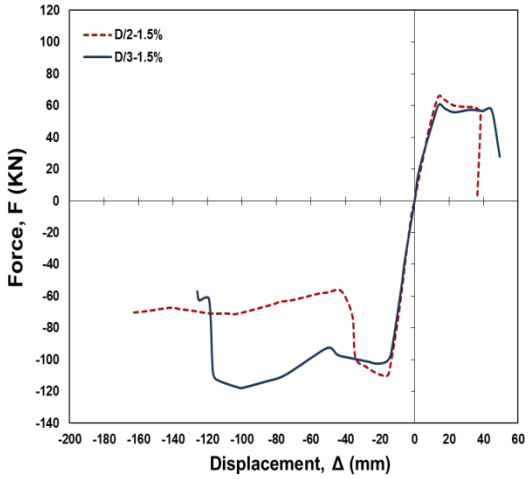

c) Comparison of experimental force-displacement curves for 1.5% series

Figure 5.6 Comparison of experimental Force-displacement response envelopes for beams with equal steel fiber contents

5.5 Effect of test parameters on energy dissipation capacity

The seismic design of ductile reinforced structures requires members to sustain large inelastic deformations and dissipate energy in a ductile manner during earthquakes. For members subjected to load reversals such as those tested in this experimental program, energy dissipation capacity can be defined as the area enclosed by the load-displacement loops in the member's hysteretic response as depicted in **Figure 5.7**.

It is to note that the "energy dissipation" referred to in this analysis consists of the total area under the load-displacement response including the area corresponding to the total "energy" in negative bending. The SFRC beams tested in this experimental program failed at relatively early drift stages due to rupture of the 15M bars during positive bending; nonetheless, comparing the total energy (while including the negative bending cycles after failure of the 15M bars) allows for an evaluation of the effects of fibers in enhancing the structural performance of beams in terms of energy dissipation capacity. In addition it allows for assessment of the improvements that could be achieved should SCFRC flexural members be detailed with equal amounts of flexural reinforcement in both positive and negative bending.

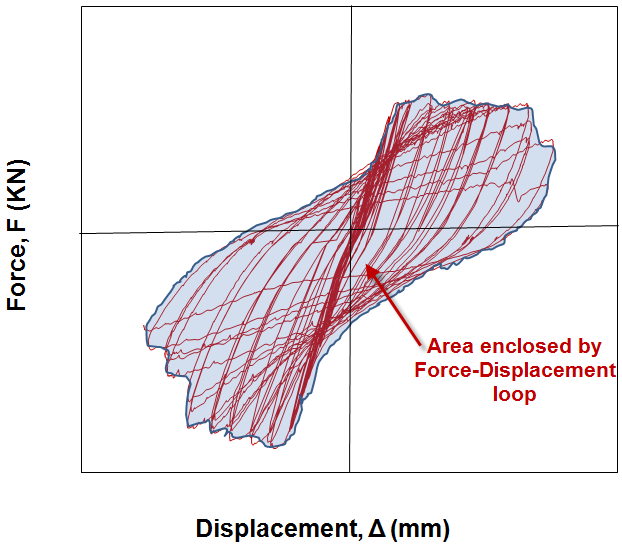

Figure 5.7 Determination Energy Dissipation Capacity

Figure 5.9 to **Figure 5.11** plot the areas enclosed by the load-displacement responses for specimens in the D/2, D/3 and D/4 series, respectively. The effect of the fibers in improving

energy dissipation was illustrated by overlaying the enclosed areas of hysteresis loops for the tested specimens. It can be seen that as the transverse reinforcement is kept constant, increasing fiber content is accompanied by increased energy dissipation as represented by increase in enclosed area. In addition overlaying the areas reveals slightly less pinching for specimens with fibers which can be associated with improvements in damage tolerance in the plastic hinge regions.

Table 5.4 and shows the total energy for the specimens in the D/2, D/3 and D/4 series. It can be seen that the total energy increases as higher fibers contents are used for beams with equal amounts of transverse reinforcement. The results are also plotted for each series in **Figure 5.8.** A slight increase in energy dissipation capacity is observed for beam D/2-0.75% when compared to the specimen without fiber, however as the fiber content increases to 1.5% there is a more significant improvement in amount of energy dissipated. A similar trend is observed when comparing the beams with 1% and 1.5% fibers in the D/3 series. Combined use of steel fibers and closely spaced transverse reinforcement in the D/4 series shows significant increase in the amount of energy dissipated.

Figure 5.12 to **Figure 5.14** compare the areas enclosed by the force-displacement curves for beams with equal amounts of steel fiber contents and varying amounts of transverse reinforcement. The amount of energy dissipated is also presented in **Figure 5.8 (b)**. In the control specimens without fibers (0% series), only a slight increase in energy dissipation capacity due to higher transverse reinforcement ratios is observed. Beams D/2-0.0% and D/4-0.0% exhibited very similar force-displacement relationships. Both beams failed in positive and negative bending at an average drift of approximately 5.0%. The gain in energy dissipation capacity of Beam D/4-0.0% due to higher transverse reinforcement ratio was about 19%. This was expected because the beams in this test program where subjected to relatively low shear stresses. Furthermore, it is observed that increasing the amount of transverse reinforcement in the control beams has led to reduced pinching due to improvements in diagonal shear capacity and increased damage tolerance in the plastic hinge regions is observed. For the case of the specimens with 1 % fibers, the increase in transverse

reinforcement in beams D/4-1.0% and D/3-1.0% when compared to beam D/2-1.0% shows important improvements in energy dissipated. The results illustrate the benefits of combining closely spaced transverse reinforcement with moderate amounts of steel fibers. At higher fiber contents of 1.5% where enhanced damage tolerance, shear capacity, and toughness of concrete is expected, the combined use of closely spaced transverse reinforcement and fibers shows improvements in energy dissipated (compare beam D/3-1.5% and beam D/2-1.5%). In beams D/3-1.5% and D/4-1%, the combined use of fibers and high transverse reinforcement ratio allows the flexural reinforcement to reach strain hardening at high drift stages which resulted in enhanced amounts of energy dissipated.

Table 5.4 Energy dissipated at failure of tested specimens

Specimen series	*0.00%*	*0.75%*	*1.00%*	*1.50%*
D/2	6.30	7.29	6.81	13.93
D/3	-	-	8.61	15.61
D/4	7.49	-	12.92	-

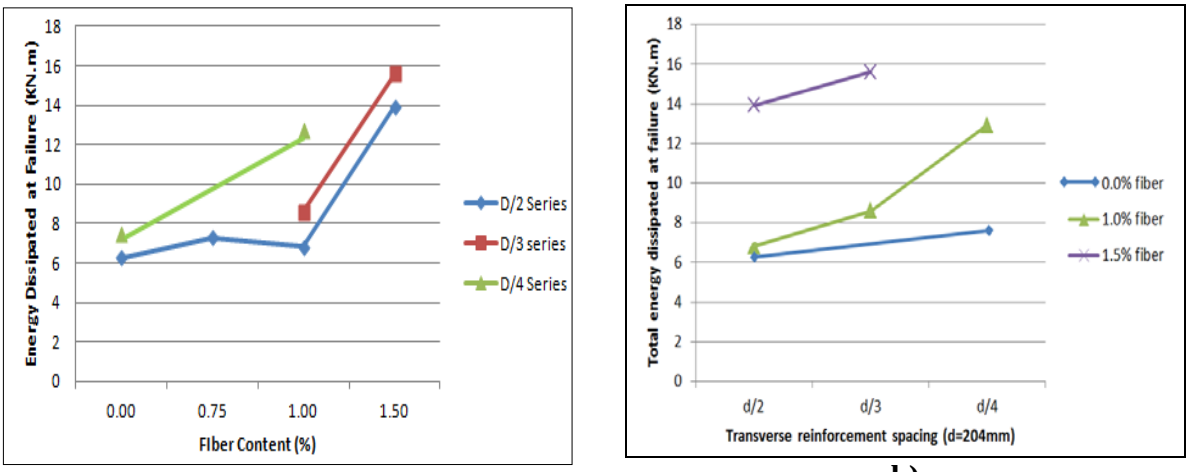

a) **b)**

Figure 5.8 Effect of (a) fibers and (b) transverse reinforcement of energy dissipation capacity

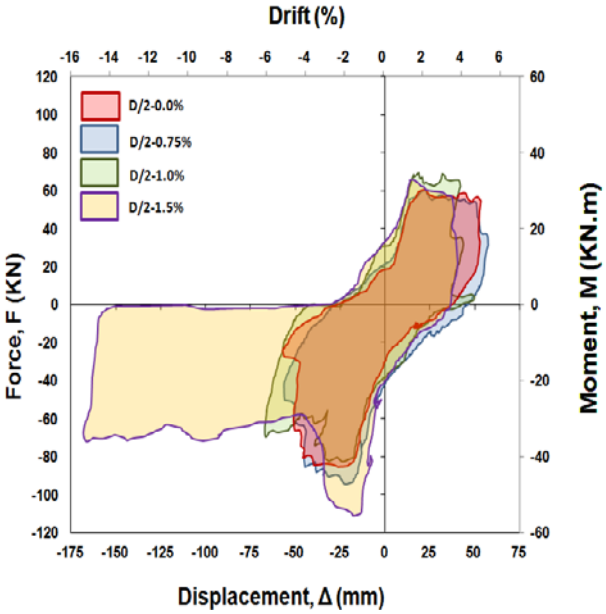

Figure 5.9 Areas enclosed by hysteresis loops for specimens in D/2 series

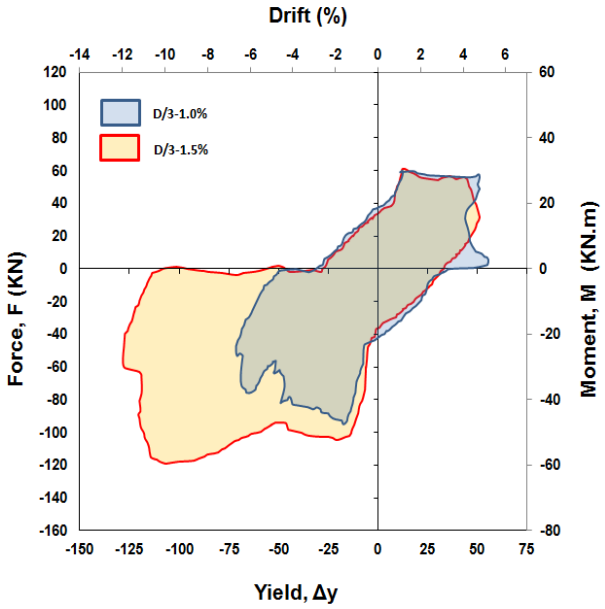

Figure 5.10 Areas enclosed by hysteresis loops for specimens in D/3 series

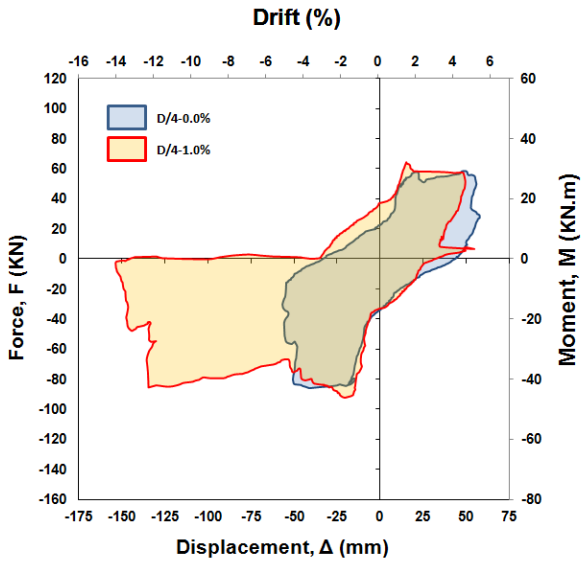

Figure 5.11 Areas enclosed by hysteresis loops for specimens in D/4 series

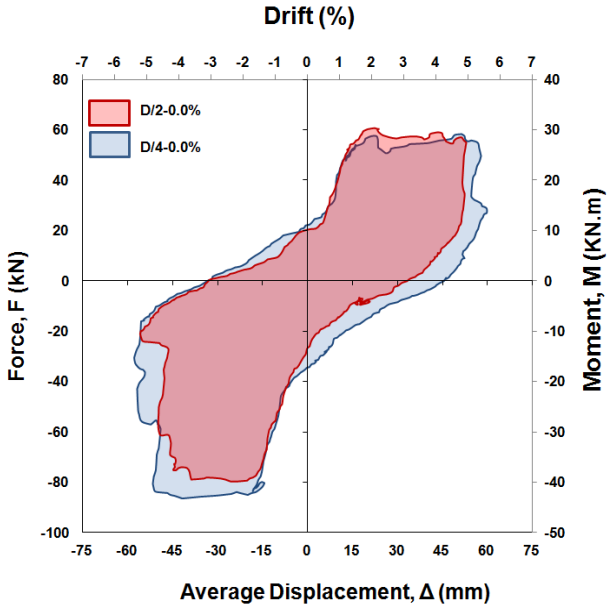

Figure 5.12 Areas enclosed by hysteresis loops for specimens with 0.0% steel fiber content

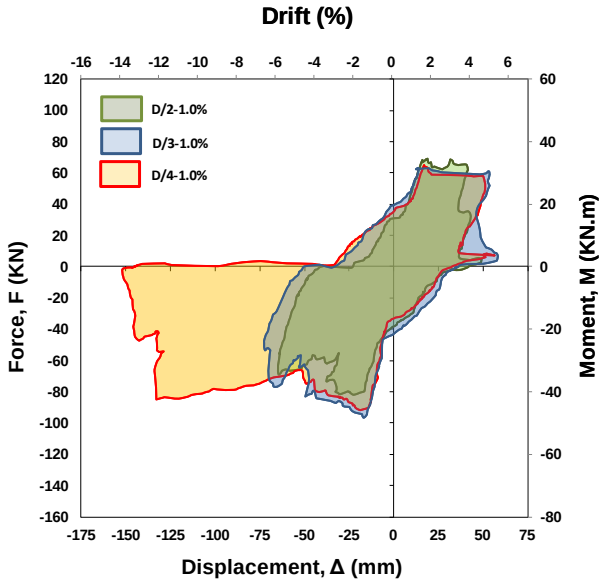

Figure 5.13 Areas enclosed by hysteresis loops for specimens with 1.0% steel fiber content

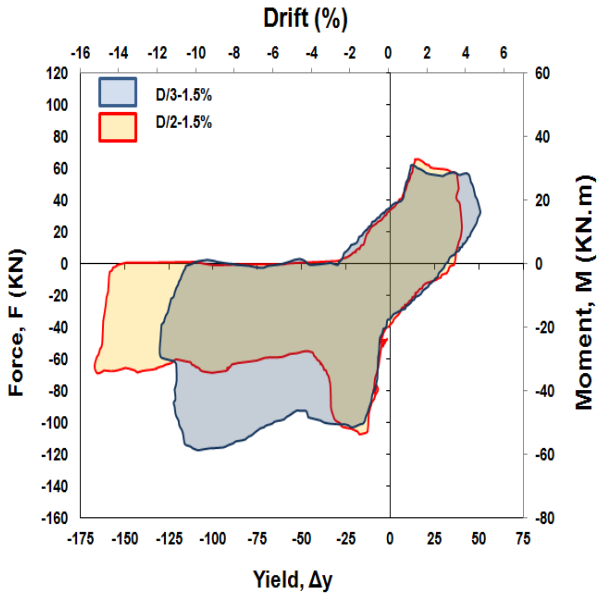

Figure 5.14 Areas enclosed by hysteresis loops for specimens with 1.5% steel fiber content

5.6 Effect of test parameters on ductility in negative bending

In this section the ductility of the specimens in negative bending is compared. In the analysis the ductility ratio at failure ($\Delta_{u/}\Delta_{y)}$ is taken as the ratio of displacement at ultimate (corresponding to failure due to complete loss of load carrying capacity due to crushing of concrete or rupture of 20M reinforcing bars) and the displacement corresponding to yielding of the 20M flexural reinforcement in negative bending. **Table 5.5** and **Figure 5.15** show the results of this analysis. The analysis reveals that for beams with equal amounts of transverse reinforcement and varying steel fiber contents, the ductility ratio at failure ($\Delta_{u/}\Delta_{y}$) improves with increased fiber content for the case of the negative bending. Ductility ratio does not follow a consistent trend in improvement due to increased transverse reinforcement ratio for beams with same steel fiber content. The only exception to this is beams with 1.0% fiber content which show improved ductility as the spacing of transverse reinforcement decreases for D/2, D/3 and D/4 series.

Table 5.5 Ductility ratios at ultimate capacity of beams in positive and negative bending

Beam	***Positive bending (Δ/Δy)***	***Negative bending (Δ/Δy)***
D-1.5%	2.5	9.8
D/2-0.0%	3.8	3.7
D/2-0.74%	4.5	2.7
D/2-1.0%	3.1	3.44
D/2-1.5%	2.84	9.8
D/3-1.0%	3.9	4.9
D/3-1.5%	3.7	8.7
D/4-0.0%	4.6	2.9
D/4-1.0%	3.2	8.4

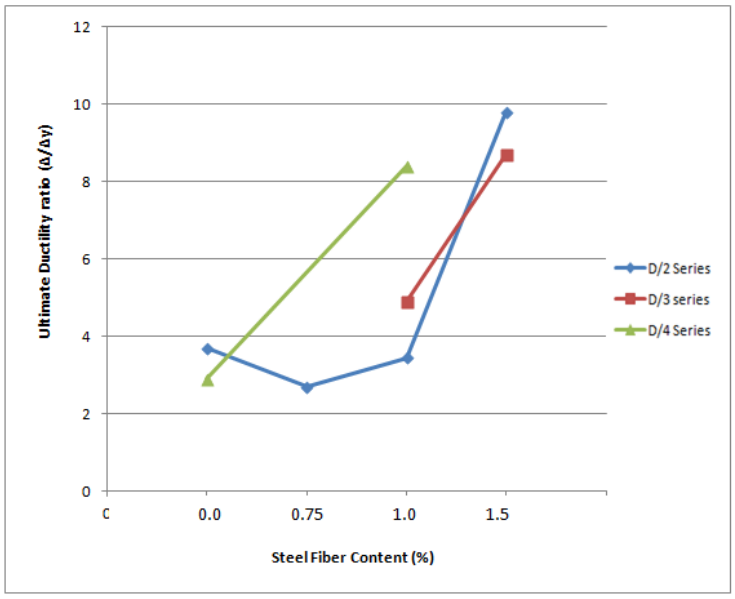

Figure 5.15 Effect of steel fibers on ductility ratio at failure in negative bending

5.7 Effect of test parameter on buckling of reinforcing bars

Buckling of the longitudinal reinforcement was only observed in beams D/2-0.0% and D-1.5%. In the case of these beams, the positive moment reinforcing bars (2-15M) buckled under compression during the negative bending cycles. In the case of the beams without fibers buckling of the reinforcement was preceded by severe spalling and loss of concrete in the cover and crushing in the core. In case of beam D/2-0.0%, severe loss of concrete within the plastic hinge region resulted in dowel action of the longitudinal reinforcement. In the case of beam D-1.5%, very large spacing of the transverse reinforcement resulted in severe buckling of the 15M reinforcing bars. Dowel action was also observed as the crack at the interface of the middle-block and beam widened under increasing displacement reversals. The results illustrate the importance of combining transverse reinforcement with at least minimum amounts of transverse reinforcement in flexural members subjected to displacement reversals to prevent buckling of compression reinforcing bars. Beams reinforced with steel fibers and at least minimum amounts of transverse reinforcement (e.g. s= d/2) did not experience buckling of the longitudinal reinforcement in compression. This is primarily due to the lateral support at this spacing of transverse reinforcement and the enhanced confinement provided by the cover due to presence of steel fibers.

5.8 Effect of test parameter on rupture of reinforcing bars

As discussed in previous sections the performance of the SFRC specimens was limited due to the early rupture of the positive moment reinforcing bars (2-15M) during the positive bending cycles. For the specimens with steel fibers rupture of positive bending reinforcement was observed at average drifts of 5.0%. In the case of negative bending, the 20M reinforcing bars ruptured at much higher drift stages; for example the 20M bars in beam D/2-1.5% ruptured at a drift of 14.5%, while for beam D/3-1.5% the bars ruptured at a drift of 11.3%.

The early rupture of the 15M bars in positive bending was primarily due to the effect of steel fibers in enhancing toughness of concrete; this increased toughness enabled longitudinal steel reinforcement bars to undergo rupturing strains at earlier drift stages compared to the case of beams with no steel fibers.

5.9 Effect of test parameters on damage tolerance

As discussed in the literature review, addition of fibers improved the behavior of concrete in tension and compression, and improves crack control, toughness and damage tolerance. Significant flexural and shear stresses develop in concrete during loading which results in development of cracks and their propagation as the beam undergoes large inelastic displacements and reverse cyclic loading. **Table 5.6** to **Table 5.8** show photos of the beams at failure for positive and negative bending**.**

Beams D/2-0.0% and D/4-0.0%, which contained no steel fibers, experienced similar cracking patterns and almost the same levels of damage at the end of the tests. Severe spalling of concrete cover and crushing of core concrete was observed in the hinging regions of these beams. These beams experienced several major cracks within the hinge region which progressed as displacements increased. Increased shear stresses and flexural stresses eventually led to complete loss of concrete material in this region. Beam D/4-0.0% showed similar behavior, although crushing was better controlled in this beam due to the higher ratio of transverse reinforcement.

As shown in **Table 5.6** to **Table 5.8**, beams reinforced with steel fibers showed an ability to control cover spalling, concrete crushing and cracking due to the enhanced toughness of SFRC in compression and tension. For example the addition of 1.5% steel fibers in beam D/2-1.5% and 1% fibers in beam D/4-1.0% resulted in pronounced improvements in damage tolerance when

compared to the control beams constructed without fibers. In general increasing the steel fiber content from 1% to 1.5% as observed in the D/2 and D/3 series resulted in significant enhancements in terms of damage tolerance.

In general, when compared to the beams constructed without fibers, the crack widths in the SFRC specimens were generally very well controlled and remained as hairline cracks until the end of the tests, with the exception of one major crack at the face of the middle block on each side. Improved crack control along the beam resulted in concentration of deformations within the major crack at the face of the middle block and continued until the end of the tests, hence these major cracks were much wider that cracks observed in beams with no steel fibers.

In addition to observations discussed above, examination of the cracking patterns indicates that the length of the plastic hinge zone is reduced in the case of beams with fibers. This behavior has also been observed by Schumacher et al. (2009) in flexural members subjected to load reversals, and recently been observed by Burrell et al. (2012) in columns tested under lateral blast loads. The plastic hinges developed in SFRC beams also function slightly different than those observed in beams with no steel fibers; hinging is limited to flexural rotation at the major cracks that develop at the face of the middle block and hence the plastic hinge length becomes very small.

Finally, for the case of beam D-1.5%, although improved control of cracking and crushing of concrete was observed, the lack of adequate lateral support for the longitudinal reinforcement resulted in buckling of the reinforcing bars in compression which resulted in spalling of the concrete cover as the bars pushed out large pieces of SFRC cover. This has also been observed in the case of columns with large spacing off hoops in the test program of Aoude et al. (2009).

Table 5.6 Comparison of damage tolerance and crcaking patterns for D/4 and D series

Beam Label	***Damage at failure in positive bending***	***Damage at failure in negative bending (end of test)***
D/4-0.0%		
D/4-1.0%	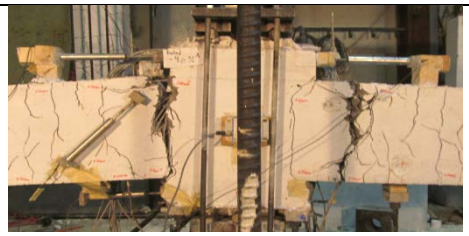	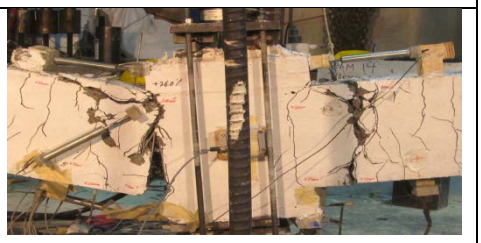
D-1.5%	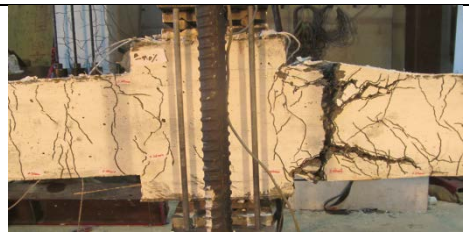	

Table 5.7 Comparison of damage tolerance and crcaking patterns for D/3 series

Beam Label	***Damage at failure in positive bending***	***Damage at failure in negative bending (end of test)***
D/3-1.0%	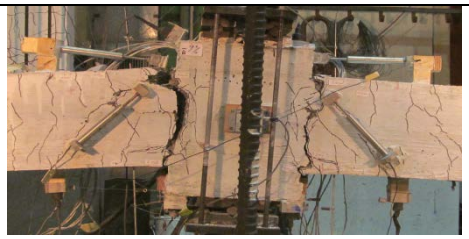	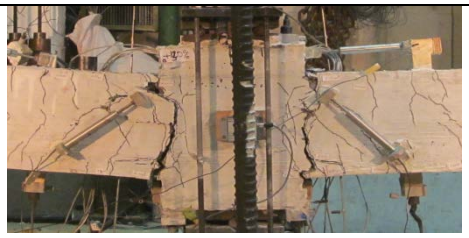
D/3-1.5%		

Table 5.8 Comparison of damage tolerance and crcaking patterns for D/2 series

Beam Label	***Damage at failure in positive bending***	***Damage at failure in negative bending (end of test)***
D/2-0.0%	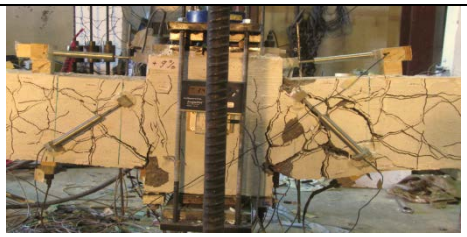	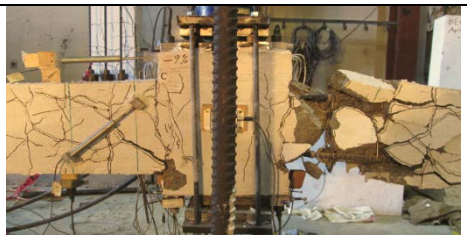
D/2-0.75%	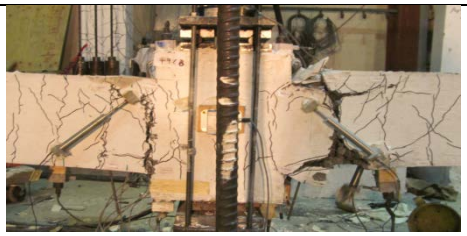	
D/2-1.0%	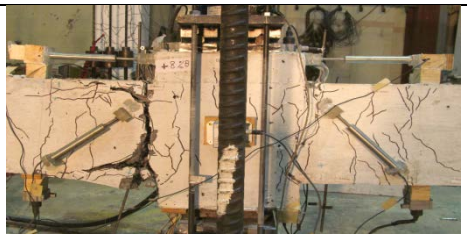	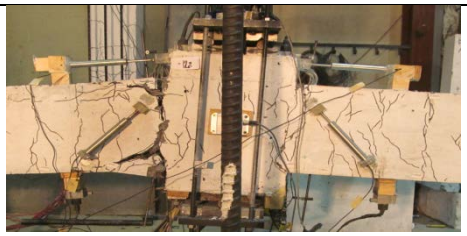
D/2-1.5%		

5.10 Ability of fibers to relax transverse reinforcement requirements in plastic hinge regions of RC flexural members

In order to illustrate the potential ability of fibers in relaxing transverse reinforcement requirements, the performance of D/4-0.0%, D/3-1.5%, D/2-1.5% and D-1.5% are compared in this section. Force-displacement response envelopes for beams D/4-0.0%, D/3-1.5%, D/2-1.5% and D-1.5% are plotted and shown in **Figure 5.16.** Maximum bending moments obtained from test results and energy dissipation capacities of these beams are listed in **Table 5.9**. It is shown in this table that flexural capacity in positive and negative bending as well as energy dissipation capacities, are higher for beams reinforced with steel fibers when compared to the control beams with seismic detailing and no steel fibers. Beams D/2-1.5% and D/3-1.5% with d/2 and d/3 hoop spacings respectively, both exhibit higher flexural strengths and energy dissipation capacities compared to beam D/4 -0.0% which has a hoop spacing of d/4 and no steel fiber reinforcement. Beam D-1.5% also has slightly higher flexural strength in negative bending and almost twice as much energy dissipation capacity compared to beam D/4-0.0%.

Table 5.9 Maximum bending moment and energy dissipation capacities

Specimen	*Max. (Positive) Moment (KN)*	*Max. (Negative) Moment (KN)*	*Energy Dissipated at failure (KN-m)*
D-1.5%	31	49	14.5
D/2-1.5%	36.13	-60.67	13.93
D/3-1.5%	33.35	-64.76	15.61
D/4-0.0%	32.46	-47.86	7.49

In addition, beams D-1.5%, D/2-1.5% and D/3-1.5% showed significant improvements in post-peak ductility in negative bending when compared to the control specimen. While beam D/4-0.0% failed at approximately 5% drift in both positive and negative bending, beams D-1.5%, D/2-1.5% and D/3-1.5% failed at 16.0%, 15% and 10.5% drifts in negative bending respectively. Failure drifts for these beams in positive bending were 4.5%, 4.0% and 4.5%, respectively. As discussed previously the SFRC beams did fail at earlier stages due to rupture of positive moment reinforcement, nonetheless the results seem to indicate that steel fiber reinforcement could potentially replace transverse reinforcement and result in improved ductility (if adequate flexural reinforcement is provided). Partial Replacement of transverse reinforcement with steel fibers can

thus have a favorable impact on the structural response of beams subjected to displacement reversals while meeting seismic design criteria with lower transverse reinforcement ratios. Further research is however required to validate this conclusion.

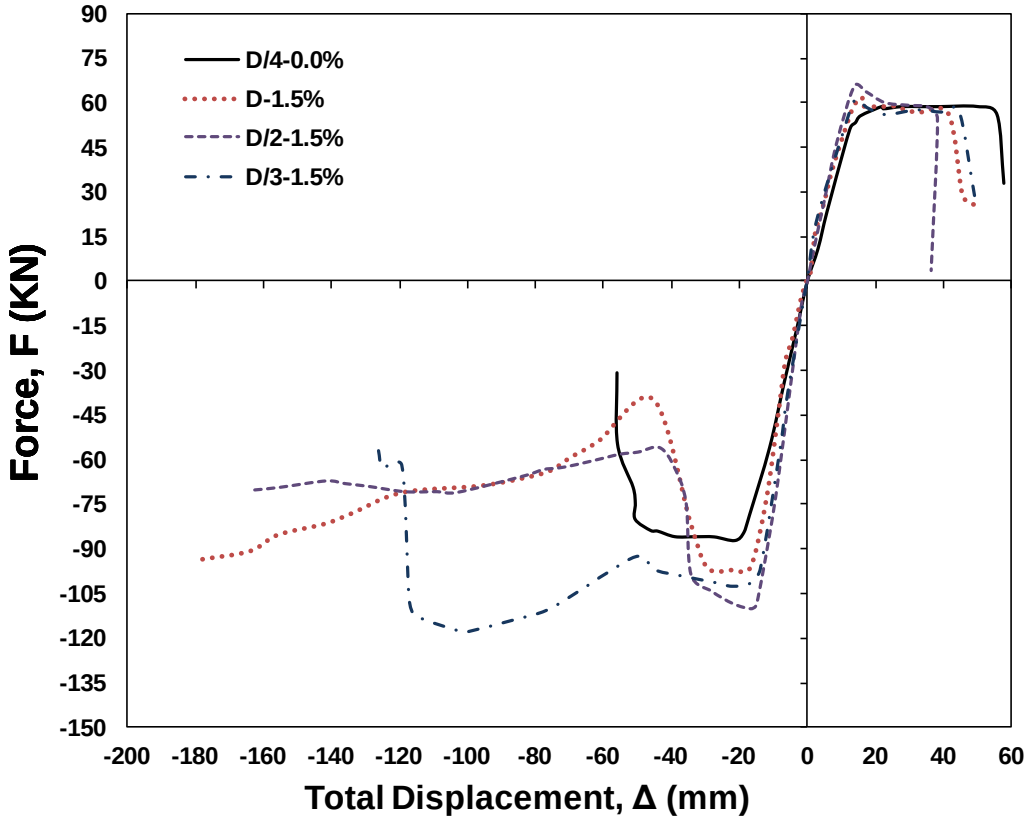

Figure 5.16 Comparison of Force-displacement response envelopes for specimens with different hoop spacing and fiber contents

5.11 Recommendation

In this section it was shown that steel fibers can potentially be used to partially replace the transverse reinforcement requirement for beams designed for seismic loads. As a preliminary research conclusion and a prescriptive research recommendation to be investigated in future research programs, the following is recommended for use in seismic design of beams: by comparing the results for beam D-1.5% with beams D/4-0.0%, D/3-0.0% and D/2-0.0%, it is shown that 1.5% steel fibers by volume of concrete seems to be adequate to achieve the same structural response for beams with lower transverse reinforcement ratios. Beams D-1.5% and D/2-1.5% which had reduced amounts of transverse reinforcement, demonstrated higher energy dissipation capacity and ductility compared to beams D/4-0.0%, D/3-0.0% and D/2-0.0%. Based on these observations the use of 1.5% fibre content is recommended for use in ductile beams subjected to seismic loads. Further research is required, however based on this research program the use of SFRC could potentially allow for a 50% reduction of transverse reinforcement if 1.5% of steel fibers are used. This would allow for reduced labour and construction costs and ease of construction by reducing congestion in beam-column joint areas. In terms of damage tolerance, beams D/2-1.5% and D-1.5% showed enhanced damage tolerance in reverse cyclic loading even at large drifts. In addition to improved seismic performance, this would be beneficial in reducing repair and retrofit costs after major earthquakes. The large hoop spacing in Beam D-1.5% resulted in buckling of longitudinal reinforcement; the result demonstrates the importance of minimum transverse reinforcement to prevent rebar buckling.

As discussed in this thesis, provision of unequal reinforcement ratios in negative and positive bending, as specified in cl. 21.3.2.3 of the CSA A23.3-04 standard, limited the performance of the SFRC beams tested in this experimental program. Early rupture of positive bending moment reinforcement (2-15M bars) resulted in early failure of the beams. Based on this observation the designer should be aware that the addition of steel fibres could result in reduced ductility; in addition, to prevent premature failure, it is recommended that the positive moment resistance at the face of joints in SFRC flexural members not be less than 100% of the negative moment resistance provided at the face of the joint (i.e. equal flexural reinforcement should be required in positive and negative bending at joints). In addition, further research is required to study the effect of equal and unequal flexural reinforcement in SFRC flexural members subjected to load reversals.

Chapter 6 Analytical Modeling of Beam Response

6.1 General

This chapter presents the results from the analysis of the nine beams under reverse cyclic loading in this experimental program. Analytical predictions of beam responses were carried out using inelastic static analysis (push-over analysis). Thereafter, sectional and member analyses using material models and beam member properties were used to derive moment-curvature relationships and moment-displacement responses for the beams. This chapter describes the analytical procedures, material models and the assumptions that were made to obtain analytical moment-displacement responses. Test results were used to verify the analytical procedures employed in this analysis. The results obtained from the analytical procedures show good agreement with the experimental results.

6.2 Sectional Analysis

6.2.1 Constitutive Model Used in Sectional Analysis

In this section constitutive model used in sectional analysis of the beams tested as part of this experimental program are presented. Models for confined and unconfined concrete and SFRC in compression are presented.

6.2.1.1 Concrete models used for RC Beams

6.2.1.1.1 Confined Concrete Model (Légeron and Paultre 2003)

Extensive research has shown that confinement of concrete results in improved compressive strength and post-peak ductility. Improved properties of confined concrete are affected by several parameters such as the volumetric ratio of the transverse reinforcements, hoop spacing and arrangement of hoops and longitudinal reinforcing bars. Over the years several authors have proposed models for predicting the stress-strain behaviour of confined concrete. Examples include models by Kent and Park (1971), Park et al. (1982), Sheik and Uzemeri (1980,1982), Mander et al. (1988), Razvi and Saatcioglu (1999) and Légeron and Paultre (2003). The model by Légeron and Paultre (2003) extends an earlier model by Cusson and Paultre (1995) to predict the complete stress-strain behaviour of confined concrete for a wide range of transverse reinforcement configurations and concrete strengths. This model has been shown to accurately

predict the stress-strain behaviour of concrete and hence is used in the analytical study to predict the confined concrete response in the beams.

In this model the confined compressive strength of concrete, f'_{cc} and corresponding strain, ε'_{cc} are computed using the following expressions:

$$f'_{cc} = f'_{cu}\left(1 + 2.4\left(I'_E\right)^{0.7}\right) \tag{6.1}$$

$$\varepsilon'_{cc} = \varepsilon'_{cu}\left(1 + 35\left(I'_E\right)^{1.2}\right) \tag{6.2}$$

$$I'_E = \frac{f'_{le}}{f'_{cu}} \tag{6.3}$$

$$f'_{le} = K_e * f'_l \tag{6.4}$$

where I'_E is the effective confinement index and f'_{le} is the effective confinement pressure that acts on the core. The effective confinement pressure is a function of the nominal lateral pressure provided by the transverse reinforcement, f'_l and the effective confinement coefficient K_e which is computed using Eq. 6.5 as proposed by Sheikh and Uzumeri (1982).

$$f'_l = \frac{f_{hcc}}{s}\left(\frac{A_{shy} + A_{shx}}{c_y + c_x}\right) \tag{6.5}$$

$$K_e = \frac{\left(1 - \frac{\sum w_i^{\,2}}{6c_x c_y}\right)\left(1 - \frac{s'}{2c_x}\right)\left(1 - \frac{s'}{2c_y}\right)}{\left(1 - \rho_c\right)} \tag{6.6}$$

In the above expressions A_{shy} and A_{shx} are the total cross-sectional areas of transverse reinforcement perpendicular to the x & y directions, ρ_c is the ratio of longitudinal reinforcement

in the core region, and f_{hcc} is the stress in the transverse steel reinforcement at maximum strength of confined concrete. The quantities s and s' refer to the centre-to-centre and clear spacing of the transverse reinforcement, and c_y & c_y refer to the widths of the concrete core parallel to the x and y axis respectively. $\sum w_i^2$ is the sum of the squares of the clear spacings between adjacent longitudinal bars.

According to Légeron and Paultre (2003), the magnitude of the stress developed in the transverse reinforcement is proportional to the amount of confinement that is provided. In other words, the more concrete is confined, the more it is able to utilize the full yield strength of the transverse reinforcement, f_{hy}, to resist lateral deformations induced by the Poisson's effect in compression. The following equations are used to calculate the stress in the transverse steel reinforcement at peak concrete stress, f'_{hcc}:

$$f'_{hcc} = \begin{cases} f_{hy} \longleftarrow \kappa \le 10 \\ \dfrac{0.25 f'_{cu}}{\rho_{sey}(\kappa - 10)} \ge 0.43\varepsilon'_{cu} E_S \longleftarrow \kappa > 10 \end{cases} \tag{6.7}$$

$$\kappa = \frac{f'_{cu}}{\rho_{sey} E_S \varepsilon'_{co}} \tag{6.8}$$

$$\rho_{sey} = \frac{K_e A_{shy}}{sc} \tag{6.9}$$

where ρ_{sey} is the effective ratio of confinement reinforcement in the y direction, κ is a parameter that is used in order to determine if yielding of the transverse reinforcement occurs at the maximum strength of confined concrete and E_S is the modulus of elasticity of the transverse reinforcement. The following equation originally developed by Popovics (1973) is used to define the ascending branch of stress-strain relationship for confined concrete:

$$f_{cc} = \frac{(f'_{cc})^* \left(k \times \frac{\varepsilon_{cc}}{\varepsilon'_{cc}} \right)}{k - 1 + (\frac{\varepsilon_{cc}}{\varepsilon'_{cc}})^k}, \quad \varepsilon_{cc} \le \varepsilon'_{cc} \tag{6.10}$$

where f_{cc} refers to the stress in the confined concrete corresponding to a chosen strain ε_{cc}. The values, f'_{cc} and ε'_{cc}, represent the peak confined stress and strain of the concrete. The constant *k*, is a parameter that controls the slope of the ascending branch of the curve and is computed as follows in Eq. 6.11:

$$k = \frac{E_c}{E_c - (\frac{f'_{cc}}{\varepsilon'_{cc}})} \tag{6.11}$$

Légeron and Paultre (2003) developed the following expressions to define the descending branch of the stress-strain curve for confined concrete:

$$f_{cc} = f'_{cc} \times \exp\left(k_1 \left(\varepsilon_{cc} - \varepsilon'_{cc}\right)^{k_2}\right), \ \varepsilon_{cc} > \varepsilon'_{cc} \tag{6.12}$$

$$k_1 = \frac{\ln(0.5)}{\left(\varepsilon_{cc50} - \varepsilon'_{cc}\right)^{k_2}} \tag{6.13}$$

$$k_2 = 1 + 25\left(I_{E50}\right)^2 \tag{6.14}$$

Where I_{E50} is the effective confinement index evaluated at the post-peak strain ε_{cc50} as defined in the following expression (Légeron and Paultre 2003):

$$\varepsilon'_{cc50} = \varepsilon'_{cu50}\left(1 + 60\left(I_{E50}\right)\right) \tag{6.15}$$

$$I_{E50} = \rho_{sey} \frac{f_{hy}}{f'_{cu}} \tag{6.16}$$

In the above expressions, the post-peak strain measured at 50% of maximum unconfined stress, ε'_{cu50} is taken as being equal to a strain of 0.004 as proposed by Cusson and Paultre in 1995.

Figure 6.1 shows the stress-strain curved for confined and unconfined concrete based on Légeron and Paultre (2003):

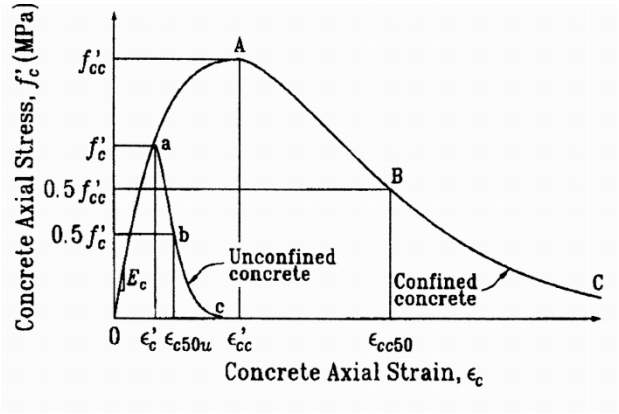

Figure 6.1 Stress-Strain curves for confined and unconfined concrete
[Adapted from Légeron and Paultre, 2003]

6.2.1.1.2 Unconfined Concrete Model

The expressions of the Légeron and Pualtre (2003) model can also be used to define the stress-strain behaviour of unconfined concrete if the confined concrete parameters in the previous equations are replaced by parameters related to unconfined concrete (namely f'_{cu}, ε'_{cu}, ε'_{c50u}) and if $k_2 = 1.5$. Note that in the analysis of the reinforced concrete beams without fibers, the unconfined concrete in the cover region was assumed to spall at a strain of 0. 3%.

6.2.1.2 Concrete models used for SFRC Beams

6.2.1.2.1 Unconfined SFRC model (Aoude 2008)

A number of empirical models have been proposed in literature for predicting the compressive stress-strain behaviour of SFRC. Aoude (2008) modified a model originally proposed by Mansur et al. (1999) for high-strength SFRC to predict the stress-strain behaviour of regular strength SFRC. Eq. 6.17 defines the ascending branch of the stress-strain curve for normal strength SFRC which is based on the work of Popovics (1973), where $f_{cu,f}$ represents the stress in the unconfined SFRC corresponding to a strain of ε_{cuf}. The constant *k* controls the slope of the ascending branch and is computed using Eq. 6.18 as follows:

$$f_{cuf} = \frac{(f'_{\text{cuf}}) * \left(k \times \frac{\varepsilon_{cuf}}{\varepsilon'_{cuf}} \right)}{k - 1 + (\frac{\varepsilon_{cu,f}}{\varepsilon'_{cuf}})^{\text{k}}}, \qquad \varepsilon_{cu,f} \le \varepsilon'_{cuf} \tag{6.17}$$

$$k = \frac{E_{\text{c}}}{E_{\text{c}} - (\frac{f'_{cuf}}{\varepsilon'_{cuf}})} \tag{6.18}$$

where f'_{cuf} and ε'_{cuf} refer to the peak stress and strain of SFRC. As discussed in previous chapters, it has been shown that SFRC shows no significant change in peak stress, peak strain or modulus of elasticity which results in a similar ascending branch. Hence f'_{cu} can be used in lieu of f'_{cuf} when the 28-day compressive strength of SFRC from cylinder tests is not available. The peak unconfined strain ε'_{cuf} is computed using Eq. 6.19:

$$\varepsilon'_{cuf} = 0.001684 + 0.000016 * f'_{cuf} \tag{6.19}$$

The equation for the descending branch of the stress-strain curve is:

$$f_{cuf} = f'_{cuf}\left[\frac{k_{f1}\beta_1\left(\frac{\varepsilon_{cuf}}{\varepsilon'_{cu}}\right)}{k_{f1}\beta_1 - 1 + \left(\frac{\varepsilon_{cuf}}{\varepsilon'_{cu}}\right)^{k_{f2}\beta_1}}\right] \quad \varepsilon_{cuf} \geq \varepsilon'_{cu} \tag{6.20}$$

where the factors k_{f1} and k_{f2} are calculated using Eq. 6.21 and Eq. 6.22 and are based on the work of Mansur et al. (1999):

$$k_{f1} = \left(\frac{C_a}{f'_{cuf}}\right)^{e_a} \times \left(1 + X_a \times \left[\frac{v_f L_f}{d_f}\right]^{e_{2a}}\right) \tag{6.21}$$

$$k_{f2} = \left(\frac{C_a}{f'_{cuf}}\right)^{e_b} \times \left(1 + X_b \times \left[\frac{v_f L_f}{d_f}\right]^{e_{2b}}\right) \tag{6.22}$$

Table 6.1 Constants used in calculation of k_{f1} and k_{f2} factors

Constants	For $\varepsilon_{cf} \leq 0.004$	For $\varepsilon_{cf} > 0.004$
C_a	30.2	4.62
e_a	0.49	0.47
X_a	-0.22	-7.8×10^{-5}
e_{2a}	24.9	-6.4
e_b	0.52	0.51
X_a	0.11	0.83
e_{2b}	-1.09	-0.34

Table 6.1 lists the constants used in calculation of k_{f1} and k_{f2} factors and are derived for normal-strength concrete by Aoude (2008) based on the results of a parametric study.

6.2.1.2.2 Confined SFRC model (Aoude 2008)

Aoude (2008) modified the confined concrete model proposed by Légeron and Paultre (2003) to predict the stress-strain behaviour of confined SFRC. Research has shown that confined SFRC experiences increased compressive strength and higher ductility (Massicotte et al., 1998, Ramesh et al., 2003, Ganesan and Murthy, 1990). The confined SFRC model proposed by Aoude(2008) accounts for these two effects.

Early research by Richart et al. (1928) demonstrated that the strength of concrete is enhanced if the concrete section is confined by an active hydrostatic pressure or passive confinement pressure in the form of spirals. The increase in peak stress due to presence of steel fibers can be related to the number of fibers per unit area N_{fibres}, and the pullout strength of the fibers. based on this approach, Foster (2001) suggested that the confinement pressure of steel fibers, $f_{l,fib}$ can be approximated using Eq. 6.23:

$$f_{l,fib} = \alpha \times \left(\frac{v_f L_f}{d} \right) \times \left[0.6 \times \left(f'_{cu} \right)^{2/3} \right] \tag{6.23}$$

where L_f refers to the length of the fiber without the hooks in the case of hooked-end steel fibers. Foster (2001) suggested using a value of 3/8 for the orientation factor, α. An approach similar to Richart (1928) was adopted by Aoude (2008) to approximate the expected contribution of steel fibers in increasing the concrete stress, Δf_{cf}:

$$\Delta f_{cf} = 4.1 \times \left(f_{l,fib} \right) \tag{6.24}$$

then $f'_{cc\,f}$ is the sum of the stress of the confined plain concrete f'_{cc} as defined by Paultre and Légeron (2003) and the stress contribution from steel fibers, Δf_{cf}:

$$f'_{cc\,f} = f'_{cc} + \Delta f_{cf} \tag{6.25}$$

$$\varepsilon'_{ccf} = \varepsilon'_{cc} = \varepsilon'_{cu}\left(1 + 35\left(\frac{f'_{le}}{f'_{cu}}\right)^{1.2}\right) \tag{6.26}$$

By substituting the corresponding values of $f'_{cc\,f}$ and $\varepsilon'_{cc\,f}$ in lieu of f'_{cc} and ε'_{cc}, in the same expression proposed by Légeron and Paultre (2003) for confined concrete the following expression is obtained for stress of confined SFRC:

$$f_{ccf} = \frac{(f'_{\mathrm{ccf}}) * \left(k \times \dfrac{\varepsilon_{ccf}}{\varepsilon'_{ccf}}\right)}{k - 1 + (\dfrac{\varepsilon_{ccf}}{\varepsilon'_{ccf}})^{\mathrm{k}}}, \qquad \varepsilon_{ccf} \le \varepsilon'_{ccf} \tag{6.27}$$

$$k = \frac{E_{\mathrm{c}}}{E_{\mathrm{c}} - (\dfrac{f'_{ccf}}{\varepsilon'_{ccf}})} \tag{6.28}$$

Research by Aoude (2008) on SFRC columns subjected to compressive axial loading has shown that the influence of the fibers in improving post-peak behaviour is directly related to the level of confinement provided by transverse reinforcement with the fibers playing a lesser role in improving post-peak ductility in the case of well-confined columns. Hence, as the ratio of the effectively confined core area, A_{KE} to the ineffectively confined core area, A_{ineff} increases, the contribution of the fibers improving the post-peak response decreases. The "ineffectively confined core area", A_{ineff}, can be computed using Eq. 6.29:

$$A_{ineff} = (1 - K_e) \times A_{core} \tag{6.29}$$

based on this approach a modified confinement index from Légeron and Paultre (2003) model is presented in Eq. 6.30:

$$I'_{E,fib} = I'_E + \left(\frac{f_{l,fib}}{f'_{cu}}\right)(1 - K_e) \tag{6.30}$$

using $f'_{cc\,f}$, $\varepsilon'_{cc\,f}$, $I'_{E,fib}$ and $I_{E50,fib}$ in lieu of f'_{cc} , ε'_{cc} , I'_E and I_{E50} in the plain confined concrete model by Legeron and Paultre (2003) for SFRC results in the following expression for $f_{cc\,f}$:

$$f_{ccf} = (f'_{cc\,f}) \times \exp\left(k_1\left(\varepsilon_{ccf} - \varepsilon'_{c\,cf}\right)^{k_2}\right), \quad \varepsilon_{ccf} > \varepsilon'_{ccf} \tag{6.31}$$

where

$$k_1 = \frac{\ln(0.5)}{\left(\varepsilon_{cc50,fib} - \varepsilon'_{c\,cf}\right)^{k_2}} \tag{6.32}$$

$$k_2 = 0.58 + 16\left(I'_{E,fib}\right)^{1.4} \tag{6.33}$$

$$\varepsilon'_{cc50,fib} = \varepsilon'_{cu50}\left[1 + 60\left(I'_{E50,fib}\right)\right] \tag{6.34}$$

$$I_{E50,fib} = I_{E50} + \left(\frac{f_{l,fib}}{f'_{cu}}\right)(1 - K_e) \tag{6.35}$$

6.2.1.3 Model for steel in tension and compression

For the analysis of all beams in this experimental program the stress-strain behaviour of steel in tension as obtained from reinforcing bar coupon tests was used for analysis. In the absence of experimental data the following generic stress-strain curve which includes elastic-plastic behaviour followed by a parabolic strain-hardening branch can be used (Jacques et al., 2012):

$$f_s = E_s \varepsilon_s \qquad \text{for } \varepsilon_s \leq \varepsilon_y \tag{6.36}$$

$$\varepsilon_y = f_y / E_s \tag{6.37}$$

$$f_s = f_y + (\varepsilon_s - \varepsilon_y)\left(\frac{f_{sh} - f_y}{\varepsilon_{sh} - \varepsilon_y}\right), \quad \text{for } \varepsilon_y < \varepsilon_s \leq \varepsilon_{sh} \tag{6.38}$$

$$f_s = f_y + (f_u - f_y)\left[2\frac{\varepsilon_s - \varepsilon_{sh}}{\varepsilon_u - \varepsilon_{sh}} - \left(\frac{\varepsilon_s - \varepsilon_{sh}}{\varepsilon_u - \varepsilon_{sh}}\right)^2\right] \tag{6.39}$$

where f_s is the steel stress at strain ε_s, E_s is the steel modulus of elasticity, f_y is the steel yield stress at steel yield strain ε_y, f_{sh} is the steel strain-hardening stress at strain ε_{sh}, and f_u is the ultimate steel stress at strain ε_u.

Research has shown that reinforcing steel in compression is prone to buckling. In order to take buckling into account, the model proposed by Yalcin and Saatcioglu (2000) can be used. This model modifies the stress-strain behaviour based on bar aspect ratio, which is defined as the ratio between the unsupported bar length and diameter. For aspect ratios greater than 8.0 the model assumes stability of the reinforcing bar is lost upon reaching yield. At values less than 8.0 and less than 4.5 the stress-strain behaviour shows limited and complete strain-hardening behaviour, respectively (see **Figure 6.2**). Details of the buckling model can be obtained by consulting the work of Yalcin and Saatcioglu (2000).

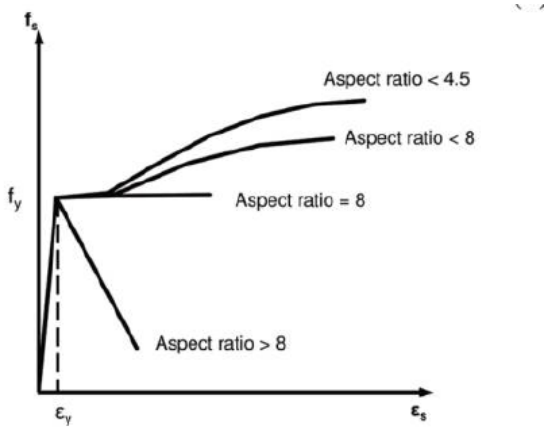

Figure 6.2 Longitudinal steel reinforcement buckling criteria
[Adopted from Yalcin and Saatciglu, 2000]

6.2.2 Validation of analytical procedures

In the first attempt to generate the moment-displacement response of the tested beams, a simplistic idealized approach was adopted to validate the analytical procedures used in this section that was used to obtain predictions of the beam responses. The experimental rotations due to flexure and anchorage slip measured during testing at each load cycle, were used to calculate the curvature of the beams which was then correlated to the vertical displacements in the beams using the assumption that the plastic hinge length of the beam, l_p remained constant and equal to the effective depth of the section, d.

Saatcioglu and Razvi (1994) showed that the plastic hinge length starts developing once yield curvature is reached in the beam and develops gradually as moment increases until it reaches its ultimate value which has been shown in previous studies to be approximately equal to the effective depth of the section, d (see **Figure 6.3** and **Figure 6.4**). For this reason an idealized moment-curvature approach introduces slight inaccuracies by assuming a constant plastic hinge length. Nonetheless it provides valuable information by generating a close approximation of the moment-curvature behaviour of the beams.

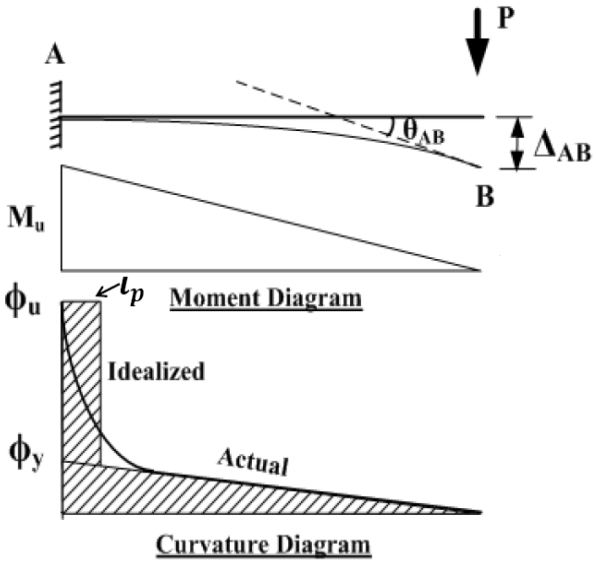

Figure 6.3 Idealized moment-curvature approach

[Adopted from Saatcioglu and Razvi, 1994]

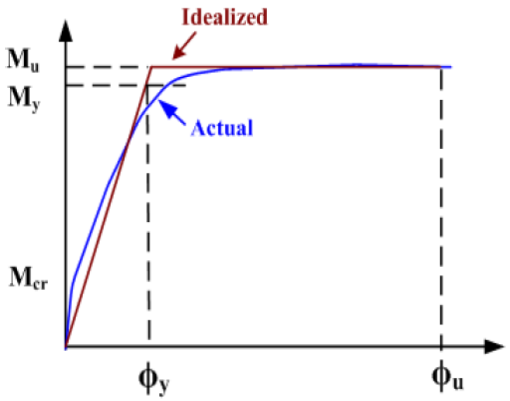

Figure 6.4 Idealized moment-curvature analysis

[Adopted from Saatcioglu and Razvi, 1994]

As mentioned in chapter 3, LVDTs were installed at the top and bottom of the beams near the faces of the middle block and at a distance equal to the theoretical plastic hinge length to measure total rotations and rotations due to anchorage slip at each load cycle. **Figure 6.5** shows schematics of a deflected plastic hinge region with rotation of θ. Eq. 6.40 was used to calculate beam rotations based on LVDT readings:

$$\theta = \frac{L_1 + L_2}{H} \tag{6.40}$$

where L_1 and L_2 are LVDT reading at the top and bottom of the beam and H is the distance between the LVDTs which is equal to the depth of the middle concrete block. The rotations obtained by this method were then used to calculate curvature of the beams and the displacement values were finally calculated by taking the moment of the area under the idealized curvature diagram.

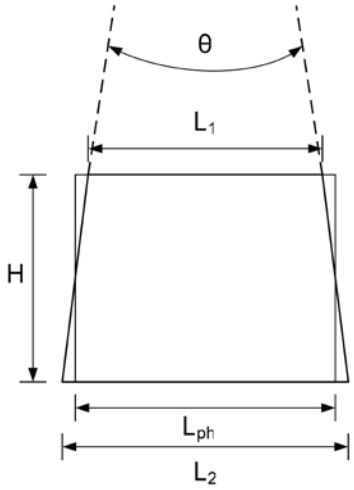

Figure 6.5 Calculation of rotations based on LVDT readings

Figure 6.6 shows the analytical moment-displacement envelope obtained using the procedure described in this section plotted against the experimental hysteretic curve for beam D/2-0.0%. As it can be seen in the figure, there is a good agreement between the analytical and experimental results which validates the methodology used in this section to predict the behaviour of beams in reverse-cyclic loading..

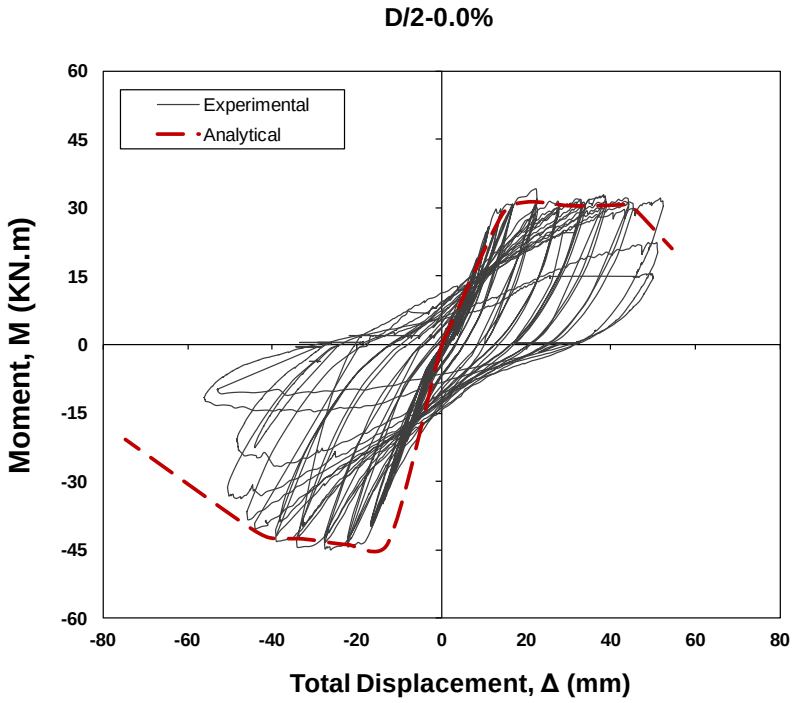

Figure 6.6 Experimental and analytical moment-displacement diagrams

6.2.3 Analytical calculation of force-displacement relationship

The moment-displacement relationships of the beams tested in this experimental program were generated analytically using an inelastic static analysis approach (push-over analysis). Well-established analytical techniques and recently developed models for confined and unconfined plain concrete and SFRC were employed to establish theoretical moment-displacement relationships. Coupon test results for the longitudinal and transverse reinforcement were used to define the stress-strain curves for the steel. The analyses were conducted manually using an MS Excel spreadsheet. The analysis procedure employed herein consisted of a sectional analysis to obtain strains and curvatures of the section at varying strain levels as well as member analysis to calculate beam deformations at various strains. This procedure is described in further details in the following sections.

6.2.3.1 Sectional Analysis

The first step in analysis of the tested beams was sectional analysis assuming that plane sections remain plane before and after bending resulting in a linear distribution of strains across the section. This assumption was used to find corresponding values of strain at various longitudinal reinforcement strains by applying the similar triangles concept. The confined and unconfined plain concrete were modelled using Légeron and Paultre (2003) models. In order to account for the contribution of the steel fibers in the stress-strain behaviour of the confined and unconfined concrete, SFRC stress-strain models for confined and unconfined concrete proposed by Aoude (2008) were adopted. Stress-strain properties of the steel reinforcement used in the sectional analyses were obtained experimentally from coupon tests which included the strain hardening effects.

The confined concrete models used for plain concrete and SFRC account for a wide range of transverse reinforcement configurations. Average effective ratios of confinement reinforcement, ρ_{sey} over x and y directions were calculated to account for the rectangular configuration of the beams in both plain concrete and SFRC confinement models.

As discussed in chapter 4 of this thesis, 7 beams out of 9, experienced early rupture of the positive bending reinforcement due to increased strength and toughness of the confined SFRC in the compression zone of the beams which enabled the 15M reinforcement to reach rupture strains

at earlier load stages than in the case of the control specimens. After this point, loading was continued in negative bending until failure of the negative moment reinforcement steel and hence a sharper descending branch in negative bending was observed as the compression steel was lost. This sudden decay in the negative moment strength was not effectively captured in the sectional analyses of the beams since the experimental stress-strain relationship of the reinforcement provided rupture strain values which were higher than those observed in the beam test results. Therefore, in order to reflect the effect of the rupture of positive moment reinforcement on the strength decay in negative bending, the contribution from the compression steel in negative bending was neglected after the point of reinforcing bar rupture (as observed experimentally). This was achieved by iteratively back-calculating the strains at the displacement at which positive steel reinforcement ruptured and assuming no contribution from compression steel for strains thereafter. This resulted in a closer prediction of the moment-displacement envelope for the tested beams. Although this procedure cannot be employed when no experimental data is available or when purely analytical results are to be obtained, it depicts a close approximation of the post-peak behaviour of the beam in negative bending. It is noted that in the present analysis, the experimental stress-strain data obtained from steel reinforcement coupon test were used.

Spalling of the cover concrete was also taken into account in the sectional analyses. For specimens without fibres, spalling of unconfined concrete in the cover region was assumed to take place at a strain of 0.3% with cover assumed to be ineffective after this strain. Aoude (2008) observed that steel fibers significantly delay cover spalling from core concrete and contributes to strength beyond a strain of 0.3%, however this contribution becomes limited in cases where buckling of the reinforcing bars occur. As such, for SFRC specimens with large L/d_b ratio (e.g. Beam D-1.5%), spalling was assumed to "effectively" occur at strains beyond 0.3%.

Yalcin and Saatcioglu (2000) derived a series of expressions to describe the effect of reinforcement stability on the static stress–strain characteristics of reinforcing steel in compression. This model suggests that buckling effect becomes significant when the aspect ratio of the reinforcing bars (L/d_b) becomes greater than 8. In the case of beam D-1.5%, the aspect-ratios (L/d_b) for the positive and negative moment reinforcement were 10.2 and 13.6,

respectively; hence buckling effects were considered for this specimen using the model proposed by Yalcin and Saatcioglu (2000).

The internal stresses and strain obtained from the sectional analyses discussed above were used to calculate the moments and curvatures at different strain profiles which resulted in a moment-curvature relationship for the beam sections.

6.2.3.2 Member Analysis

Moment-curvature relationships obtained from the sectional analyses were used to compute vertical displacements of the beams. Two separate components of deformations were used to compute the total displacement of the beams: flexural deformations and anchorage slip deformations. Based on results obtained from testing a number of columns under inelastic load reversals, Saatcioglu and Ozcebe (1989) indicated that flexure-dominant columns experience deflections resulting from two components of deformations: flexure and anchorage slip (where flexural deformations refer to the deformations due to the bending of the beam and anchorage slip is the deformation due to extension and/or slippage of the longitudinal reinforcement).

It is to note that anchorage slip deformations can be significant when axial stresses are low or no axial stress is present, which is the case in the beams tested in this experimental program. Shear deformations were predicted to be small as the beams were designed to be flexure-dominant hence they were neglected in this analysis. This was verified during the testing by visual inspection of diagonal cracking and measurement of shear deformations in the plastic hinge region of the beams.

6.2.3.2.1 Flexural Deformations

Flexural deformations were computed by first establishing the curvature distribution along the length of the beams. The curvature relationship within the ascending branch can be directly established from this curvature distribution. The post-peak behaviour of the beams requires consideration of the plastic hinging. Similar to the analysis described in Section 6.2.2, in the post-peak region, the plastic hinge length was approximated to be equal to the effective depth of the section, d and was assumed to be constant as bending moment increased.

This approach theoretically tends to slightly overestimate the flexural deformations as the plastic hinge length is taken to be greater than what it actually is. Nonetheless, an idealized approach was used in this study as it avoids the complexity of calculating the actual plastic hinge lengths as bending moments increase.

Finally, member rotations were obtained by integrating the curvatures along the length of the beam. Displacements due to flexure were then computed by taking the moment of the area under the curvature diagram. The procedure outlined above is based on accepted principles of strain compatibility and equilibrium and has been shown to be applicable to normal strength and high strength concrete (Baingo 1996).

6.2.3.2.2 Deformations due to Anchorage Slip

Anchorage slip results in member end rotations that are not accounted for in flexural analysis. Deformations due to anchorage deformation consist of two components: deformation due to extension of the reinforcing bars and deformation due to slip of the reinforcement. Well-anchored reinforcing bars do not exhibit deformations due to slip of reinforcement. Research has shown that deformations due to extension of the reinforcement bars can be significant if the bars reach hardening strain (Alsiwat and Saatcioglu, 1992). The analytical model proposed by Alsiwat and Saatcioglu (1992) was adopted in this section to compute anchorage slip deformations. The anchorage slip deformation due to the slip of the reinforcement has been neglected in this analysis assuming well-anchored reinforcing bars.

The model developed by Alsiwat and Saatcioglu (1992) is based on construction of the stress-strain diagram along the embedment length of the reinforcement to obtain stress and strain in the reinforcement at the that location by first performing sectional analysis of the critical section and then using the elastic and inelastic bond stresses to compute the length of each region within the embedment length. **Figure 6.7** depicts the strains and stresses along the length of the reinforcement within the adjoining member.

In the analysis presented in this section, extension of the reinforcing bars within the elastic region as well as the strain hardening region of the steel stress-strain diagram was calculated. The yield plateau of the reinforcement steel was experimentally found to be flat and hence was assumed to not contribute to any anchorage slip deformations.

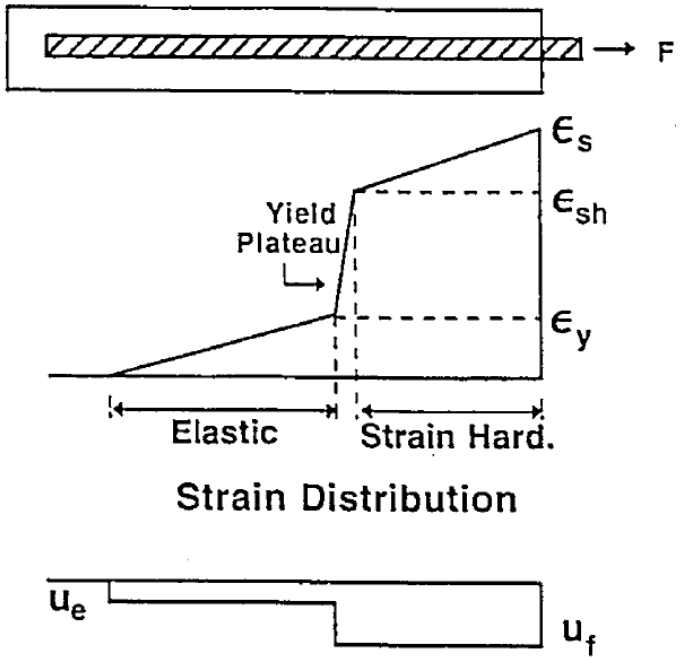

Figure 6.7 Strain and Bond Stress in Anchorage Reinforcement
[Adopted from Baingo 1996 based on Alsiwat and Saatcioglu, 1992]

6.3 Comparison of Analytical Results with Experimental Data

This section presents a comparison between the moment-displacement relationships that were obtained analytically as described in the previous sections with the experimental moment-displacement hysteretic curves. The analytical curves were obtained for monotonically increasing loads whereas the experimental curves on the other hand were obtained as hysteretic moment-displacement relationships. It was assumed that the monotonically loaded analytical curves would result in envelope curves which would match the envelope of the experimental hysteretic curves. The comparisons of the analytical and experimental results for the tested beams are presented in **Figure 6.8** to **Figure 6.16**. The results of the comparisons show good

agreement between the analytical and experimental results as the analytical envelope curves match the envelope of the experimental hysteretic curves well.

Table 6.2 also shows that the peak flexural capacities of the beams as predicted analytically match well with the experimentally obtained peak moment capacities.

Table 6.2 Experimental and Analytical flexural strengths of tested beams

Specimen	***Flexural Strength in Positive Bending***		***Flexural Strength in Negative Bending***	
	Experimental	***Analytical***	***Experimental***	***Analytical***
D/2-0/0%	34.1	33.2	-45.1	-47
D/2-0.75%	34.2	33.8	-49.5	-52
D/2-1.0%	37.7	36.5	-43.3	-44
D/2-1.5%	36.1	35.2	-60.7	-53
D/3-1.0%	33	33.1	-51.5	-52.1
D/3-1.5%	33.4	33.8	-64.8	-58.9
D/4-0.0%	32.5	33.6	-47.9	-48.5
D/4-1.5%	34.9	33.1	-50.6	-53.6
D-1.5%	33.8	33	-52.3	-50.6

6.3.1 Discussion of Analytical Results

6.3.1.1 Effect of Tension-hardening in SFRC

As noted in the previous section, the peak moment capacities of the control beams without fibers and the SFRC beams with fibers contents of up to 1.0% are in good agreement with the experimental results. However, in beams reinforced with 1.5% fiber content, the analytical procedure that was used generally underestimates peak strengths with a few minor exceptions. It is to note that the procedures used in the present analysis neglected the tensile capacity of concrete for simplicity. As discussed in the literature review, SFRC has the ability to carry tensile stresses after cracking and therefore neglecting this tensile strength can result in underestimation of moment capacity. Although this effect may be negligible in beams with SFRC having low fiber contents, this tensile contribution may be more important for SFRC having higher fiber content, such as in the case of the 1.5% series beams, since tensile behaviour can transform from tension-softening into tension-hardening at higher fiber contents. In addition to effects of higher fiber content on tensile response, it should also be noted that behaviour in

compression (in terms of peak stress) has also been shown to be more strongly influenced at higher fiber contents. According to Aoude (2008), this enhancement in behaviour is related to the enhanced resistance of concrete against lateral deformations (i.e. Poisson's effect) in SFRC with tension-hardening properties. Further research is required to investigate this effect on confined SFRC in compression.

6.3.1.2 Effect of strain-hardening in longitudinal steel reinforcement

The strain hardening effect of the longitudinal reinforcement was not captured effectively in the analytical results. The stress-strain behaviour of the longitudinal reinforcement was defined based on experimental data obtained from coupon tests which resulted in higher hardening and rupture strains than strain-hardening and rupture strains during experimental testing of the beams.

6.3.1.3 Effect of buckling

Buckling of longitudinal reinforcements was observed in beam D-1.5% in which the spacing of the hoops were equal to the effective depth of the section, d=204mm. Based on work of Yalcin and Saatcioglu (2000), when the bar aspect ratio (L/d_b) is greater than 8.0, stability of reinforcement is lost immediately upon reaching yield, resulting in loss of strength. In the case of beam D-1.5%, the bar aspect ratios for the positive and negative bending were 10.2 and 13.3 respectively and hence buckling of the longitudinal reinforcement was expected. The buckling effect was accounted for in this beam and as it can be seen in **Figure 6.16**, the analytical method used in this chapter was able to predict the strength decay in positive bending due to buckling of positive moment reinforcement in compression showing good agreement with the experimental results.

6.3.1.4 Effect of plastic hinge length

Analytical results for the SFRC specimens may have also been affected by the definition of plastic hinge length in SFRC members. During testing it was observed that the SFRC beams showed a slightly different behaviour in developing plastic hinging when compared to the beams without fibres. In the case of the SFRC beams although hinging was apparent, it was observed that a single major crack developed in the plastic hinge section near the face of the middle block (maximum moment section). This crack widened as the beams deformed vertically under

positive and negative bending moments while most secondary cracks remained well controlled. This behaviour can be related to the ability of fibres to bridge and control cracks as they form and hence only cracks at the critical sections widened under loading. Other researchers have also observed that SFRC typically results in reduced plastic hinge length in specimens subjected to load reversals (Schumacher et al., 2009). Consequently the plastic hinge lengths assumed in the analysis could be different in the case of SFRC.

6.3.1.5 Effect of Dowel action

Beam D/2-0.0% which contained no steel fibers, did not experience rupture of reinforcing bars in negative bending unlike other beams and a shear mode of failure was observed after spalling and severe loss of material due to flexural deformations. Dowel action of the longitudinal reinforcement was observed at this stage. This was primarily due to extensive loss of concrete in the plastic hinge region which results in a complete loss of shear strength and hence the minimal shear forces were taken by the longitudinal reinforcing bars. It is well known that longitudinal reinforcing bars cannot resist shear forces applied perpendicular to the direction of the reinforcing bars and therefore the bars deform laterally resulting in a dowel action. It should be noted that dowel action of the reinforcing bars was not directly accounted for in the present analysis due to lack of an analytical procedure for computing the effects of this behaviour.

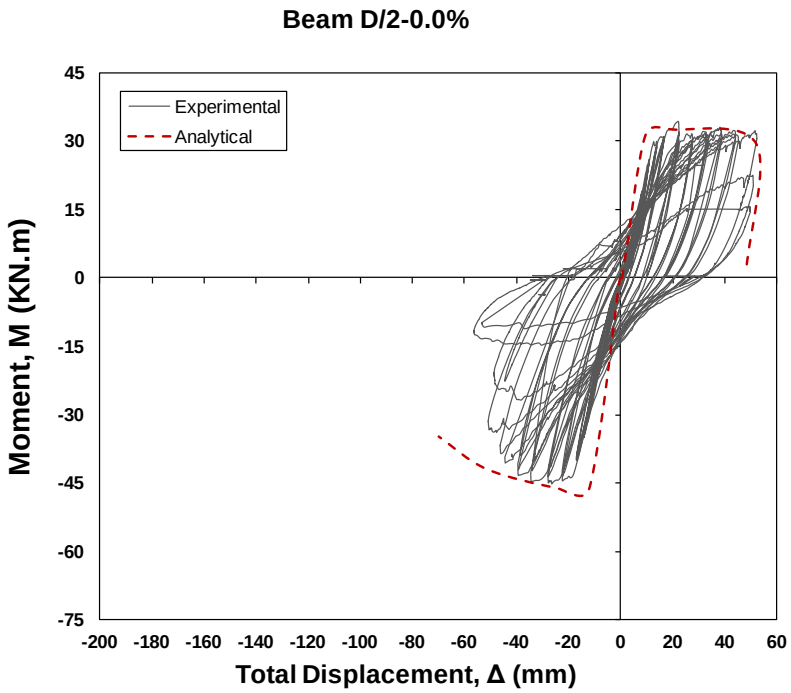

Figure 6.8 Comparison of analytical and experimental results for Beam D/2-0.0%

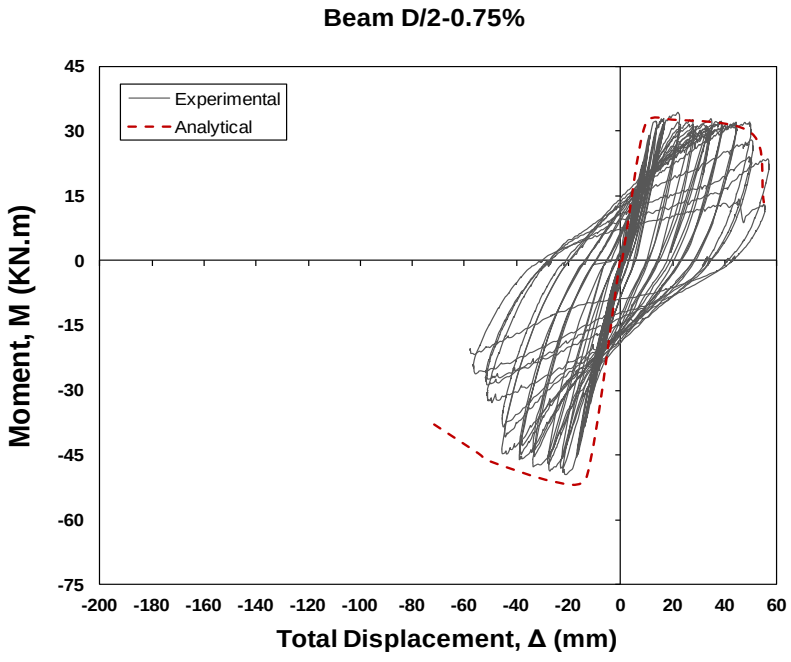

Figure 6.9 Comparison of analytical and experimental results for Beam D/2-0.75%

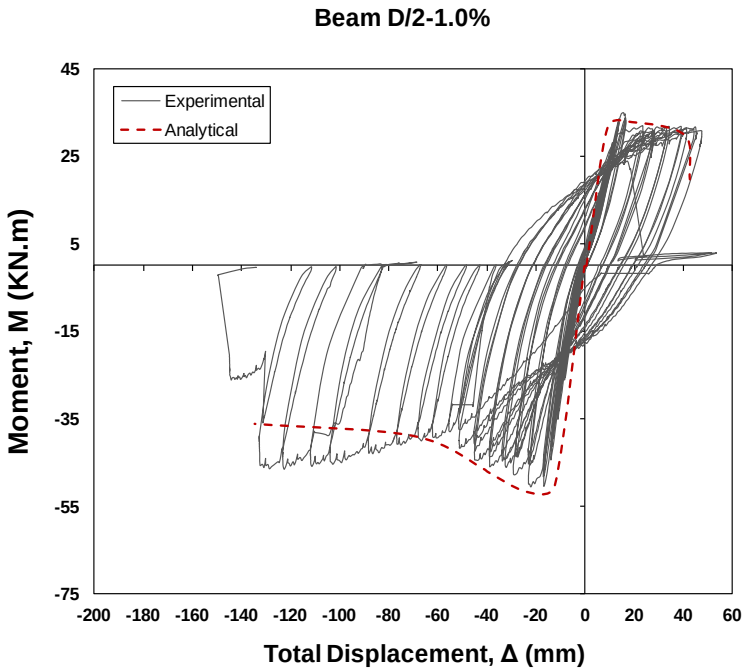

Figure 6.10 Comparison of analytical and experimental results for Beam D/2-1.0%

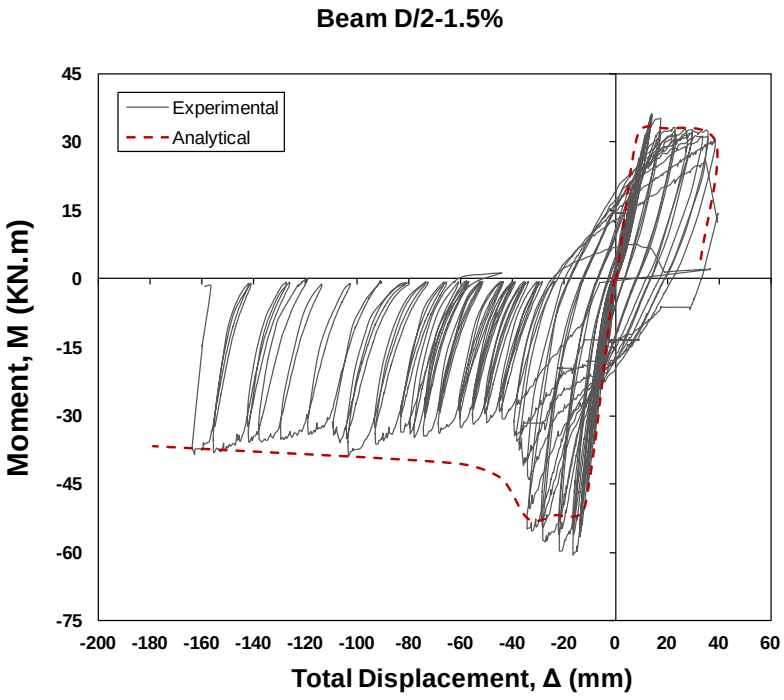

Figure 6.11 Comparison of analytical and experimental results for Beam D/2-1.5%

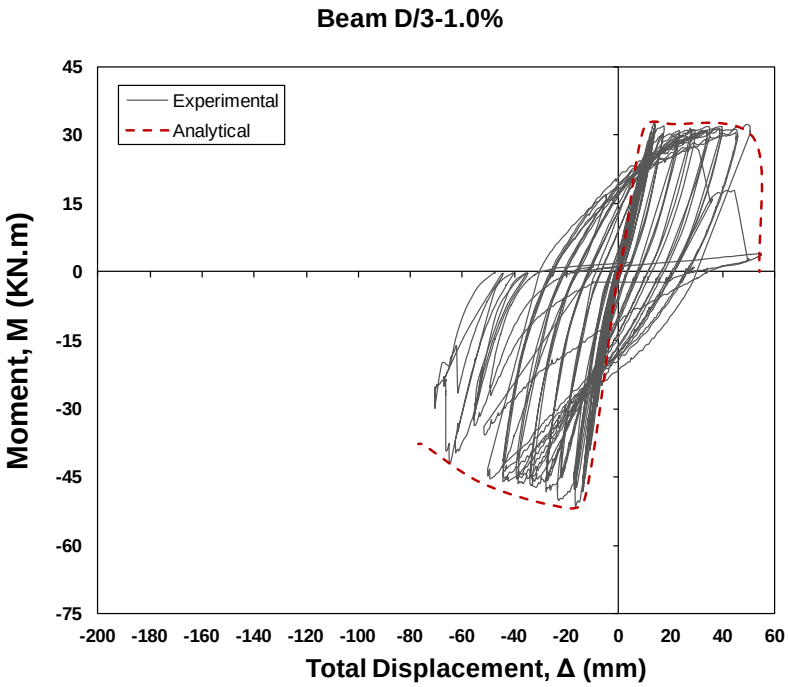

Figure 6.12 Comparison of analytical and experimental results for Beam D/3-1.0%

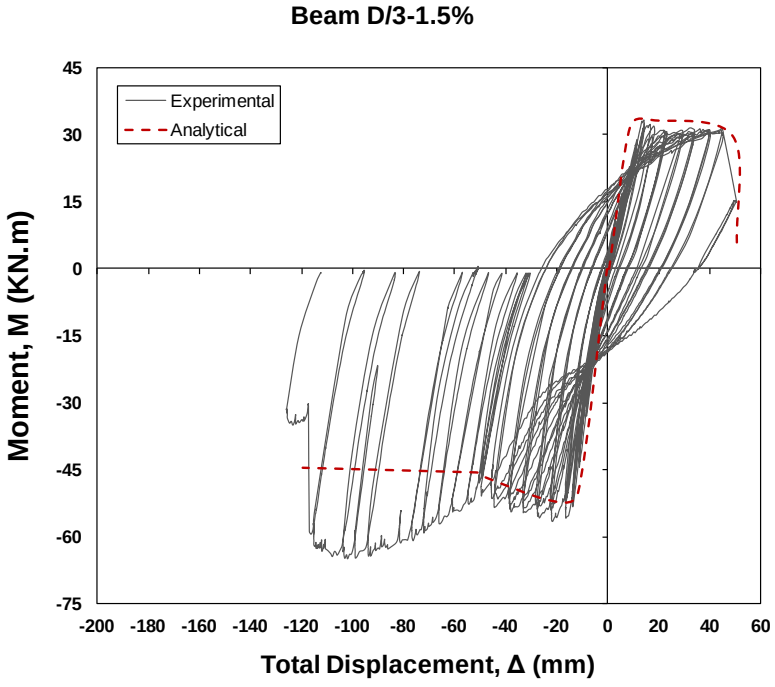

Figure 6.13 Comparison of analytical and experimental results for Beam D/3-1.5%

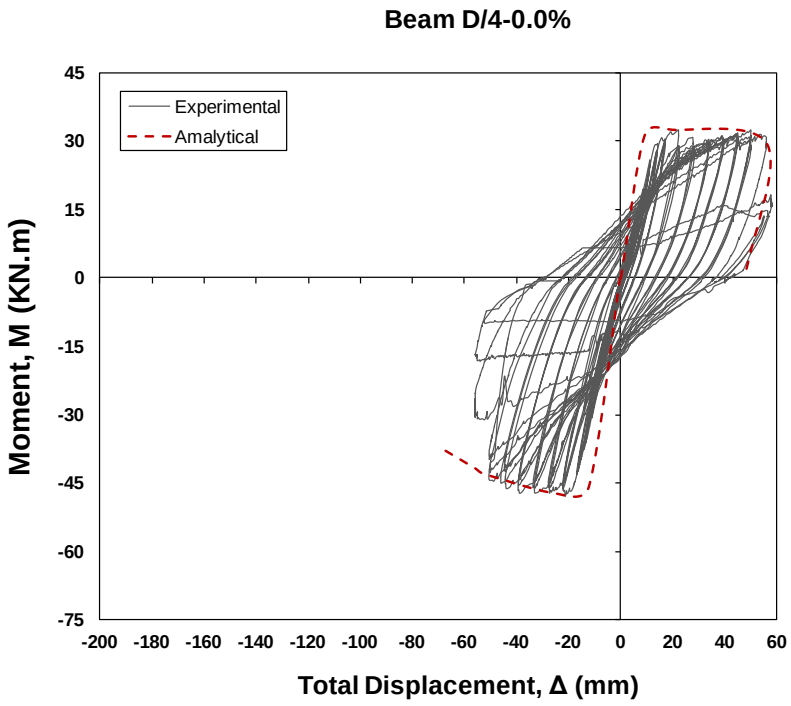

Figure 6.14 Comparison of analytical and experimental results for Beam D/4-0.0%

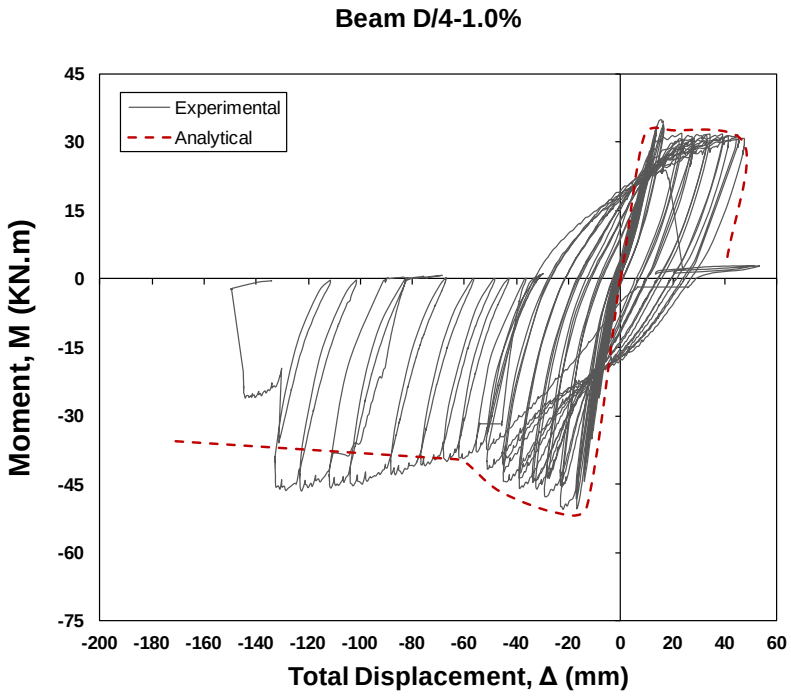

Figure 6.15 Comparison of analytical and experimental results for Beam D/4-1.0%

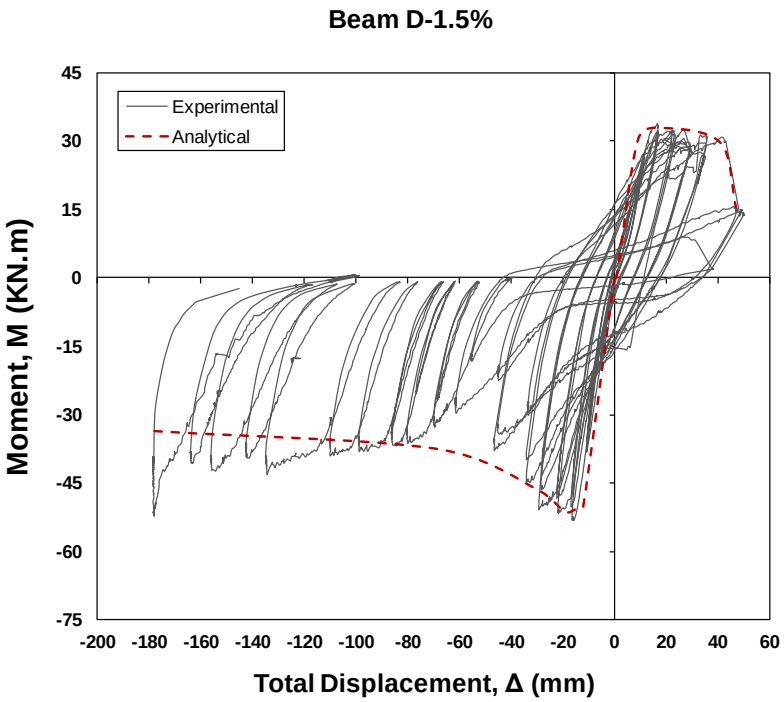

Figure 6.16 Comparison of analytical and experimental results for Beam D-1.5%

.

6.4 Concluding Remarks

The inelastic static (push-over) analysis approach adopted in this study was presented in this chapter. Material models for concrete, SFRC and steel were used to establish sectional moment-curvature and member moment-displacement responses of the tested beams. Generally the analytical moment-displacement envelopes obtained in this chapter showed good agreement with the experimental results.

Chapter 7 Conclusions

The primary objective of this research program was to study the performance enhancements that can be gained from the use of steel fibers in reinforced concrete beams subjected to large displacement reversals. An additional objective was to examine the potential of using steel fibers to partially replace transverse reinforcement in flexural members designed for ductile performance during earthquakes. The conclusions based on the experimental and analytical studies are summarized in the following sections.

7.1 Experimental Program

In this experimental program, nine steel fiber reinforced concrete (SFRC) dual-cantilever specimens constructed with SCC were tested under reverse-cyclic loading. Specimens containing varying fiber contents and reinforced with varying amounts of transverse reinforcement were tested in order to investigate the influence of steel fibres on the structural response of RC beam elements under large displacement reversals. The following conclusions were drawn from the experimental results:

(i) The use of self-consolidating concrete mix allows for good workability at moderate and high steel fiber contents;

(ii) Addition of steel fibres leads to an improved post-peak ductility and energy dissipation capacity in beams subjected to large displacement reversals;

(iii) Addition of steel fibres leads to increased flexural capacity, particularly at higher fiber contents, in beams subjected to large displacement reversals;

(iv) Addition of steel fibres can potentially be used to partially replace conventional transverse and relax seismic detailing requirements in flexural members.

(v) Inclusion of fibers leads to improved damage tolerance in beams subjected to displacement reversals. In particular, the addition of fibers improves crack control, delays cover spalling and provides better resistance against crushing;

(vi) Although addition of steel fibers increases resistance to cover spalling and enhances concrete confinement, minimum amounts of transverse reinforcement are still required to prevent buckling of longitudinal steel reinforcement;

(vii) Due to increased toughness of SFRC in compression, positive bending reinforcement (2-15M), which was designed in accordance with cl. 21.3.3.2 of the CSA A23.3-04 design standard, underwent large tensile strains during positive bending cycles resulting in early rupture and failure of the SFRC beams tested in this experimental program. In contrast, improved ductility was observed in negative bending due to the higher amount of bending reinforcement (2-20M).

(viii) Based on the observations in this experimental program, it is recommended that equal amounts of positive and negative bending moment reinforcements be provided in SFRC beams subjected to load reversals in order utilize the full toughness of SFRC and achieve increased ductility in both positive and negative bending. Further research is recommended.

7.2 Analytical Program

The load-displacement responses of the nine specimens tested in this experimental program were analytically predicted using inelastic static (push-over) analysis. Sectional and member analyses were conducted to establish the moment-curvature and moment-displacement relationships for the tested beams. Analytical results were compared to the hysteretic moment-displacement curves obtained from experimental results and the following conclusions were drawn:

i. Using the inelastic static (push-over) analysis, and accounting for the effect of steel fibers on concrete behaviour in compression in the sectional analysis, reliable analytical moment-displacement relationships can be established for SFRC beams tested under revered-cyclic loading;

ii. Predicting effect of strain-hardening in longitudinal reinforcement on member response may be difficult using a moment-curvature analysis that relies on experimental stress-strain data from coupon tests. An analytical model may be developed for predicting the stress-strain relationship of steel for computation of moment-displacement relationship;

iii. The buckling effect of longitudinal reinforcement should be considered in establishing moment-displacement relationship for beams with rebar aspect ratios, $L/db > 8.0$.

iv. SFRC beams exhibit different pattern in developing plastic hinge length as only one major crack develops and widens while smaller cracks are prevented from widening due

to the bridging effect of steel fibers. This may need to be taken into accounting when analyzing SFRC beams using a plastic hinge analysis approach in order to avoid overestimation of displacement;

v. Dowel effect in longitudinal reinforcement can be expected in beams tested under reverse-cyclic loading due to material loss in the hinging region in beams with no steel fibers. Dowel effect of longitudinal rebars can also occur in beams reinforced with steel fibers and transverse reinforcement with large spacings as a result of wide cracks at the shear critical section. Further research is required

7.3 Future Research

Suggestions for future research are given below:

(i) Studying the effect of unequal positive and negative moment reinforcement in SFRC beams subjected to reverse-cyclic loading;

(ii) Studying the effect of shear stress demand on the behaviour of SFRC beams subjected to reverse-cyclic loading (this can be achieved by testing beams having different a/d ratios);

(iii) Further fibre typologies could be used to examine the influence of fibre geometry on the response of structural members constructed with SFRC under reverse-cyclic loading;

(iv) Based on further experimental tests, expressions that can be used to introduce the influence of fibres in reducing the required hoop spacing in RC beams could be developed and implemented in codes of practice.

List of References

ACI Committee 544, (1988). "Design Considerations for Steel Fiber Reinforced Concrete (ACI 544.4R-88)." *American Concrete Institute*, Farmington Hills, Michigan, USA, 18 pp.

Altoubat, S. A., Lange, D. A. (2001), "Creep, Shrinkage, and Cracking of Early Age Concrete," *ACI Materials Journal*, 98(4), 323-31.

Alwan, J. M., Namman, A. E. & HNSEN, W. (1991) "Pull-Out Work of Steel Fibers From Cementitious Composites: Analytical Investigation." *Cement and Concrete Composites*, 13 (4), 247-255.

Alwan, J. M., Naaman, A. E., & Guerrero, P. (1999) "Effect of Mechanical Clamping on the Pullout Response of Hooked Steel Fibers Embedded in Cementitious Matrices." *Concrete Science and Engineering*, 1,15-25.

Aoude, H. (2008) "Structural Behaviour of Steel Fiber Reinforced Concrete Members." PhD thesis, Department of Civil Engineering and Applied Mechanics, McGill University, Montreal, Canada.

ASTM C1609 (2010b) "*Standard Test Method for Flexural Performance of Fiber Reinforced Concrete (Using Beam with Third-Point Loading).*" Philadelphia, American Society of Testing and Materials.

ASTM C1018 (1998) "*Standard Test Method for Flexural Toughness and First Crack Strength of Fiber Reinforced Concrete.*" Philadelphia, American Society of Testing and Materials.

ASTM C1399 (1998b) " *Test Method for Obtaining Average Residual-Strength of Fiber Reinforced Concrete.*" Philadelphia, American Society of Testing and Materials.

ASTM C1550 (2010a) "*Standard Test Method for Flexural Toughness of Fiber Reinforced Concrete (Using centrally loaded round panel).*" Philadelphia, American Society of Testing and Materials.

Banthia, N. & Mindess, S. (2004) "Toughness Characterization of Fiber-Reinforced Concrete: Which Standard to Use." *Journal of Testing and Evaluation*, 32 (2), 138-42.

Banthia, N. and Trottier, J.-F.(1994). "Concrete Reinforced with Deformed Steel Fibers, Part I: Bond Slip Mechanisms." *ACI Materials J.*, 91(5), 435-446.

Batson, G., Ball, C., Bailey, L., Lenders, E. and Hooks, J. "Flexural Fatigue Strength of Steel Fiber Reinforced Concrete Beams." *ACI Journal, Proceedings*, Vol. 69, No. 11 November 1972, pp 673 – 677.

Bayramov F., C. Tas_demir and M.A. Tas_demir. (2004). “Optimization of Steel Fiber Reinforced Concretes by Means of Statistical Response Surface Method.” *Cem. Conc. Res.*, 26, 665-675.

Bernard, S. (2003) “Release of New ASTM Round Panel Test.” *Shotcrete Corner*, 5 (2), 20-23.

Burrel R. (2012). "Performance of Steel Fiver Reinforced Concrete Columns under Shock Tube Induced Shock Wave Loading." M.S. thesis, Dept. Civil. Eng., Ottawa. Univ., Ottawa., ON , 2012.

Campione G. (2008) "Simplified Flexural Response of Steel Fiber-Reinforced Concrete Beams." *Journal of Materials in Civil Engineering*, 20(4).

Chanvillard, G. & Aiticin, P.C. (1996) “Pull-Out Behaviour of Corrugated Steel Fibers Qualitative and Statistical Analysis.” *Advanced Cement Based Materials*, 4 (1), 28-41.

Chompreda, P. and Parra-Montesinos, G. J. (2005). "Deformation Capacity and Shear Strength of Fiber Reinforced Cement Composite Flexural Members Subjected to Displacement Reversals." Research Report No. UMCEE 05-03, Department of Civil and Environmental Engineering, University of Michigan, 186 pages.

Colajanni, P., La Mendola, L., Priolo, S., and Spinella, N. (2008). “Experimental Tests and FEM Model for SFRC Beams under Flexural and Shear Loads.” *SEISMIC ENGINEERING CONFERENCE: Commemorating the 1908 Messina and Reggio Calabria Earthquake*, 1020, 872-879.

Cohen, M. (2012). “Structural Behaviour of Self Consolidating Steel Fiber Reinforced Concrete Beams,” M.S. thesis, Dept. Civil. Eng., Ottawa. Univ., Ottawa., ON , 2012.

CSA (2004) “CSA A23.3-04: Design of Concrete Structures.” Canadian Standards Association, Mississauga, Canada.

Dupont, D. (2003) “Modeling and Experimental Validation of the Constitutive Law and Cracking Behaviour of Steel Fiber Reinforced Concrete.” Department of Civil Engineering. Heverlee, Catholic University of Leuven, Belgium.

Fantilli, A. P. (2009). “Multiple Cracking and Strain Hardening in Uniaxial Tension.” *Cement and Concrete Research*, 39, 1217–1229.

Fenwick, R. C., Fong, A. (1979). "The Behaviour of Reinforced Concrete Beams under Cyclic Loading.", Report No. 176, Department of Civil Engineering, University of Auckland.

Foster, S. J. & Attard, M. M. (2001) “Strength and Ductility of Fiber-Reinforced High-Strength Concrete Columns.” *Journal of Structural Engineering*, 127 (1), 28-34.

Foster, J. & VOO, J., (2003) “Variable Engagement Model for Fiber Reinforced Concrete in Tension.” University of New South Wales, Sydney, Australia.

Ganesan and J.V. Ramana Murthy, "Strength and Behaviour of Confined steel Fibre Reinforced Concrete Columns", ACI Materials Journal, American Concrete Institute, Vol.87, No.3, May-June 1990, pp. 221-227.

Greenough, T & Nehdi, M. (2008) “Shear Behaviour of Fiber-Reinforced Self-Consolidating Concrete Slender Beams.”. *ACI Structural Journal*, 105 (5), 468-477.

Cusson D. and P. Paultre (1945). "Stress-strain model for confined high strength concrete." *ASCE Journal of Structural Engineering*, 121 (3), 468-477.

Grunewald, S. (2004) “Performance-Based Design of Self-Compacting Fiber Reinforced Concrete.” Department of Structural and Building Engineering, Delft University of Technology, Delft, Germany, 20-24 .

Gurjar, A. (2004) “Mix Design and Testing of Self-Consolidating Concrete Using Florida Materials.” Report No. BD 503, Daytona Beach, the Florida Department of Transportation.

Hameed R., Turatsinze A., Duprat F., Sellier A. (2009). "Study on the flexural properties of metallic-hybrid-fibre reinforced concrete". PhD thesis, University of Toulouse, France.

Hannant, D. J. (1978) “Fiber Cements and Fiber Concretes.” John Wiley and Sons Ltd., New York, USA.

Johnston, C. D. (2001). “Advance in Concrete Technology.” *International Centre for Sustainable Development of Cement and Concrete.*

Kang,S.T., Lee, Y., Park,Y.,and Kim, J.K.(2010).“Tensile fracture properties of an Ultra High Performance Fiber Reinforced Concrete (UHPFRC) with steel fiber”, *Composite Structures.*, 92(1), 61-71.

Kent, D.C, and Park, R. (1971). “Flexural Members with Confined Concrete.” *Journal of the Structural Division. Vol. 97, No. 7*, 1969-1990.

Khayat, K. H., Tremblay, S. y Paultre, P.: “Structural response of self-consolidating concrete columns”, Proceedings of 1st international RILEM symposium on self-compacting concrete, Stockholm, 1999, pp. 291-306.

Konig, G., Kutzing, L., (1999). "Modeling the Increase of Ductility of HPC Under Compressive Forces – A Fracture Mechanics Approach by RILEM TC 148-SSC.Materials and Structures.", 30, 250-260.

Kooiman, A.G (2000).″ Modelling Steel Fibre Reinforced Concrete for Structural Design".

PhD thesis, TU Delft.

Kosmatka, S., B. Kerkhoff, and W. Panarese (2008). "Design and Control of Concrete Mixtures. 14th Edition". Item Code: EB001. Portland Cement Association, Skokie, IL.

Kutzing, L.; Koning, G. (2000). "Punching Behaviour of High Performance Concrete Columns with Fibre Cocktails." Lacer 5, 253-260.

Lankard, D.R., 1984. “Properties, Application: Slurry Infiltrated fibre concrete,” *Journal Concrete Design and construction*, 61(12), 44-47.

Lee, C. D. (1990) “Constitutive Modeling and Flexural Analysis of Steel Fiber Reinforced Concrete for Structural Applications.” Department of Civil and Environmental Engineering. Ann Arbor, Michigan State University.

Legeron, F., and Paultre,P., (2003) “Uniaxial confinement model for normal and high strength concrete columns.” *ASCE Journal of Structural Engineering*, 2003, 29(2), 241-252.

Liao W., Chao S., Park S., & Naaman A. (2006) “Self-Consolidating High Performance Fiber Reinforced Concrete (SCHPFRC)-Preliminary Investigation.” Department of Civil and Environmental Engineering, University of Michigan, USA.

Liao, W. C., Chao, S. H., Park, S. Y. and Naaman, A. E. (2006),“Self-Consolidating High Performance Fiber Reinforced Concrete (SCHPFRC) – Preliminary Investigation,” Report No. UMCEE 06-02, University of Michigan, Ann Arbor, MI, 68.

Lok T.S., Pei J.S., (1996). "Flexural Behaviour of Teel Fiber-reinforced Concrete." *Journal of Materials in Civil Engineering, ASCE,* 10(2), 86-97.

Maidl, B., Dietrich J. (1995). "Steel fibre reinforced concrete.", Ernst & Sohn, Berlin.

Marefat, M.S., Shirazi, S.M.H., Rostamshirazi, R. and Khanmohammadi, M. (2009). "Cyclic response of concrete beams reinforced by plain bars." Journal of Earthquake Engineering 13(4), 463-481.

Minelli, F. (2005) “*Plain and Fiber Reinforced Concrete Beams under Shear Loading*.” PhD Thesis, Department of Civil Engineering, University of Brescia, Italy.

Mohammadi, Y., Singh S.P., and Kaushik, S.K. (2008). “Properties of steel fibre concrete containing mixed fibres in fresh and hardened state”. *Journal of Construction and Building materials,* 22, 956-965.

Massicotte, B., MacGregor, J., and Elwi, A. (1990). ”Behavior of Concrete Panels Subjected to Axial and Lateral Loads.” *J. Struct. Eng*., 116(9), 2324–2343.

Mansur, M. A., Chin, M. S. & Wee, T. H. (1999) “Stress-Strain Relationship of High-

Strength Fiber Concrete in Compression." *Journal of Materials in Civil Engineering*, 11 (1), 21-29.

Mander, J. B., Priestley, M. J. N., and Park, R. (1988). "Observed stress strain behavior of confined concrete." *J. Struct. Eng*., 1148, 1827–1849.

Naaman, A. E., and Reinhardt, H. W.(1996). "Characterization of High Performance Fiber Reinforced Cement Composites," *High Performance Fiber Reinforced Cement Composites (HPFRCC 2)*, 1-23.

Naaman Antoine E (2003). "Engineered Steel Fibers with Optimal Properties for Reinforcement of Cement Composites." *Journal of Advanced Concrete Technology*. 1(3), 241-252.

Nataraja, M. C., Dhang, N. & Gupta, A. P. (1999) "Stress-Strain Curves for Steel-Fiber Reinforced Concrete Under Compression." *Cement and Concrete Composites*, 21 (5), 383-390.

Naaman, A. E., and Reinhardt H. W. (2006) "High Performance Fiber Reinforced Cement Composites: Classification and Application." *Proceedings of the Second International RILEM Workshop*, RILEM Publications, Cachan Cedex, France, pp. 1-24.

Nemegeer D. (1997). "Dramix: Design guidelines for Dramix steel wire fibre reinforced concrete". N.V. Bekaert S.A., Harelbeke, Belgium.

Nowak A.S.; Laumet P., Czarnecki A.A., Kaszynska M., Szerszen M.M., Podhorecki P.J. (2005). "US-Specific Self-Consolidating Concrete for Bridges," Final Report.

Okamura, H., and Ouchi, M.m(2003)."Self-Compacting Concrete." *Journal of Advanced Concrete Technology*, 1(1), 5-15.

Ouchi M., Nakamura S. Osterberg T., Hallberg S., & Lwin M. (2003). "Applications of Self-Compacting Concrete in Japan, Europe and the United States". *ISHPC*, 1-20.

Ozyildirim, C., and Lane, D.S. (2003). "Evaluation of Self-Consolidating Concrete." *National Technical Information Service.*

Ozcebe, G., and Saatcioglu, M. (1989). "Response of Reinforced Concrete Columns to Simulated Seismic Loading." *Structural Journal*. 86(1), 3-12.

Park R., Priestley M. J. N., and Gill W. D. (1982). "Ductility of square confined concrete columns." *J. Struct. Div., ASCE*, 108(4), 929-950.

Parra-Montesinos, G. J. (2006) "Shear Strength of Beams with Deformed Steel Fibers", *Journal of American Concrete Institute*, 28 (11), 57-66.

Popovics, S. (1973). "A numerical approach to the complete stress-strain curves for concrete." *Cent. Concr. Res.*, 3(5), 583-599.

Popovics, S. (1973). "A numerical approach to the complete stress-strain curves for concrete." Cent. Concr. Res., 3(5), 583-599.

Popovics, S. (1973). "A numerical approach to the complete stress-strain curves for concrete." Cent. Concr. Res., 3(5), 583-599.

Popovics, S. (1973). "A numerical approach to the complete stress-strain curves for concrete." Cent. Concr. Res., 3(5), 583-599.

Ramesha , K., Seshu, D.R., and Prabhakar, M. (2003). “Constitutive Behaviour of Confined Fibre Reinforced Concrete Under Axial Compression.” *Cement and Concrete Composites*. 25(3), 343–350

Razvi, S., and Saatcioglu, M. (1999). ”Confinement Model for High-Strength Concrete.” *J. Struct. Eng.*, 125(3), 281–289.

Razvi, s., and Saatcioglu, M. (1994). “Strength and Deformability of Confined High-Strength Concrete Columns.” *Structural Journal*. 91(6), 678-687.

Richart, F. E., Brandtzaeg, A., and Brown, R. L. (1928). “A study of the failure of concrete under combined compressive stresses.” Univ. of Illinois Bulletin, 185.

Saatcioglu, M. and Baingo, D. (1999). “Circular High-Strength Concrete Columns under Simulated Seismic Loading.” *J. Struct. Eng.*, 125(3), 272–280.

Saatcioglu, M., Alsiwat, J., and Ozcebe, G. (1992). ”Hysteretic Behavior of Anchorage Slip in R/C Members.” *J. Struct. Eng.*, 118(9), 2439–2458.

Saatcioglu, Murat; and Ozcebe, Guney, "Response of Reinforced Concrete Columns to Simulated Seismic Loading," American Concrete Institute, ACI Structural Journal, January - February, 1989, pp. 3-12

Sheikh, S. A., and Uzumeri, S. M. (1982). "Analytical model for concrete confinement in tied columns." *Struct, Div., ASCE*, 108(12), 2703-2722.

Van Gysel A. (2000). "Study of the pullout behaviour of steel fibers embedded in cement-bonded matrix with application on the fiber reinforced concrete in bending." PhD Thesis, Laboratorium Magnel voor Betononderzoek, faculty of applied sciences, University of Gent, Belgium.

Van Mier, J.G.M., et al., 1997. Strain-softening of Concrete in Uniaxial Compression- Report of the round Robin test carried out by RILEM TC 148-SSC.Materials and Structures 30, 195-209.

Weiler, B., Grosse, C. And Reinhardt, H. W. (1999). “Acoustic emission investigations of the damage zone in steel fiber reinforced beams.” *Proceedings of the Third International RILEM Workshop*, RILEM Publications, Mainz, Germany, pp. 487-496.

Wang, J.Y., Van Tittelboom, K., De Belie, N., and Verstraete, W. (2010). “Potential of applying bacteria to heal cracks in concrete.” Proceedings of the second international conference on sustainable construction materials and technologies. Ancona, Italy.

Yalcin, C., and Saatcioglu, M. (2000). “Inelastic Analysis of Reinforced Concrete Columns.” *Computers & Structures*. 77(5), 539–555.